Dynamical Reconstruction of Multi-Dimensional Image Sequences Using Optical Flows

Dissertation
zur Erlangung des Doktorgrades
der Fakultät für Mathematik, Informatik
und Naturwissenschaften
der Universität Hamburg

vorgelegt
im Fachbereich Mathematik
von

Marcel Kumbartzky

aus Oststeinbek

Hamburg, 2016

Day of oral defense: May 31, 2017

The following evaluators recommend the admission of the dissertation:

Prof. Dr. Michael Hinze
Prof. Dr. Jan Modersitzki

Contents

List of Figures

List of Tables

1. Introduction

1.1. Motivation

This thesis is concerned with the dynamical reconstruction of image sequences. Before formulating the concrete mathematical problem, we first motivate it with some practical applications:

Medicine: In 2013, a quarter of all cases of death in Germany were due to cancer. Among the various kinds of cancer, lung and bronchial cancer had been second most frequently detected [23].

Radiotherapy is often applied to combat the tumour. In this treatment, the lung tumour is simultaneously irradiated from all sides. At any time, we have to ensure that the tumour receives the necessary dose rate. However, this is hard to realize, since the lung tumour is moved by the respiratory act. Therefore, a larger security domain around the contour of the tumor is often used in radiotherapy. But this may have the consequence that also healthy tissue, lying directly next to the tumour, is destroyed. Hence, we are interested in minimizing this security domain.

Thus, the aim is to reconstruct the periodical movement of a lung to ensure a precise localisation of the tumour at each time. To be more precise, we are given 3-dimensional radiographs of a lung at discrete points in time, and we are interested in reconstructing a continuous movement of this lung. This way, we obtain a $(3 + 1)$-dimensional reconstruction problem (in space $+$ time).

Animation: An animation consists of a sequence of single frames differing slightly from each other which is displayed rapidly, i.e., around 24 frames per second. This rapid display gives the illusion to the observer that this is a smooth motion.

However, an animation with a running time of 90 minutes consists of 129,600 pictures. Hence, the effort for the animators to draw all these single frames is very large. This effort can be reduced by a factor k if we only draw every k-th single frame and generate the remaining single frames by using a sequence interpolation.

Video restoration: If we play old VHS cassettes, we often observe strokes on the video. If only a few sequential single frames per video scene are affected, then one possibility to denoise the video could be to use a sequence interpolation. This means we reconstruct each perturbed video scene by interpolating the unperturbed single frames of this video scene.

In summary, we observe that we have to solve a sequence interpolation problem in any of these different applications which reads.

Problem (Sequence Interpolation Problem)**.**
Given a sequence of image samples $I_n \colon \Omega \to \mathbb{R}$ with domain $\Omega := [0,1]^d$ of dimension $d > 1$ at discrete time points $0 = t_0 < t_1 < ... < t_N = T$, we seek a continuous function $I \colon [0,T] \times \Omega \to \mathbb{R}$ which interpolates these samples, i.e.,

$$I(t_n, x) = I_n(x) \quad for \ n = 0, ..., N \ and \ all \ x \in \Omega. \tag{1.1}$$

There are, of course, many ways this could be done.

1.2. Introduction to Optical Flows

A convenient way to solve the sequence interpolation problem (1.1) is to use optical flows, as we will show in this thesis. For further explanation, an optical flow describes the projection of a $(d+1)$-dimensional movement onto a d-dimensional hyperplane. Mathematically, an optical flow can be represented by a vector field which describes the speed and direction of the motion of each pixel point in a sequence of images. In Figure 1.1, the optical flow is illustrated for the Hamburg taxi sequence, which is a famous benchmark in the context of optical flows, see e.g. [4, 8, 9, 18, 46].

Nowadays, optical flows are already used in many application fields, for example:

In robot navigation, the optical flow gives important information about the motion of surrounding objects, such that the robot is able to orientate and navigate autonomously in space. Consider for example a river and a bridge to cross it. In this case, we observe a nonzero optical flow along the river, but a zero optical flow at the location of the bridge. Hence, the robot is able to locate the bridge and to cross it autonomously [13].

In video compression, the optical flow allows us to find redundant information in a video sequence. These are areas where no motion appears in the optical flow. Thus, we can compress the video size by storing these redundant information only once [13].

In computer science, the motion of an optical mouse is scanned by identification of the optical flow [47].

Unfortunately, the optical flow is a function which is not physically measurable. But we know the intensity function $I \colon [0,T] \times \Omega \to \mathbb{R}$ at discrete time points t_n. This intensity function I measures the grey value of an image pixel point $x \in \Omega$ at time $t \in [0,T]$. Hence, the aim is to set the optical flow in relation to the intensity function I. For this purpose, we require $I \in \mathcal{C}^1([0,T] \times \Omega)$. Moreover, we assume that the intensity

of an image pixel point does not change during its movement, which is described by a C^1-curve $(t, x(t))$ with $x \colon [0, T] \to \Omega$. Thus, we obtain

$$I\big(t, x(t)\big) = I\big(0, x(0)\big) =: I_0\big(x_0\big), \qquad (1.2)$$

or, equivalently,

$$\frac{\mathrm{d}}{\mathrm{d}t} I\big(t, x(t)\big) = 0. \qquad (1.3)$$

Applying the chain rule, we get

$$0 = \frac{\mathrm{d}}{\mathrm{d}t} I\big(t, x(t)\big) = I_t\big(t, x(t)\big) + \dot{x}(t) \cdot \nabla I\big(t, x(t)\big) \qquad (1.4)$$

where $I_t(t, x) := \frac{\partial}{\partial t} I(t, x)$, $\nabla I(t, x) := (\frac{\partial}{\partial x_1} I(t, x), ..., \frac{\partial}{\partial x_d} I(t, x))^T$ and $\dot{x}(t) = \frac{\mathrm{d}}{\mathrm{d}t} x(t)$.

Altogether, from (1.2) and (1.4) we obtain the *optical flow constraint*

$$I_t(t, x) + \omega(t, x) \cdot \nabla I(t, x) = 0 \quad \text{with } I(0, x) = I_0(x), \qquad (\text{OFC})$$

where $\omega = \omega(t, x(t)) := \dot{x}(t)$ denotes the *optical flow*. Alternatively, this optical flow constraint (OFC) can be derived by using a Taylor expansion series, see [33].

Next, we observe that the optical flow constraint (OFC) is characterized by a semi-linear transport equation. Hence, for given $\omega \in \mathcal{C}([0, T] \times \Omega; \mathbb{R}^d)$ and $I_0 \in \mathcal{C}^1(\Omega)$ we deduce existence of a solution $I \in \mathcal{C}^1([0, T] \times \Omega)$ from Peano's theorem (cf. Chapter 3).

Regarding the assumption $I \in \mathcal{C}^1([0, T] \times \Omega)$ in the derivation of the optical flow constraint (OFC), we note that image samples are not necessarily differentiable or at least continuous (in space). But in Chapter 5 we show that the optical flow constraint (OFC) is also reasonable in a weak sense for $I \in \mathcal{C}([0, T], L^p(\Omega)), 1 \le p < \infty$. In particular, we prove that the optical flow constraint (OFC) admits a unique weak solution $I \in \mathcal{C}([0, T], L^p(\Omega)), 1 \le p < \infty$, if the vector field ω lies in the Bochner space $\big(L^1((0, T), W_0^{1,1}(\Omega))\big)^d$ and the initial value I_0 is bounded in $L^\infty(\Omega)$.

As a consequence, if we know the optical flow ω corresponding to the given sequence of images I_n, we can solve the sequence interpolation problem (1.1) by solving the optical flow constraint (OFC).

1.3. Horn and Schunck's Approach

For solving the sequence interpolation problem (1.1), we first have to solve the inverse problem, i.e., we have to reconstruct ω from a given sequence of image samples $I_n, n = 0, ..., N$, with $I_n(x) = I(x, t_n)$. Considering the optical flow constraint (OFC) more carefully, we observe that this problem is under-determined for $d > 1$. In fact, we have one equation, but d unknown velocity components. Hence, this inverse problem

has in general no unique solution.

This inverse problem was first analysed by Horn and Schunck in 1981 [33]. They proposed a linear Tikhonov regularization (cf. Chapter 4),

$$\min_{\omega \in \mathcal{U}} J(\omega) = \int_{\Omega} \left(I_t + \omega \cdot \nabla I \right)^2 \mathrm{d}x + \alpha\, R(\omega) \quad \text{for } t \in [0, T] \text{ and } \alpha > 0, \tag{1.5}$$

to reduce the space of admissible vector fields. Here, $\mathcal{U}$ denotes the space of admissible vector fields ω and $R(\omega)$ is a regularization term. More concretely, Horn and Schunck used $R(\omega) = \|\omega\|_{\mathcal{U}}^2$ with $\mathcal{U} = H_0^1(\Omega)$ as regularization term. Since the reconstruction quality of the optical flow depends essentially on the choice of regularization, further regularization terms were suggested in the last few decades, for instance a BV-regularization, see [4, 16, 18]. Further regularization terms are collected in [46]. In [46], it is also suggested to exploit the complete discrete sequence of image samples $I_n, n = 0, ..., N$, to reconstruct the optical flow, i.e., to solve

$$\min_{\omega \in \mathcal{U}} J(\omega) = \int_{\Omega} \int_0^T \left(I_t + \omega \cdot \nabla I \right)^2 \mathrm{d}x\, \mathrm{d}t + \alpha\, R(\omega) \quad \text{for } \alpha > 0, \tag{1.6}$$

where $\mathcal{U}$ denotes again the space of admissible vector fields ω.

Figure 1.1.: Reconstruction of the optical flow using Horn and Schunck's algorithm: Here the 5th, 10th and 15th image frame of the Hamburg taxi sequence with corresponding optical flow are pictured.

A frequently used method for solving numerically problem (1.5) for an H^1-regularization term is Horn and Schunck's algorithm given in [33]. The reconstructed optical flow for the Hamburg taxi sequence obtained by this algorithm is depicted in Figure 1.1.

We observe that the motion of the white car is well identified, whereas the motion of the two black cars and the pedestrian are not clearly distinguishable from the noise in the image frames. Moreover, the optical flow is computed in real time. This efficiency is of particular importance in robot navigation or in scanning the motion of an optical mouse.

1.4. Sequence Interpolation Problem

A disadvantage of Horn and Schunck's approach is that any algorithm for solving numerically problem (1.5) or (1.6) needs to compute approximate time derivatives I_t from the samples I_n. Hence, the reconstruction results are depending on the sampling time $\Delta t_n := t_{n+1} - t_n$ since

$$I_t(t, \cdot) = \frac{I_{n+1} - I_n}{\Delta t_n} + \mathcal{O}(\Delta t_n) \quad \text{for } t \in [t_n, t_{n+1}].$$

Consequently, the sampling rate Δt_n has to be chosen small for accurate reconstruction results of the optical flow ω. Therefore, Horn and Schunck's approach (1.5) is inappropriate to solve the sequence interpolation problem (1.1), where we do not necessarily have a sufficiently high sampling rate.

Introducing the solution operator of the optical flow constraint (OFC),

$$\mathcal{T} : \mathcal{U} \times \mathcal{Z} \to \mathcal{Y}$$
$$(\omega, I_0) \mapsto I$$

with appropriate function spaces $\mathcal{U}, \mathcal{Y}$ and $\mathcal{Z}$, we can reformulate the sequence interpolation problem (1.1) as follows:

Problem (Sequence Interpolation Problem).
Given a sequence of image samples $I_n \in \mathcal{Z}$ at discrete time points

$$0 = t_0 < t_1 < ... < t_N = T,$$

we seek a vector field $\omega \in \mathcal{U}$ such that

$$\mathcal{T}(\omega, I_0)(t_n, \cdot) = I_n \quad \text{for } n = 0, ..., N. \tag{SIP}$$

In Chapter 6, we show that this problem is not stable. This means small errors in the input samples I_n, caused, e.g., by physical measurements, can generate arbitrarily large errors in the reconstruction. Hence, we also use a Tikhonov regularization in this case to stabilize this problem and obtain

$$\min_{(\omega, I) \in \mathcal{U} \times \mathcal{Y}} J(\omega, I) = \sum_{n=0}^{N} \|I(x, t_n) - I_n\|^2_{L^2(\Omega)} + \alpha R(\omega) \tag{1.7}$$

subject to the optical flow constraint

$$I_t(t, x) + \omega(t, x) \cdot \nabla I(t, x) = 0 \quad \text{with } I(0, x) = I_0(x). \tag{OFC}$$

This optimal control formulation for computing the optical flow was already suggested by Borzi, Ito and Kunisch in 2002 [8, 9]. A benefit of this approach is that the image samples I_n and the corresponding intensity function I are different quantities. Consequently, in

numerical methods we are able to use for I and ω a finer time discretisation than induced by the given sampling rate Δt_n.

In [8, 9], it is illustrated by a few numerical experiments that this optimal control approach (1.7) leads indeed to better reconstruction results of the optical flow ω in comparison to Horn and Schunck's algorithm. But on the other hand, the computational costs are much higher. Hence, this approach is inappropriate in real time applications, like robot navigation. Moreover, in 2011, the optimal control approach (1.7) was applied by Chen [15] for solving the sequence interpolation problem (SIP).

A similar approach was proposed by Hinterberger and Scherzer in 2001 [30] to solve the sequence interpolation problem (SIP). They consider the minimization problem

$$\min_{(\omega, I) \in \mathcal{U} \times \mathcal{Y}} J(\omega, I) = \int_0^T \|I(x, \tau) - I_N\|_{L^2(\Omega)}^2 \, \mathrm{d}\tau + \alpha \, R(\omega) \qquad (1.8)$$

subject to the optical flow constraint (OFC).

In this approach (1.8), we seek for a solution I which approaches the final state I_N as fast as possible. However, this approach is inappropriate if we want to interpolate more than two images frames because intermediate image frames are not involved into the solution process.

Therefore, in the following we use for solving the sequence interpolation problem (SIP) ansatz (1.7). However, proving existence of a solution to problem (1.7) is much more complicated than for the Horn and Schunck approach (1.5). The squared term in (1.5) is a linear equation in ω (for given I).

(a) I_0 (b) $2\,\mathcal{T}(\omega, I_0)(1, \cdot)$ (c) $\mathcal{T}(2\,\omega, I_0)(1, \cdot)$
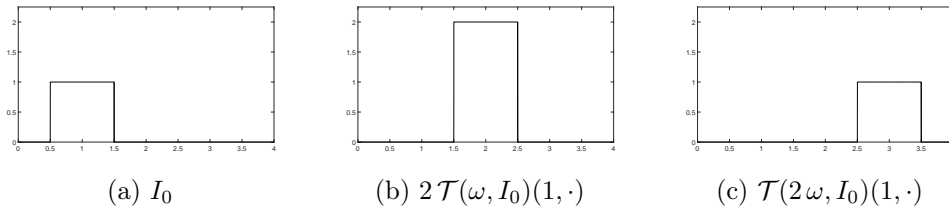
Figure 1.2.: Graphical Visualisation of the Non-Linearity of the solution operator $\mathcal{T}$

On the contrary, we have a non-linear solution operator $\mathcal{T}$ in ω in problem (1.7). In fact, if we consider a constant and nonzero vector field ω, then we obtain (cf. Section 3.2)

$$2\,\mathcal{T}(\omega, I_0) = 2\,I_0(x - \omega\,t) \neq I_0(x - 2\,\omega\,t) = \mathcal{T}(2\,\omega, I_0).$$

This inequality is also graphically illustrated in Figure 1.2. Hence, for proving existence of a solution to problem (1.7) a crucial step is to analyse the non-linear operator $\mathcal{T}$ of

the optical flow constraint (OFC) (cf. Chapter 5).

In [15], existence of a solution to problem (1.7) for an H^3- and a smoothened TV_ε-regularization was discussed for divergence-free optical flows. This means for example that deformations are excluded as solutions. However, we show in Chapter 6 existence and stability of a solution to problem (1.7) for an H^1-regularization in space (and time), as well as for a $W^{1,1+\tau}$-regularization without any restriction on the divergence of the optical flow.

1.5. Optical Flow vs. Motion Field

In this section, we want to emphasize that the optical flow only represents the movement of brightness patterns in a sequence of image samples and is, in particular, a different quantity as the motion field. To illustrate this fact we consider the following examples.

Barber Pole Illusion: Consider a cylinder with spiral lines on the surface. If we now rotate this object around the z-axis, we will observe a motion in vertical direction, although the movement is in horizontal direction. An animation can be found on Wikipedia [48].

Rotating ball: Consider a ball with an arbitrary uniform surface. If we now rotate this ball through its balance point along an arbitrary axis, we obtain a zero optical flow, although there is a movement.

Ball in equilibrium: Consider the same ball, but this time in equilibrium. If we now illuminate it by a moving light source, we will observe a non zero optical flow, although there is no motion of the ball.

Nevertheless, the optical flow is in many situations a good representation of the real motion field.

1.6. Outline of the Thesis

The outline of this thesis is divided into three parts. In the first part we introduce some basics, which are useful for the following discussion. To be more precise, in Chapter 2 we briefly introduce the function spaces occurring in the later discussion and state some useful properties of these spaces. In Chapter 3, we present the solution theory on various kinds of partial differential equations appearing later on in the analysis of the sequence interpolation problem (SIP). In Chapter 4, we show how to stabilize a linear inverse problem, like problem (1.5). Here, in particular, we motivate the H^1-regularization and the BV-regularization, which we also like to use for the stabilization of the non-linear sequence interpolation problem (SIP).

In the main theoretical part of this thesis, we present in Chapter 5 the weak solution

theory on transport equations. Here, we adapt the work of [10] to show existence and uniqueness of a weak solution to the transport equation (OFC), as well as the weak-* sequential closedness of the solution operator $\mathcal{T}$, without restriction on the divergence of the optical flow ω. Finally, this theory enables us to show in Chapter 6 existence of an optimal solution to problem (1.7) for an H^1-regularization in space (and time) and a $W^{1,1+\tau}$-regularization in space. Moreover, we show in Chapter 6 that problem (1.7) is a stable approximation of the sequence interpolation problem (SIP).

In the last part of this thesis we present in Chapter 7 the gradient method for solving problem (1.7) numerically. Since the computation of the gradient of the cost functional J defined in (1.7) requires to solve sequentially several kinds of partial differential equations, we also discuss in Chapter 7 how to numerically solve these partial differential equations. In particular, we present some new results in the numerical analysis of a transport equation with variable coefficient vector field ω. Furthermore, in Chapter 8, we test the regularized reconstruction method (1.7) with sequences of synthetic and real image frames.

Finally, in Chapter 9, we give a conclusion of this thesis.

Part I.

Basics

2. Function Spaces

This chapter briefly introduces the function spaces occurring in the analysis of the sequence interpolation problem (SIP). Here, we start with the notation of continuous function spaces. Subsequently, we define Lebesgue, Sobolev and Bochner spaces, as well as the space of functions with bounded variation. Additionally, we state some important properties of these function spaces, for use in the following chapters. For more details on these function spaces, we refer to [2, 3, 7, 10, 11, 26, 49].

2.1. Continuous Functions

Notations 2.1.
Let $\Omega \subset \mathbb{R}$ be an open set. Then:

- *$\mathcal{C}^k(\Omega)$ denotes the set of all functions $u \colon \Omega \to \mathbb{R}$ which are k-times continuously differentiable.*

- *$\mathcal{C}^k(\Omega; \mathbb{R}^d)$ denotes the set of all functions $u \colon \Omega \to \mathbb{R}^d$ which are k-times continuously differentiable.*

- *$\mathcal{C}^{0,1}(\Omega)$ denotes the set of all Lipschitz continuous functions $u \colon \Omega \to \mathbb{R}$.*

- *$\mathcal{C}^k_c(\Omega)$ denotes the set of all functions $u \colon \Omega \to \mathbb{R}$ with compact support in Ω which are k-times continuously differentiable.*

2.2. Lebesgue Spaces

Definition 2.2 (Lebesgue Spaces)**.**
Let Ω be an open set and $1 \leq p \leq \infty$. Then the Banach space

$$L^p(\Omega) := \left\{ u \colon \Omega \to \mathbb{R} : \text{ with } u \text{ Lebesgue integrable and } \|u\|_{L^p(\Omega)} < \infty \right\}$$

with norm

$$\|u\|_{L^p(\Omega)} := \begin{cases} \left(\int_\Omega |u(x)|^p \, \mathrm{d}x \right)^{\frac{1}{p}}, & \text{for } 1 \leq p < \infty, \\ \operatorname*{ess\,sup}_{x \in \Omega} |u(x)| = \inf_{\substack{N \subset \Omega \\ |N| = 0}} \sup_{x \in \Omega \setminus N} |u(x)|, & \text{for } p = \infty \end{cases}$$

is called Lebesgue *or L^p-space.*

2.3. Sobolev Spaces

Definition 2.3 (Sobolev Spaces).
Let Ω be an open set, $k \geq 0$ and $1 \leq p \leq \infty$. Then the Sobolev space $W^{k,p}(\Omega)$ is defined by

$$W^{k,p}(\Omega) := \left\{ u \in L^p(\Omega) : \text{ with } D^\alpha u \in L^p(\Omega) \text{ for all } |\alpha| \leq k \right\},$$

where $D^\alpha u$ denotes the weak derivative of u with multi-index α. The Sobolev space $W^{k,p}$ equipped with the norm

$$\|u\|_{W^{k,p}(\Omega)} := \begin{cases} \left(\displaystyle\sum_{|\alpha| \leq k} \|D^\alpha u\|_{L^p(\Omega)}^p \right)^{\frac{1}{p}}, & \text{for } 1 \leq p < \infty, \\ \displaystyle\sum_{|\alpha| \leq k} \|D^\alpha u\|_{L^\infty(\Omega)}, & \text{for } p = \infty \end{cases}$$

is a Banach space.
Moreover, in the case $p = 2$ we set $H^k(\Omega) := W^{k,2}(\Omega)$ and we have $W^{0,p}(\Omega) = L^p(\Omega)$ for $k = 0$.

Definition 2.4.
We denote by $W_0^{k,p}(\Omega)$ the closure of $\mathcal{C}_c^\infty(\Omega)$ in $W^{k,p}(\Omega)$. Equivalently, the space can be characterized as

$$W_0^{k,p}(\Omega) = \left\{ u \in W^{k,p}(\Omega) : \text{ with } D^\alpha u = 0 \text{ on } \partial\Omega \text{ for } |\alpha| \leq k - 1 \right\},$$

where "$D^\alpha u = 0$ on $\partial\Omega$" is defined in the sense of traces, see e.g. [22].

Theorem 2.5.
The spaces $W^{k,p}(\Omega)$ and $W_0^{k,p}(\Omega)$ are reflexive, if and only if $1 < p < \infty$.

Proof.
A proof can be found in [11]. $\qquad\square$

Theorem 2.6 (Generalized Poincaré Inequality).
Let Ω be a bounded, connected, Lipschitz domain of $\mathbb{R}^n$. Let Γ_1 be a part of the boundary $\partial\Omega$ with a nonzero surface measure. For $1 \leq p < \infty$ we define

$$W_{0,\Gamma_1}^{1,p}(\Omega) := \{ u \in W^{1,p}(\Omega) : \text{ with } u = 0 \text{ on } \Gamma_1 \}.$$

Then there exists a constant $C > 0$, such that for all functions $u \in W_{0,\Gamma_1}^{1,p}(\Omega)$ there holds

$$\|u\|_{L^p(\Omega)} \leq C \, \|\nabla u\|_{L^p(\Omega)}.$$

Proof.
A proof can be found in [10]. $\qquad\square$

Remark 2.7.
As a consequence of Theorem 2.6, we can equip the space $W_{0,\Gamma_1}^{1,p}(\Omega)$ with the norm

$$\|u\|_{W_0^{1,p}(\Omega)} = \|\nabla u\|_{L^p(\Omega)},$$

too. In fact, this norm is equivalent to the Sobolev-norm $\|\cdot\|_{W^{1,p}(\Omega)}$, since there exists a constant $C > 0$ with

$$\|\nabla u\|_{L^p(\Omega)} \leq \|u\|_{W^{1,p}} \leq (1+C)\|\nabla u\|_{L^p}.$$

Theorem 2.8 (Sobolev Imbedding Theorem)**.**
Let $\Omega \subset \mathbb{R}^n$ be an open and bounded set with Lipschitz boundary. Assume $k_1, k_2 \geq 0$, $1 \leq p_1, p_2 < \infty$ and

$$m_1 - \frac{d}{p_1} \geq m_2 - \frac{d}{p_2} \quad and \quad m_1 \geq m_2, \tag{2.1}$$

then we have the continuous embedding

$$W^{k_1,p_1}(\Omega) \hookrightarrow W^{k_2,p_2}(\Omega).$$

Additionally , the embedding is compact, denoted by

$$W^{k_1,p_1}(\Omega) \hookrightarrow\hookrightarrow W^{k_2,p_2}(\Omega),$$

if strict convexity holds in (2.1), i.e.,

$$m_1 - \frac{d}{p_1} > m_2 - \frac{d}{p_2} \quad and \quad m_1 > m_2.$$

The same statements hold for the space $W_0^{k,p}(\Omega)$ instead of $W^{k,p}(\Omega)$.

Proof.
A proof can be found in [2]. □

Theorem 2.9.
Let $\Omega \subset \mathbb{R}^d$ be an open set and $u\colon \Omega \to \mathbb{R}$ be a bounded Lipschitz continuous function. Then it holds that $u \in W^{1,\infty}(\Omega)$.

Proof.
A proof can be found in [10]. □

2.4. Bochner Spaces

Definition 2.10 (Bochner Spaces)**.**
Let $\mathcal{X}$ be a Banach space, $0 < T < \infty$ and $u\colon [0,T] \to \mathcal{X}$ be a Lebesgue measurable function on $[0,T]$ with values in $\mathcal{X}$.

(i) Then we define the Banach space

$$L^p((0,T);\mathcal{X}) := \big\{ u\colon [0,T] \to \mathcal{X} : \ with \ \|u\|_{L^p((0,T);\mathcal{X})} < \infty \big\}$$

with norm

$$\|u\|_{L^p((0,T);\mathcal{X})} := \begin{cases} \left(\int\limits_0^T \|u(t)\|_{\mathcal{X}}^p \, \mathrm{d}t \right)^{\frac{1}{p}}, & \text{for } 1 \leq p < \infty, \\ \underset{t\in[0,T]}{\mathrm{ess\,sup}} \|u(t)\|_{\mathcal{X}}, & \text{for } p = \infty. \end{cases}$$

(ii) Then we define the Banach space

$$\mathcal{C}([0,T];\mathcal{X}) := \big\{ u\colon [0,T] \to \mathcal{X} \ is \ continuous \big\}$$

with norm

$$\|u\|_{\mathcal{C}([0,T];\mathcal{X})} = \max_{t\in[0,T]} \|u(t)\|_{\mathcal{X}}.$$

The spaces $L^p((0,T);\mathcal{X})$ and $\mathcal{C}([0,T];\mathcal{X})$ are called Bochner spaces.

Theorem 2.11.
Let $\mathcal{X}$ be a reflexive space. Then the Bochner spaces $L^p((0,T);\mathcal{X})$ are reflexive for $1 < p < \infty$.

Proof.
A proof can be found in [49]. □

Theorem 2.12 (Aubin-Lions Lemma)**.**
Let $1 < \alpha, \beta < \infty$. Let $\mathcal{X}$ be a Banach space and let $\mathcal{X}_0, \mathcal{X}_1$ be separable and reflexive Banach spaces. Provided that $\mathcal{X}_0 \hookrightarrow\hookrightarrow \mathcal{X} \hookrightarrow \mathcal{X}_1$, we have

$$\left\{ u \in L^\alpha((0,T);\mathcal{X}_0); \frac{\mathrm{d}u}{\mathrm{d}t} \in L^\beta((0,T);\mathcal{X}_1) \right\} \hookrightarrow\hookrightarrow L^\alpha((0,T);\mathcal{X}).$$

Proof.
A proof can be found in [10]. □

2.5. Functions of Bounded Variation

Definition 2.13.
Let $\Omega \subset \mathbb{R}^d$ be an open set. Then we define the space of functions with bounded variation
by

$$\mathrm{BV}(\Omega) := \left\{ u \in L^1(\Omega) : \text{ with } \mathrm{TV}_\Omega(u) < \infty \right\},$$

with total variation

$$\mathrm{TV}_\Omega(u) := \sup \left\{ \int_\Omega u \operatorname{div} \varphi \, \mathrm{d}x : \text{ with } \varphi \in \mathcal{C}_c^1(\Omega; \mathbb{R}^d) \text{ and } \|\varphi\|_{L^\infty(\Omega)} \leq 1 \right\}.$$

The space $\mathrm{BV}(\Omega)$ equipped with the norm

$$\|u\|_{\mathrm{BV}(\Omega)} := \|u\|_{L^1(\Omega)} + TV_\Omega(u)$$

is a Banach space.

Moreover we define

$$\mathrm{BV}_0(\Omega) := \left\{ u \in \mathrm{BV}(\Omega) : \text{ with } u = 0 \text{ on } \partial\Omega \right\},$$

where "$u = 0$ on $\partial\Omega$" is defined in the sense of traces, see e.g. [3, 26].

Furthermore, any function $u \in \mathrm{BV}_\Omega$ admits a derivative Du in the distributional sense and there holds

$$\int_\Omega |Du| \, \mathrm{d}x = \mathrm{TV}_\Omega \,.$$

Theorem 2.14 (Poincaré-Wirtinger Inequality)**.**
Let $\Omega \subset \mathbb{R}^n$ be an open subset of $\mathbb{R}^n$. Then there exists a constant $C > 0$ such that for all $u \in \mathrm{BV}_0(\Omega)$ the following inequality holds

$$\|u\|_{L^1(\Omega)} \leq C \, \mathrm{TV}_\Omega(u).$$

Proof.
A proof can be found in [7]. □

Remark 2.15.
As a consequence of Theorem 2.14, we can equip the space $\mathrm{BV}_0(\Omega)$ with the norm

$$\|u\|_{\mathrm{BV}_0(\Omega)} = \mathrm{TV}_\Omega(u),$$

too. In fact, this norm is equivalent to the BV-norm $\| \cdot \|_{\mathrm{BV}(\Omega)}$, since there exists a constant $C > 0$ with

$$\mathrm{TV}_\Omega(u) \leq \|u\|_{\mathrm{BV}(\Omega)} \leq (1 + C) \, \mathrm{TV}_\Omega(u).$$

3. Differential Equations

In this chapter we introduce a few *partial differential equations* (PDEs), which appear later on in this thesis. In practice, differential equations are used for instance to formulate laws of nature or to model population dynamics or electric circuits. Mathematically, a PDE is an equation that relates a multivariate function u with its partial derivatives. In abstract form, a PDE of $k-th$ order is given by

$$F\big(D^k u(x), D^{k-1} u(x), ..., Du(x), u(x), x\big) = 0, \tag{3.1}$$

where

$$F \colon \mathbb{R}^{d^k} \times \mathbb{R}^{d^{k-1}} \times ... \times \mathbb{R}^d \times \mathbb{R} \times \Omega \to \mathbb{R}$$

is a given function, $\Omega \subset \mathbb{R}^d$ an open set and $u \colon \Omega \to \mathbb{R}$ is the unknown function. In the univariate case, i.e., $d = 1$, we call (3.1) *ordinary differential equation* (ODE).

An example for a PDE is the so called transport equation

$$u_t(t,x) + a \cdot \nabla u(t,x) = 0 \quad \text{in } \mathbb{R} \times \mathbb{R}^d,$$

where $a \in \mathbb{R}^d$ is given. Here, t denotes the time and x the space variable.

A *(classical) solution* of a differential equation of $k-th$ order is a sufficiently smooth function u, i.e., $u \in \mathcal{C}^k(\Omega)$, which satisfies the differential equation. Later we will also introduce the concept of *weak solutions*. Moreover, in many cases boundary and / or initial conditions are additionally prescribed by the model, which have to be satisfied by the solution, too. In fact, these conditions are also necessary to ensure uniqueness. But these are not sufficient, as we will see in the following section.

However, a general solution theory on differential equations is not available, since the range of various differential equations is too large. Therefore, we restrict our presentation only on the PDEs occurring later on. More precisely, we introduce in the following the solution theory on elliptic PDEs, transport and Stokes equations.

3.1. Ordinary Differential Equations

Since we will show in the next section that we can solve a transport equation by solving a system of ODEs, we briefly introduce ODEs before starting the analysis of the transport equation, for more details on the solution theory of ODEs we refer to [29, 37, 40]. An

ODE (of first order) is given by

$$\dot{x}(t) = f\big(t, x(t)\big) \tag{3.2a}$$
$$x(t_0) = x_0 \tag{3.2b}$$

with $f\colon \mathbb{R} \times \Omega \to \mathbb{R}$, $t_0 \in \mathbb{R}$ and $x_0 \in \Omega$, where $\Omega \subset \mathbb{R}$ denotes an open set. In this case $x\colon \mathbb{R} \to \Omega$ is denoted as state (variable) at time $t \in \mathbb{R}$. In the case $\Omega \subset \mathbb{R}^d$ with $d > 1$ and $f\colon \mathbb{R} \times \Omega \to \mathbb{R}^d$, (3.2) is called system of ODEs.

We ask ourselves about assumptions on f and x_0 that guarantee solvability of this problem (3.2). Before discussing the solvability of the initial value problem (3.2), we consider two examples which demonstrate the difficulties of finding a solution to problem (3.2).

Example 3.1.
Let $f = x^2$ and $x(0) = 1$. Then by using the method of separation of variables we find

$$x(t) = \frac{1}{1 - t}$$

as solution to the initial value problem (3.2). Thus, we observe that the solutions exists only locally on $(-\infty, 1)$.

Example 3.2.
For $f = 3\,x^{\frac{2}{3}}$ and $x_0 = 0$ the initial value problem (3.2) admits two different solution. In fact, $x(t) = t^3$ and $x(t) = 0$ solve the problem.

In summary, we have seen that solutions to the initial value problem (3.2) are not necessarily unique or globally defined. Indeed, in many cases there exist only a *local solution* $x\colon I \to \Omega$ to problem (3.2) defined on an interval I around the initial time t_0. Additionally, for many ODEs it is not so easy to find a solution. But Peano has shown in 1890, that the initial value problem (3.2) admits at least a local solution, if f is continuous, see e.g. in [29, 37]. Moreover, at the end of the 19th century Picard and Lindelöf have shown, that Lipschitz continuity of the function f is sufficient for uniqueness of a solution to problem (3.2).

Theorem 3.3 (Picard-Lindelöf)**.**

1) *(Local version) Let $f\colon [t_0 - a, t_0 + a] \times \overline{B_R(x_0)} \to \mathbb{R}^d$ be a continuous function, where $\overline{B_R(x_0)} := \{x \in \mathbb{R}^d;\ \text{with } \|x - x_0\| \le R\}$ denotes a closed ball around x_0 with radius $R > 0$. Assume that f is locally Lipschitz continuous with respect to x, i.e., there exists a constant L with*

   $$\|f(t, x) - f(t, \tilde{x})\| \le L\,\|x - \tilde{x}\| \quad \text{for all } (t, x), (t, \tilde{x}) \in [t_0 - a, t_0 + a] \times \overline{B_R(x_0)}.$$

   Then there exists a local unique solution $x\colon [t_0 - \alpha, t_0 + \alpha] \to \Omega$ to the initial value problem (3.2), where

   $$\alpha := \min\left(a, \frac{R}{M}\right) \quad \text{with} \quad M := \max_{(t,x)} |f(t, x)|.$$

2) (Global version) Let $f\colon [a,b] \times \mathbb{R}^d \to \mathbb{R}^d$ be continuous with $t_0 \in [a,b]$. Assume that f is globally Lipschitz continuous with respect to x, i.e.,

$$\|f(t,x) - f(t,\tilde{x})\| \leq L \|x - \tilde{x}\| \quad \text{for all } (t,x), (t,\tilde{x}) \in [a,b] \times \mathbb{R}^d.$$

Then the initial value problem (3.2) admits a global unique solution $x\colon [a,b] \to \mathbb{R}^d$.

Proof.
A proof can be found in [29, 37]. □

Next, we introduce the concept of flows. For the sake of convenience, we only consider the global case, i.e., $\Omega = \mathbb{R}^d$, which is the only relevant one in the later discussion.

Definition 3.4.
Assume that f satisfies the (global) assumption of Picard-Lindelöf's theorem. Furthermore, we denote by $x\colon [a,b] \to \mathbb{R}^d$ the unique solution of the initial value problem (3.2). Then for $t + t_0 \in [a,b]$ the mapping

$$\Phi\colon \mathbb{R}^d \times [a,b] \times [a,b] \to \mathbb{R}^d,$$
$$(x_0, t_0, t) \mapsto x(t + t_0)$$

is called flow *of the differential equation (3.2).*

Moreover, it is customary to write $\Phi_{t_0}^t(x_0)$ instead of $\Phi(x_0, t_0, t)$.

The flow of a differential equation possesses the following useful properties.

Theorem 3.5.
Let $\Phi_{t_0}^t(x_0)$ define the flow of the initial value problem (3.2) on the time interval $[a,b]$. Moreover, we assume $t + t_0 \in [a,b]$ and $s + t + t_0 \in [a,b]$. Then it holds:

(i) $\Phi_{t_0}^0(x_0) = x_0$,

(ii) $\Phi_{t+t_0}^s(\Phi_{t_0}^t(x_0)) = \Phi_{t_0}^{s+t}(x_0)$,

(iii) $\Phi_{t_0}^{-t}(\Phi_{t_0}^t(x_0)) = x_0$.

Proof.
In [40], it is shown that the mapping

$$\phi\colon \left(\mathbb{R}^d \times [a,b]\right) \times [a,b] \to \mathbb{R}^d \times [a,b],$$
$$(x_0, t_0, t) \mapsto (\Phi_{t_0}^t(x_0), t + t_0)$$

satisfies the following properties:

(i) $\phi(x_0, t_0, 0) = (x_0, t_0)$,

(ii) $\phi(\phi(x_0, t_0, t), s) = \phi(x_0, t_0, s + t)$,

(iii) $\phi(\phi(x_0, t_0, t), -t) = (x_0, t_0)$.

From these properties of the mapping ϕ, we immediately follow the statement of the theorem. □

3.2. Transport Equation with Variable Coefficients

This section introduces the *transport equation with variable coefficients.* The classical transport equation with constant vector field $a \in \mathbb{R}^d$ is defined by

$$I_t(t, x) + a \cdot \nabla I(t, x) = 0 \quad \text{with } I(0, x) = I_0(x), \tag{3.3}$$

where $I_0 \colon \mathbb{R}^d \to \mathbb{R}$ denotes an initial state and $I \colon \mathbb{R}_+ \times \mathbb{R}^d \to \mathbb{R}$ is the unknown function. It is well known that this problem (3.3) admits a unique solution, which is given by

$$I(t, x) = I_0(x - at) \in \mathcal{C}^1(\mathbb{R}_+ \times \mathbb{R}^d)$$

under the assumption that $I_0 \in \mathcal{C}^1(\mathbb{R}^d)$.

Now, we generalize the transport equation (3.3) such that we have a variable vector field $\omega \colon \mathbb{R}_+ \times \mathbb{R}^d \to \mathbb{R}^d$ depending on time and space instead of the constant vector field $a \in \mathbb{R}^d$. However, this generalization is not unique. In fact, both the *transport equation in conservative form,*

$$p_t(t, x) + \text{div}\big(\omega(t, x)\, p(t, x)\big) = 0 \quad \text{with } p(0, x) = p_0(x), \tag{cTPE}$$

and the *transport equation in non-conservative form,*

$$I_t(t, x) + \omega(t, x) \cdot \nabla I(t, x) = 0 \quad \text{with } I(0, x) = I_0(x), \tag{OFC}$$

are generalizations to equation (3.3).

3.2.1. The Non-Conservative Transport Equation

A standard ansatz for solving problem (OFC) is the method of characteristics, for more details on this method we refer to [22]. For the transport equation with constant vector field (3.3) we have seen that the solution is constant along the curve $\big(t, x(t)\big)$ with $x(t) = x_0 + a\, t$. Thus, the idea is now to find also for problem (OFC) an appropriate curve $\big(t, x(t)\big)$, such that we can compute the solution $I(t, x)$ along this curve.

For this aim, we initially assume that $I \in \mathcal{C}^1(\mathbb{R}_+ \times \mathbb{R}^d)$ is a solution to problem (OFC) and define

$$z(t) = I\big(t, x(t)\big). \tag{3.4}$$

Furthermore, we suppose that $x(t)$ solves

$$\dot{x}(t) = \omega\big(t, x(t)\big).$$

Next, we compute

$$\begin{aligned}
\dot{z}(t) &= I_t\big(t, x(t)\big) + \dot{x}(t) \cdot \nabla I\big(t, x(t)\big) \\
&= I_t\big(t, x(t)\big) + \omega\big(t, x(t)\big) \cdot \nabla I\big(t, x(t)\big) = 0
\end{aligned}$$

and

$$z(0) = I\big(0, x(0)\big) = I_0(x_0).$$

Altogether, we have converted the PDE problem (OFC) into a system of ODEs

$$\dot{x}(t) = \omega\big(t, x(t)\big) \qquad \text{with} \qquad x(0) = x_0, \qquad (3.5\text{a})$$
$$\dot{z}(t) = 0 \qquad \text{with} \qquad z(0) = I_0(x_0), \qquad (3.5\text{b})$$

which is called *system of characteristics*. The solution $\big((t, x(t)), z(t)\big)$ is called *characteristic*.

On the other hand, any solution $z(t) = I\big(t, x(t)\big)$ to the system of characteristics (3.5), solves also the transport equation (OFC), since

$$\begin{aligned} 0 = \dot{z}(t) &= I_t\big(t, x(t)\big) + \dot{x}(t) \cdot \nabla I\big(t, x(t)\big) \\ &= I_t\big(t, x(t)\big) + \omega\big(t, x(t)\big) \cdot \nabla I\big(t, x(t)\big) \end{aligned}$$

and

$$I(0, x_0) = I\big(0, x(0)\big) = z(0) = I_0(x_0).$$

Consequently, we conclude that problem (OFC) admits a (unique) solution, if and only if the characteristic system (3.5) admits a (unique) solution. Thus, existence and uniqueness of a solution to problem (OFC) can be deduced from Picard-Lindelöf's theorem.

Theorem 3.6.
Let $I_0 \in \mathcal{C}^1(\mathbb{R}^d)$ and $\omega \in \mathcal{C}(\mathbb{R}_+ \times \mathbb{R}^d; \mathbb{R}^d)$. Assume that the vector field ω is additionally Lipschitz continuous in the space variable. Then problem (OFC) admits a unique solution, which is given by

$$I(t, x) = I_0(\Phi_t^{-t}(x)) \in \mathcal{C}^1(\mathbb{R}_+ \times \mathbb{R}^d),$$

where $\Phi_t^{-s}(x) = \Phi_t^{-s}(\Phi_0^t(x_0)) = \Phi_0^{t-s}(x_0)$ for $s \in [0, t]$ denotes the flow to the differential equation (3.5a).

Proof.
The vector field ω satisfies the assumptions of Picard-Lindelöf's theorem. As a consequence equation (3.5a) admits a unique solution and we denote the flow of (3.5a) by $\Phi_0^t(x_0)$. Moreover, the unique solution to (3.5b) is given by

$$z(t) = z(0) = I_0(x_0) = I_0(\Phi_t^{-t}(x)).$$

Finally, we deduce the statement from (3.4). $\qquad\square$

3.2.2. The Conservative Transport Equation

For solving the conservative transport equation (cTPE), we first rewrite the equation as

$$p_t(t,x) + \omega(t,x) \cdot \nabla p(t,x) = -\operatorname{div}(\omega(t,x))\, p(t,x) \quad \text{with } p(0,x) = p_0(x).$$

We observe, that we obtain a non-conservative transport equation with source term

$$-\operatorname{div}(\omega(t,x))\, p(t,x).$$

As a consequence, a solution to problem (cTPE) is only constant along a characteristic if and only if the vector field ω is divergence free. Instead of that, we can show at least that a solution to (cTPE) is conservative. We exploit this property later on to design a finite difference scheme for solving the conservative transport equation (cTPE) (cf. Section 7.4.2) numerically .

Theorem 3.7.
The solution of the conservative transport equation (cTPE) *is* conservative, *i.e.,*

$$\int_{\mathbb{R}^d} p(t,x)\,\mathrm{d}x = \int_{\mathbb{R}^d} p_0(x)\,\mathrm{d}x.$$

Proof.
A proof can be found in [10]. □

Remark 3.8.
Assume that the conservative transport equation is only defined on a bounded domain $\Omega \subset \mathbb{R}^d$. If the vector field ω vanishes on the boundary $[0,T] \times \partial\Omega$, then the statement is still valid, i.e.,

$$\int_{\Omega} p(t,x)\,\mathrm{d}x = \int_{\Omega} p_0(x)\,\mathrm{d}x \in \mathcal{C}^1(\mathbb{R}_+ \times \mathbb{R}^d).$$

However, the procedure for solving the conservative transport equation (cTPE) is analogous to the non-conservative case (OFC) and we obtain as characteristic system

$$\dot{x}(t) = \omega\big(t, x(t)\big) \qquad\qquad \text{with} \qquad x(0) = x_0, \qquad\qquad \text{(3.6a)}$$
$$\dot{z}(t) = -\operatorname{div}\big(\omega(t, x(t))\big)\, p\big(t, x(t)\big) \qquad \text{with} \qquad z(0) = p_0(x_0), \qquad \text{(3.6b)}$$

Finally, we again deduce the solvability from Picard-Lindelöf's theorem.

Theorem 3.9.
Let $I_0 \in \mathcal{C}^1(\mathbb{R}^d)$ and $\omega \in \mathcal{C}(\mathbb{R}_+ \times \mathbb{R}^d; \mathbb{R}^d)$. Assume that the vector field ω is additionally Lipschitz continuous in the space variable. Then problem (cTPE) admits a unique solution, which is given by

$$p(t,x) = p_0\big(\Phi_t^{-t}(x)\big) \, \exp\left(-\int\limits_0^t \operatorname{div}\Big(\omega\big(s, \Phi_t^{s-t}(x)\big)\Big) \, \mathrm{d}s \right)$$

where $\Phi_t^{-s}(x) = \Phi_t^{-s}(\Phi_0^t(x_0)) = \Phi_0^{t-s}(x_0)$ for $s \in [0,t]$ denotes the flow to the differential equation (3.6a).

Proof.
The proof is analogous to the non-conservative case (cf. Theorem 3.6). But in this case, the unique solution to (3.6b) is given by

$$z(t) = z(0) \, \exp\left(-\int\limits_0^t \operatorname{div}\Big(\omega\big(s, x(s)\big)\Big) \right)$$

$$= p_0\big(\Phi_t^{-t}(x)\big) \, \exp\left(-\int\limits_0^t \operatorname{div}\Big(\omega\big(s, \Phi_t^{s-t}(x)\big)\Big) \, \mathrm{d}s \right),$$

where we used the method of separation of variables. $\qquad \square$

At the end, we remark that we can also apply the method of characteristics, if (OFC) and (cTPE) are only defined on an open and bounded domain $\Omega \subset \mathbb{R}^d$. In this case, the only difference is, that the problem is solved along characteristics starting either at initial time $t = 0$ or at the boundary $[0,T] \times \partial\Omega$.

3.3. Elliptic Partial Differential Equations

In this section we present two elliptic PDEs appearing later on in this thesis and discuss their solution theory. In the following $\Omega \subset \mathbb{R}^d$ denotes an open and bounded set.

3.3.1. Poisson Equation

We start with the *Poisson problem*

$$-\alpha \, \Delta u = f \quad \text{in } \Omega, \tag{3.7a}$$

$$u = 0 \quad \text{on } \partial\Omega, \tag{3.7b}$$

where $\alpha > 0$ and $f \in L^2(\Omega)$. First, note that for a given discontinuous function f it is not possible to find a classical solution $u \in \mathcal{C}^2(\Omega) \cup \mathcal{C}(\overline{\Omega})$. Therefore, we seek for

a weak solution to the Poisson Problem (3.7). For this purpose, we initially assume, that problem (3.7) admits a classical solution u. Then we multiply equation (3.7a) by a smooth test function $v \in \mathcal{C}_0^\infty(\Omega)$ and integrate over Ω, i.e.,

$$-\alpha \int_\Omega \Delta u \, v \, \mathrm{d}x = \int_\Omega f \, v \quad \text{for all } v \in \mathcal{C}_0^\infty(\Omega).$$

Integration by part leads to

$$\alpha \int_\Omega \nabla u \cdot \nabla v \, \mathrm{d}x = \int_\Omega f \, v \quad \text{for all } v \in \mathcal{C}_0^\infty(\Omega). \tag{3.8}$$

Since $\mathcal{C}_0^\infty(\Omega)$ is dense in $H_0^1(\Omega)$, equation (3.8) is valid for all $v \in H_0^1(\Omega)$, too. Moreover, equation (3.8) is still reasonable, if $u \in H_0^1(\Omega)$.

Thus, a function $u \in H_0^1(\Omega)$ satisfying the *weak formulation*

$$\alpha \int_\Omega \nabla u \cdot \nabla v \, \mathrm{d}x = \int_\Omega f \, v \quad \text{for all } v \in H_0^1(\Omega). \tag{3.9}$$

is called *weak solution* to the Poisson problem (3.7).

Note, that the Dirichlet boundary condition (3.7b) is incorporated in the function space $H_0^1(\Omega)$. For proving existence and uniqueness of a weak solution to the Poisson problem (3.7) we use Lax Milgram's Theorem.

Theorem 3.10 (Lax Milgram)**.**
Let $\mathcal{U}$ be a Hilbert space. Assume that $a \colon \mathcal{U} \times \mathcal{U} \to \mathbb{R}$ is a bilinear-form satisfying:

(i)	*the continuity condition:*	$\lvert a(u,v) \rvert \leq \alpha \lVert u \rVert_{\mathcal{U}} \lVert v \rVert_{\mathcal{U}}$	*for all $u, v \in \mathcal{U}$,*
(ii)	*the coercivity condition:*	$a(u,u) \geq \beta \lVert u \rVert_{\mathcal{U}}^2$	*for all $u \in \mathcal{U}$,*

for given constants $\alpha, \beta > 0$. Furthermore, let $F \colon \mathcal{U} \to \mathbb{R}$ be a bounded linear functional.

Then there exists a unique element $u \in \mathcal{U}$ such that

$$a(u, v) = F(v) \quad \text{for all } v \in \mathcal{U}.$$

Proof.
A proof can be found in [11, 22]. $\qquad\square$

For applying Lax Milgram's theorem, we define the bilinear form

$$a \colon H_0^1(\Omega) \times H_0^1(\Omega) \to \mathbb{R}, \quad a(u, v) := \alpha \int_\Omega \nabla u \cdot \nabla v \, \mathrm{d}x$$

and the linear functional

$$F \colon H_0^1(\Omega) \to \mathbb{R}, \quad F(v) := \int_\Omega f\, v \, \mathrm{d}x.$$

We easily verify

$$
\begin{aligned}
|a(u,v)| &\leq \alpha \, \|\nabla u\|_{L^2(\Omega)} \, \|\nabla v\|_{L^2(\Omega)} = \alpha \, \|u\|_{H_0^1(\Omega)} \, \|v\|_{H_0^1(\Omega)} \\
a(u,u) &\geq \alpha \, \|\nabla u\|_{L^2(\Omega)}^2 = \alpha \, \|u\|_{H_0^1(\Omega)}^2
\end{aligned}
\tag{3.10}
$$

and

$$|F(v)| \leq \|f\|_{L^2(\Omega)} \, \|v\|_{L^2(\Omega)} \leq C \, \|f\|_{L^2(\Omega)} \, \|v\|_{H_0^1(\Omega)}$$

by using Poincore's inequality (Theorem 2.6) in the last estimate. Finally, we obtain existence and uniqueness of a solution by using Lax Milgram's theorem.

Theorem 3.11.
Assume $f \in H^{-1}(\Omega)$. Then the Poisson problem (3.7) admits a unique weak solution $u \in H_0^1(\Omega)$.

For more details to the Poisson problem, like higher regularity of the weak solution than H^1-regularity, we refer to [11, 22].

3.3.2. Time-Dependent Elliptic PDE

Next, we consider a time-dependent elliptic PDE problem given by

$$
\begin{aligned}
-\beta \, u_{tt} - \alpha \, \Delta u &= f && \text{in } \Omega_T := (0,T) \times \Omega, & \text{(3.11a)} \\
u &= 0 && \text{on } \Gamma_x := (0,T) \times \partial\Omega, & \text{(3.11b)} \\
u_t &= 0 && \text{on } \Gamma_t := \{0,T\} \times \Omega, & \text{(3.11c)}
\end{aligned}
$$

where $\alpha, \beta > 0$ and $f \in L^2(\Omega_T)$. To obtain the weak formulation of the problem, we multiply (3.11a) by a test function $\mathcal{C}^1(\overline{\Omega_T})$ and integrate over Ω_T, i.e.,

$$-\beta \int_{\Omega_T} u_{tt} \, v \, \mathrm{d}x - \alpha \int_{\Omega_T} \Delta u \, v \, \mathrm{d}x = \int_{\Omega_T} f \, v \, \mathrm{d}x \quad \text{for all } v \in \mathcal{C}^1(\overline{\Omega_T}),$$

where we assume that $u \in \mathcal{C}^2(\Omega_T) \cap \mathcal{C}^1(\overline{\Omega_T})$ is a classical solution to problem (3.11).

By using integration by parts formula we obtain

$$\beta \int\limits_{\Omega_T} u_t\, v_t \,\mathrm{d}x - \beta \int\limits_{\Gamma_t} \underbrace{u_t}_{=0}\, v \,\mathrm{d}S$$

$$+ \alpha \int\limits_{\Omega_T} \nabla u \cdot \nabla v \,\mathrm{d}x - \alpha \int\limits_{\Gamma_x} (\nabla u \cdot \eta)\, v \,\mathrm{d}S = \int\limits_{\Omega_T} f\, v \,\mathrm{d}x \tag{3.12}$$

for all $v \in \mathcal{C}^1(\overline{\Omega_T})$, where η denotes the outer unit normal vector of Γ_x. Since $\mathcal{C}^1(\overline{\Omega_T})$ is dense in $H^1(\Omega_T)$, equation (3.12) is valid for $v \in H^1(\Omega_T)$, too, and makes sense even if we only have $u \in H^1(\Omega_T)$. Moreover, to incorporate the Dirichlet boundary condition (3.11b), we additionally require $u, v \in H^1_{\Gamma_x}(\Omega_T) \subset H^1(\Omega_T)$, where

$$H^1_{\Gamma_x}(\Omega_T) := \left\{ u \in H^1(\Omega_T): \text{ with } u|_{\Gamma_x} = 0 \right\}$$

$$= \left\{ u \in L^2\big((0,T), H^1_0(\Omega)\big): \text{ with } u_t \in L^2\big((0,T), L^2(\Omega)\big) \right\}$$

equipped with the norm

$$\|u\|_{H^1_{\Gamma_x}(\Omega_T)} := \|u\|_{L^2((0,T),H^1_0(\Omega))} + \|u_t\|_{L^2((0,T),L^2(\Omega))}$$

is a Hilbert space (see [10]). The Neumann boundary condition (3.11c) do not need to be incorporated in the solution space, since we have already exploited it for the derivation of the weak formulation (3.12).

Consequently, we call a function $u \in H^1_{\Gamma_x}(\Omega_T)$ *weak solution* of the elliptic problem (3.11), if it satisfies the *weak formulation*

$$\beta \int\limits_{\Omega_T} u_t\, v_t \,\mathrm{d}x + \alpha \int\limits_{\Omega_T} \nabla u \cdot \nabla v \,\mathrm{d}x = \int\limits_{\Omega_T} f\, v \,\mathrm{d}x \quad \text{for all } v \in H^1_{\Gamma_x}(\Omega_T).$$

To apply Lax Milgram's theorem, we define the linear functional $F \colon H^1_{\Gamma_x}(\Omega_T) \to \mathbb{R}$ by

$$F(v) := \int\limits_{\Omega_T} f\, v \,\mathrm{d}x$$

and the bilinear form $a \colon H^1_{\Gamma_x}(\Omega_T) \times H^1_{\Gamma_x}(\Omega_T) \to \mathbb{R}$ by

$$a(u, v) := \beta \int\limits_{\Omega_T} u_t\, v_t \,\mathrm{d}x\,\mathrm{d}t + \alpha \int\limits_{\Omega_T} \nabla u \cdot \nabla v \,\mathrm{d}x\,\mathrm{d}t.$$

A simple calculation shows, that the bilinear form is bounded and coercive:

$$|a(u,v)| \le \beta \int\limits_0^T \|u_t\|_{L^2(\Omega)} \|v_t\|_{L^2(\Omega)} \, \mathrm{d}t + \alpha \int\limits_0^T \|u\|_{H_0^1(\Omega)} \|v\|_{H_0^1(\Omega)} \, \mathrm{d}t$$

$$\le \beta \|u_t\|_{L^2((0,T),L^2(\Omega))} \|v_t\|_{L^2((0,T),L^2(\Omega))}$$

$$+ \alpha \|u\|_{L^2((0,T),H_0^1(\Omega))} \|v\|_{L^2((0,T),H_0^1(\Omega))}$$

$$\le \max(\alpha,\beta) \|u\|_{H_{\Gamma_x}^1(\Omega_T)} \|v\|_{H_{\Gamma_x}^1(\Omega_T)}$$

and

$$a(u,u) = \beta \|u_t\|_{L^2((0,T),L^2(\Omega))}^2 + \alpha \|u\|_{L^2((0,T),H_0^1(\Omega))}^2 \ge \min(\alpha,\beta) \|u\|_{H_0^1(\Omega_T)}^2.$$

Moreover, the linear functional F is bounded, since

$$F(v) \le \|f\|_{L^2((0,T),L^2(\Omega))} \|v\|_{L^2((0,T),L^2(\Omega))}$$

$$\le C \|f\|_{L^2((0,T),L^2(\Omega))} \|v\|_{L^2((0,T),H_0^1(\Omega))}$$

$$\le \tilde{C} \|v\|_{H_{\Gamma_x}^1(\Omega_T)},$$

where we used Poincore's inequality (Theorem 2.6) in the second estimate. Finally, by applying Lax Milgram's theorem we obtain existence and uniqueness of a solution.

Theorem 3.12.
Let $f \in \left(H_{\Gamma_x}^1(\Omega_T)\right)^*$. Then problem (3.11) admits a unique weak solution $u \in H_{\Gamma_x}^1(\Omega_T)$.

3.4. Stokes Equation

Finally, we present the Stokes problem defined by

$$-\Delta u + \nabla\lambda = f \qquad \text{in } \Omega, \tag{3.13a}$$

$$-\operatorname{div}(u) = 0 \qquad \text{in } \Omega, \tag{3.13b}$$

$$u = 0 \qquad \text{on } \partial\Omega, \tag{3.13c}$$

where $\Omega \subset \mathbb{R}^d$ denotes an open and bounded set. First, note that the problem cannot have a unique solution pair $(y,\lambda) \in \left(\mathcal{C}^2(\Omega;\mathbb{R}^d) \cap \mathcal{C}_0(\overline{\Omega};\mathbb{R}^d)\right) \times \mathcal{C}^1(\Omega)$ because the solution λ can only be uniquely determined up to an additive constant. Therefore, we additionally impose the normalization condition

$$\int\limits_\Omega \lambda \, \mathrm{d}x = 0. \tag{3.14}$$

Now, analogous to the examinations of the elliptic PDEs, we derive the weak formulation of the Stokes problem. Hence, we initially assume that the problem admits a classical

solution $(y, \lambda) \in \left(\mathcal{C}^2(\Omega; \mathbb{R}^d) \cap \mathcal{C}_0(\overline{\Omega}; \mathbb{R}^d)\right) \times \mathcal{C}^1(\Omega)$. Multiplying equation (3.13a) by a smooth test function $v \in \mathcal{C}_0^\infty(\Omega; \mathbb{R}^d)$ and integrating lead to

$$\int_\Omega \left(\nabla u \cdot \nabla v - \lambda \operatorname{div}(v)\right) \mathrm{d}x = \int_\Omega f \, v \, \mathrm{d}x \quad \text{for all } v \in \mathcal{C}_0^\infty(\Omega; \mathbb{R}^d). \tag{3.15}$$

Since $\mathcal{C}_0^\infty(\Omega; \mathbb{R}^d)$ is dense in $\left(H_0^1(\Omega)\right)^d$, equation (3.15) is valid for $v \in \left(H_0^1(\Omega)\right)^d$, too. Moreover, equation (3.15) is still valid if $u \in \left(H_0^1(\Omega)\right)^d$ and $\lambda \in L^2(\Omega)$. Additionally, to incorporate the normalization condition (3.14) we require

$$\lambda \in L_0^2(\Omega) := \left\{ \varphi \in L^2(\Omega) : \text{ with } \int_\Omega \varphi \, \mathrm{d}x = 0 \right\}.$$

Next, we multiply (3.13b) with a test function $\mu \in L_0^2(\Omega)$ and integrate equation to obtain

$$-\int_\Omega \operatorname{div}(u) \, \mu \, \mathrm{d}x = 0 \quad \text{for all } \mu \in L_0^2(\Omega).$$

In summary, a function pair $(u, \lambda) \in \left(H_0^1(\Omega)\right)^d \times L_0^2(\Omega)$ satisfying the *weak formulation*

$$\int_\Omega \left(\nabla u \cdot \nabla v - \lambda \operatorname{div}(v)\right) \mathrm{d}x = \int_\Omega f \, v \, \mathrm{d}x \qquad \text{for all } v \in \left(H_0^1(\Omega)\right)^d$$

and
$$-\int_\Omega \operatorname{div}(u) \, \mu \, \mathrm{d}x = 0 \qquad \text{for all } \mu \in L_0^2(\Omega)$$

is called *weak solution* of the Stokes problem (3.13).

Introducing the bilinear forms

$$a \colon H_0^1(\Omega) \times H_0^1(\Omega) \to \mathbb{R}, \qquad\qquad a(u, v) = \int_\Omega \nabla u \cdot \nabla v \, \mathrm{d}x$$

$$b \colon H_0^1(\Omega) \times L_0^2(\Omega) \to \mathbb{R}, \qquad\qquad b(u, \lambda) = -\int_\Omega \lambda \operatorname{div}(u) \, \mathrm{d}x$$

and the linear functional

$$F \colon H_0^1(\Omega) \to \mathbb{R}, \qquad\qquad F(v) = \int_\Omega f \, v \, \mathrm{d}x,$$

we observe, that the weak formulation of the Stokes Problem can be characterized by a saddle point problem,

$$a(u, v) + b(v, \lambda) = F(v) \qquad \text{for all } v \in \left(H_0^1(\Omega)\right)^d, \tag{3.16a}$$
$$b(u, \mu) = 0 \qquad \text{for all } \mu \in L_0^2(\Omega). \tag{3.16b}$$

Hence, existence and uniqueness of a weak solution can be deduced from the following theorem.

Theorem 3.13.
Let $\mathcal{U}$ and Λ be two Hilbert spaces. Assume that $a\colon \mathcal{U} \times \mathcal{U} \to \mathbb{R}$ and $b\colon \mathcal{U} \times \Lambda \to \mathbb{R}$ are two bilinear-forms satisfying

$$
\begin{array}{lll}
(i) & \text{the inf-sup condition:} & \displaystyle \inf_{\lambda \in \Lambda} \sup_{u \in \mathcal{U}} \frac{b(u,\lambda)}{\|u\|_{\mathcal{U}} \, \|\lambda\|_{\Lambda}} \geq \alpha > 0 \\[2ex]
(ii) & \text{the coercivity condition:} & a(u,u) \geq \beta \|u\|_{\mathcal{U}}^2 \quad \text{for all } u \in \mathcal{U}
\end{array}
$$

for given constants $\alpha, \beta > 0$. Furthermore, let $F : \mathcal{U} \to \mathbb{R}$ be a bounded linear functional.

Then the saddle point problem

$$
\begin{aligned}
a(u,v) + b(v,\lambda) &= F(v) && \text{for all } v \in \mathcal{U}, \\
b(u,\mu) &= 0 && \text{for all } \mu \in \Lambda
\end{aligned}
$$

admits a unique solution pair $(u,p) \in \mathcal{U} \times \Lambda$.

Proof.
A proof can be found in [25]. □

Remark 3.14.
The inf-sup condition is also known as Babuška-Brezzi condition or the LBB condition (for Ladyzhenskaya-Babuška-Brezzi).

Hence, for proving existence and uniqueness of a weak solution to the Stokes problem (3.13) we have to check the assumptions of Theorem 3.13. The coercivity condition we have already verified for the Poisson problem (cf. inequality (3.10)). For the inf-sup condition we use the following lemma.

Lemma 3.15 (Ladyzhenskaya)**.**
Let $\mu \in L_0^2(\Omega)$. Then there exists a $v \in \left(H_0^1(\Omega)\right)^d$ with

$$
\mu = -\operatorname{div} v \quad \text{and} \quad \|v\|_{\left(H_0^1(\Omega)\right)^d} \leq C \, \|\mu\|_{L^2(\Omega)}.
$$

Proof.
A proof can be found in [25]. □

Using this lemma, we compute

$$
\sup_{u \in \left(H_0^1(\Omega)\right)^d} \frac{b(u,\mu)}{\|u\|_{\left(H_0^1(\Omega)\right)^d}} \geq \frac{b(v,\mu)}{\|v\|_{\left(H_0^1(\Omega)\right)^d}} = \frac{\|\mu\|_{L^2(\Omega)}^2}{\|v\|_{\left(H_0^1(\Omega)\right)^d}} \geq \frac{1}{C} \, \|\mu\|_{L^2(\Omega)}
$$

and, consequently, we obtain

$$\inf_{\mu \in L_0^2(\Omega)} \sup_{u \in \left(H_0^1(\Omega)\right)^d} \frac{b(u, \mu)}{\|u\|_{\left(H_0^1(\Omega)\right)^d} \|\mu\|_{L^2(\Omega)}} \geq \frac{1}{C} > 0.$$

In conclusion, we have shown.

Theorem 3.16 (cf. [25])**.**
Let $f \in \left(H^{-1}(\Omega)\right)^d$. Then the Stokes problem (3.13) admits a unique weak solution pair $(u, p) \in \left(H_0^1(\Omega)\right)^d \times L_0^2(\Omega)$.

4. Inverse Problems

In engineering disciplines, as well as in natural and social sciences mathematical models are used to study systems. A *mathematical model* is a mapping

$$A : \mathcal{U} \to \mathcal{Y},$$

where $\mathcal{U}$ denotes the set of *causes (parameters)* and $\mathcal{Y}$ the set of *effects (observations)*. We speak of a *direct problem*, if we calculate the effect $Au = y \in \mathcal{Y}$ for given parameters $u \in \mathcal{U}$. Conversely, we have an *inverse problem* if we conclude the cause $u \in \mathcal{U}$ from the observation $y \in \mathcal{Y}$.

In the context of optical flows the model equation is given by the optical flow constraint

$$I_t(t, x) + \omega(t, x) \cdot \nabla I(t, x) = 0 \quad \text{with } I(0, x) = I_0(x). \tag{OFC}$$

In this case, for a given vector field ω and an initial image I_0 the computation of the intensity function I is denoted as the direct problem. Conversely, the inverse problem is given by the estimation of the optical flow ω for a given intensity function I (cf. Chapter 1).

In the following we analyse linear inverse problems, i.e, we restrict ourselves to the case that A is a linear operator.

In general, inverse problems are more difficult to solve than the corresponding direct problem. In fact, inverse problems often tend to be ill-posed in the sense of Jacques Hadamard. This means, at least one of the following conditions is violated:

  (i) The problem admits a solution.

 (ii) The solution is unique.

(iii) The solution depends continuously on the input data.

Usually, this ill-posedness is caused by violation of the third condition. This has the effect, that small noises in the input data, which are unavoidable by physical measurements, can generate arbitrary large errors in the solution. Consequently, the calculated solution is completely useless. This instability is illustrated in the following example.

Example 4.1 (cf. [42]).
Let $\mathcal{U} = L^2(0,1)$ and $\mathcal{Y} = \{y \in L^2(0,1) : y' \text{ exists in the weak sense}\}$. Then we consider the integration operator

$$A : \mathcal{U} \to \mathcal{Y}, \quad u(t) \mapsto \int_0^t u(s)\,\mathrm{d}s$$

and the differentiation operator

$$A^{-1} : \mathcal{Y} \to \mathcal{U}, \quad y(t) \mapsto y'(t).$$

These two problems are inverse to each other. The integration operator admits a unique solution and is continuous since it is linear and bounded by

$$
\begin{aligned}
\|Au(t)\|_{L^2(0,1)}^2 &= \int_0^1 (Au(t))^2 \,\mathrm{d}t = \int_0^1 \left(\int_0^t u(s)\,\mathrm{d}s \right)^2 \mathrm{d}s \\
&\leq \int_0^1 \left(\int_0^1 |u(s)|\,\mathrm{d}s \right)^2 \mathrm{d}t = \left(\int_0^1 |u(s)|\,\mathrm{d}s \right)^2 \\
&\leq \left(\left(\int_0^1 1^2 \,\mathrm{d}s \right)^{\frac{1}{2}} \left(\int_0^1 |u(s)|^2 \,\mathrm{d}s \right)^{\frac{1}{2}} \right)^2 = \int_0^1 |u(s)|^2 \,\mathrm{d}s \\
&= \|u\|_{L^2(0,1)}^2.
\end{aligned}
$$

For the differentiation operator and a given $y \in \mathcal{Y}$ we consider the sequence of perturbed data

$$y_k(t) = y(t) + \frac{1}{k\pi} \sin(k^2 \pi t)$$

and compute

$$u_k(t) = y_k'(t) = u(t) + k \cos(k^2 \pi t),$$

where we set $u(t) = y'(t)$. Then, we obtain

$$\|y_k - y\|_{L^2(0,1)}^2 = \frac{1}{(k\pi)^2} \int_0^1 |\sin(k^2 \pi t)|^2 \,\mathrm{d}t = \frac{1}{2(k\pi)^2} \to 0$$

for $k \to \infty$, but on the other hand it holds that

$$\|A^{-1}(y_k) - A^{-1}(y)\|_{L^2(0,1)}^2 = \|u_k - u\|_{L^2(0,1)}^2 = k \int_0^1 |\cos(k^2 \pi t)|^2 \,\mathrm{d}t = \frac{k}{2} \to \infty$$

for $k \to \infty$, i.e., A^{-1} is discontinuous. Hence, the direct problem of integration is well-posed (all the three conditions of Hadamard are satisfied), whereas the inverse problem of differentiation is ill-posed.

Due to the instability, we have to stabilize the solution process. For this purpose, the idea is to approximate the problem by a suitable stable model.

The outline of this chapter is as follows: In Section 4.1 we introduce a generalized solution of an inverse problem to guarantee existence and uniqueness of the solution. This generalization leads to the so called Moore-Penorse inverse. Additionally, we state an explicit representation of the Moore-Penrose inverse of a compact linear operator. With the help of this representation we analyse the instability of an inverse problem and motivate the classical Tikhonov regularization for stabilizing the solution. In particular, in Section 4.2 we show existence, uniqueness and stability of the solution for the Tikhonov regularization.

At the end of the chapter we are focussing on inverse problems, where $\mathcal{U}$ and $\mathcal{Y}$ are function spaces. Here, we discuss that the Tikhonov regularization is inappropriate, if we seek for a discontinuous solution. Therefore, we also introduce the BV-Regularization in Section 4.3.

4.1. Moore-Penrose Inverse

Before generalizing the solution of an inverse problem, we want to mention that the well-posedness of the problem depends on the operator $\mathcal{A}$ as well as on the function spaces $\mathcal{U}$ and $\mathcal{Y}$. Obviously, the existence and uniqueness rely on the function spaces $\mathcal{U}$ and $\mathcal{Y}$. But also the continuity of the operator depends on the metric in which we measure the distance. In fact, if we use the function space $\mathcal{Y} = H^1(0,1)$ in Example 4.1, then the differentiation operator A^{-1} is continuous since

$$\|A^{-1}(y)\|_{L^2(0,1)} = \|y'\|_{L^2(0,1)} \leq \|y\|_{L^2(0,1)} + \|y'\|_{L^2(0,1)} = \|y\|_{H^1(0,1)}.$$

However, the function spaces are usually prescribed by the application. Hence, we cannot artificially define the function spaces $\mathcal{U}$ and $\mathcal{Y}$ to obtain well-posedness of the inverse problem.

In the following, we restrict our discussion on Hilbert spaces $\mathcal{U}$ and $\mathcal{Y}$. To guarantee the existence of a solution, we only seek for a least-squares solution of the inverse problem, i.e., we consider the surrogate problem

$$u = \operatorname*{argmin}_{\varphi \in \mathcal{U}} \|A\varphi - y\|_{\mathcal{Y}}. \tag{LSS}$$

In fact, we can show that this problem admits a solution if and only if $y \in \mathcal{R}(A) \oplus \mathcal{R}(A)^{\perp}$. Moreover, the set of solutions to problem (LSS) is closed and convex. As a consequence, we can find a unique element of minimal norm in the set of solutions to problem (LSS), see e.g. [21, 38, 42]. This motivates the following definition.

Definition 4.2 (Moore-Penrose inverse)**.**
Let $A \in L(\mathcal{U}, \mathcal{Y})$ with Hilbert spaces $\mathcal{U}$ and $\mathcal{Y}$. Then the mapping $A^\dagger$ which maps $y \in \mathcal{D}(A^\dagger) := \mathcal{R}(A) \oplus \mathcal{R}(A)^\perp$ onto the unique minimal-norm-solution $u^\dagger \in \mathcal{U}$ to problem (LSS) is called (generalized) Moore-Penrose inverse.

For further properties of the (generalized) Moore-Penrose inverse we refer to [21, 42]

We just mention that, for compact linear operators $K \in \mathcal{K}(\mathcal{U}, \mathcal{Y})$ we can derive an explicit representation of the Moore-Penrose inverse. Indeed, by using the spectral theorem we can represent the Moore-Penrose inverse by a singular value decomposition.

Theorem 4.3.
Let $K \in \mathcal{K}(\mathcal{U}, \mathcal{Y})$ with Hilbert spaces $\mathcal{U}$ and $\mathcal{Y}$. Moreover, we denote by

$$K^*Ku = \sum_{j=0}^{\infty} \lambda_j \big(u, \varphi_j \big)_{\mathcal{U}} \varphi_j$$

the eigenvalue expansion of K^*K, where $\{\varphi_j\} \subset \mathcal{U}$ denotes an orthonormal sequence of eigenvectors and $\{\lambda_j\} \subset \mathbb{R}$ denotes the corresponding zero sequence of eigenvalues with $\lambda_1 \geq \lambda_2 \geq ... > 0$. Then, the Moore-Penrose inverse of K is given by

$$u^\dagger = K^\dagger y = \sum_{j=1}^{\infty} \sigma_j^{-1} \big(y, \psi_j \big)_{\mathcal{Y}} \varphi_j \quad \text{for } y \in D(K^\dagger), \tag{4.1}$$

where $\sigma_j = \sqrt{\lambda_j}$ and $\{\psi_j\} \subset \mathcal{Y}$ is defined by $\psi_j = \sigma_j^{-1} K \varphi_j$ and forms an orthonormal sequence. The set $\{(\sigma_j, \varphi_j, \psi_j)\} \subset \mathbb{R} \times \mathcal{U} \times \mathcal{Y}$ is called singular value system *of K.*

Proof.
A proof can be found in [21, 42]. $\qquad\square$

Remark 4.4.
For $K \in \mathcal{K}(\mathcal{U}, \mathcal{Y})$ with $N := \dim(\mathcal{R}(K)) < \infty$ we have

$$u^\dagger = K^\dagger y = \sum_{j=1}^{N} \sigma_j^{-1} \big(y, \psi_j \big)_{\mathcal{Y}} \varphi_j.$$

With the help of the singular value representation of $K^\dagger$ (4.1) we are in a position to analyse the stability of the corresponding inverse problem. In practical applications we usually have noisy measurements, i.e., we are only given $y^\varepsilon \in \mathcal{Y}$ with $\|y - y^\varepsilon\|_{\mathcal{Y}} \leq \varepsilon$. If we assume a finite singular value system we can estimate the reconstruction error by

$$\|x^\dagger - K^\dagger y^\varepsilon\|_{\mathcal{U}} = \|K^\dagger y - K^\dagger y^\varepsilon\|_{\mathcal{U}} = \left\| \sum_{j=1}^{N} \sigma_j^{-1} \big(y - y^\varepsilon, \varphi_j \big)_{\mathcal{Y}} \psi_j \right\|_{\mathcal{U}}$$
$$\leq \frac{1}{\sigma_N} \|y - y^\varepsilon\|_{\mathcal{Y}} \leq \frac{\varepsilon}{\sigma_N}. \tag{4.2}$$

Thus, the reconstruction error is bounded, even though it can be very large. On the other hand, for an infinite singular value system $\{(\sigma_j, \varphi_j, \psi_j)\} \subset \mathbb{R} \times \mathcal{U} \times \mathcal{Y}$ we consider the sequence of perturbed measurements $\{y^\varepsilon\} \subset \mathcal{Y}$ given by $y^\varepsilon = y + \varepsilon \, \psi_j$. In this case, the reconstruction error is given by

$$\|K^\dagger y - K^\dagger y^\varepsilon\|_\mathcal{U} = \frac{\varepsilon}{\sigma_j} \to \infty \quad \text{for } j \to \infty.$$

Altogether, we conclude that the Moore-Penrose inverse of a compact linear operator is continuous if and only if the range $\mathcal{R}(K)$ is finite dimensional.

4.2. Tikhonov Regularization

We have seen that the generalized inverse $K^\dagger$ is discontinuous if the range of K is infinite dimensional. Therefore, we have to stabilize the solution process. For this purpose, the idea is to approximate the Moore-Penrose inverse by a suitable family of linear operators R_α. The question is now: What does suitable mean? To answer this, we estimate the reconstruction error by

$$\|u^\dagger - R_\alpha y^\varepsilon\|_\mathcal{U} \leq \|u^\dagger - R_\alpha y\|_\mathcal{U} + \|R_\alpha(y - y^\varepsilon)\|_\mathcal{U}$$
$$= \|(K^\dagger - R_\alpha)y\|_\mathcal{U} + \|R_\alpha(y - y^\varepsilon)\|_\mathcal{U},$$

where $u^\dagger$ denotes the exact solution, i.e. $u^\dagger = K^\dagger y$. We observe that we can divide the reconstruction error into an approximation error, caused by the approximation of $K^\dagger$ by R_α, and a data error, which occurs due to noisy measurements. To control both errors terms, we require that the family of approximations R_α satisfies the following conditions:

$$\text{Stability:} \qquad R_\alpha \in \mathcal{L}(\mathcal{Y}, \mathcal{U}) \qquad \text{for all } \alpha > 0 \qquad (4.3)$$
$$\text{Pointwise convergence:} \qquad R_\alpha y \xrightarrow{\alpha \to 0} K^\dagger y \qquad \text{for all } y \in \mathcal{D}(K^+). \qquad (4.4)$$

However, we note that both conditions typically exclude each other. Indeed, the smaller α the smaller the approximation error $\|(K^\dagger - R_\alpha)y\|$, but the larger the data error $\|R_\alpha(y - y^\varepsilon)\|$, since $\|R_\alpha\| \to \infty$ for $\alpha \to 0$. The behaviour of both error terms is illustrated in Figure 4.1. Therefore, the regularization parameter α has to be chosen appropriately such that the summation of approximation and data error is minimized. An a priori parameter choice rule is presented at the end of this section.

First, we introduce two approximations satisfying the conditions (4.3) and (4.4), namely the truncated singular value decomposition and the Tikhonov regularization. Considering the singular value representation of the Moore-Penrose inverse (4.1) more carefully, we observe that error components (with respect to the basis $\{\varphi_j\}$) are amplified by the factor σ_j^{-1}. These amplifications are harmless for large singular values. But for small

singular values, these amplifications are severe. Hence, the idea of the *truncated singular value decomposition* is to omit these severe summands and, thus, the regularization is given by

$$R_\alpha y = \sum_{\sigma_j \geq \alpha} \sigma_j^{-1} (y, \psi_j)_{\mathcal{Y}} \varphi_j \quad \text{with } \alpha > 0.$$

This regularization is linear and bounded (cf. (4.2)). To argue the pointwise convergence, we interpret $R_\alpha y$ as a series of partial sums which converge to $K^\dagger y$ since the limit exists for $y \in \mathcal{D}(K^\dagger)$.

In contrast, the so called *Tikhonov regularization* is given by

$$R_\alpha y = \sum_{j=1}^{\infty} \frac{\sigma_j}{\sigma_j^2 + \alpha} (y, \psi_j)_{\mathcal{Y}} \varphi_j \quad \text{with } \alpha > 0. \tag{4.5}$$

The motivation of this regularization is to damp the amplifications by translating the eigenvalues σ_j from zero to the positive part of the real axis.

Obviously, the Tikhonov regularization is linear and pointwise convergent to $K^\dagger$. To show the boundedness we estimate

$$\|R_\alpha y\|_{\mathcal{U}} \leq \left\| \frac{\sigma_1}{\alpha} \sum_{j=1}^{\infty} (y, \psi_j)_{\mathcal{Y}} \varphi_j \right\|_{\mathcal{U}} \leq \frac{\sigma_1}{\alpha} \|y\|_{\mathcal{Y}}.$$

In comparison to the truncated singular value decomposition, an advantage of the Tikhonov regularization is that we do not need to compute the singular value system of K. In fact, we can formulate (4.5) as a minimization problem (cf. [21]):

$$u^* = \operatorname*{argmin}_{u \in \mathcal{U}} J(u) := \|Ku - y\|_{\mathcal{Y}}^2 + \alpha \|u\|_{\mathcal{U}}^2 \quad \text{with } \alpha > 0.$$

Regularization paramter $\alpha \rightarrow$
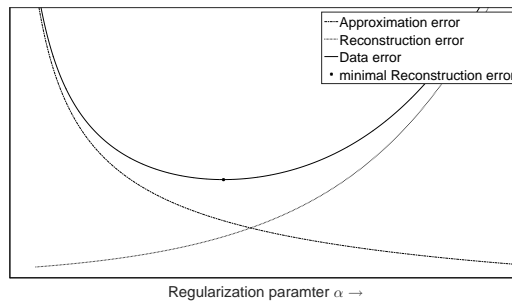
Figure 4.1.: Typical behaviour of the approximation and data error

In particular, this formulation enables us to generalize the Tikhonov regularization also to operators $A\colon \mathcal{U} \to \mathcal{Y}$ which are not necessarily linear or compact. For this, we set

$$u^* = \underset{u \in \mathcal{U}}{\operatorname{argmin}} \, J(u) := \|Au - y\|_{\mathcal{Y}}^2 + \alpha \|u\|_{\mathcal{U}}^2 \quad \text{with } \alpha > 0. \tag{4.6}$$

Indeed, in a moment we show existence, uniqueness and stability of a solution for operators A, which are just linear and bounded. Moreover, we discuss the Tikhonov regularization for the non-linear solution operator $\mathcal{T}$ of the optical flow constraint (OFC) in Chapter 6.

For the following analysis let $A \in \mathcal{L}(\mathcal{U}, \mathcal{Y})$ with Hilbert spaces $\mathcal{U}$ and $\mathcal{Y}$. We show existence and uniqueness of an optimal solution to problem (4.6) by using standard techniques from optimization theory, see [31, 44]. These techniques exploit the strict convexity and the weak lower semicontinuity of the cost functional $J(u)$.

Lemma 4.5 (Strict convexity).
Let $A \in \mathcal{L}(\mathcal{U}, \mathcal{Y})$ with Hilbert spaces $\mathcal{U}$ and $\mathcal{Y}$. Then the cost functional $J(u)$ defined in (4.6) is strictly convex.

Proof.
We have

$$v^T J''(u) v = \|Av\|_{\mathcal{Y}}^2 + \alpha \|v\|_{\mathcal{U}}^2 > 0 \quad \text{for all } v \in \mathcal{U} \setminus \{0\}.$$

Thus, we conclude that $J''(u)$ is positiv definit and, consequenlty, $J(u)$ is strictly convex. □

Lemma 4.6 (Weakly lower semicontinuity).
Let $A \in \mathcal{L}(\mathcal{U}, \mathcal{Y})$ with Hilbert spaces $\mathcal{U}$ and $\mathcal{Y}$. Then the cost functional $J(u)$ defined in (4.6) is weakly lower semicontinuous, i.e.,

$$u^k \rightharpoonup u \in \mathcal{U} \implies \liminf_{k \to \infty} J(u_k) \geq J(u).$$

Proof.
By using the linearity of the inner product we compute

$$
\begin{aligned}
\|Au - y\|_{\mathcal{Y}}^2 &= \big(Au - y, Au - y\big)_{\mathcal{Y}} \\
&= \big(A(u - u^k + u^k) - y, Au - y\big)_{\mathcal{Y}} \\
&= \big(Au^k - y, Au - y\big)_{\mathcal{Y}} + \big(u - u^k, A^*(Au - y)\big)_{\mathcal{U}} \\
&\leq \|Au - y\|_{\mathcal{Y}} \|Au^k - y\|_{\mathcal{Y}} + \big(u - u^k, A^*(Au - y)\big)_{\mathcal{U}}.
\end{aligned}
$$

Letting $k \to \infty$ and by exploiting the weak convergence of the sequence $\{u^k\}$, we obtain

$$\|Au - y\|_{\mathcal{Y}} \leq \liminf_{k \to \infty} \|Au^k - y\|_{\mathcal{Y}}.$$

With the same argumentation we conclude

$$\|u\|_{\mathcal{U}} \leq \liminf_{k \to \infty} \|u^k\|_{\mathcal{U}}.$$

In summary, we get

$$J(u) = \|Au - y\|_{\mathcal{Y}}^2 + \|u\|_{\mathcal{U}}^2 \leq \liminf_{k \to \infty} \left(\|Au^k - y\|_{\mathcal{Y}}^2 + \|u^k\|_{\mathcal{U}}^2 \right) = \liminf_{k \to \infty} J(u^k).$$

$\square$

Remark 4.7.
In [20] it is shown that any continuous convex functional $F \colon \mathcal{U} \to \mathbb{R}$ is weakly lower semicontinuous if $\mathcal{U}$ is a Banach space.

Finally, we are in a position to prove the existence and uniqueness of an optimal solution to problem (4.6).

Theorem 4.8.
Let $A \in \mathcal{L}(\mathcal{U}, \mathcal{Y})$ with Hilbert spaces $\mathcal{U}$ and $\mathcal{Y}$. Then the minimization problem (4.6) admits a unique solution $u^* \in \mathcal{U}$.

Proof.
For existence, we consider a monotone minimizing sequence $\{u^k\}$ with

$$J(u^k) \to \inf_{u \in \mathcal{U}} J(u) =: d > 0.$$

This sequence is bounded by

$$\|u^k\|_{\mathcal{U}}^2 \leq \frac{1}{\alpha} J(u^k) \leq \frac{1}{\alpha} J(u^0).$$

Consequently, we conclude that there exists a subsequence $\{u^{k_i}\}$ which weakly converges towards $u^* \in \mathcal{U}$ since $\mathcal{U}$ is reflexive.

Finally, we deduce the existence of an optimal solution from the weak lower semicontinuity of J,

$$d = \lim_{k \to \infty} J(u^k) = \liminf_{k_i \to \infty} J(u^{k_i}) \geq J(u^*) \geq d.$$

For uniqueness, we assume that there exist two distinct optimal solution u_1^* and u_2^*. Then by exploiting the strict convexity of J, we get

$$J(\lambda \, u_1^* + (1 - \lambda) \, u_2^*) < \lambda \, J(u_1^*) + (1 - \lambda) \, J(u_2^*) \quad \text{for } \lambda \in (0, 1).$$

But this is a contradiction to the optimality of u_1^* and u_2^*. Thus, problem (4.6) admits a unique solution. $\square$

Next, we state a result on how to choose the regularization parameter such that the Tikhonov regularization converges towards the Moore-Penrose inverse if the noise level ε tends to zero, i.e., if $\|y - y^\varepsilon\|_\mathcal{Y} \leq \varepsilon \to 0$.

Theorem 4.9 (Stability).
Assume $\|y - y^\varepsilon\|_\mathcal{Y} \leq \varepsilon$ with $y \in \mathcal{D}(A^\dagger)$. Moreover, we choose $\alpha \colon (0, \infty) \to (0, \infty)$ such that

$$\alpha(\varepsilon) \to 0 \quad and \quad \varepsilon^2/\alpha(\varepsilon) \to 0 \quad for \quad \varepsilon \to 0.$$

Then,

$$\|u^\dagger - R_{\alpha(\varepsilon)} y^\varepsilon\|_\mathcal{U} = \|K^\dagger y - R_{\alpha(\varepsilon)} y^\varepsilon\|_\mathcal{U} \to 0 \quad for\ \varepsilon \to 0.$$

Proof.
This statement is a special case of Corollary 6.13. □

Finally, we exemplify the Tikhonov-regularization by considering the (linear) optical flow problem (cf. Section 1.3).

Example 4.10.
Determine $\omega \in \mathcal{U}$ such that

$$\nabla I(t, x) \cdot \omega(t, x) = -I_t(t, x) \quad for\ t \in [0, T],$$

where $I \in \mathcal{C}^1(\overline{(0, T) \times \Omega}) \subset H^1((0, T) \times \Omega)$ is a measured observation. First note, that in this case the linear operator $\nabla I(t, x)$ is perturbed, too, if the measured function I is noisy. However, in [39] the Tikhonov-regularization (4.6) is also analysed for noisy operators.

In [33] Horn and Schunck proposed to seek for a solution ω in the space $\mathcal{U} = \left(H_0^1(\Omega) \right)^d$. This is motivated by the fact that image pixels belonging to the same object are moving with the same speed and in the same direction. Hence, it is reasonable to seek for a smooth solution. Additionally, for the computation of the optimality system it is useful to require that ω vanishes on the boundary. Altogether, by using a Tikhonov-regularization we obtain the minimization problem

$$\omega^* = \underset{\omega \in \mathcal{U}}{\operatorname{argmin}} J(\omega) := \|\nabla I \cdot \omega - (-I_t)\|_{L^2(\Omega)}^2 + \alpha \|\omega\|_{H_0^1(\Omega)}^2 \quad for\ t \in [0, T],$$

which we have already mentioned in Section 1.3.

4.3. BV Regularization

For a general linear operator $A : H_0^1(\Omega) \to L^2(\Omega)$ and observation $y \in L^2(\Omega)$ the Tikhonov- or H^1-regularization reads as

$$u^* = \underset{u \in H_0^1(\Omega)}{\operatorname{argmin}} J(u) := \frac{1}{2}\|Au - y\|_{L^2(\Omega)}^2 + \frac{\alpha}{2}\|u\|_{H_0^1(\Omega)}^2 \quad \text{with } \alpha > 0. \tag{4.7}$$

An essential benefit of a Tikhonov regularization is its differentiability. Hence, we can easily compute the optimality condition of the solution,

$$
\begin{aligned}
0 = J'(u)\tilde{u} &= \int_\Omega A^*\big(Au - y\big)\,\tilde{u}\,\mathrm{d}x + \alpha \int_\Omega \nabla u \cdot \nabla \tilde{u}\,\mathrm{d}x \\
&= \int_\Omega A^*\big(Au - y\big)\,\tilde{u}\,\mathrm{d}x - \alpha \int_\Omega \Delta u\,\tilde{u}\,\mathrm{d}x \qquad \text{for all } \tilde{u} \in \mathcal{U}.
\end{aligned}
\tag{4.8}
$$

As a consequence, we can use for instance gradient method (cf. Chapter 7) for solving the problem numerically. Nevertheless, from (4.8) we conclude that the optimal solution u to problem (4.7) satisfies the Poisson equation

$$
\alpha \Delta u = A^*\big(Au - y\big),
\tag{4.9}
$$

which can be interpreted as the limit of a diffusion process. Consequently, discontinuities in the solution u are smoothed out. However, if we consider for example a sequence of two objects touching each other but moving in different directions, then we observe that the optical flow is represented by a discontinuous vector field (cf. Section 8.5). Thus, a H^1-regularization is inappropriate in this case. For preserving discontinuities in the solution, a BV-regularization, given by

$$
u^* = \operatorname*{argmin}_{u \in \mathcal{U}} J(u) := \frac{1}{2}\|Au - y\|^2_{L^2(\Omega)} + \alpha \int_\Omega |\nabla u|\,\mathrm{d}x \quad \text{with } \alpha > 0,
$$

is more suited. In the following we motivate the BV-regularization for the 2-dimensional case, i.e., $\Omega \subset \mathbb{R}^2$, by adopting the work of [5], as well as [4] and [18]. As a starting point, we consider the regularized problem

$$
u^* = \operatorname*{argmin}_{u \in \mathcal{U}} J(u) := \frac{1}{2}\|Au - y\|^2_{L^2(\Omega)} + \alpha \int_\Omega \Phi(|\nabla u|)\,\mathrm{d}x \quad \text{with } \alpha > 0,
\tag{4.10}
$$

where $\Phi \colon \mathbb{R}^+ \to \mathbb{R}^+$ is for now an arbitrary function and $\mathcal{U}$ a function space which we suitably design later on. Again, we derive the optimality condition

$$
\alpha \operatorname{div}\left(\frac{\Phi'(|\nabla u|)}{|\nabla u|}\nabla u\right) = A^*\big(Au - y\big)
\tag{4.11}
$$

and observe, that the Laplacian term in (4.9) is replaced by a divergence term, i.e.,

$$
\alpha \Delta u \to \alpha \operatorname{div}\left(\frac{\Phi'(|\nabla u|)}{|\nabla u|}\nabla u\right).
$$

This replacement allows us to design the function Φ in such away, that we have a smoothing process inside homogeneous regions, while we preserve discontinuities in inhomogeneous regions. Here, the key idea is to separate the divergence term into two

parts, where one part describes the smoothing process in gradient direction $\xi = \frac{(\omega_x, \omega_y)^T}{|\nabla \omega|}$ and the other part describes the smoothing process in direction $\eta = \frac{(-\omega_y, \omega_x)^T}{|\nabla \omega|}$ orthogonal to ξ. This separation is given by the following theorem.

Theorem 4.11.
Let u be a twice continuously differentiable function. Then, the following identity holds

$$\mathrm{div}\left(\frac{\Phi'(|\nabla u|)}{|\nabla u|} \nabla u\right) = \frac{\Phi'(|\nabla u|)}{|\nabla u|} u_{\xi\xi} + \Phi''(|\nabla u|) u_{\eta\eta},$$

where

$$\xi = \frac{(u_x, u_y)^T}{|\nabla u|} \quad and \quad \eta = \frac{(-u_y, u_x)^T}{|\nabla u|} \perp \xi. \tag{4.12}$$

Proof.
By applying the chain and product rule for differentiation we obtain

$$\mathrm{div}\left(\frac{\Phi'(|\nabla u|)}{|\nabla u|} \nabla u\right) = \frac{\mathrm{d}}{\mathrm{d}x}\left(\frac{\Phi'(|\nabla u|)}{|\nabla u|} u_x\right) + \frac{\mathrm{d}}{\mathrm{d}y}\left(\frac{\Phi'(|\nabla u|)}{|\nabla u|} u_y\right)$$

$$= \frac{\Phi''(|\nabla u|)}{|\nabla u|^2} \left(\left(u_x^2 u_{xx} + u_x u_y u_{xy}\right) + \left(u_y u_x u_{xy} + u_y^2 u_{yy}\right)\right)$$

$$+ \frac{\Phi'(|\nabla u|)}{|\nabla u|} \left(u_{xx} + u_{yy}\right)$$

$$- \frac{\Phi'(|\nabla u|)}{|\nabla u|^2} \frac{\left(u_x^2 u_{xx} + u_x u_y u_{yx}\right) + \left(u_y u_x u_{xy} + u_y^2 u_{yy}\right)}{|\nabla u|}.$$

A simplification of this expression leads to

$$\mathrm{div}\left(\frac{\Phi'(|\nabla u|)}{|\nabla u|} \nabla u\right) = \Phi''(|\nabla u|) \frac{u_x^2 u_{xx} + 2 u_x u_y u_{xy} + u_y^2 u_{yy}}{|\nabla u|^2}$$

$$+ \frac{\Phi'(|\nabla u|)}{|\nabla u|} \frac{u_y^2 u_{xx} - 2 u_x u_y u_{xy} + u_x^2 u_{yy}}{|\nabla u|^2}.$$

Finally, we deduce the statement from the following Lemma 4.12. □

Lemma 4.12.
Let $u = u(x,y)$ be twice continuously differentiable. Then the second order derivatives of $u = u(x,y)$ in direction ξ and η defined in (4.12) are given by

$$u_{\xi\xi} = \frac{u_x^2 u_{xx} + 2 u_x u_y u_{xy} + u_y^2 u_{yy}}{|\nabla u|^2},$$

$$u_{\eta\eta} = \frac{u_y^2 u_{xx} - 2 u_x u_y u_{xy} + u_x^2 u_{yy}}{|\nabla u|^2}.$$

Proof.
By a simple calculation we get

$$
\begin{aligned}
u_{\xi\xi} = \xi^T D^2 u\, \xi &= \frac{1}{|\nabla u|^2} \left(u_x, u_y\right) \begin{bmatrix} u_{xx} & u_{xy} \\ u_{yx} & u_{yy} \end{bmatrix} \begin{pmatrix} u_x \\ u_y \end{pmatrix} \\
&= \frac{u_x^2\, u_{xx} + 2\, u_x\, u_y\, u_{xy} + u_y^2\, u_{yy}}{|\nabla u|^2}, \\
u_{\eta\eta} = \eta^T D^2 u\, \eta &= \frac{1}{|\nabla u|^2} \left(-u_y, u_x\right) \begin{bmatrix} u_{xx} & u_{xy} \\ u_{yx} & u_{yy} \end{bmatrix} \begin{pmatrix} -u_y \\ u_x \end{pmatrix} \\
&= \frac{u_y^2\, u_{xx} - 2\, u_x\, u_y\, u_{xy} + u_x^2\, u_{yy}}{|\nabla u|^2}.
\end{aligned}
$$

$\square$

Now, with this separation we are in the position to design the function Φ. First, note that the gradient is small in homogeneous regions, whereas it is large in inhomogeneous regions, i.e., $|\nabla u| \to 0$ or $|\nabla u| \to \infty$, respectively. In order to achieve the diffusion in homogeneous regions we require

$$
\lim_{s \to 0} \frac{\Phi'(s)}{s} = \lim_{s \to 0} \Phi''(s) = \Phi''(0) = c > 0, \tag{RTC1}
$$

because in this case equation (4.11) using Theorem 4.11 leads to a Poisson equation

$$
\alpha \operatorname{div}\left(\frac{\Phi'(|\nabla u|)}{|\nabla u|} \nabla u \right) = c\,\alpha\,\Delta u = A^*\big(Au - y\big).
$$

On the other hand, in inhomogeneous regions we would like to smooth only parallel to the edges, but not across them. We enforce this by stopping the diffusion in gradient direction η, while keeping a stable diffusion along the direction ξ being parallel to the edge. Thus, we impose

$$
\lim_{s \to \infty} \frac{\Phi'(s)}{s} = 0, \tag{4.13}
$$

$$
\lim_{s \to \infty} \Phi''(s) = b > 0, \tag{4.14}
$$

which by using Theorem 4.11 leads to

$$
\alpha \operatorname{div}\left(\frac{\Phi'(|\nabla u|)}{|\nabla u|} \nabla u \right) = b\,\alpha\,u_{\eta\eta} = A^*\big(Au - y\big).
$$

However, the two conditions (4.13) and (4.14) exclude each other. Therefore, we require, that we have much more diffusion in direction ξ than along the gradient direction η, i.e.,

$$
\lim_{s \to \infty} \Phi''(s) = \lim_{s \to \infty} \frac{\Phi'(s)}{s} = 0, \tag{RTC2}
$$

$$
\lim_{s \to \infty} \frac{\Phi''(s)}{\frac{\Phi'(s)}{s}} = 0. \tag{RTC3}
$$

A function which satisfies the conditions (RTC1) to (RTC3) is given by Aubert [4, 18],

$$\Phi(s) = \sqrt{s^2 + \delta}. \tag{4.15}$$

In fact, by calculating

$$\Phi'(s) = \frac{s}{\sqrt{s^2 + \delta}} \quad \text{and}$$

$$\Phi''(s) = \varepsilon \, (s^2 + \delta)^{-\frac{3}{2}},$$

we verify that the conditions (RTC1) to (RTC3) are satisfied:

$$\lim_{s \to 0} \Phi''(s) = \lim_{s \to 0} \frac{\Phi'(s)}{s} = \frac{1}{\sqrt{\delta}} > 0,$$

$$\lim_{s \to \infty} \Phi''(s) = \lim_{s \to \infty} \frac{\Phi'(s)}{s} = 0,$$

$$\lim_{s \to \infty} \frac{\Phi''(s)}{\frac{\Phi'(s)}{s}} = 0.$$

Inserting Aubert's function (4.15) in the generalized regularized problem (4.10) leads to

$$u^* = \operatorname*{argmin}_{u \in \mathcal{U}} J_\delta(u) := \frac{1}{2} \|Au - y\|_{L^2}^2 + \int_\Omega \sqrt{|\nabla u|^2 + \delta} \, \mathrm{d}x. \tag{4.16}$$

Letting $\varepsilon \to 0$, we obtain the total variation as regularization term

$$u^* = \operatorname*{argmin}_{u \in \mathcal{U}} J(u) := \frac{1}{2} \|Au - y\|_{L^2}^2 + \int_\Omega |\nabla u| \, \mathrm{d}x. \tag{4.17}$$

Note, that the total variation is not differentiable. However, from the inequality

$$J(u) = \frac{1}{2} \|Au - y\|_{L^2}^2 + \int_\Omega |\nabla u| \, \mathrm{d}x$$

$$\leq \frac{1}{2} \|Au - y\|_{L^2}^2 + \int_\Omega \sqrt{|\nabla u|^2 + \delta} \, \mathrm{d}x = J_\delta(u)$$

$$\leq \frac{1}{2} \|Au - y\|_{L^2}^2 + \int_\Omega \left(\sqrt{|\nabla u|^2} + \sqrt{\delta} \right) \mathrm{d}x = J(u) + \sqrt{\delta} \, |\Omega|$$

we conclude that both regularizations (4.16) and (4.17) admit comparable optimal solutions for $\delta > 0$ sufficiently small. Hence, (4.16) can be interpreted as a smoothened total variation, which gives certain advantages in numerical calculations, like differentiability.

Now the question is: What is an appropriate control space $\mathcal{U}$ for finding a solution to

problem (4.17) or (4.16), respectively? As a reminder, the aim of this section was to design a regularization which allows discontinuous solution. Hence, classical Sobolev spaces are inappropriate in this case. Additionally, we are not able to find a solution to problem (4.16) or (4.17) in the space $W^{1,p}(\Omega), 1 \leq p \leq \infty$ (cf. discussion in Section 6.2.3), respectively. Therefore, in the following we seek for a solution in the space of bounded variational functions. Indeed, in [1] it is shown that we can find a unique solution in the space $\mathcal{U} = \big(BV_0(\Omega)\big)^d$.

Theorem 4.13.
Let $\mathcal{U} := \big(BV_0(\Omega)\big)^d$ and $\mathcal{Y}$ be a Hilbert space. Assume that $A \colon \mathcal{U} \to \mathcal{Y}$ is a linear operator. Then the minimization problems (4.16) and (4.17) admit unique solutions $u_\delta^* \in \mathcal{U}$ and $u^* \in \mathcal{U}$, respectively.

Proof.
We deduce the statement from Theorem 3.1 in [1], which additionally requires that the cost functional J is BV-coercive. The BV-coercivity assumption can be verified by using the Poincoré inequality for functions of bounded variation (cf. Theorem 2.14). $\qquad\square$

Moreover, also the stability of the BV-regularization is analysed in [1].

Theorem 4.14 (Stability).
Let $\mathcal{U} := \big(BV_0(\Omega)\big)^d$, $\mathcal{Y}$ be a Hilbert space and u^* be the exact solution to problem (4.17). Assume $\|y - y^\varepsilon\|_\mathcal{Y} \leq \varepsilon$ with $y, y^\varepsilon \in \mathcal{Y}$. We denote by u_ε^* the unique solution to problem

$$\min_{u \in \mathcal{U}} J(u) := \frac{1}{2} \|Au - y^\varepsilon\|_{L^2}^2 + \int_\Omega |\nabla u| \, \mathrm{d}x$$

Moreover, we choose $\alpha \colon (0, \infty) \to (0, \infty)$ such that

$$\alpha(\varepsilon) \to 0 \quad and \quad \varepsilon^2 / \alpha(\varepsilon) \to 0 \quad for \quad \varepsilon \to 0.$$

Then, u_ε^* converges towards u^* in $L^p(\Omega)$ if $1 \leq p < \frac{d}{d-1}$. The convergence is weak in $L^p(\Omega)$ if $p = \frac{d}{d-1}$.

Analogously, the statement holds for problem (4.16).

Part II.

Theory

5. Weak Solutions of Transport Equations

In this chapter we analyse the solution operator

$$\mathcal{T} : \mathcal{U} \times \mathcal{Z} \to \mathcal{Y}$$
$$(\omega, I_0) \mapsto I$$

of the optical flow constraint

$$I_t + \omega \cdot \nabla I = 0 \quad \text{with } I(0, x) = I_0(x) \tag{OFC}$$

with $I \colon (0, T) \times \Omega \to \mathbb{R}$, $\omega \colon (0, T) \times \Omega \to \mathbb{R}^d$ and $I_0 \colon \Omega \to \mathbb{R}$, where $\Omega \subset \mathbb{R}^d$ denotes an open and bounded set. In particular, we will argue a suitable choice for the function spaces $\mathcal{U}, \mathcal{Y}$ and $\mathcal{Z}$.

If I_0 is a $\mathcal{C}^1$-function and ω is a Lipschitz continuous vector field, then a standard ansatz for solving a transport equation analytically is the method of characteristics, see Section 3.2. In fact, in this case existence and uniqueness of a solution follows by Picard-Lindelöf's theorem, as we have shown in Theorem 3.6. However, in our case the samples $I_n, n = 0, ..., N$, are not necessarily differentiable. Furthermore, also the vector fields ω which we consider in the next chapter are not necessarily Lipschitz continuous. This means Picard-Lindelöf's theorem is not applicable. Therefore in the following we consider weak solutions of transport equations. The weak formulation is obtained by multiplying the transport equation (OFC) by a test function φ and integration by parts.

Definition 5.1 (Local Weak Solution).
Let $\omega \in \big(L^1((0, T) \times \Omega) \big)^d$, $\operatorname{div}(\omega) \in L^1((0, T) \times \Omega)$ and $I_0 \in L^1(\Omega)$. A function $I \in L^\infty((0, T) \times \Omega)$ is said to be a local weak solution *of* (OFC), *if it satisfies the equation*

$$\int_0^T \int_\Omega I \Big(\varphi_t + \omega \cdot \nabla\varphi + \operatorname{div}(\omega)\, \varphi \Big) \, \mathrm{d}x \, \mathrm{d}t = - \int_\Omega I_0(x)\, \varphi(0, x) \, \mathrm{d}x,$$

for any Lipschitz continuous test function $\varphi \in \mathcal{C}^{0,1}(\overline{(0, T) \times \Omega})$ such that $\varphi(T, \cdot) = 0$ and $\varphi = 0$ on $[0, T] \times \partial\Omega$.

In this chapter we show existence and uniqueness of a weak solution, as well as the weak-* sequential closedness of the solution operator $\mathcal{T}$, which is useful for proving the

weak lower semicontinuity of the cost functional $J(\omega)$ in problem (NP) or (1.7).

A useful tool for proving the uniqueness of weak solutions is the renormalization property of weak solutions. This renormalization property was originally introduced by DiPerna and Lions in 1989 [19]. However, in the following we will adapt the work of Boyer and Fabrie [10], which is also based on [19]. They in a simplified version showed the following properties of weak solutions to (OFC).

Theorem 5.2 (Existence, Uniqueness & Stability [10])**.**
Let

$$\omega \in \left(L^1((0,T), W_0^{1,1}(\Omega)) \right)^d,$$
$$\operatorname{div}(\omega) \in L^1((0,T), L^\infty(\Omega)) \qquad and$$
$$I_0 \in L^\infty(\Omega).$$

Then the transport equation (OFC) admits a unique solution

$$I \in \mathcal{C}^0([0,T], L^r(\Omega)), 1 \le r < \infty.$$

Moreover the solution I is stable, too. This means, if $\{I^k\} \subset \mathcal{C}^0([0,T], L^r(\Omega))$ denotes the unique sequence of weak solutions corresponding to the sequence $\{\omega^k\}$ with

$$\omega^k \in \left(L^1((0,T), W_0^{1,1}(\Omega)) \right)^d \qquad and$$
$$\operatorname{div}(\omega^k) \in L^1((0,T), L^\infty(\Omega)),$$

then the sequence $\{I^k\}$ converges strongly towards $I \in \mathcal{C}^0([0,T], L^r(\Omega))$, if $\omega^k \to \omega \in \mathcal{U}$.

Remark 5.3.
To be more precise, in [10] existence, uniqueness and stability is shown for the more general transport equation

$$I_t(t,x) + \operatorname{div}\left(\omega(t,x)\, I(t,x) \right) + c(t,x)\, I(t,x) = 0$$

with initial and inflow boundary conditions

$$I(0,x) = I_0(x) \quad and$$
$$I(t,x) = I^{in}(t,x) \quad on\ \partial\Omega^{In},$$

where $\partial\Omega^{In} := \{(t,x) \in [0,T] \times \partial\Omega : \text{ with } \omega(t,x) \cdot \nu(t,x) < 0\}$ with outer unit normal vector ν on $[0,T] \times \partial\Omega$.

In particular, the vector field does not necessarily vanish on the spatial boundary $\partial\Omega$.

However, with the regularity condition $\operatorname{div}(\omega) \in L^1((0,T), L^\infty(\Omega))$ it is difficult to show existence of an optimal solution to problem (NP) without any additional assumptions.

To prove existence of an optimal solution to problem (NP), one possibility is to additionally assume $\text{div}(\omega) = 0$ as in [15]. But this would mean to exclude deformation vector fields as solutions.

Therefore, we will show next that we can omit the L^∞- boundedness assumption on the divergence of ω, if we require instead that the vector field ω vanishes on the spatial boundary $\partial\Omega$. We remark at this point, that this requirement is not really a restriction, because for the computation of the optimality system to problem (NP) we will require it anyway, as in [15] (or in [8, 9]).

5.1. Existence

We start with analysing existence of a local weak solution. For this we require that the vector field ω is a Bochner function with values in the Sobolev space $W_0^{1,1}(\Omega)$, i.e., $\omega \in \left(L^1((0,T), W_0^{1,1}(\Omega))\right)^d$. The fact that ω vanishes on the spatial boundary $\partial\Omega$ allows us to use a continuation of ω from $(0,T) \times \Omega$ to $(0,T) \times \mathbb{R}^d$ given by

$$\bar{\omega}(x,t) = \begin{cases} \omega(x,t) & \text{if } x \in \Omega \\ 0 & \text{if } x \in \mathbb{R}^d \setminus \Omega \end{cases}.$$

Hence, the procedure for proving existence is as follows. Firstly, we look for a global weak solution. Here, the idea is to approximate ω and I_0 by smooth functions and, subsequently, to conclude the existence of a solution from the global version of Picard Lindelöf's theorem. Secondly, we deduce from global existence also local existence of a weak solution by using the continuation above.

We now define a global weak solution.

Definition 5.4 (Global Weak Solution).
Let $\omega \in \left(L_{loc}^1((0,T) \times \mathbb{R}^d)\right)^d$, $\text{div}(\omega) \in L_{loc}^1((0,T) \times \mathbb{R}^d)$ and $I_0 \in L_{loc}^1(\mathbb{R}^d)$. A function $I \in L^\infty((0,T) \times \mathbb{R}^d)$ is said to be a global weak solution *of* (OFC)*, if it satisfies the equation*

$$\int_0^T \int_{\mathbb{R}^d} I \left(\varphi_t + \omega \cdot \nabla\varphi + \text{div}(\omega)\,\varphi\right) \mathrm{d}x\,\mathrm{d}t = -\int_{\mathbb{R}^d} I_0(x)\,\varphi(0,x)\,\mathrm{d}x,$$

for any test function $\varphi \in \mathcal{C}_c^{0,1}([0,T] \times \mathbb{R}^d)$.

For proving existence of a global weak solution to (OFC), we adapt the proof in [17].

Theorem 5.5 (Existence).
Let $\omega \in \left(L^1((0,T), W_{loc}^{1,1}(\mathbb{R}^d))\right)^d$ and $I_0 \in L^\infty(\mathbb{R}^d)$ with compact support. Then there exists a global weak solution $I \in L^\infty((0,T) \times \mathbb{R}^d)$ to the transport equation (OFC).

Proof.

First we smoothen the vector field ω and the initial value I_0 by using a mollifier function, i.e, we define $\omega^\varepsilon = \omega * \rho_\varepsilon$ and $I_0^\varepsilon = I_0 * \eta_\varepsilon$, where ρ_ε denotes a mollifier function on $\mathbb{R}^{d+1}$ and η_ε a mollifier function on $\mathbb{R}^d$ (cf. Appendix A.1). Then we deduce from the theorem of Picard and Lindelöf (cf. Theorem 3.6), that for every $\varepsilon > 0$ the regularized problem

$$I_t + \omega^\varepsilon \cdot \nabla I = 0 \quad \text{with } I(0, \cdot) = I_0^\varepsilon$$

has a (unique) solution on $[0, T] \times \mathbb{R}^d$. We denote this solution by I^ε. Furthermore, we know from the method of characteristics (cf. Section 3.2.1), that

$$\|I^\varepsilon\|_{L^\infty((0,T)\times\mathbb{R}^d)} \leq \|I_0^\varepsilon\|_{L^\infty(\mathbb{R}^d)} \leq \|I_0\|_{L^\infty(\mathbb{R}^d)}.$$

Thus, we deduce that there exists a subsequence I^{ε_k} which converges weakly-* towards a function $I \in L^\infty((0, T) \times \mathbb{R}^d)$. Finally we show that the pair (ω, I) satisfies the weak formulation of a transport equation:

$$\int_0^T \int_{\mathbb{R}^d} I \left(\varphi_t + \omega \cdot \nabla\varphi + \text{div}(\omega)\,\varphi \right) \mathrm{d}x\,\mathrm{d}t$$

$$- \int_0^T \int_{\mathbb{R}^d} I^{\varepsilon_k} \left(\varphi_t + \omega^{\varepsilon_k} \cdot \nabla\varphi + \text{div}(\omega^{\varepsilon_k})\,\varphi \right) \mathrm{d}x\,\mathrm{d}t$$

$$+ \int_{\mathbb{R}^d} I_0(x)\,\varphi(0, x)\,\mathrm{d}x - \int_{\mathbb{R}^d} I_0^{\varepsilon_k}(x)\,\varphi(0, x)\,\mathrm{d}x$$

$$= \int_0^T \int_{\mathbb{R}^d} (I - I^{\varepsilon_k}) \left(\varphi_t + \omega \cdot \nabla\varphi + \text{div}(\omega)\,\varphi \right) \mathrm{d}x\,\mathrm{d}t$$

$$+ \int_0^T \int_{\mathbb{R}^d} I^{\varepsilon_k} \left((\omega - \omega^{\varepsilon_k}) \cdot \nabla\varphi + \text{div}(\omega - \omega^{\varepsilon_k})\,\varphi \right) \mathrm{d}x\,\mathrm{d}t$$

$$+ \int_{\mathbb{R}^d} \left(I_0(x) - I_0^{\varepsilon_k}(x) \right) \varphi(0, x)\,\mathrm{d}x,$$

The first integral vanishes for $\varepsilon_k \to 0$, since the sequence I^{ε_k} converge weakly-* towards I in $L^\infty((0, T) \times \mathbb{R}^d)$.

Denoting by $K \subset [0, T) \times \mathbb{R}^d$ the compact support of the test function φ we can estimate

the second integral by

$$\int\limits_0^T \int\limits_{\mathbb{R}^d} I^{\varepsilon_k} \Big((\omega - \omega^{\varepsilon_k}) \cdot \nabla\varphi + \operatorname{div}(\omega - \omega^{\varepsilon_k})\,\varphi \Big)\,\mathrm{d}x\,\mathrm{d}t$$

$$= \int\limits_K I^{\varepsilon_k} \Big((\omega - \omega^{\varepsilon_k}) \cdot \nabla\varphi + \operatorname{div}(\omega - \omega^{\varepsilon_k})\,\varphi \Big)\,\mathrm{d}x\,\mathrm{d}t$$

$$\leq \|I_0\|_{L^\infty(\mathbb{R}^d)} \|\nabla\varphi\|_{L^\infty((0,T)\times\mathbb{R}^d)} \int\limits_K |\omega - \omega^{\varepsilon_k}|\,\mathrm{d}x\,\mathrm{d}t$$

$$+ \|I_0\|_{L^\infty(\mathbb{R}^d)} \|\varphi\|_{L^\infty((0,T)\times\mathbb{R}^d)} \int\limits_K \big| \operatorname{div}(\omega - \omega^{\varepsilon_k}) \big|\,\mathrm{d}x\,\mathrm{d}t,$$

From this estimate we conclude that the second integral also vanishes when $\varepsilon_k \to 0$, because of the strong convergence of ω^{ε_k} towards ω in $\big(L^1((0,T), W^{1,1}_{loc}(\mathbb{R}^d)) \big)^d$ (cf. Theorem A.5).

For the third integral we have the estimate

$$\int\limits_{\mathbb{R}^d} \Big(I_0(x) - I_0^{\varepsilon_k}(x) \Big)\varphi(0,x)\,\mathrm{d}x = \int\limits_{K_0} \Big(I_0(x) - I_0^{\varepsilon_k}(x) \Big)\varphi(0,x)\,\mathrm{d}x$$

$$\leq \|\varphi\|_{L^\infty((0,T)\times\mathbb{R}^d)} \int\limits_{K_0} \Big(I_0(x) - I_0^{\varepsilon_k}(x) \Big)\,\mathrm{d}x,$$

where $K_0 \subset \mathbb{R}^d$ denotes the compact spatial support of the test function φ at initial time $t = 0$. Thus, also the third integral vanishes for $\varepsilon_k \to 0$, because of the strong convergence of $I_0^{\varepsilon_k} \to I_0$ in $L^1_{loc}(\mathbb{R}^d)$ (cf. Theorem A.5).

Since $(\omega^{\varepsilon_k}, I^{\varepsilon_k})$ solves the transport equation, we conclude that the pair (ω, I) is a weak solution of the transport equation, too. $\qquad\square$

Remark 5.6.
In contrast to [17] we do not need the assumption that $\omega \in \big(L^\infty((0,T) \times \mathbb{R}^d) \big)^d$.

Finally, existence of a local weak solution is deduced from Theorem 5.5 by using a continuation of ω and I_0 from $(0,T) \times \Omega$ to $(0,T) \times \mathbb{R}^d$ and from Ω to $\mathbb{R}^d$, respectively.

Corollary 5.7.
Let $\omega \in \big(L^1((0,T), W^{1,1}_0(\Omega)) \big)^d$ and $I_0 \in L^\infty(\Omega)$. Then there exists a local weak solution $I \in L^\infty((0,T) \times \Omega)$ to the transport equation (OFC).

Proof.
We define the continuations

$$\bar{\omega}(x,t) = \begin{cases} \omega(x,t) & \text{if } x \in \Omega \\ 0 & \text{if } x \in \mathbb{R}^d \setminus \Omega \end{cases} \quad \text{and} \quad \bar{I}_0(x) = \begin{cases} I_0(x) & \text{if } x \in \Omega \\ 0 & \text{if } x \in \mathbb{R}^d \setminus \Omega \end{cases}.$$

Then $\bar{\omega}$ and $\bar{I}_0$ satisfy the assumptions of Theorem 5.5 and we deduce a global weak solution in $[0,T] \times \mathbb{R}^d$. If we now only use test functions $\varphi \in \mathcal{C}^{0,1}(\overline{(0,T) \times \Omega})$ such that $\varphi(0,\cdot) = \varphi(T,\cdot) = 0$ and $\varphi(t,x) = 0$ for $x \in \mathbb{R}^d \setminus \Omega$, then we immediately obtain the statement of the corollary. $\qquad\square$

Remark 5.8.
This technique for proving existence of a solution cannot be applied to vector fields with nonzero boundary values. Therefore, in [10] the assumption $\mathrm{div}(\omega) \in L^\infty(\Omega)$ is necessary to prove the existence of a solution for vector fields with nonzero boundary values.

5.2. Uniqueness

Next, we analyse uniqueness of a weak solution. We begin with two useful properties of weak solutions to the optical flow constraint (OFC).

Theorem 5.9 (cf. [10]).
Let $\omega \in \big(L^1((0,T), W_0^{1,1}(\Omega))\big)^d, I_0 \in L^\infty(\Omega)$ and $I \in L^\infty((0,T) \times \Omega)$, be any weak solution of the transport equation (OFC). *Then the following properties hold:*

1. *For any $1 \le r < \infty$, we have $I \in \mathcal{C}^0([0,T], L^r(\Omega))$.*

2. *I is a renormalized solution, this means that for any $\mathcal{C}^1$-function $\beta \colon \mathbb{R} \mapsto \mathbb{R}$, for any $\varphi \in \mathcal{C}^{0,1}([0,T] \times \overline{\Omega})$ and any $[t_0,t_1] \subset [0,T]$, we have*

$$\begin{aligned} 0 = &\int_{t_0}^{t_1} \int_\Omega \beta(I)\big(\varphi_t + \omega \cdot \nabla\varphi\big)\,\mathrm{d}x\,\mathrm{d}t + \int_{t_0}^{t_1} \int_\Omega \mathrm{div}(\omega)\,\beta(I)\,\varphi\,\mathrm{d}x\,\mathrm{d}t \\ &+ \int_\Omega \beta\big(I(\cdot,t_0)\big)\,\varphi(t_0)\,\mathrm{d}x - \int_\Omega \beta\big(I(\cdot,t_1)\big)\,\varphi(t_1)\,\mathrm{d}x \end{aligned} \qquad \text{(RenSol)}$$

Lemma 5.10 ([10]).
For any $\delta > 0$ the function $\beta_\delta : \mathbb{R} \to \mathbb{R}$ defined by

$$\beta_\delta(\xi) = \frac{\xi^2}{\sqrt{\xi^2 + \delta}}$$

is of class $\mathcal{C}^\infty$ and satisfies

$$\begin{aligned} |\beta_\delta(\xi)| &\le |\xi| &&\text{for all } \xi \in \mathbb{R}, \\ |\beta_\delta'(\xi)| &\le 2 &&\text{for all } \xi \in \mathbb{R} \quad \text{and} \\ \beta_\delta(\xi) &\to |\xi| &&\text{for } \delta \to 0 \text{ and } \xi \in \mathbb{R}. \end{aligned}$$

Proof of Theorem 5.9.
The proof is essentially based on the proof of Theorem VI.1.3. in [10]. For the first part of the proof we have to introduce the concept of mollifier operators. Since we can adopt this part of the proof from [10], we only sketch this part and refer to [10] for more details.

First we consider a family of mollifier operators $\{S^\varepsilon\}$, which were introduced in [10], and set $I^\varepsilon(\cdot, t) = S^\varepsilon I(\cdot, t)$ for all $t \in [0, T]$. Then from the properties of mollifier operators we know that

$$I^\varepsilon \in L^\infty((0,T), \mathcal{C}^k(\overline{\Omega})) \quad \text{for all } k \geq 0,$$
$$\|I^\varepsilon\|_{L^\infty((0,T)\times\Omega)} \leq \|I\|_{L^\infty((0,T)\times\Omega)} \tag{5.1}$$

and that

$$I^\varepsilon(t) \to I(t) \qquad \text{in } L^r(\Omega) \text{ for any } r < \infty \text{ and any } t \in [0,T], \text{ and}$$
$$I^\varepsilon \to I \qquad \text{in } L^r((0,T)\times\Omega) \text{ for any } r < \infty.$$

Further I^ε solves the following equation in the distributional sense:

$$I_t^\varepsilon + \omega \cdot \nabla I^\varepsilon = R^\varepsilon, \tag{5.2}$$

where $R^\varepsilon \in L^1((0,T)\times\Omega)$ satisfies $\|R^\varepsilon\|_{L^1((0,T)\times\Omega)} \to 0$ as $\varepsilon \to 0$. Since I^ε is smooth in space, we deduce from (5.2) that

$$I_t^\varepsilon = R^\varepsilon - \omega \cdot \nabla I^\varepsilon \in L^1((0,T)\times\Omega) \tag{5.3}$$

holds for any $\varepsilon > 0$. From (5.3) we get

$$I^\varepsilon \in W^{1,1}((0,T)\times\Omega) \subset \mathcal{C}^0([0,T], L^1(\Omega)).$$

Finally by using (5.1) we conclude that

$$I^\varepsilon \in \mathcal{C}^0([0,T], L^r(\Omega)), \quad \text{for } 1 \leq r < \infty.$$

In order to prove the convergence of the sequence $\{I^\varepsilon\}$ for $\varepsilon \to 0$ towards a function $I \in \mathcal{C}^0([0,T], L^1(\Omega))$, we show that $\{I^\varepsilon\}$ is a Cauchy sequence in $\mathcal{C}^0([0,T], L^1(\Omega))$. Let $\varepsilon_1, \varepsilon_2 > 0$, then by using equation (5.2) we obtain

$$I_t^{\varepsilon_1} - I_t^{\varepsilon_2} + \omega \cdot \nabla(I^{\varepsilon_1} - I^{\varepsilon_2}) = R^{\varepsilon_1} - R^{\varepsilon_2}.$$

Next we multiply the equation by $\beta_\delta'(I^{\varepsilon_1} - I^{\varepsilon_2})$, with β_δ as defined in Lemma 5.10:

$$\beta_\delta'(I^{\varepsilon_1} - I^{\varepsilon_2})\,(R^{\varepsilon_1} - R^{\varepsilon_2})$$
$$= \beta_\delta'(I^{\varepsilon_1} - I^{\varepsilon_2})\left(I_t^{\varepsilon_1} - I_t^{\varepsilon_2} + \omega \cdot \nabla(I_1^\varepsilon - I^{\varepsilon_2})\right)$$
$$= \frac{\partial}{\partial t}\left(\beta_\delta(I^{\varepsilon_1} - I^{\varepsilon_2})\right) + \operatorname{div}\left(\beta_\delta(I^{\varepsilon_1} - I^{\varepsilon_2})\,\omega\right) - \operatorname{div}(\omega)\,\beta_\delta(I^{\varepsilon_1} - I^{\varepsilon_2}).$$

Now we multiply the equation by a time independent Lipschitz continuous test function $\varphi \in \mathcal{C}^{0,1}(\overline{\Omega})$, which satisfies $\varphi = 0$ on the boundary $\partial\Omega$ and $0 \leq \varphi \leq 1$ in Ω, integrate over Ω and get

$$\int_{\Omega} \beta_{\delta}'(I^{\varepsilon_1} - I^{\varepsilon_2})(R^{\varepsilon_1} - R^{\varepsilon_2})\,\varphi\,\mathrm{d}x$$

$$= \frac{\mathrm{d}}{\mathrm{d}t}\left(\int_{\Omega} \beta_{\delta}(I^{\varepsilon_1} - I^{\varepsilon_2})\,\varphi\,\mathrm{d}x\right) - \int_{\Omega} \beta_{\delta}(I^{\varepsilon_1} - I^{\varepsilon_2})\,\omega \cdot \nabla\varphi$$

$$- \int_{\Omega} \mathrm{div}(\omega)\,\beta_{\delta}(I^{\varepsilon_1} - I^{\varepsilon_2})\,\varphi\,\mathrm{d}x.$$

Then we integrate the equation over $[0,s] \subset [0,T]$ and obtain

$$\int_{\Omega} \left(\beta_{\delta}(I^{\varepsilon_1} - I^{\varepsilon_2})\,\varphi\right)(s,\cdot)\,\mathrm{d}x - \int_0^s \int_{\Omega} \mathrm{div}(\omega)\beta_{\delta}(I^{\varepsilon_1} - I^{\varepsilon_2})\,\varphi\,\mathrm{d}x\,\mathrm{d}t$$

$$= \int_{\Omega} \left(\beta_{\delta}(I^{\varepsilon_1} - I^{\varepsilon_2})\,\varphi\right)(0,\cdot)\,\mathrm{d}x + \int_0^s \int_{\Omega} \beta_{\delta}'(I^{\varepsilon_1} - I^{\varepsilon_2})(R^{\varepsilon_1} - R^{\varepsilon_2})\,\varphi\,\mathrm{d}x\,\mathrm{d}t$$

$$+ \int_0^s \int_{\Omega} \beta_{\delta}(I^{\varepsilon_1} - I^{\varepsilon_2})\,\omega \cdot \nabla\varphi\,\mathrm{d}x\,\mathrm{d}t$$

$$\leq \int_{\Omega} \left(|I^{\varepsilon_1} - I^{\varepsilon_2}|\right)(0,\cdot)\,\mathrm{d}x + C\int_0^s \int_{\Omega} |R^{\varepsilon_1} - R^{\varepsilon_2}|\,\mathrm{d}x\,\mathrm{d}t$$

$$+ \int_0^s \int_{\Omega} |I^{\varepsilon_1} - I^{\varepsilon_2}|\,|\omega \cdot \nabla\varphi|\,\mathrm{d}x\,\mathrm{d}t,$$

where we use in the estimation the properties of β_{δ} which are given in Lemma 5.10 and that $0 \leq \varphi \leq 1$. Finally, by using the dominated convergence theorem we pass to the limit in this inequality for $\delta \to 0$ and obtain

$$\int_{\Omega} \left(\varphi\,|I^{\varepsilon_1} - I^{\varepsilon_2}|\right)(s,\cdot)\,\mathrm{d}x$$

$$\leq \int_{\Omega} \left(|I^{\varepsilon_1} - I^{\varepsilon_2}|\right)(0,\cdot)\,\mathrm{d}x + C\int_0^s \int_{\Omega} |R^{\varepsilon_1} - R^{\varepsilon_2}|\,\mathrm{d}x\,\mathrm{d}t \tag{5.4}$$

$$+ \int_0^s \int_{\Omega} |I^{\varepsilon_1} - I^{\varepsilon_2}|\,|\omega \cdot \nabla\varphi|\,\mathrm{d}x\,\mathrm{d}t + \int_0^s \int_{\Omega} \mathrm{div}(\omega)\,|I^{\varepsilon_1} - I^{\varepsilon_2}|\,\mathrm{d}x\,\mathrm{d}t.$$

Next we define for $h > 0$ a function φ_h via

$$\varphi_h(x) := \frac{1}{h} \min(h, \delta(x)), \quad \text{for all } x \in \Omega,$$

where $\delta(x)$ denotes the distance from x to the boundary $\partial\Omega$. This function is Lipschitz continuous and satisfies $0 \leq \varphi_h \leq 1$. Further we have

$$|\nabla\varphi| = \begin{cases} 0 & \text{in } \Omega_h := \{x \in \Omega, \delta(x) > h\} \\ \frac{1}{h} & \text{in } \mathcal{O}_h := \{x \in \Omega, \delta(x) < h\} \end{cases}.$$

Then the estimate

$$\int_\Omega (1 - \varphi_h) \, |I^{\varepsilon_1} - I^{\varepsilon_2}|(s, \cdot) \, \mathrm{d}x \leq 2 \, \|I\|_{L^\infty((0,T)\times\Omega)} \int_\Omega (1 - \varphi_h) \, \mathrm{d}x$$

$$\leq 2 \, \|I\|_{L^\infty((0,T)\times\Omega)} |\mathcal{O}_h|$$

holds for any $h, \varepsilon_1, \varepsilon_2 > 0$, which by using (5.4) leads us to

$$\|(I^{\varepsilon_1} - I^{\varepsilon_2})(s, \cdot)\|_{L^1(\Omega)} \leq 2 \, \|I\|_{L^\infty((0,T)\times\Omega)} \, |\mathcal{O}_h| + \|(I^{\varepsilon_1} - I^{\varepsilon_2})(0, \cdot)\|_{L^1(\Omega)}$$

$$+ C \, \|R^{\varepsilon_1} - R^{\varepsilon_2}\|_{L^1((0,T)\times\Omega)}$$

$$+ \frac{1}{h} \int_0^s \int_{\mathcal{O}_h} |I^{\varepsilon_1} - I^{\varepsilon_2}| \, |\omega| \, \mathrm{d}x \, \mathrm{d}t$$

$$+ \int_0^s \int_\Omega \operatorname{div}(\omega) \, |I^{\varepsilon_1} - I^{\varepsilon_2}| \, \mathrm{d}x \, \mathrm{d}t.$$

Here we only have to estimate the last two integrals on the right-hand side. To this end, let $v \in \left(\mathcal{C}^\infty(\overline{(0,T)\times\Omega})\right)^d$, and by using the inequality $|\omega| \leq |\omega - v| + |v|$ we get

$$\|(I^{\varepsilon_1} - I^{\varepsilon_2})(s, \cdot)\|_{L^1(\Omega)} \leq 2 \, \|I\|_{L^\infty((0,T)\times\Omega)} \, |\mathcal{O}_h| + \|(I^{\varepsilon_1} - I^{\varepsilon_2})(0, \cdot)\|_{L^1(\Omega)}$$

$$+ C \, \|R^{\varepsilon_1} - R^{\varepsilon_2}\|_{L^1((0,T)\times\Omega)}$$

$$+ \frac{2}{h} \, \|I\|_{L^\infty(\Omega)} \, \|\omega - v\|_{L^1((0,T)\times\Omega)}$$

$$+ \frac{1}{h} \, \|\omega\|_{L^\infty((0,T)\times\Omega)} \, \|I^{\varepsilon_1} - I^{\varepsilon_2}\|_{L^1((0,T)\times\Omega)}$$

$$+ 2 \, \|\operatorname{div}(\omega - v)\|_{L^1((0,T)\times\Omega)} \, \|I\|_{L^\infty((0,T)\times\Omega)}$$

$$+ \|\operatorname{div}(v)\|_{L^\infty((0,T)\times\Omega)} \, \|I^{\varepsilon_1} - I^{\varepsilon_2}\|_{L^1((0,T)\times\Omega)}.$$

Finally, for a given $\xi > 0$, we can choose $v, h, \varepsilon_1, \varepsilon_2$ such that

$$\|(I^{\varepsilon_1} - I^{\varepsilon_2})(\cdot, s)\|_{L^1(\Omega)} \leq \xi,$$

because of the convergence of $R^\varepsilon \to 0$ in $L^1((0,T) \times \Omega)$, the convergence of $I^\varepsilon \to I$ in $L^p((0,T) \times \Omega)$ and the density of $\left(\mathcal{C}^\infty(\overline{(0,T) \times \Omega})\right)^d$ in $\left(L^1((0,T) \times \Omega)\right)^d$. We conclude that $\{I^\varepsilon\}$ is a Cauchy sequence in $\mathcal{C}^0([0,T], L^1(\Omega))$. Together with the convergence of $\{I^\varepsilon\}$ in $L^1((0,T) \times \Omega)$ it follows that

$$I \in \mathcal{C}^0([0,T], L^1(\Omega)),$$
$$I^\varepsilon \to I \text{ in } \mathcal{C}^0([0,T], L^1(\Omega)) \quad \text{for } \varepsilon \to 0.$$

Further from (5.1) we deduce that this convergence also holds in $\mathcal{C}^0([0,T], L^r(\Omega))$ for $1 \le r < \infty$.

In the next step, we show the renormalization property by multiplying the equation (5.2) by $\beta'(I^\varepsilon)$, where $\beta \colon \mathbb{R} \to \mathbb{R}$ is a $\mathcal{C}^1$-function, and get

$$\beta'(I^\varepsilon)\, R^\varepsilon = \beta'(I^\varepsilon)\, I_t^\varepsilon + \beta'(I^\varepsilon)\, \omega \cdot \nabla I^\varepsilon = \frac{\partial \beta(I^\varepsilon)}{\partial t} + \omega \cdot \nabla \beta(I^\varepsilon).$$

Next we multiply the equation by a test function $\varphi \in \mathcal{C}^1(\overline{(t_0, t_1) \times \Omega})$ and, using integration by parts, we obtain

$$\int\limits_{t_0}^{t_1} \int\limits_\Omega \beta(I^\varepsilon) \left(\frac{\partial \varphi}{\partial t} + \omega \cdot \nabla \varphi\right) \mathrm{d}x\,\mathrm{d}t + \int\limits_{t_0}^{t_1} \int\limits_\Omega \operatorname{div}(\omega)\, \beta(I^\varepsilon)\, \varphi\, \mathrm{d}x\,\mathrm{d}t$$
$$+ \int\limits_\Omega \beta\big(I^\varepsilon(0,\cdot)\big)\, \varphi(0,\cdot)\, \mathrm{d}x - \int\limits_\Omega \beta\big(I^\varepsilon(T,\cdot)\big)\, \varphi(T,\cdot)\, \mathrm{d}x$$
$$= \int\limits_{t_0}^{t_1} \int\limits_\Omega \beta'(I^\varepsilon)\, R^\varepsilon\, \varphi\, \mathrm{d}x\,\mathrm{d}t.$$

Due to the convergences we have shown above, we finally obtain equation (RenSol) by passing to the limit for $\varepsilon \to 0$.

$\square$

Remark 5.11.
Note that the proof is similar to the proof of Theorem VI.1.3. in [10], except that we have to estimate the integral

$$\int\limits_0^T \int\limits_\Omega \operatorname{div}(\omega)\, |I^{\varepsilon_1} - I^{\varepsilon_2}|\, \varphi\, \mathrm{d}x\,\mathrm{d}t$$

in inequality (5.4) differently.

Corollary 5.12. *[10]*
The renormalization property given in (RenSol) *also holds for* $\beta(s) = |s|$.

Proof.
We use the smooth approximation β_δ given in Lemma 5.10 and pass to the limit for $\delta \to 0$. $\qquad\square$

With these two properties we are prepared to prove the uniqueness of the weak solution.

Theorem 5.13 (Uniqueness)**.**
Let $\omega \in \left(L^1((0,T), W_0^{1,1}(\Omega))\right)^d$ *and* $I_0 \in L^\infty(\Omega)$. *Then there exists a unique weak solution* $I \in \mathcal{C}([0,T], L^r(\Omega)), 1 \le r < \infty$, *to the transport equation* (OFC).

In comparison to [10], the proof is more technical in this case, since we cannot exploit that the divergence of ω is bounded in $L^1((0,T), L^\infty(\Omega))$. Therefore, we need the following lemma.

Lemma 5.14.
Let $\varphi \in L^\infty((0,T) \times \Omega))$ *with* $\|\varphi(t, \cdot)\|_{L^1(\Omega)} \ge \varepsilon > 0$ *for all* $t \in [0,T]$. *Then there exists a constant* C_ε *(depending on* ε*), such that*

$$\|\varphi(t, \cdot)\|_{L^\infty(\Omega)} \le C_\varepsilon \|\varphi(t, \cdot)\|_{L^1(\Omega)} \quad \text{for all } t \in [0,T].$$

Proof.
It holds that

$$\|\varphi(t, \cdot)\|_{L^\infty(\Omega)} \le \|\varphi\|_{L^\infty((0,T)\times\Omega)} \le \underbrace{\frac{1}{\varepsilon}\|\varphi\|_{L^\infty((0,T)\times\Omega)}}_{:=C_\varepsilon} \|\varphi(t, \cdot)\|_{L^1(\Omega)}$$

for all $t \in [0,T]$. $\qquad\square$

Proof of Theorem 5.13.
From Corollary 5.7 and Theorem 5.9 we already know that problem (OFC) admits a weak solution $I \in \mathcal{C}^0([0,T], L^r(\Omega)) \cap L^\infty((0,T) \times \Omega), 1 \le r < \infty$.

We assume that there exist two distinct weak solutions I_1, I_2, and set $\bar{I} = I_1 - I_2$. Since $\bar{I}$ is continuous in time by Theorem 5.9, we can find an interval $[\delta, s] \subset [0,T]$ for which $\|\bar{I}(t, \cdot)\|_{L^1(\Omega)} \ge \varepsilon > 0$ holds for all $t \in [\delta, s]$.

Then by using the renormalization property (RenSol), we obtain

$$\int\limits_\delta^s \int\limits_\Omega |\bar{I}| \left(\frac{1}{s-\delta}\right) \, dx \, dt - \int\limits_\delta^s \int\limits_\Omega \text{div}(\omega) \, |\bar{I}| \left(\frac{t-\delta}{s-\delta}\right) \, dx \, dt - \int\limits_\Omega |\bar{I}(s)| \, dx = 0,$$

where we have chosen $\beta(\bar{I}) = |\bar{I}|$ and $\varphi(t,x) = \frac{t-\delta}{s-\delta}$. Then it follows that

$$
\begin{aligned}
\|\bar{I}(s,\cdot)\|_{L^1(\Omega)} &= \int_\Omega |\bar{I}(s,\cdot)| \,\mathrm{d}x\,\mathrm{d}t \\
&\leq \int_\delta^s \int_\Omega |\bar{I}| \left| \mathrm{div}(\omega)\,\frac{t-\delta}{s-\delta} - \frac{1}{s-\delta} \right| \,\mathrm{d}x\,\mathrm{d}t \\
&\leq \frac{1}{s-\delta} \int_\delta^s \int_\Omega |\bar{I}| \left(|\mathrm{div}(\omega)\,s| + 1 \right) \,\mathrm{d}x\,\mathrm{d}t \\
&\leq \frac{1}{s-\delta} \int_\delta^s s\,\|\bar{I}(t,\cdot)\|_{L^\infty(\Omega)}\,\|\mathrm{div}(\omega)\|_{L^1(\Omega)} + \|\bar{I}(t,\cdot)\|_{L^1(\Omega)} \,\mathrm{d}t \\
&\leq \frac{1}{s-\delta} \int_\delta^s \left(s\,C_\varepsilon\,\|\mathrm{div}(\omega)\|_{L^1(\Omega)} + 1 \right) \|\bar{I}(t,\cdot)\|_{L^1(\Omega)} \,\mathrm{d}t,
\end{aligned}
$$

where we used Lemma 5.14 in the last inequality. Finally, by using Gronwall's Lemma (cf. Theorem A.1), we obtain

$$
\|\bar{I}(s,\cdot)\|_{L^1(\Omega)} \leq 0 \cdot \exp\left(\frac{1}{s-\delta} \int_\delta^s s\,C_\varepsilon\,\|\mathrm{div}(\omega)\|_{L^1(\Omega)} + 1 \,\mathrm{d}t \right) = 0,
$$

but this is a contradiction to $\|\bar{I}(t,\cdot)\|_{L^1(\Omega)} > 0$ in $[\delta, s]$. Hence $\bar{I} = 0$, and thus the solution I is unique. $\qquad\square$

5.3. Weak-* Sequential Closedness

Finally, we show that the solution operator $\mathcal{T}$ is weakly-* sequentially closed.

Theorem 5.15 (Weak-* Sequential Closedness)**.**
Let $\omega \in \mathcal{U} := \left(L^p((0,T), W_0^{1,q}(\Omega)) \right)^d, 1 < p,q < \infty, \{\omega^k\} \subset \mathcal{U}, I_0 \in \mathcal{Z} := L^\infty(\Omega)$ and $\{I_0^k\} \subset \mathcal{Z}$ with $\|I_0^k\|_{L^\infty(\Omega)} \leq C\,\|I_0\|_{L^\infty(\Omega)}$ for a given constant $C > 0$. Then the solution operator $\mathcal{T}$ of the transport equation (OFC) *is weakly-* sequentially closed, i.e.,*

$$
\omega^k \rightharpoonup \omega \ \text{in } \mathcal{U} \quad \text{and} \quad I_0^k \rightharpoonup I_0 \ \text{in } L^r(\Omega), 1 < r < \infty,
$$

imply

$$
\mathcal{T}(\omega^k, I_0^k) = I^k \overset{*}{\rightharpoonup} I = \mathcal{T}(\omega, I_0) \ \text{in } L^\infty((0,T) \times \Omega).
$$

Proof.

First we note that the sequence $\{I^k\}$ is bounded by

$$I^k(t,x) \leq \|I_0^k(x)\|_{L^\infty(\Omega)} \leq C \, \|I_0(x)\|_{L^\infty(\Omega)}.$$

Thus, we deduce that there exists a subsequence $\{I^{k_j}\}$ and an $R \in L^\infty((0,T) \times \Omega)$, such that

$$I^{k_j} \overset{*}{\rightharpoonup} R \text{ in } L^\infty((0,T) \times \Omega).$$

Now we show that the pair (R, ω) satisfies the weak formulation of the transport equation (OFC), too:

$$\int_0^T \int_\Omega R \left(\varphi_t + \omega \cdot \nabla\varphi + \operatorname{div}(\omega)\,\varphi \right) - I^{k_j} \left(\varphi_t + \omega^{k_j} \cdot \nabla\varphi + \operatorname{div}(\omega^{k_j})\,\varphi \right) \mathrm{d}x\,\mathrm{d}t$$

$$+ \int_\Omega \left(I_0 - I_0^{k_j} \right) \varphi(0, \cdot) \, \mathrm{d}x$$

$$= \int_0^T \int_\Omega (R - I^{k_j}) \left(\varphi_t + \omega \cdot \nabla\varphi + \operatorname{div}(\omega)\,\varphi \right) \mathrm{d}x\,\mathrm{d}t$$

$$+ \int_0^T \int_\Omega I^{k_j} \left((\omega - \omega^{k_j}) \cdot \nabla\varphi + \operatorname{div}(\omega - \omega^{k_j})\,\varphi \right) \mathrm{d}x\,\mathrm{d}t + \int_\Omega \left(I_0 - I_0^{k_j} \right) \varphi(0, \cdot) \, \mathrm{d}x$$

For the first integral there holds

$$\int_0^T \int_\Omega (R - I^{k_j}) \left(\varphi_t + \omega \cdot \nabla\varphi + \operatorname{div}(\omega)\,\varphi \right) \mathrm{d}x\,\mathrm{d}t \to 0 \quad \text{for } k \to \infty,$$

because of the weak-* convergence of I^{k_j} towards R in $L^\infty((0,T) \times \Omega)$.

For the second integral we have that

$$\int_0^T \int_\Omega I^{k_j} \left((\omega - \omega^{k_j}) \cdot \nabla\varphi + \operatorname{div}(\omega - \omega^{k_j})\,\varphi \right) \mathrm{d}x\,\mathrm{d}t$$

$$\leq \|I_0\|_{L^\infty(\Omega)} \int_0^T \int_\Omega (\omega - \omega^{k_j}) \cdot \nabla\varphi + \operatorname{div}(\omega - \omega^{k_j})\,\varphi \, \mathrm{d}x\,\mathrm{d}t \to 0 \quad \text{for } k \to \infty,$$

due to the weak convergence $\omega^{k_j} \rightharpoonup \omega$ in $\left(L^p((0,T), W_0^{1,q}(\Omega)) \right)^d, 1 < p, q < \infty$. Note that $\varphi \in \mathcal{C}^{0,1}(\overline{(0,T) \times \Omega}) \subset W^{1,\infty}((0,T) \times \Omega)$ by Theorem 2.9.

For the third integral we obtain

$$\int\limits_{\Omega} \left(I_0 - I_0^{k_j}\right)\varphi(0, \cdot)\,\mathrm{d}x \to 0 \quad \text{for } k \to \infty,$$

because of the weak convergence $I_0^{k_j} \rightharpoonup I_0$ in $L^r(\Omega), 1 < r < \infty$.

We conclude that the pair (R, ω) solves the transport equation (OFC). Finally, from the uniqueness of the weak solution (Theorem 5.13) it follows that $R = I$. $\qquad\square$

6. Sequence Interpolation Problem

With the help of the previous chapter, we now have at hand all the tools to analyse the sequence interpolation problem, which we recall from Section 1.4.

Problem (Sequence Interpolation Problem).
Let $\mathcal{U}, \mathcal{Y}$ and $\mathcal{Z}$ be Banach spaces specified below. Given image samples $I_n \in \mathcal{Z}$ at discrete times $0 = t_0 < t_1 < ... < t_N = T$, find a vector field $\omega \in \mathcal{U}$, such that

$$\mathcal{T}(\omega, I_0)(t_n, \cdot) = I_n \quad \text{for } n = 0, ..., N \tag{SIP}$$

where $\mathcal{T} \colon \mathcal{U} \times \mathcal{Z} \to \mathcal{Y}, (\omega, I_0) \mapsto I$ denotes the solution operator of the optical flow constraint

$$I_t(t, x) + \omega(t, x) \cdot \nabla I(t, x) = 0 \quad \text{with } I(0, x) = I_0(x). \tag{OFC}$$

In view of the discussion in the previous chapter we initially set:

$$\mathcal{U} := \left(L^p((0, T), W_0^{1,q}(\Omega)) \right)^d, \qquad \text{for } 1 < p, q < \infty, \tag{6.1a}$$

$$\mathcal{Y} := \mathcal{C}([0, T], L^r(\Omega)), \qquad \text{for } 1 \leq r < \infty \qquad \text{and} \tag{6.1b}$$

$$\mathcal{Z} := L^\infty(\Omega). \tag{6.1c}$$

With the established theory on weak solutions in the previous chapter, we show next that the sequence interpolation problem (SIP) is ill-posed. Hence, we have to regularize the problem. In [15], an H^3- and a smoothened TV_ε-regularization were discussed for divergence-free optical flows. This means for example that deformations are excluded as solutions. However, we introduce in the following an H^1-regularization in space (and time), as well as a $W^{1,1+\tau}$-regularization, without any restriction on the divergence of the optical flow. In particular, we show for these regularizations the existence of a solution. Additionally, we show the stability of a solution for the H^1-regularization.

6.1. Local Ill-Posedness

Let us start with the ill-posedness of the sequence interpolation problem (SIP). Since in general a non-linear problem has no unique solution, we have to redefine the well-posedness of a non-linear problem. Moreover, we assume in this chapter that the sequence interpolation problem (SIP) admits a solution ω^+ for given (unperturbed) image samples $I_n, n = 0, ..., N$.

Definition 6.1 (Local well-posedness, [42])**.**
Let $\mathcal{U}$ and $\mathcal{Y}$ be Banach spaces. A non-linear operator equation $\mathcal{A}\omega = y$ with $\mathcal{A} \colon \mathcal{U} \to \mathcal{Y}$ is called locally well-posed *at $\omega^+ \in \mathcal{U}$, if there exists an $r > 0$, such that for all sequences $\{\omega_r^k\} \subset B_r(\omega^+)$ there holds*

$$\lim_{k \to \infty} \|\mathcal{A}(\omega_r^k) - \mathcal{A}(\omega^+)\|_{\mathcal{Y}} = 0 \implies \lim_{k \to \infty} \|\omega_r^k - \omega^+\|_{\mathcal{U}} = 0.$$

Otherwise the problem is called locally ill-posed*, for each $r > 0$ there exists a sequence $\{\omega_r^k\} \subset B_r(\omega^+)$, such that*

$$\lim_{k \to \infty} \|\mathcal{A}(\omega_r^k) - \mathcal{A}(\omega^+)\|_{\mathcal{Y}} = 0, \text{ but } w_r^k \not\to \omega^+ \text{ in } \mathcal{U} \text{ for } k \to \infty.$$

In particular, a non-linear problem is locally ill-posed:

- if ω^+ is not locally unique or

- if ω^+ does not depend continuously on the input data.

In [21, 42] it is shown that a non-linear inverse problem $\mathcal{A}\omega = f$ is locally ill-posed, if $\mathcal{A} \colon \mathcal{U} \to \mathcal{Y}$ is a continuous, compact operator, which additionally is weakly sequentially closed. Basically, this proof exploits that continuity, compactness and weak sequential closedness of the operator $\mathcal{A}$ imply that

$$\omega^k \rightharpoonup \omega \text{ in } \mathcal{U} \implies \mathcal{A}\omega^k \to \mathcal{A}\omega \in \mathcal{Y} \tag{6.2}$$

and, consequently, the ill-posedness of $\mathcal{A}$, if $\omega^k \not\to \omega$ in $\mathcal{U}$. However, in our case we cannot ensure the compactness of the operator $\mathcal{T}$. But we can show that property (6.2) holds at least for a suitably chosen subspace of $\mathcal{U}$ by using the Aubin-Lions Lemma (Theorem 2.12) and the stability result of Boyer and Fabrie (Theorem 5.2).

Theorem 6.2.
Let $\mathcal{U}, \mathcal{Y}$ and $\mathcal{Z}$ be given as in (6.1) with $p = q = 2$. Moreover, we define the function space $\mathcal{V} := \left(\{ \varphi \in L^2((0,T), H_0^1(\Omega)) \colon \text{ with } \varphi_t \in L^2((0,T), L^2(\Omega)) \} \right)^d$, which is a Banach space (cf. [10]) equipped with the norm

$$\|v\|_{\mathcal{V}} := \|v\|_{L^2((0,T), H_0^1(\Omega))} + \|v_t\|_{L^2((0,T), L^2(\Omega))}.$$

Note that $\mathcal{V} \subset \mathcal{U}$. Then the sequence interpolation problem (SIP) is (at least) locally ill-posed at any point $\omega^+ \in \mathcal{V}$ with $\operatorname{div}(\omega^+) \in L^1((0,T), L^\infty(\Omega))$.

Proof.
We set $\mathcal{V}_{\mathrm{div}} := \{ v \in \mathcal{V} \colon \text{ with } \operatorname{div}(v) = 0 \}$ and assume that $\{\varphi^k\}$ is an orthonormal basis of $\mathcal{V}_{\mathrm{div}}$.

Moreover, let $\omega^+ \in \mathcal{V} \subset \mathcal{U}$ with $\operatorname{div}(\omega^+) \in L^1((0,T), L^\infty(\Omega))$ be an inner point of $\mathcal{V}$, i.e., there exists an r, such that $B_r(\omega^+) \subset \mathcal{V}$. Then we consider the sequence

$$\omega_r^k = \omega^+ + r\,\varphi^k,$$

which weakly converges towards ω^+ in $\mathcal{V}$. Note that $\text{div}(w_r^k) \in L^1((0,T), L^\infty(\Omega))$ for $k \in \mathbb{N}_0$.

Next, by applying the Aubin-Lions Lemma (Theorem 2.12) we obtain

$$\omega_r^k \to \omega^+ \text{ in } \left(L^2((0,T), L^2(\Omega))\right)^d.$$

Finally, by using the stability result of Boyer and Fabrie (Theorem 5.2) we get

$$\mathcal{T}(\omega_r^k, I_0) = I_r^k \to I = \mathcal{T}(\omega^+, I_0) \text{ in } \mathcal{C}^0([0,T], L^r(\Omega)),$$

for $1 \leq r < \infty$, but

$$\|\omega_r^k - \omega^+\|_\mathcal{V} = r.$$

As a consequence, we conclude that the problem is locally ill-posed at $\omega^+ \in \mathcal{V}$ with $\text{div}(\omega^+) \in L^1((0,T), L^\infty(\Omega))$. $\qquad\square$

6.2. Regularization of the Problem

As we have seen the sequence interpolation problem (SIP) is locally ill-posed. Hence, small errors in the image samples $I_n, n = 0, ..., N$, can lead to large errors in the reconstruction of the optical flow ω and the video sequence I. As discussed in Chapter 4, we can counteract this error amplification by adding one or more regularization terms, which involve a priori information of the solution, to the objective functional. Finally, this regularization leads to the minimization problem

$$\left(\omega^*, I^*\right) = \operatorname*{argmin}_{(\omega, I) \in \mathcal{U} \times \mathcal{Y}} J(\omega, I) := \sum_{n=0}^{N} \int_\Omega |I(t_n, x) - I_n(x)|^2 \, dx \tag{NP}$$
$$+ \alpha \, R^x(\omega) + \beta \, R^t(\omega)$$

subject to

$$I_t(t, x) + \omega(t, x) \cdot \nabla I(t, x) = 0 \quad \text{with } I(0, x) = I_0(x), \tag{OFC}$$

where $\alpha > 0$, $\beta \geq 0$ and $I_n \in \mathcal{Z}, n = 0, ..., N$. Here, $R^x \colon \mathcal{U} \to \mathbb{R}$ denotes a regularization in space and $R^t \colon \mathcal{U} \to \mathbb{R}$ a regularization in time. In the last chapter we have shown that the optical flow constraint (OFC) admits a unique solution $I = I(\omega)$, thus, problem (NP) is equivalent to the reduced problem

$$\omega^* = \operatorname*{argmin}_{\omega \in \mathcal{U}} \hat{J}(\omega) := J(\omega, I(\omega)) = \sum_{n=0}^{N} \int_\Omega |I(t_n, x) - I_n(x)|^2 \, dx \tag{$\widehat{\text{NP}}$}$$
$$+ \alpha \, R^x(\omega) + \beta \, R^t(\omega).$$

The existence of a solution to problem (NP) can be ensured under the following assumptions, as we will see.

Assumptions 6.3.

  (i) $\mathcal{U}$ is a reflexive space and there exist $1 < p, q < \infty$ such that

$$\mathcal{U} \hookrightarrow \left(L^p((0,T), W_0^{1,q}(\Omega))\right)^d,$$

  (ii) $\mathcal{Y} := \mathcal{C}([0,T], L^2(\Omega))$,

  (iii) $I_n \in \mathcal{Z} := L^\infty(\Omega)$, for $n = 0, ..., N$,

  (iv) $R^x, R^t \colon \mathcal{U} \to \mathbb{R}$ are continuous and convex functionals,

  (v) $R^x + R^t \colon \mathcal{U} \to \mathbb{R}$ is $\mathcal{U}$-coercive, i.e.,

$$\|\omega\|_{\mathcal{U}} \to \infty \quad \Longrightarrow \quad R^x(\omega) + R^t(\omega) \to \infty.$$

If $\beta = 0$, we demand the preceding conditions with $R^t(\omega) := 0$.

The procedure for proving the existence of a solution to problem (NP) is similar to the linear case (cf. Theorem 4.8). However, note that for an arbitrary non-linear and non-convex operator $\mathcal{A} \colon \mathcal{U} \to \mathcal{Y}$ and $f \in \mathcal{Y}$ the term $\|\mathcal{A}\omega - f\|_{\mathcal{Y}}$ is not necessarily weakly lower semicontinuous. But with the help of the weak-* sequential closedness of $\mathcal{T}$ we can still ensure the weak lower semicontinuity of $\hat{J}$.

Lemma 6.4.
Let Assumptions 6.3 hold. Then the cost functional $\hat{J}$ defined in $\widehat{(\text{NP})}$ is weakly lower semicontinuous, i.e.,

$$\omega^k \rightharpoonup \omega \text{ in } \mathcal{U} \quad \Longrightarrow \quad \hat{J}(\omega) \le \liminf_{k \to \infty} \hat{J}(\omega^k).$$

Proof.
Let $\{\omega^k\}$ be a sequence, weakly convergent towards ω in $\mathcal{U}$. Then from the weak-* sequential closedness of $\mathcal{T}$ (cf. Theorem 5.15) it follows that

$$\mathcal{T}(\omega^k, I_0) = I^k \overset{*}{\rightharpoonup} I = \mathcal{T}(\omega, I_0) \quad \text{in } L^\infty((0,T) \times \Omega)$$

and, consequently, we conclude

$$\mathcal{T}(\omega^k, I_0) = I^k \rightharpoonup I = \mathcal{T}(\omega, I_0) \quad \text{in } L^2((0,T) \times \Omega).$$

Furthermore, since a continuous convex functional mapping from a Banach space to $\mathbb{R}$ is weakly lower semicontinuous (cf. [20]), we have

$$\sum_{n=0}^{N} \|I(t_n, x) - I_n(x)\|_{L^2(\Omega)}^2 \le \liminf_{k \to \infty} \sum_{n=0}^{N} \|I^k(t_n, x) - I_n(x)\|_{L^2(\Omega)}^2$$

and

$$\alpha\, R^x(\omega) + \beta\, R^t(\omega) \le \liminf_{k \to \infty} \left(\alpha\, R^x(\omega^k) + \beta\, R^t(\omega^k)\right).$$

Thus, we immediately deduce the statement of the lemma. $\qquad\square$

Finally, we show, similarly to the linear case, the existence of an optimal solution to problem (NP) or $(\widehat{\mathrm{NP}})$, respectively.

Theorem 6.5.
Let Assumptions 6.3 hold. Then the optimization problem

$$\left(\omega^*, I^*\right) = \underset{(\omega,I)\in\mathcal{U}\times\mathcal{Y}}{\operatorname{argmin}} J(\omega, I) := \sum_{n=0}^{N} \int_{\Omega} |I(t_n, x) - I_n(x)|^2 \, \mathrm{d}x \tag{NP}$$
$$+ \alpha \, R^x(\omega) + \beta \, R^t(\omega)$$

subject to

$$I_t(t, x) + \omega(t, x) \cdot \nabla I(t, x) = 0 \quad \text{with } I(0, x) = I_0(x), \tag{OFC}$$

where $\alpha > 0$ and $\beta \geq 0$, admits a solution $(\omega^*, I^*) \in \mathcal{U} \times \mathcal{Y}$.

Proof.
Consider a monotone minimizing sequence $\{\omega^k\}$ with

$$\hat{J}(\omega^k) \to \inf_\omega \hat{J}(\omega) =: d \geq 0.$$

From the estimate

$$\alpha \, R^x(\omega^k) + \beta \, R^t(\omega^k) \leq \hat{J}(\omega^k) \leq \hat{J}(\omega^0)$$

and the $\mathcal{U}$-coercivity of $\alpha \, R^x + \beta \, R^t$ we deduce the boundedness of the sequence $\{\omega^k\}$.

Thus, there exists a subsequence $\{\omega^{k_j}\}$, which converges weakly towards $\omega^* \in \mathcal{U}$, since $\mathcal{U}$ is reflexive.

Hence, from the weak lower semicontinuity of $\hat{J}$ we conclude

$$d = \lim_{k\to\infty} \hat{J}(\omega^k) = \liminf_{k_j\to\infty} \hat{J}(\omega^{k_j}) \geq \hat{J}(\omega^*) \geq d.$$

Therefore, ω^* is a solution to problem $(\widehat{\mathrm{NP}})$. Finally, from Theorem 5.13 we deduce that $(\omega^*, I^*) = (\omega^*, \mathcal{T}(\omega^*, I_0)) \in \mathcal{U} \times \mathcal{Y}$ is a solution to problem (NP). $\qquad\square$

Remark 6.6.
Basically, we use the same techniques as in the existence proof of Chen for the TV_ε-regularization (cf. Theorem 4.5. in [15]). Both proofs only differ in their theories on weak solutions of transport equations, which enables us to show the existence of a solution without restriction on divergence-free vector fields. However, in [15] the weak sequential closedness of $\mathcal{T}$ is deduced from a stability result on weak solutions established by DiPerna and Lions (cf. Theorem II.4. in [19] or Theorem 4.4. in [15]). Unfortunately, this stability result requires the strong convergence of the subsequence ω^{k_j} and consequently is not applicable. But by using the more general Theorem II.7. in [19] the statement of Theorem 4.5. in [15] still holds.

In the following we introduce an H^1-regularization in space (and time), as well as a $W^{1,1+\tau}$-regularization. Here, if not stated otherwise, we restrict ourselves to the case $\beta = 0$, i.e., without regularization in time.

6.2.1. H^1-Regularization in Space

We start with the H^1-regularization in space given by

$$R^x(\omega) := \frac{1}{2} \int_0^T \int_\Omega |\nabla \omega|^2 \, \mathrm{d}x \, \mathrm{d}t. \tag{6.3}$$

As control space, we choose $\mathcal{U} := \left(L^2((0,T), H_0^1(\Omega)) \right)^d$, because in this case the solution operator $\mathcal{T}$, as well as the integrals in the cost functional, are well-defined and the regularization term defined in (6.3) is $\mathcal{U}$-corecive, since $\frac{1}{2}\|\omega\|_{\mathcal{U}}^2 = R^x(\omega)$. Thus, we deduce the existence of an optimal solution from Theorem 6.5.

Corollary 6.7 (Existence).
Consider $\mathcal{U} := \left(L^2((0,T), H_0^1(\Omega)) \right)^d$, $\mathcal{Y} := \mathcal{C}([0,T], L^2(\Omega))$ and $I_n \in \mathcal{Z} := L^\infty(\Omega)$ for $n = 0, ..., N$. Then the optimization problem

$$(\omega^*, I^*) = \operatorname*{argmin}_{(\omega, I) \in \mathcal{U} \times \mathcal{Y}} J(\omega, I) = \sum_{n=0}^N \int_\Omega |I(t_n, x) - I_n(x)|^2 \, \mathrm{d}x$$

$$+ \frac{\alpha}{2} \int_0^T \int_\Omega |\nabla \omega|^2 \, \mathrm{d}x \, \mathrm{d}t$$

subject to

$$I_t(t, x) + \omega(t, x) \cdot \nabla I(t, x) = 0 \quad \text{with } I(0, x) = I_0(x), \tag{OFC}$$

where $\alpha > 0$, admits a solution $(\omega^*, I^*) \in \mathcal{U} \times \mathcal{Y}$.

6.2.2. H^1-Regularization in Space and Time

In this section, we consider the case of additional regularization in time, that is $\beta > 0$. To be more precise, we use an H^1-regularization in space and time, i.e.,

$$R^x(\omega) := \frac{\alpha}{2} \int_0^T \int_\Omega |\nabla \omega|^2 \, \mathrm{d}x \, \mathrm{d}t \quad \text{and} \quad R^t(\omega) := \frac{\beta}{2} \int_0^T \int_\Omega |\omega_t|^2 \, \mathrm{d}x \, \mathrm{d}t. \tag{6.4}$$

In this case, we choose as the space of admissible vector fields ω

$$
\begin{aligned}
\mathcal{U} &:= \left(H^1_{\Gamma_x}((0,T) \times \Omega) \right)^d \\
&:= \left(\left\{ u \in H^1((0,T) \times \Omega) : \text{ with } u|_{\Gamma_x} = 0 \right\} \right)^d \\
&= \left(\left\{ u \in L^2\big((0,T), H^1_0(\Omega)\big) : \text{ with } u_t \in L^2\big((0,T), L^2(\Omega)\big) \right\} \right)^d,
\end{aligned}
$$

where $\Gamma_x = [0,T] \times \partial\Omega$. This space equipped with the norm

$$
\|u\|_{\mathcal{U}} := \|u\|_{L^2((0,T), H^1_0(\Omega))} + \|u_t\|_{L^2((0,T), L^2(\Omega))}
$$

is a Hilbert space (cf. [10]). Note that we only have a spatial boundary condition, which is necessary due to the theory of weak solutions of transport equations (cf. Chapter 5). For the $\mathcal{U}$-coercivity of the regularization $\alpha\, R^x(\omega) + \beta\, R^t(\omega)$ defined in (6.4) we estimate

$$
\begin{aligned}
\alpha\, R^x(\omega) + \beta\, R^t(\omega) &\geq \frac{1}{2}\min(\alpha,\beta) \left(\int_0^T \int_\Omega |\nabla\omega|^2 \,\mathrm{d}x\,\mathrm{d}t + \int_0^T \int_\Omega |\omega_t|^2 \,\mathrm{d}x\,\mathrm{d}t \right) \\
&= \frac{1}{2}\min(\alpha,\beta)\|\omega\|^2_{\mathcal{U}}.
\end{aligned}
$$

Consequently, we obtain the existence of an optimal solution from Theorem 6.5.

Corollary 6.8 (Existence).
Consider $\mathcal{U} := \left(H^1_{\Gamma_x}((0,T) \times \Omega) \right)^d$, $\mathcal{Y} := \mathcal{C}([0,T], L^2(\Omega))$ and $I_n \in \mathcal{Z} := L^\infty(\Omega)$ for $n = 0, ..., N$. Then the optimization problem

$$
(\omega^*, I^*) = \operatorname*{argmin}_{(\omega, I) \in \mathcal{U} \times \mathcal{Y}} J(\omega, I) = \sum_{n=0}^N \int_\Omega |I(t_n, x) - I_n(x)|^2 \,\mathrm{d}x
$$

$$
+ \frac{\alpha}{2} \int_0^T \int_\Omega |\nabla\omega|^2 \,\mathrm{d}x\,\mathrm{d}t + \frac{\beta}{2} \int_0^T \int_\Omega |\omega_t|^2 \,\mathrm{d}x\,\mathrm{d}t
$$

subject to

$$
I_t(t,x) + \omega(t,x) \cdot \nabla I(t,x) = 0 \quad \text{with } I(0,x) = I_0(x), \tag{OFC}
$$

where $\alpha, \beta > 0$, admits a solution $(\omega^*, I^*) \in \mathcal{U} \times \mathcal{Y}$.

6.2.3. $W^{1,1+\tau}$-Regularization

In Chapter 8, we illustrate with numerical test examples, that the H^1-regularization leads to accurate reconstruction results, if we seek a smooth optical flow. But if we look

for a discontinuous vector field, then the reconstruction is very imprecise (cf. Section 8.5). This is caused by the fact, that we can only obtain smooth solutions with an H^1-regularization, as we have already discussed in Chapter 4. However, in Chapter 4 we have also motivated, that a total variation term, i.e.,

$$R^x(\omega) := \int_0^T \int_\Omega |\nabla\omega|\,\mathrm{d}x\,\mathrm{d}t,$$

is more suitable for the regularization of the sequence interpolation problem (SIP).

Unfortunately, for this regularization term we are not able to show existence of a solution. In fact:

- For $\mathcal{U} := \left(L^1((0,T), BV_0(\Omega))\right)^d$ we do not have established a theory of weak solutions for the transport equation.

- For $\mathcal{U} := \left(L^1((0,T), W_0^{1,1}(\Omega))\right)^d$ the control space is not dual or reflexive, which we would need to exploit in the existence proof.

- For $\mathcal{U} := \left(L^p((0,T), W_0^{1,q}(\Omega))\right)^d, 1 < p,q < \infty$, the cost functional J is not $\mathcal{U}$-coercive, which we need for the existence proof.

In [15] it is suggested to use a smoothened total variation as regularization term, i.e.,

$$R^x(\omega) := \int_0^T \int_\Omega \sqrt{|\nabla\omega|^2 + \delta}\,\mathrm{d}x\,\mathrm{d}t \tag{6.5}$$

for some $\delta > 0$, and to seek a solution ω in the space $\mathcal{U} = \left(L^2((0,T), W_0^{1,1+\tau}(\Omega))\right)^d$ for $\tau > 0$ sufficiently small. This is motivated in [15] by the claim, that for a given $\delta > 0$ there exist constants $\tau > 0$ and $C > 0$, such that the following inequality hold

$$\int_\Omega \sqrt{|\nabla\omega|^2 + \delta}\,\mathrm{d}x \geq C\,\|\omega\|_{W_0^{1,1+\tau}} \quad \text{for all } \omega \in W_0^{1,1+\tau}. \tag{6.6}$$

But this inequality does not necessarily hold as the following counterexample shows. Therefore, the existence proof in [15] for a minimizer of problem (NP) with regularization term (6.5) is incorrect since in [15] the $\mathcal{U}$-coercivity of the regularization term $R^x(\omega)$ is deduced from inequality (6.6).

Counterexample 6.9.
Let $\Omega := [-1, 1] \subset \mathbb{R}$. We define for $0 < \varepsilon < 1$ a sequence of functions

$$\omega_\varepsilon(x) = \begin{cases} 1 - \left|\frac{x}{\varepsilon}\right| & , x \in [-\varepsilon, \varepsilon] \\ 0 & , x \in \Omega \setminus [-\varepsilon, \varepsilon] \end{cases}.$$

Then the weak derivative ω_ε' is given by

$$\omega_\varepsilon'(x) = \begin{cases} \frac{1}{\varepsilon} & , x \in [-\varepsilon, 0] \\ -\frac{1}{\varepsilon} & , x \in [0, \varepsilon] \\ 0 & , else \end{cases}.$$

Finally, we obtain

$$\|\omega_\varepsilon\|_{W_0^{1,1+\tau}(\Omega)} = \left(\int\limits_{-\varepsilon}^{\varepsilon} \left| \frac{1}{\varepsilon} \right|^{1+\tau} dx \right)^{\frac{1}{1+\tau}} = \left(\frac{2}{\varepsilon^\tau} \right)^{\frac{1}{1+\tau}} \to \infty, \quad for \ \varepsilon \to 0, \ and \ \tau > 0,$$

but on the other hand it holds that

$$\int\limits_{\Omega} \sqrt{|\omega_\varepsilon'|^2 + \delta} \, dx \leq \int\limits_{\Omega} \left(|\omega_\varepsilon'| + \sqrt{\delta} \right) dx$$

$$= \int\limits_{-\varepsilon}^{\varepsilon} \left| \frac{1}{\varepsilon} \right| dx + \int\limits_{-1}^{1} \sqrt{\delta} \, dx = 2 + 2\sqrt{\delta} \to 2 \quad , \ for \ \delta \to 0.$$

Hence, there exist no constants $\tau > 0$ and $C > 0$ such that inequality (6.6) holds.

As a remedy, we propose to use a $(1+\tau)$-energy functional as regularization term given by

$$R^x(\omega) := \int\limits_0^T \int\limits_\Omega |\nabla\omega|^{1+\tau} \, dx \, dt \tag{6.7}$$

or a smoothened $(1+\tau)$-energy functional given by

$$R_\delta^x(\omega) := \int\limits_0^T \int\limits_\Omega \left(|\nabla\omega|^2 + \delta \right)^{\frac{1+\tau}{2}} \, dx \, dt \tag{6.8}$$

for $\tau > 0$ and $\delta > 0$ sufficiently small. Due to the inequality

$$R^x(\omega) = \int\limits_0^T \int\limits_\Omega |\nabla\omega|^{1+\tau} \, dx \, dt$$

$$\leq \int\limits_0^T \int\limits_\Omega \left(|\nabla\omega|^2 + \delta \right)^{\frac{1+\tau}{2}} \, dx \, dt = R_\delta^x(\omega)$$

$$\leq \int\limits_0^T \int\limits_\Omega \left(|\nabla\omega|^{1+\tau} + \delta^{\frac{1+\tau}{2}} \right) dx \, dt = R^x(\omega) + \delta^{\frac{1+\tau}{2}} |\Omega| \, T$$

both regularization terms (6.7) and (6.8) differ only slightly and thus are supposed to lead to comparable optimal solutions. We note that the second inequality holds for $0 < \tau \leq 1$. Regarding to the calculation of the optimality system (cf. Theorem 6.14) we prefer the smoothened $(1+\tau)$-energy functional in the following discussion, since this term is differentiable.

Subsequently, we look for a solution ω in the space $\mathcal{U} := \left(L^{1+\tau}((0,T), W_0^{1,1+\tau}(\Omega)) \right)^d$.

Indeed, this regularization term is $\mathcal{U}$-coercive, as the following estimate shows

$$
\begin{aligned}
\|\omega\|_{\mathcal{U}}^{1+\tau} &= \int_0^T \int_\Omega |\nabla\omega|^{1+\tau} \, \mathrm{d}x \, \mathrm{d}t \\
&= \int_0^T \int_\Omega \left(|\nabla\omega|^2\right)^{\frac{1+\tau}{2}} \, \mathrm{d}x \, \mathrm{d}t \leq \int_0^T \int_\Omega \left(|\nabla\omega|^2 + \delta\right)^{\frac{1+\tau}{2}} \, \mathrm{d}x \, \mathrm{d}t.
\end{aligned}
$$

In particular, it is reasonable to use this regularization term in order to preserve discontinuities. We show this by verifying the conditions (RTC1) to (RTC3), which we have derived in Section 4.3. With the notation in Section 4.3 we have

$$
\Phi(s) = (s^2 + \delta)^{\frac{1+\tau}{2}},
$$

and calculate

$$
\begin{aligned}
\Phi'(s) &= (1+\tau)(s^2+\delta)^{\frac{\tau-1}{2}} s, &&\text{and} \\
\Phi''(s) &= (\tau^2-1)(s^2+\delta)^{\frac{\tau-3}{2}} s^2 + (1+\tau)(s^2+\delta)^{\frac{\tau-1}{2}} \\
&= \left(\delta + \tau\, s^2\right)(1+\tau)\left(s^2+\delta\right)^{\frac{\tau-3}{2}}.
\end{aligned}
$$

Finally, we obtain

$$
\begin{aligned}
\lim_{s\to 0} \Phi''(s) &= \lim_{s\to 0} \frac{\Phi'(s)}{s} = (1+\tau)\delta^{\frac{\tau-1}{2}}, \\
\lim_{s\to\infty} \Phi''(s) &= \lim_{s\to\infty} \frac{\Phi'(s)}{s} = 0, \quad \text{for } \tau < 1 \quad \text{and} \\
\lim_{s\to\infty} \frac{\Phi''(s)}{\frac{\Phi'(s)}{s}} &= \tau.
\end{aligned}
$$

Hence, all the conditions (RTC1) to (RTC3) are (approximately) satisfied for τ sufficiently small.

Furthermore, we deduce the convexity of the regularization term $R^x(\omega)$ from the fact that $\Phi' \colon [0,\infty) \to \mathbb{R}$ is non-negative.

Finally, the existence of a solution follows from Theorem 6.5.

Corollary 6.10 (Existence).
Consider the spaces $\mathcal{U} := \left(L^{1+\tau}((0,T), W_0^{1+\tau}(\Omega))\right)^d$ for some $\tau > 0$ sufficiently small, $\mathcal{Y} := \mathcal{C}([0,T], L^2(\Omega))$ and $\mathcal{Z} := L^\infty(\Omega)$. Assume $I_n \in \mathcal{Z}$ for $n = 0, ..., N$. Then the optimization problem

$$(\omega^*, I^*) = \operatorname*{argmin}_{(\omega, I) \in \mathcal{U} \times \mathcal{Y}} J(\omega, I) = \sum_{n=0}^{N} \int_{\Omega} |I(t_n, x) - I_n(x)|^2 \, \mathrm{d}x$$

$$+ \alpha \int_0^T \int_\Omega \left(|\nabla \omega|^2 + \delta\right)^{\frac{1+\tau}{2}} \, \mathrm{d}x \, \mathrm{d}t$$

subject to

$$I_t(t,x) + \omega(t,x) \cdot \nabla I(t,x) = 0 \quad \text{with } I(0,x) = I_0(x), \tag{OFC}$$

where $\alpha > 0$ and $\delta \geq 0$, admits a solution $(\omega^*, I^*) \in \mathcal{U} \times \mathcal{Y}$.

6.3. Stability of the Regularized Problem

In this section we analyse the stability of problem (NP) by adapting the more general work of Engl, Hanke and Neubauer [21] to our concrete non linear inverse problem (SIP). Stability shall be understood as follows:

$$I_n^\varepsilon \to I_n \text{ in } \mathcal{Z}, \quad \text{for all } n = 0, ..., N \quad \implies \quad \omega^\varepsilon \to \omega^+ \in \mathcal{U},$$

where $\omega^+ \in \mathcal{U}$ denotes an exact solution of the sequence interpolation problem (SIP) for given (unperturbed) image samples $I_n \in \mathcal{Z}, n = 0, ..., N$, and ω^ε denotes a solution of the regularized problem (NP) for given perturbed image samples $I_n^\varepsilon \in \mathcal{Z}, n = 0, ..., N$.

For the stability analysis, we set

$$I_\# = \left(I_0, I_1, ..., I_N\right) \in \mathcal{Z}^{N+1}$$
$$I_\#^\varepsilon = \left(I_0^\varepsilon, I_1^\varepsilon, ..., I_N^\varepsilon\right) \in \mathcal{Z}^{N+1}$$

and define

$$I_\#^\varepsilon \to I_\# \text{ in } \mathcal{Z}^{N+1}, \quad \text{if and only if} \quad I_n^\varepsilon \to I_n \text{ in } \mathcal{Z}, \quad \text{for all } n = 0, ..., N.$$

In a first step, we now show that a solution to the regularized problem (NP) for fixed $\alpha > 0$ and $\beta \geq 0$ depends continuously on the input data $I_\#^\varepsilon$.

Theorem 6.11.
Let Assumptions 6.3 hold and let $I_\#^\varepsilon$ be a sequence of image samples which converges towards $I_\#$ in $\mathcal{Z}^{N+1}$. Furthermore, we denote by $\{\omega^\varepsilon\} \subset \mathcal{U}$ a corresponding sequence of minimizers of

$$\hat{J}(\omega; I_\#^\varepsilon) := \sum_{n=0}^N \int_\Omega |I(x,t_n) - I_n^\varepsilon(x)|^2 \, \mathrm{d}x + \alpha \, R^x(\omega) + \beta \, R^t(\omega),$$

where $\alpha > 0$ and $\beta \geq 0$, which exists by Theorem 6.5. Then there exists a convergent subsequence $\{\omega^{\varepsilon_k}\}$ and any convergent subsequence converges towards a minimizer $\omega^* \in \mathcal{U}$ of $\hat{J}(\,\cdot\,; I_\#)$. Additionally, if the optimal solution ω^* is unique, then the complete sequence $\{\omega^\varepsilon\}$ converges towards ω^*.

Proof.
Since ω^ε is a minimizer of $\hat{J}(\,\cdot\,; I_\#^\varepsilon)$, we get, by using the coercivity of $\hat{J}$,

$$\sum_{n=0}^N \|\mathcal{T}(\omega^\varepsilon, I_0^\varepsilon)(t_n, \cdot) - I_n^\varepsilon\|_{\mathcal{Y}}^2 + \alpha \, R^x(\omega^\varepsilon) + \beta \, R^t(\omega^\varepsilon) = \hat{J}(\omega^\varepsilon; I_\#^\varepsilon)$$

$$\leq \hat{J}(\omega; I_\#^\varepsilon) = \sum_{n=0}^N \|\mathcal{T}(\omega, I_0^\varepsilon)(t_n, \cdot) - I_n^\varepsilon\|_{\mathcal{Y}}^2 + \alpha \, R^x(\omega) + \beta \, R^t(\omega)$$

$$\leq \sum_{n=0}^N \left(\|\mathcal{T}(\omega, I_0^\varepsilon)(t_n, \cdot) - I_n\|_{\mathcal{Y}}^2 + \|I_n - I_n^\varepsilon\|_{\mathcal{Y}}^2 \right) + \alpha \, R^x(\omega) + \beta \, R^t(\omega)$$

for all $\omega \in \mathcal{U}$. Hence, the sequence $\{\omega^\varepsilon\}$ is bounded due to the coercivity of $\hat{J}$ and we deduce the existence of a subsequence $\{\omega^{\varepsilon_k}\}$ which weakly converges towards $\tilde{\omega} \in \mathcal{U}$, since $\mathcal{U}$ is reflexive. Next, by using the weak-* sequential closedness of $\mathcal{T}$ (see Theorem 5.15), we get

$$\mathcal{T}(\omega^{\varepsilon_k}, I_0^{\varepsilon_k}) = I^{\varepsilon_k} \overset{*}{\rightharpoonup} \tilde{I} = \mathcal{T}(\tilde{\omega}, I_0) \quad \text{in } L^\infty((0,T) \times \Omega)$$

and, consequently, we conclude

$$\mathcal{T}(\omega^{\varepsilon_k}, I_0^{\varepsilon_k}) = I^{\varepsilon_k} \rightharpoonup \tilde{I} = \mathcal{T}(\tilde{\omega}, I_0) \quad \text{in } L^2((0,T) \times \Omega).$$

Finally, by using the weak lower semicontinuity of $\hat{J}$, we obtain

$$\hat{J}(\tilde{\omega}; I_\#) \leq \liminf_{k \to \infty} \hat{J}(\omega^{\varepsilon_k}; I_\#^{\varepsilon_k}) \leq \limsup_{k \to \infty} \hat{J}(\omega^{\varepsilon_k}; I_\#^{\varepsilon_k})$$

$$\leq \lim_{k \to \infty} \hat{J}(\omega; I_\#^{\varepsilon_k}) = \hat{J}(\omega; I_\#)$$

for all $\omega \in \mathcal{U}$. In particular, $\tilde{\omega}$ is a minimizer of $J(\,\cdot\,; I_\#)$ and

$$\lim_{j \to \infty} J(\omega^{\varepsilon_k}, I_\#^{\varepsilon_k}) = J(\tilde{\omega}, I_\#). \tag{6.9}$$

For proving strong convergence, we define

$$R(\omega) := \alpha\, R^x(\omega) + \beta\, R^t(\omega)$$

and assume $\{\omega^{\varepsilon_k}\}$ does not converge strongly towards $\tilde{\omega}$. Then

$$D := \limsup_{k \to \infty} R\big(\omega^{\varepsilon_k}\big) > R\big(\tilde{\omega}\big)$$

and there exists a subsequence $\{\omega^{\varepsilon_{k_j}}\}$ which satisfies $\omega^{\varepsilon_{k_j}} \rightharpoonup \tilde{\omega}, \mathcal{T}(\omega^{\varepsilon_{k_j}}, I_0^{\varepsilon_{k_j}}) \rightharpoonup \mathcal{T}(\tilde{\omega}, I_0)$ and $R\big(\omega^{\varepsilon_{k_j}}\big) \to D$. As a consequence of equation (6.9) we obtain

$$\sum_{n=0}^{N} \|\mathcal{T}\big(\tilde{\omega}, I_0\big)(t_n, \cdot) - I_n\|_{\mathcal{U}}^2 = \lim_{k \to \infty} \sum_{n=0}^{N} \|\mathcal{T}\big(\omega^{\varepsilon_{k_j}}, I_0^{\varepsilon_{k_j}}\big)(t_n, \cdot) - I_n^{\varepsilon_{k_j}}\|_{\mathcal{U}}^2 + D - R(\tilde{\omega})$$

$$> \lim_{k \to \infty} \sum_{n=0}^{N} \|\mathcal{T}\big(\omega^{\varepsilon_{k_j}}, I_0^{\varepsilon_{k_j}}\big)(t_n, \cdot) - I_n^{\varepsilon_{k_j}}\|_{\mathcal{U}}^2.$$

But this is a contradiction to the weak lower semicontinuity of the $\|\cdot\|_{\mathcal{U}}$-norm. Hence, the sequence $\{\omega^{\varepsilon_k}\}$ converges strongly towards $\tilde{\omega}$ in $\mathcal{U}$.

Finally, if ω^* is unique, then any subsequence $\{\omega^{\varepsilon_k}\}$ converges strongly towards ω^* and, consequently, the complete sequence $\{\omega^{\varepsilon}\}$ converges towards ω^*. $\qquad\square$

Secondly, we now show how to choose the regularization parameters α and β, such that solutions $\omega_{\alpha,\beta}^{\varepsilon}$ to the regularized problem (NP) converge towards a minimal energy solution ω^+ of the sequence interpolation problem (SIP), if the noise level ε tends to zero. A good choice of α and β is necessary, because the larger the regularization parameters α and β are, the more stable is the problem (NP) is, but, on the other hand, the larger is the distance of the regularized solution $\omega_{\alpha,\beta}^{\varepsilon}$ to an exact solution ω^+ of the sequence interpolation problem (SIP).

Theorem 6.12.
Let Assumptions 6.3 hold, let $\{I_{\#}^{\varepsilon}\} \subset \mathcal{Z}^{N+1}$ be a sequence of (perturbed) image samples satisfying $\sum_{n=0}^{N} \|I_n^{\varepsilon_n} - I_n\|_{L^2(\Omega)}^2 < \varepsilon^2$, and let ω^+ be a solution to the sequence interpolation problem (SIP) with minimal energy

$$R(\omega) := R^x(\omega) + \frac{\beta}{\alpha}\, R^t(\omega),$$

i.e, $R(\omega^+) \leq R(\omega)$ for all $\omega \in \mathcal{U}$ solving the sequence interpolation problem (SIP).

Furthermore, we choose the regularization parameters $\alpha, \beta \colon (0, \infty) \to (0, \infty)$ such that

$$\alpha(\varepsilon) \to 0, \quad \frac{\varepsilon^2}{\alpha(\varepsilon)} \to 0 \quad and \quad \frac{\beta(\varepsilon)}{\alpha(\varepsilon)} = \mathrm{const} \quad for \quad \varepsilon \to 0, \qquad (6.10)$$

and denote by $\omega_{\alpha_\varepsilon,\beta_\varepsilon}^\varepsilon$ a minimizer of

$$J_{\alpha_\varepsilon,\beta_\varepsilon}(\cdot, I_\#^\varepsilon) := \sum_{n=0}^{N} \|\mathcal{T}(\omega, I_0^\varepsilon)(t_n, \cdot) - I_n^\varepsilon\|_{L^2(\Omega)}^2 + \alpha(\varepsilon)\, R^x(\omega) + \beta(\varepsilon)\, R^t(\omega).$$

Then $\{\omega_{\alpha_\varepsilon,\beta_\varepsilon}^\varepsilon\}$ admits a weak convergent subsequence and any weak convergent subsequence converges weakly towards a solution of the sequence interpolation problem (SIP) *with minimal energy.*

Proof.
Since $\omega_{\alpha_\varepsilon,\beta_\varepsilon}^\varepsilon$ is a minimal energy solution of $J_{\alpha_\varepsilon,\beta_\varepsilon}(\cdot; I_\#^\varepsilon)$, we have

$$\sum_{n=0}^{N} \|\mathcal{T}(\omega_{\alpha_\varepsilon,\beta_\varepsilon}^\varepsilon, I_0^\varepsilon)(t_n, \cdot) - I_n^\varepsilon\|_{L^2(\Omega)}^2 + \alpha(\varepsilon)\, R^x(\omega_{\alpha_\varepsilon,\beta_\varepsilon}^\varepsilon) + \beta(\varepsilon)\, R^t(\omega_{\alpha_\varepsilon,\beta_\varepsilon}^\varepsilon)$$

$$= J_{\alpha_\varepsilon,\beta_\varepsilon}(\omega_{\alpha_\varepsilon,\beta_\varepsilon}^\varepsilon; I_\#^\varepsilon) \le J_{\alpha_\varepsilon,\beta_\varepsilon}(\omega^+; I_\#^\varepsilon) \le \varepsilon^2 + \alpha(\varepsilon)\, R^x(\omega^+) + \beta(\varepsilon)\, R^t(\omega^+).$$

Using assumptions (6.10) this implies

$$\lim_{\varepsilon \to 0} \sum_{n=0}^{N} \|\mathcal{T}(\omega_{\alpha_\varepsilon,\beta_\varepsilon}^\varepsilon, I_0^\varepsilon)(t_n, \cdot) - I_n\|_{L^2(\Omega)}^2 = 0 \tag{6.11}$$

and

$$\limsup_{\varepsilon \to 0} R(\omega_{\alpha_\varepsilon,\beta_\varepsilon}^\varepsilon) \le R(\omega^+). \tag{6.12}$$

In particular, the sequence $\{\omega_{\alpha_\varepsilon,\beta_\varepsilon}^\varepsilon\}$ is bounded due to the coercivity of R and, consequently, there exists a subsequence $\{\omega_{\alpha_{\varepsilon_k},\beta_{\varepsilon_k}}^{\varepsilon_k}\}$ which converges weakly towards $\tilde{\omega} \in \mathcal{U}$, since $\mathcal{U}$ is reflexive. Moreover, from the weak-* sequential closedness of $\mathcal{T}$ and equation (6.11) we conclude

$$\mathcal{T}(\tilde{\omega}, I_0)(t_n, \cdot) = I_n, \quad \text{for all } n = 0, ..., N. \tag{6.13}$$

From (6.12) and the weak lower semicontinuity of R we obtain

$$R(\tilde{\omega}) \le \liminf_{k \to \infty} R(\omega_{\alpha_{\varepsilon_k},\beta_{\varepsilon_k}}^{\varepsilon_k}) \le R(\omega^+). \tag{6.14}$$

Thus, from (6.13) and (6.14) we conclude that $\tilde{\omega}$ is a minimal energy solution of the sequence interpolation problem (SIP), too.

$\square$

Corollary 6.13 (Stability).
The statements of Theorem 6.12 hold with strong convergence, if there exists a bilinear form $(\cdot, \cdot)_R$ such that

$$(\omega, \omega)_R = R(\omega) = R^x(\omega) + \frac{\beta}{\alpha} R^t(\omega) \quad \text{for all } \omega \in \mathcal{U}.$$

Moreover, if the minimal energy solution denoted by ω^+ is unique, then we have

$$\lim_{\varepsilon \to 0} \|\omega^\varepsilon_{\alpha_\varepsilon, \beta_\varepsilon} - \omega^+\|_R = 0.$$

Proof.
From Theorem (6.12) we know that $\{\omega^\varepsilon_{\alpha_\varepsilon, \beta_\varepsilon}\}$ admits a subsequence $\{\omega^{\varepsilon_k}_{\alpha_{\varepsilon_k}, \beta_{\varepsilon_k}}\}$ which weakly converges towards a minimal energy solution of the sequence interpolation problem (SIP), which we denote by ω^+.

Now, we show the strong convergence of the sequence $\{\omega^{\varepsilon_k}_{\alpha_{\varepsilon_k}, \beta_{\varepsilon_k}}\}$ towards ω^+ in $\mathcal{U}$. Here, we need the identity

$$\|\omega^{\varepsilon_k}_{\alpha_{\varepsilon_k}, \beta_{\varepsilon_k}} - \omega^+\|_R^2 = \|\omega^{\varepsilon_k}_{\alpha_{\varepsilon_k}, \beta_{\varepsilon_k}}\|_R^2 + \|\omega^+\|_R^2 - 2 \operatorname{Re} \left(\omega^{\varepsilon_k}_{\alpha_{\varepsilon_k}, \beta_{\varepsilon_k}}, \omega^+ \right)_R, \tag{6.15}$$

and obtain, together with equation (6.12) and (6.15), the statement

$$\limsup_{k \to \infty} \|\omega^{\varepsilon_k}_{\alpha_{\varepsilon_k}, \beta_{\varepsilon_k}} - \omega^+\|_R \le 2 \|\omega^+\|_R^2 - 2 \lim_{k \to \infty} \operatorname{Re} \left(\omega^{\varepsilon_k}_{\alpha_{\varepsilon_k}, \beta_{\varepsilon_k}}, \omega^+ \right)_R = 0.$$

Thus, we conclude the strong convergence.

Finally, if ω^+ is unique, then any subsequence $\{\omega^{\varepsilon_k}_{\alpha_{\varepsilon_k}, \beta_{\varepsilon_k}}\}$ converges strongly towards ω^+ and, consequently, the complete sequence $\{\omega^\varepsilon_{\alpha_\varepsilon, \beta_\varepsilon}\}$ converges towards ω^+. □

The assumptions of Corollary 6.13 are satisfied for both H^1-regularizations introduced in Section 6.2.1 and 6.2.2. In particular in these cases, the sequence $\{\omega^\varepsilon_{\alpha(\varepsilon), \beta(\varepsilon)}\}$ converges also strongly towards a minimal norm solution, i.e. with respect to the $\| \cdot \|_\mathcal{U}$-norm, since $\| \cdot \|_\mathcal{U}$ and $\| \cdot \|_R$ are norm equivalent.

6.4. Optimality System

After proving the existence and stability of a solution to problem (NP), we have to compute it numerically. For this purpose we characterize a solution by a system of optimality conditions.

Theorem 6.14 (Optimality System, cf. [8, 9]).
Let (ω, I) be a solution to problem (NP) with regularization term defined by (6.3), (6.4) or (6.8), then there exists an adjoint variable $p \in \mathcal{Q} := \left(\mathcal{C}^{0,1}(\overline{(0,T) \times \Omega}) \right)^{**}$, such that the following (optimality) conditions hold:

1. *The transport equation*

$$I_t + \omega \cdot \nabla I = 0 \ \text{ with } I(0, \cdot) = I_0 \qquad\qquad \text{(OFC)}$$

2. *The adjoint equation*

$$p_t + \nabla(\omega\, p) = \sum_{n=1}^{N-1} [\delta(t - t_n)(I(t_n, \cdot) - I_n)]$$

$$\text{with } p(T, \cdot) = -(I(T, \cdot) - I_N)$$

(adjEq)

where δ denotes the Dirac delta distribution.

3. *Depending on the choice of regularization term*

$$\text{for (6.3):} \qquad\qquad \alpha\,\Delta\omega = p\,\nabla I, \qquad\qquad (6.16)$$
$$\text{for (6.4):} \qquad\qquad \beta\,\omega_{tt} + \alpha\,\Delta\omega = p\,\nabla I, \qquad\qquad (6.17)$$

where we additionally have assumed that $\omega_t = 0$ for $t \in \{0, T\}$,

$$\text{for (6.8):} \qquad \alpha\,\mathrm{div}\left(\frac{(1 + \tau)\,\nabla\omega}{(|\nabla\omega|^2 + \varepsilon)^{\frac{1-\tau}{2}}}\right) = p\,\nabla I. \qquad\qquad (6.18)$$

Proof.
First we introduce the Lagrange functional

$$L(\omega, I, p) = J(\omega, I) + \int_0^T \int_\Omega p\left(I_t + \omega \cdot \nabla I\right) \mathrm{d}x\,\mathrm{d}t.$$

From the optimization theory, we know if there exists some $p \in \mathcal{Q}$ such that the derivative of the Lagrange functional vanishes at (ω, I, p), then (ω, I) is a local extremum of the cost functional J.

(i) From

$$0 = L_p(\omega, I, p)\tilde{p} = \int_0^T \int_\Omega \tilde{p}\left(I_t + \omega \cdot \nabla I\right) \mathrm{d}x\,\mathrm{d}t \quad \text{ for all } \tilde{p} \in \mathcal{Q},$$

we conclude equation (OFC).

(ii) We obtain the adjoint equation (adjEq) by differentiating the Lagrange functional with respect to I:

$$0 = L_I(\omega, I, p)\tilde{I} = \int\limits_{\Omega} \sum_{n=0}^{N}(I(t_n, \cdot) - I_n))\tilde{I}(t_n, \cdot)\,\mathrm{d}x + \int\limits_{0}^{T}\int\limits_{\Omega} p\,(\tilde{I}_t + \omega \cdot \nabla\tilde{I})\,\mathrm{d}x\,\mathrm{d}t$$

$$= \int\limits_{0}^{T}\int\limits_{\Omega} \sum_{n=0}^{N}(I(t, \cdot) - I_n))\delta(t - t_n)\tilde{I}(t, \cdot)\,\mathrm{d}x\,\mathrm{d}t$$

$$+ \int\limits_{0}^{T}\int\limits_{\Omega} p\,\tilde{I}_t\,\mathrm{d}x\,\mathrm{d}t + \int\limits_{0}^{T}\int\limits_{\Omega} p\,w \cdot \nabla\tilde{I}\,\mathrm{d}x\,\mathrm{d}t$$

$$= \int\limits_{0}^{T}\int\limits_{\Omega} \sum_{n=0}^{N}(I(t, \cdot) - I_n))\delta(t - t_n)\tilde{I}(t, \cdot)\,\mathrm{d}x\,\mathrm{d}t$$

$$+ \int\limits_{\Omega} \left(p(T, \cdot)\tilde{I}(T, \cdot) - p(0, \cdot)\tilde{I}(0, \cdot)\right)\,\mathrm{d}x - \int\limits_{0}^{T}\int\limits_{\Omega} p_t\,\tilde{I}\,\mathrm{d}x\,\mathrm{d}t$$

$$- \int\limits_{0}^{T}\int\limits_{\Omega} \nabla(\omega\,p)\tilde{I}\,\mathrm{d}x\,\mathrm{d}t,$$

for all $\tilde{I} \in \mathcal{Y}$ which satisfy $\tilde{I}(0, x) = 0$, because $I(0, x) + \tilde{I}(0, x) = I_0(x)$ has to satisfy the initial condition of the transport equation. In the last equality we also used the fact that ω is zero on the boundary. Therefore, we obtain

$$0 = L_I(\omega, I, p)\tilde{I} = \int\limits_{0}^{T}\int\limits_{\Omega} \sum_{n=1}^{N}(I(t, \cdot) - I_n)\delta(t - t_n)\tilde{I}(t, \cdot)\,\mathrm{d}x\,\mathrm{d}t$$

$$- \int\limits_{0}^{T}\int\limits_{\Omega}(p_t + \nabla(\omega\,p))\tilde{I}\,\mathrm{d}x\,\mathrm{d}t + \int\limits_{\Omega} p(T, \cdot)\tilde{I}(T, \cdot)\,\mathrm{d}x.$$

Next, we test the equation with an arbitrary $\tilde{I} \in \mathcal{Y}$ which satisfies the boundary condition $\tilde{I}(0, x) = \tilde{I}(T, x) = 0$ and get

$$\int\limits_{0}^{T}\int\limits_{\Omega} \sum_{n=1}^{N-1}(I(t, \cdot) - I_n))\delta(t - t_n)\tilde{I}(t, \cdot)\,\mathrm{d}x\,\mathrm{d}t = \int\limits_{0}^{T}\int\limits_{\Omega}(p_t + \nabla(\omega\,p))\tilde{I}\,\mathrm{d}x\,\mathrm{d}t.$$

Finally, by testing with an arbitrary $\tilde{I} \in \mathcal{Y}$ which satisfies $\tilde{I}(0, \cdot) = 0$ we obtain

$$-(I(t_N, \cdot) - I_N) = p(t_N, \cdot),$$

and thus condition (adjEq).

(iii) The equations (6.16) to (6.18) are obtained by differentiating the Lagrange functional with respect to ω.

For the H^1-regularization we have

$$0 = L_\omega(\omega, I, p)\tilde{\omega}$$

$$= \alpha \int_0^T \int_\Omega \nabla\omega \cdot \nabla\tilde{\omega} \, dx \, dt + \beta \int_0^T \int_\Omega \omega_t \, \tilde{\omega}_t \, dx \, dt + \int_0^T \int_\Omega p \tilde{\omega} \cdot \nabla I \, dx \, dt$$

$$= -\alpha \int_0^T \int_\Omega \Delta\omega \, \tilde{\omega} \, dx \, dt - \beta \int_0^T \int_\Omega \omega_{tt} \, \tilde{\omega} \, dx \, dt + \int_0^T \int_\Omega p \tilde{\omega} \cdot \nabla I \, dx \, dt$$

since $\tilde{\omega} \in \mathcal{U}$ is zero on $(0, T) \times \partial\Omega$ and $\omega_t = 0$ on $\{0, T\} \times \Omega$. From this equation we deduce (6.16) and (6.17).

For the $W^{1,1+\tau}$-regularization (6.8) we obtain

$$0 = L_\omega(\omega, I, p)\tilde{\omega}$$

$$= \alpha \int_0^T \int_\Omega \frac{1 + \tau}{\left(|\nabla\omega|^2 + \varepsilon\right)^{\frac{1-\tau}{2}}} \nabla\omega \cdot \nabla\tilde{\omega} \, dx \, dt + \int_0^T \int_\Omega p \tilde{\omega} \cdot \nabla I \, dx \, dt$$

$$= -\alpha \int_0^T \int_\Omega \text{div}\left(\frac{(1 + \tau)\, \nabla\omega}{\left(|\nabla\omega|^2 + \varepsilon\right)^{\frac{1-\tau}{2}}}\right) \tilde{\omega} + \int_0^T \int_\Omega p \tilde{\omega} \cdot \nabla I \, dx \, dt,$$

where we used the fact that $\tilde{\omega} \in \mathcal{U}$ is zero on the boundary $(0, T) \times \partial\Omega$. From this equation we finally obtain equation (6.18).

$\square$

Remark 6.15.
In the proof of Theorem 6.14 we have not shown the solveability of the adjoint equation (adjEq). Interpreting the delta impulse in the adjoint equation (adjEq) as in [8, 9] or in Section 7.1, respectively, we can prove, analogously, to the existence of a weak solution to the optical flow constraint (OFC) (cf. Corollary 5.7) that the adjoint equation (adjEq) admits a weak solution $p \in L^\infty((0, T) \times \Omega)$. Nevertheless, the $\left(\mathcal{C}^{0,1}(\overline{(0, T) \times \Omega})\right)^{**}$-regularity of this weak solution still needs to be verified.

Remark 6.16.
The additional assumption $\omega_t = 0$ on $\{0, T\} \times \Omega$ is necessary to eliminate the boundary integral in the computation of J_ω. Theoretically, it would also be possible to require $\omega = 0$ on $\{0, T\} \times \Omega$, but this requirement would exclude vector fields being constant in time as solutions.

Part III.

Numerical Simulation

7. Numerical Algorithm

In this chapter we discuss how to numerically solve problem (NP). We start with presenting the gradient method. Subsequently, we show that the computation of the gradient of the cost functional $J(\omega)$ defined in (NP) with H^1-regularization term involves solving a conservative and a non-conservative transport equation, as well as an elliptic PDE. Moreover, in the case, where we seek for a divergence free optical flow we use a projected gradient method. In this case, we additionally have to solve a Stokes equation. Hence, in the main part of this chapter we develop for each of these appearing PDEs a finite difference scheme for solving these PDEs numerically.

7.1. Gradient Method

A standard scheme for solving a minimization problem of the form

$$\min_{\omega \in \mathcal{U}} J(\omega),$$

where $\mathcal{U}$ is a Banach space and $J \colon \mathcal{U} \to \mathbb{R}$ is Fréchet-differentiable, is the *method of deepest descent.* The idea of this algorithm is very simple: We start with an initial value $\omega^0 \in \mathcal{U}$ and seek for a *descent direction* d^0, which satisfies

$$J(\omega^0 + t\, d^0) < J(\omega^0) \quad \text{for all } t \in (0, \bar{t}] \tag{7.1}$$

with $\bar{t} > 0$. Then we set $\omega^1 := \omega^0 + t\, d^0$ and seek again for a descent direction. We do this procedure iteratively until we converge towards a solution (cf. Algorithm 7.4).

Now the question is, how to compute a descent direction? If we assume that $\mathcal{U}$ is a Hilbert Space, then a descent direction at the point ω^k is given by $d^k = -\nabla J(\omega^k)$. In fact, using Riesz representation theorem (Theorem A.2) and a Taylor expansion series we obtain

$$\frac{J(\omega^k + t\, d^k) - J(\omega^k)}{t} + \mathcal{O}(t) = \left\langle J'(\omega^k), d^k \right\rangle_{\mathcal{U}^*, \mathcal{U}} = -\|\nabla J(\omega^k)\|_{\mathcal{U}}^2 \leq 0. \tag{7.2}$$

We conclude that $d_k = -\nabla J(\omega_k)$ is indeed a descent direction for a sufficiently small $t > 0$.

At this point, we recall that we are interested in solving the minimization problem

$$\left(\omega^+, I^+\right) = \operatorname*{argmin}_{(\omega, I) \in \mathcal{U} \times \mathcal{Y}} J(\omega, I) := \sum_{n=0}^{N} \int_{\Omega} |I(x, t_n) - I_n(x)|^2 \, \mathrm{d}x + \alpha\, R(\omega) \tag{NP}$$

subject to

$$I_t(t, x) + \omega(t, x) \cdot \nabla I(t, x) = 0 \quad \text{with } I(0, x) = I_0(x). \tag{OFC}$$

For this problem the gradients of the cost functional $J(\omega)$ for an H^1-regularization in space (6.3), as well as for an H^1-regularization in space and time (6.4), are given by the following theorem.

Theorem 7.1 (Gradient of J).
Consider the minimization problem (NP). *Let $\omega \in \mathcal{U}$ be given, where $\mathcal{U}$ denotes the control space depending on the regularization term (cf. Theorem 6.7 and Theorem 6.8). Moreover, we denote by $I \in \mathcal{C}([0, T], L^r(\Omega))$, for $1 \leq r < \infty$, and $p \in \left(\mathcal{C}^{0,1}(\overline{(0, T) \times \Omega})\right)^{**}$ the solutions of the optical flow constraint*

$$I_t + \omega \cdot \nabla I = 0 \quad \text{with } I(0, \cdot) = I_0 \tag{OFC}$$

and the adjoint equation

$$p_t + \nabla(\omega\, p) = \sum_{n=1}^{N-1} [\delta(t - t_n)(I(t_n, \cdot) - I_n)] \tag{adjEq}$$
$$\text{with } p(T, \cdot) = -(I(T, \cdot) - I_N),$$

respectively. Then we obtain the gradient $\nabla J \in \mathcal{U}$ by solving an elliptic PDE problem.

(i) For the H^1-regularization in space (6.3) we solve the Poisson equation

$$-\Delta\big(\nabla J(\omega)\big) = -\alpha\, \Delta\omega + p\, \nabla I \tag{7.3}$$

with $\omega, \nabla J(\omega) \in \mathcal{U} := \left(L^2((0, T), H_0^1(\Omega))\right)^d$.

(ii) For the H^1-regularization in space and time (6.4) we solve the time-dependent elliptic PDE problem

$$-\big(\nabla J(\omega)\big)_{tt} - \Delta\big(\nabla J(\omega)\big) = -\beta\, \omega_{tt} - \alpha\, \Delta\omega + p\, \nabla I \tag{7.4}$$

with $\omega, \nabla J(\omega) \in \mathcal{U} := \left(\{\varphi \in H^1_{\Gamma_x}((0, T) \times \Omega) : \text{ with } \varphi_t = 0 \text{ on } \{0, T\} \times \Omega\}\right)^d$, where we recall that the function space $H^1_{\Gamma_x}((0, T) \times \Omega)$ consists of all functions $u \in H^1((0, T) \times \Omega)$ which vanish on the spatial boundary $\Gamma_x := (0, T) \times \partial\Omega$.

We remark that the solvability of (7.3) and (7.4) was already shown in Section 3.3.

We proof this theorem by using the following Lemma.

Lemma 7.2 (Riesz Isomorphism).
The Riesz isomorphism $R : F \mapsto f$ which maps an element from $\mathcal{U}^*$ onto $\mathcal{U}$, such that

$$\langle F, \varphi \rangle_{\mathcal{U}^*, \mathcal{U}} = (f, \varphi)_{\mathcal{U}} \quad \text{for all } \varphi \in \mathcal{U},$$

is given by solving an elliptic PDE problem:

$$\begin{aligned}
&(i)\ F = -\Delta f &&\text{for } \mathcal{U} := L^2((0,T), H_0^1(\Omega)), \\
&(ii)\ F = -f_{tt} - \Delta f &&\text{for } \mathcal{U} := \big\{ \varphi \in H_{\Gamma_x}^1((0,T) \times \Omega) : \\
&&&\qquad \text{with } \varphi_t = 0 \text{ on } \{0, T\} \times \Omega \big\}.
\end{aligned}$$

Proof.
In the case $\mathcal{U} = \big\{ \varphi \in H_{\Gamma_x}^1((0,T) \times \Omega) : \text{ with } \varphi_t = 0 \text{ on } \{0, T\} \times \Omega \big\}$ we compute by using Riesz representation theorem (Theorem A.2)

$$\langle F, \varphi \rangle_{\mathcal{U}^*, \mathcal{U}} = (f, \varphi)_{\mathcal{U}} = \int_0^T \int_\Omega \left(\nabla f \cdot \nabla \varphi + f_t\, \varphi_t \right) \mathrm{d}x\, \mathrm{d}t$$

$$= -\int_0^T \int_\Omega \left(\Delta f + f_{tt} \right) \varphi \,\mathrm{d}x\, \mathrm{d}t = \big\langle -\Delta f - f_{tt}, \varphi \big\rangle_{\mathcal{U}^*, \mathcal{U}}$$

for all $\varphi \in \mathcal{U}$.
Analogously, we can calculate the Riesz isomorphism for $\mathcal{U} = L^2((0,T), H_0^1(\Omega))$. $\qquad\square$

Proof of Theorem 7.1.
In the derivation of the optimality system (cf. proof of Theorem 6.14) we have shown that the derivative $J'(\omega) \in \mathcal{U}^*$ for the H^1-regularization in space and time (6.4) is given by

$$J'(\omega) = -\beta\, \omega_{tt} - \alpha\, \Delta \omega + p\, \nabla I,$$

where I and p denote the solutions of the optical flow constraint (OFC) and the adjoint equation (adjEq), respectively.

Hence, applying the Riesz isomorphism we immediately deduce the statement of the theorem. Analogously, we can show the statement for the H^1-regularization in space (6.3). $\qquad\square$

Remark 7.3.
For the $W^{1,1+\tau}$-regularization (6.8) we cannot use the gradient as descent direction, since this space is not a Hilbert space. However, the computation of a descent direction for the $W^{1,1+\tau}$-regularization is not discussed in this thesis.

In the following, for solving the adjoint equation (adjEq) we use a linear transformation in time, $\tau := T - t$, and obtain

$$p_\tau + \nabla(-\omega\, p) = -\sum_{n=1}^{N-1} [\delta(\tau - \tau_n)(I(\tau_n, \cdot) - I_{N-n})]$$

$$\text{with } p(0, \cdot) = -(I(T, \cdot) - I_N)$$

with $\tau_n := T - t_n = t_{N-n}$ for equidistant time points.

Moreover as in [8, 9], the delta impulse in the adjoint equation (adjEq) can be interpreted as follows

$$p_\tau + \nabla\big(-\omega\, p\big) = 0 \qquad\qquad \text{on } \tau \in (\tau_n, \tau_{n+1}) \text{ for } n = 0, ..., N-1$$
$$p(\tau_n^+, \cdot) - p(\tau_n^-, \cdot) = -\big(I(\tau_n, \cdot) - I_n\big) \qquad \text{for } n = 1, ..., N-1.$$

Hence, for solving the adjoint equation (adjEq) we iteratively solve on each interval $[\tau_n, \tau_{n+1})$ a conservative transport equation of the form

$$p_t + \operatorname{div}\big(-\omega\, p\big) = 0$$

with initial condition

$$p(\tau_n, x) = \begin{cases} -(I(T, \cdot) - I_N) & \text{for } n = 0 \\ p(\tau_n^-, \cdot) - (I(\tau_n, \cdot) - I_{N-n}) & \text{for } n = 1, ..., N-1 \end{cases}$$

where $p(\tau_n^-, \cdot)$ for $n = 1, ..., N-1$ is given as solution of the previous time interval $[\tau_{n-1}, \tau_n)$.
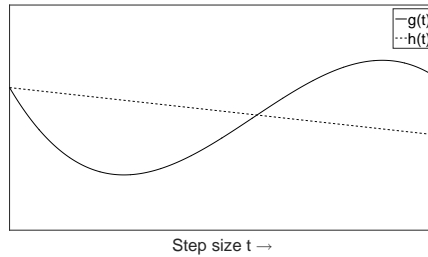
Figure 7.1.: Armijo step size rule: Here, the set of feasible step sizes is given by the set of all $t \in (0, \infty)$ for which the graph $g(t) := J(\omega + t^k d^k)$ is below the linear function $h(t) := J(\omega) + \sigma\, t_k \big\langle J'(\omega^k), d^k \big\rangle_{\mathcal{U}^*\mathcal{U}}$.

After computing a descent direction we have to choose an appropriate step size t_k. From (7.2) we conclude that the step size cannot be chosen too large, because otherwise condition (7.1) is not satisfied. On the other hand, if we choose the step size too small, then we need a lot of iterations, until we converge to a solution, and, consequently, the

computational costs are too large. Therefore, we use in the following the Armijo step size rule. For a given descent direction d^k of J at the point ω^k the Armijo step size is defined as the maximum $t^k \in \{\gamma^l, l \in \mathbb{N}_0\}$ which satisfies

$$J(\omega^k + t^k\, d^k) - J(\omega^k) \leq \sigma\, t_k \left\langle J'(\omega^k), d^k \right\rangle_{\mathcal{U}^*\mathcal{U}},$$

where $\sigma, \gamma \in (0,1)$ are given constants. The Armijo step size rule is also graphically illustrated in Figure 7.1.

Finally, we need a criterion for stopping the iterative process, if we are close enough to the solution. Here, we use a stopping criterion $\|\nabla J(\omega_k)\| < \text{Tol}$ for a given $\text{Tol} > 0$. In summary, we have presented the following algorithm:

Algorithm 7.4 (Gradient method)**.**

> *(S1) Set $\sigma \in (0,1), \gamma \in (0,1)$ # parameter of Armijo step size rule*
>
> *(S2) Set $\text{Tol} > 0$ # for stop criterion*
>
> *(S3) Set ω^0 # initial vector field*
>
> *(S4) **repeat***
>
> *(S5)   Compute $\nabla J(\omega^k)$*
>
> *(S6)   Set $d^k = -\nabla J(\omega^k)$*
>
> *(S7)   Determine step size t^k by using Armijo step size rule*
>
> *(S8)   Set $\omega^{k+1} = \omega^k + t^k\, d^k$*
>
> *(S9) **until** $\left\|\nabla J(\omega^k)\right\| < Tol$*

Remark 7.5.
We remark that in our case the algorithm only converge to a local minimum in the neighbourhood of the initial value ω^0, since the problem is non-linear. Nevertheless, in chapter 8 it is illustrated that we still obtain reasonable reconstruction results.

For more details on the gradient method with Armijo step size rule, like convergence analysis, or for further optimization methods we refer to [24] and [34].

7.2. Projected Gradient Method

In comparison to [15] an essential improvement of our existence analysis to problem (NP) (cf. Chapter 6) is that we do not need to restrict the optical flow ω to be divergence free. Thus, the aim is to illustrate with numerical experiments that this benefit leads indeed to better reconstruction results. For this purpose, we also have to solve problem

(NP) for divergence free optical flows ω. However, we note that $\omega \in \mathcal{U}$ with $\operatorname{div}(\omega) = 0$ does not necessarily imply $\operatorname{div}\left(\nabla J(\omega)\right) = 0$. Therefore, we use in this case a projected gradient method [31], i.e., line (S8) in Algorithm 7.4 is substituted by

$$\omega^{k+1} = \mathcal{P}\left(\omega^k + t^k\, d^k\right), \tag{7.5}$$

where $\mathcal{P}$ denotes the orthogonal projection from $\mathcal{U}$ onto its divergence free subspace $\mathcal{U}_{\mathrm{div}} := \{\omega \in \mathcal{U}; \operatorname{div}(\omega) = 0\}$. Moreover, we have to use a projected Armijo rule, too. This means for a given descent direction d^k of J at the point ω^k we choose the maximum $t^k \in \{\gamma^l, l \in \mathbb{N}_0\}$ which satisfies

$$J\left(\mathcal{P}\left(\omega^k + t^k\, d^k\right)\right) - J\left(\omega^k\right) \le -\frac{\sigma}{t^k}\left\|\mathcal{P}\left(\omega^k + t^k\, d^k\right) - \omega^k\right\|_{\mathcal{U}}^2, \tag{7.6}$$

where $\sigma, \gamma \in (0, 1)$ are given constants and $\mathcal{U}$ is a Hilbert space.

For the H^1-regularization in space (6.3) the orthogonal projection $\mathcal{P}$ onto the divergence free subspace is given by the following theorem.

Theorem 7.6.
Let $\mathcal{U} := \left(L^2((0, T), H_0^1(\Omega))\right)^d$ and $\mathcal{U}_{\mathrm{div}} := \{u \in \mathcal{U} : \text{ with } \operatorname{div}(u) = 0\}$. Then the orthogonal projection

$$\mathcal{P} : \mathcal{U} \to \mathcal{U}_{\mathrm{div}}$$
$$u \mapsto z$$

at each time t is given as solution of the Stokes problem

$$\begin{aligned} -\Delta z + \nabla \lambda &= -\Delta u \\ -\operatorname{div}(z) &= 0, \end{aligned} \tag{7.7}$$

where $\lambda \in \Lambda := L^2((0, T) \times \Omega)$.

Proof.
By using the definition of an orthogonal projection, we seek for a vector field z which satisfies

$$\min_{z \in \mathcal{U}_{\mathrm{div}}} H(z) = \|z - u\|_{\mathcal{U}}^2$$

or, equivalently,

$$\min_{z \in \mathcal{U}} H(z) = \|z - u\|_{\mathcal{U}}^2 \quad \text{subject to } \operatorname{div}(z) = 0.$$

This problem admits a unique solution, since the function $H(z)$ is strictly convex and $\mathcal{U}_{\mathrm{div}}$ is a convex set.

As a consequence, we can find the optimal solution by solving the corresponding optimality system. For this purpose, we use the Lagrange ansatz. We define

$$L(z, \lambda) = \|z - u\|_{\mathcal{U}}^2 - \int_0^T \int_\Omega \lambda \, \mathrm{div}(z)$$

with $\lambda \in \Lambda$.

Differentiating the Lagrange functional L with respect to z and λ leads to

$$0 = \langle L_z(z, \lambda), \tilde{z} \rangle_{\mathcal{U}^*\mathcal{U}} = \int_0^T \int_\Omega \nabla(z - u) \cdot \nabla \tilde{z} - \lambda \, \mathrm{div}(\tilde{z}) \, \mathrm{d}x$$

$$= \int_0^T \int_\Omega \left(-\Delta(z - u) + \nabla \lambda \right) \tilde{z}$$

and

$$0 = \langle L_\lambda(z, \lambda), \tilde{\lambda} \rangle_{\Lambda^*\Lambda} = -\int_0^T \int_\Omega \mathrm{div}(z) \, \tilde{\lambda} \, \mathrm{d}x.$$

Consequently, the orthogonal projection is given by solving the weak formulation of the Stokes problem. Finally, we remark, that existence of a solution to the Stokes problem was already shown in Section 3.4. $\qquad \square$

Finally, we observe that this orthogonal projection is linear. As a consequence (7.5) and (7.6) can be simplified to

$$\omega^{k+1} = \omega^k - t^k \, \mathcal{P}\big(\nabla J(\omega^k)\big)$$

and

$$J\Big(\omega^k - t^k \, \mathcal{P}\big(\nabla J(\omega^k)\big)\Big) - J\Big(\omega^k\Big) \leq -\sigma \, t^k \Big\| \mathcal{P}\big(\nabla J(\omega^k)\big) \Big\|_{\mathcal{U}}^2,$$

respectively.

Here, due to Theorem 7.6 the orthogonal projection $\mathcal{P}\big(\nabla J(\omega^k)\big) \in \mathcal{U}_{\mathrm{div}}$ is given by solving the Stokes problem

$$-\Delta\Big(\mathcal{P}\big(\nabla J(\omega^k)\big)\Big) + \nabla \lambda = -\Delta\Big(\nabla J(\omega^k)\Big) \qquad \text{in } \Omega, \tag{7.8a}$$

$$-\mathrm{div}\Big(\mathcal{P}\big(\nabla J(\omega^k)\big)\Big) = 0 \qquad \text{in } \Omega, \tag{7.8b}$$

$$\nabla J(\omega^k) = 0 \qquad \text{on } \partial\Omega. \tag{7.8c}$$

7.3. Discretisation of the Mesh

As we have seen in Theorem 7.1, we have to numerically solve three PDEs for computing the gradient of J, namely a conservative, a non conservative transport equation and an elliptic PDE. In the case, where we seek for a divergence free optical flow, we additionally have to solve a Stokes equation. We solve each of these PDEs by using the method of finite differences. The numerical treatment of these PDEs is discussed in detail in the following sections.

<table>
<tr><td>(a) mesh of I and p</td><td>(b) mesh of u</td><td>(c) mesh of v</td></tr>
</table>
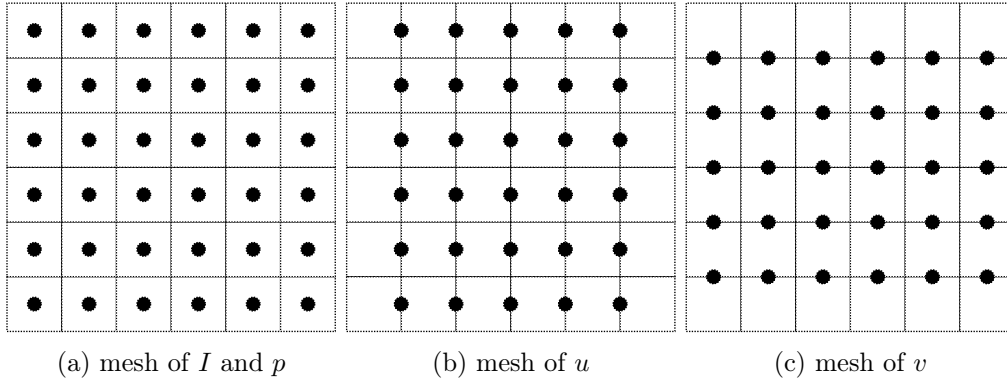
Figure 7.2.: Staggered grid in space at time level m for the functions I, p, u and v

For this purpose, we first have to discretise the domain. For the discretisation we assume, that we are given a sequence of images I_n at discrete time points $0 = t_0 < t_1 < ... < t_N = T$ of size $N_x \times N_y$ pixels. Then we set $\Omega = [0, N_x \, \Delta x] \times [0, N_y \, \Delta x]$ with mesh size $\Delta x = \frac{1}{\max(N_x, N_y)}$. Moreover, we use M time steps, i.e., $T = M \, \Delta t$. Later we show, that M cannot be choosen arbitrarily, since the mesh size ratio $\lambda = \frac{\Delta x}{\Delta t}$ has to satisfy a CFL-condition. Hence, we assume for the following discussion that the mesh ratio λ remains constant, if we refine the mesh size Δx. Finally, we obtain the following discretisation for the 2-dimensional case, i.e., $x \in \Omega \subset \mathbb{R}^2$:

$$I^m_{i+1/2,j+1/2} = I\big((i+1/2) \, \Delta x, (j+1/2) \, \Delta x, m \, \Delta t\big) \qquad \text{with} \qquad i = 0, ..., N_x - 1$$
$$j = 0, ..., N_y - 1$$
$$m = 0, ..., M$$

$$p^m_{i+1/2,j+1/2} = p\big((i+1/2) \, \Delta x, (j+1/2) \, \Delta x, m \, \Delta t\big) \qquad \text{with} \qquad i = 0, ..., N_x - 1$$
$$j = 0, ..., N_y - 1$$
$$m = 0, ..., M$$

$$u^m_{i,j+1/2} = u\big(i \, \Delta x, (j+1/2) \, \Delta x, m \, \Delta t\big) \qquad \text{with} \qquad i = 1, ..., N_x - 1$$
$$j = 0, ..., N_y - 1$$
$$m = 0, ..., M$$

and

$$v^m_{i+1/2,j} = v\big((i+1/2)\,\Delta x, j\,\Delta x, m\,\Delta t\big) \qquad \text{with} \qquad i = 0, ..., N_x - 1$$
$$j = 1, ..., N_y - 1$$
$$m = 0, ..., M.$$

Here, u and v denotes the two velocity components of the optical flow ω. This kind of discretisation, where the functions I and p are stored in the cell centres and the velocity components are stored on the cell boundaries, is called *staggered grid*. The discretisation is also visualized in Figure 7.2. Note, that we do not have any degree of freedom on the boundary $[0,T] \times \partial\Omega$, since the optical flow vanishes on the spatial boundary. We remark at this point, that the numerical schemes presented in the following sections can be generalized straightforward to higher dimensions.
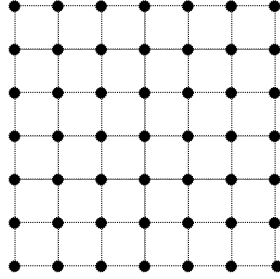
Figure 7.3.: Collocated grid in space at time level m for the functions I, p, u and v

In comparison to [8, 9, 15] we emphasize that we use for the discretisation of the functions I and p another grid as for the velocity components u and v. Indeed, in [8, 9, 15] a *collocated grid* arrangement is used, i.e., the functions I, p, u and v are discretised at the same grid points $(m\,\Delta t, i\,\Delta x, j\,\Delta x)$ for $i = 0, ..., N_x, j = 0, ..., N_y$ and $m = 0, ..., M$, see Figure 7.3.

This fact, that we use a staggered grid, has two reasons. The first reason is that we find it more reasonable to evaluate the function I representing the grey of an image pixel at the cell midpoints. Whereas, we prefer to evaluate the optical flow at the cell boundaries to incorporate with the boundary conditions of the elliptic PDEs (7.3) and (7.4). The second and more significant reason is that the velocity components u and v has to be discretised for numerical stability on different grids for solving the Stokes equation, as we will discuss in Section 7.6.

7.4. Finite Difference Scheme for the Transport Equation

We start with the numerical treatment of the optical flow constraint

$$I_t(t,x) + \omega(t,x) \cdot \nabla I(t,x) = 0 \quad \text{with } I(0,x) = I_0(x), \qquad \text{(OFC)}$$

as well as the conservative transport equation

$$p_t(t, x) + Div\big(\omega(t, x)\, p(t, x)\big) = 0 \quad \text{with } p(0, x) = p_0(x). \qquad \text{(cTPE)}$$

Note that the adjoint equation (adjEq) can be reformulated in the form (cTPE) due to the discussion in Section 7.1.

In the literature, there are many finite difference schemes for solving a transport equation, see for instance [32, 35, 36]. However, the theory on finite differences is only well established for transport equations with constant vector field $\omega(t, x) = a \in \mathbb{R}^d$.

Hence, the outline of this section is as follows: Firstly, we introduce the concept of finite differences for the constant case by orientating to the work of [32, 36]. Here, we define a finite difference scheme and derive sufficient conditions for the convergence of this scheme. These conditions are illustrated with two examples, namely the first order Upwind scheme and the second order Lax-Wendroff scheme.

Secondly, we show that in the Upwind scheme discontinuities of the exact solution are smoothened out, whereas in the Lax-Wendroff scheme oscillations occur around discontinuities. Therefore, we introduce also the concept of flux limiters, which combine both schemes to obtain more accurate results. In this part, we adopt the work of [32].

Thirdly, we generalize the Upwind and Lax-Wendroff scheme straightforward for solving transport equations with variable vector fields, i.e., ω depends on t and x. In this way we obtain in each case for solving the conservative (cTPE) and the non-conservative transport equation (OFC) a generalized Upwind and Lax-Wendroff scheme, which were originally introduced by LeVeque in 2004 [35]. However, in [35] the schemes were only motivated for time-independent and monotone vector fields, i.e., $\omega(x) \geq 0$ or $\omega(x) \leq 0$ for all $x \in \Omega \subset \mathbb{R}^d$, by considering the analytical solution of the Riemann problem at the cell boundaries. In the following, we show that these generalized schemes are also reasonable for time-dependent and non-monotone vector fields by doing a consistency analysis for the more general case. Moreover, in contrast to [35] we do a stability analysis for the generalized Upwind schemes, which is sufficient for convergence of the Upwind schemes due to Lax's Equivalence theorem. Since discrete solutions of the generalized Upwind and Lax-Wendroff admit the damping or oscillating behaviour, we also generalize the concept of flux limiters for non constant vector fields. Basically, we only have to redefine in this case the so called gradient ratios, which measure the local smoothness of a function.

Finally, we want to emphasize that in our case the conservative (cTPE) and the non-conservative transport equation (OFC) are numerically solved by different FD schemes, whereas in [8, 9, 15] both equations are solved with the same conservative FD scheme. Hence, for a non divergence free vector field ω the numerical solution of the non-conservative transport equation (OFC) obtained by the FD scheme in [8, 9, 15] will not be constant along a characteristic.

7.4.1. Transport Equation with Constant Vector Field

Now, we start with the numerical treatment of the transport equation with constant vector field $a \in \mathbb{R}$ in the 1-dimensional case, i.e.,

$$I_t(t,x) + a\, I_x(t,x) = 0 \quad \text{with } I(0,x) = I_0(x), \tag{TPE}$$

with $x \in \Omega \subset \mathbb{R}$ and $t \in [0,T]$. For higher dimensions d we use a directional splitting approach, see Section 7.4.4, which reduces the problem to d 1-dimensional problems. Moreover, for simplification in the notation we propose $\Omega = \mathbb{R}$. Because in this case we do not need to take care about inflow boundary conditions.

In the following the aim is to find a discrete solution $I_{\Delta x}$, which approximates the exact (analytical) solution $\tilde{I}$ of the transport equation (TPE). For this purpose, for a given time step size Δt we discretise the time interval $[0,T]$ by an equidistant mesh, $0 = t_0 < t_1 < ... < t_M = T$. Subsequently, for a given mesh size Δx we define on each time level m a piecewise constant function

$$I_{\Delta x}(m\,\Delta t, x) = \sum_{j \in \mathbb{Z}} I_{j+1/2}^m \chi_{[j\,\Delta x, (j+1)\,\Delta x)}, \tag{7.9}$$

where the coefficients $I_{j+1/2}^m \in \mathbb{R}, j \in \mathbb{Z}$ are approximations to cell average values

$$\tilde{I}_{j+1/2}^m = \frac{1}{\Delta x} \int\limits_{j\,\Delta x}^{(j+1)\,\Delta x} \tilde{I}(m\,\Delta t, x)\, \mathrm{d}x \tag{7.10}$$

of the exact solution $\tilde{I}$. Thus, $I_{\Delta x}(m\,\Delta t, \cdot)$ is an approximation to the exact solution $\tilde{I}$ at time $t := m\,\Delta t$. Finally, we define the approximation $I_{\Delta x}$ to the exact solution $\tilde{I}$ at any time t by

$$I_{\Delta x}(t,x) = \sum_{m=0}^{M} \sum_{j \in \mathbb{Z}} I_{j+1/2}^m \chi_{[(m-1/2)\,\Delta t, (m+1/2)\,\Delta t) \times [j\,\Delta x, (j+1)\,\Delta x)}. \tag{7.11}$$

At this point we would like to mention that the values $I_{j+1/2}^m$ are often interpreted as approximations to the exact solution $\tilde{I}$ at the grid points $(m\,\Delta t, (j+1/2)\,\Delta x)$, too.

For the computation of the approximations $I_{j+1/2}^m$ we use the method of finite differences. A *finite difference scheme* (FD scheme) is defined by

$$I_{j+1/2}^{m+1} = \mathcal{H}_{j+1/2}(I_{\Delta x}^m) := \sum_{k \in \mathbb{Z}} b_{k+j+1/2}\, I_{k+j+1/2}^m, \tag{7.12}$$

where $I_{\Delta x}^m = \{I_{j+1/2}^m, j \in \mathbb{Z}\}, b_{k+1/2} \in \mathbb{R}$ for $k \in \mathbb{Z}$ and $\mathcal{H}$ is called a *finite difference operator*. Moreover, we set $I_{\Delta x}^{m+1} = \mathcal{H}(I_{\Delta x}^m) := \{\mathcal{H}_{j+1/2}(I_{\Delta x}^m), j \in \mathbb{Z}\}$.

In relation (7.12) we observe, that the coefficients $I_{j+1/2}^m, m = 1, ..., M$ are recursively computed from the values $I_{j+1/2}^{m-1}, j \in \mathbb{Z}$ of the previous time level $m - 1$. Hence, for the computation of the coefficients $I_{j+1/2}^m$ we only need to know the coefficients $I_{j+1/2}^0$ at initial time $t = 0$. But these are given by the initial value condition of the differential equation (TPE), i.e.,

$$I_{j+1/2}^0 = \frac{1}{\Delta x} \int\limits_{j \, \Delta x}^{(j+1) \, \Delta x} I_0(x) \, \mathrm{d}x.$$

Next we derive two established FD-Schemes. In the case $\alpha > 0$, we replace in the transport equation (TPE) the time and spatial derivative by forward finite difference quotients and obtain the discrete equation

$$\frac{I_{j+1/2}^{m+1} - I_{j+1/2}^m}{\Delta t} + \frac{I_{j+1/2}^m - I_{j-1/2}^m}{\Delta x} = 0$$

or, equivalently,

$$I_{j+1/2}^{m+1} = I_{j+1/2}^m - \lambda \, a \big(I_{j+1/2}^m - I_{j-1/2}^m \big), \tag{7.13}$$

with mesh size ratio $\lambda = \frac{\Delta t}{\Delta x}$. Relation (7.13) is called *forward Upwind scheme*. Analogously, if $a < 0$, we use a forward finite difference quotient in time and a backward finite difference quotient in space to obtain the *backward Upwind scheme*

$$I_{j+1/2}^{m+1} = I_{j+1/2}^m - \lambda \, a \big(I_{j+3/2}^m - I_{j+1/2}^m \big). \tag{7.14}$$

A combination of both cases leads to the *Upwind scheme*

$$\begin{aligned} I_{j+1/2}^{m+1} = I_{j+1/2}^m &- \frac{\lambda \, a}{2} \big(I_{j+3/2}^m - I_{j-1/2}^m \big) \\ &+ \frac{|\lambda a|}{2} \big(I_{j+3/2}^m - 2 \, I_{j+1/2}^m + I_{j-1/2}^m \big). \end{aligned} \tag{7.15}$$

Next, we derive the Lax-Wendroff scheme. Here, we consider a second order Taylor expansion series of I in time, i.e.,

$$I(t + \Delta t, x) = I(t, x) + I_t(t, x) \, \Delta t + I_{tt}(t, x) \frac{(\Delta t)^2}{2} + \mathcal{O}((\Delta t)^3) \tag{7.16}$$

and substitute the time derivative I_{tt} in (7.16) by spatial derivatives via

$$I_{tt} = (-a \, I_x)_t = -a \, I_{tx} = -a \, (-a \, I_x)_x = a^2 \, I_{xx} \tag{7.17}$$

by exploiting the transport equation (TPE). Moreover, we replace the spatial derivatives I_x in (TPE) and I_{xx} in (7.17) by central finite differences and obtain, finally, the *Lax-Wendroff scheme*

$$
\begin{aligned}
I_{j+1/2}^{m+1} = I_{j+1/2}^m &- \frac{\lambda\,a}{2}\left(I_{j+3/2}^m - I_{j-1/2}^m\right) \\
&+ \frac{(\lambda a)^2}{2}\left(I_{j+3/2}^m - 2\,I_{j+1/2}^m + I_{j-1/2}^m\right).
\end{aligned}
\tag{7.18}
$$

For further examples of FD schemes, like the method of Lax-Friedrich or Leapfrog, we refer to [32, 35, 36].

Now the question is: Is the discrete solution $I_{\Delta x}$ defined by the Upwind (7.15) or Lax-Wendroff scheme (7.18) convergent towards the exact solution $\tilde{I}$ of the transport equation (TPE)? Here, convergence means,

$$
\|I_{\Delta x} - \tilde{I}\| \to 0 \quad \text{for } \Delta x, \Delta t \to 0
$$

in some suitable norm $\|\cdot\|$, which we discuss explicitly later on. For proving the convergence, we use Lax's Equivalence theorem. This theorem states that consistency and stability of a linear FD scheme is necessary and sufficient for convergence. Here, roughly speaking, consistency means that the FD scheme approximates the differential equation (TPE) and stability means, that the summation of the unavoidable discretisation errors at each time step remains bounded, if we use infinite many time steps, i.e., if $\Delta t \to 0$.

Conservativity

However, before analysing these two properties, we first discuss the conservativity property of a FD scheme. This conservativity property is useful later on for the generalization of the Upwind and Lax-Wendroff scheme for solving the conservative transport equation (cTPE). In Theorem 3.7 we have shown that the exact solution $\tilde{I}$ to the transport equation (TPE) is conservative, i.e.,

$$
\int_{\mathbb{R}} \tilde{I}(t,x)\,\mathrm{d}x = \int_{\mathbb{R}} I_0(x)\,\mathrm{d}x \quad \text{for all } t \in [0,T].
$$

This property written in the discrete sense

$$
\sum_{j\in\mathbb{Z}} I_{j+1/2}^m = \sum_{j\in\mathbb{Z}} I_{j+1/2}^0 \quad \text{for } m = 0,...,M.
$$

Integrating the transport equation (TPE) over a grid cell $(m, j+1/2)$ defined by

$$
(m, j+1/2) := [(m-1/2)\,\Delta t, (m+1/2)\,\Delta t) \times [j\,\Delta x, (j+1)\,\Delta x)
$$

and multiplying by $\frac{1}{\Delta x}$ leads to

$$\tilde{I}^{m+1}_{j+1/2} = \tilde{I}^m_{j+1/2} - \lambda \left(\frac{1}{\Delta t} \int\limits_{(m-1/2)\,\Delta t}^{(m+1/2)\,\Delta t} f(\tilde{I}(t, (j+1)\,\Delta x))\, \mathrm{d}t \right.$$

$$\left. - \frac{1}{\Delta t} \int\limits_{(m-1/2)\,\Delta t}^{(m+1/2)\,\Delta t} f(\tilde{I}(t, j\,\Delta x))\, \mathrm{d}t \right),$$

where we have used the notation (7.10). Here, the integral on the right hand side describes the mass, which flows into or rather out of the grid cell $(m, j+1/2)$ during one time step. However, in general we cannot exactly compute these flows. Therefore, we have to approximate them by numerical flux functions

$$F_j(I^m_{\Delta x}) \approx \frac{1}{\Delta t} \int\limits_{(m-1/2)\,\Delta t}^{(m+1/2)\,\Delta t} f(\tilde{I}(t, j\,\Delta x))\, \mathrm{d}t.$$

Altogether, this motivates the following definition of a conservative finite difference scheme.

Definition 7.7.
A FD scheme is called conservative, *if we can rewrite the scheme (7.12) as*

$$I^{m+1}_{j+1/2} = I^m_{j+1/2} - \lambda \left(F_{j+1}(I^m_{\Delta x}) - F_j(I^m_{\Delta x}) \right), \tag{7.19}$$

where

$$F_j(I^m_{\Delta x}) := \sum_{k \in \mathbb{Z}} c_{k+j+1/2} I^m_{k+j+1/2} \quad \text{with} \quad c_{k+1/2} \in \mathbb{R}, k \in \mathbb{Z}$$

is called the numerical flux function.

A simple calculation

$$\int\limits_{\mathbb{R}} I^{m+1}_{\Delta x} = \Delta x \sum_{j \in \mathbb{Z}} I^{m+1}_{j+1/2}$$

$$= \Delta x \sum_{j \in \mathbb{Z}} \left(I^m_{j+1/2} - \lambda \underbrace{\left(\sum_{k \in \mathbb{Z}} c_{k+j+3/2} I^m_{k+j+3/2} - \sum_{k \in \mathbb{Z}} c_{k+j+1/2} I^m_{k+j+1/2} \right)}_{=0} \right)$$

$$= \Delta x \sum_{j \in \mathbb{Z}} I^m_{j+1/2} = \int\limits_{\mathbb{R}} I^m_{\Delta x}.$$

shows, that a FD scheme (7.12) which can be rewritten in the form (7.19) is indeed conservative. Here, we have exploited in the calculation, that there is a telescoping sum in the second line.

Furthermore, we can rewrite the Upwind (7.15) and Lax-Wendroff scheme (7.18) in conservative form (7.19) by using the Upwind flux

$$
\begin{aligned}
F_j^{Up}(I_{\Delta x}^m) &= \begin{cases} a\, I_{j-1/2}^m & , \text{ for } a \geq 0 \\ a\, I_{j+1/2}^m & , \text{ for } a < 0 \end{cases} \\
&= \frac{1}{2}\, a\, \left(I_{j+1/2}^m + I_{j-1/2}^m\right) - \frac{1}{2}\, |a|\, \left(I_{j+1/2}^m - I_{j-1/2}^m\right),
\end{aligned}
\tag{7.20}
$$

and the Lax-Wendroff flux

$$
F_j^{LW}(I_{\Delta x}^m) = \frac{1}{2}\, a\, \left(I_{j+1/2}^m + I_{j-1/2}^m\right) - \frac{1}{2}\, a^2\, \lambda\, \left(I_{j+1/2}^m - I_{j-1/2}^m\right),
\tag{7.21}
$$

respectively.

Consistency

Next, we analyse the consistency of a FD scheme. For this purpose we assume that $\tilde{I}$ is a smooth solution of the differential equation (TPE). Hence, we compute the Taylor epansion series given as

$$
\begin{aligned}
\tilde{I}_{j+1/2}^{m+1} &= \tilde{I}(t,x) + \tilde{I}_t(t,x)\, \Delta t + \tilde{I}_{tt}(t,x)\, \frac{(\Delta t)^2}{2} + ... \quad \text{ and} \\
\tilde{I}_{k+j+1/2}^m &= \tilde{I}(t,x) + \tilde{I}_x(t,x)\, k\, \Delta x + \tilde{I}_{xx}(t,x)\, \frac{(k\, \Delta x)^2}{2} + ...
\end{aligned}
\tag{7.22}
$$

at the points $(t,x) = (m\, \Delta t, (j+1/2)\, \Delta x)$.

Now a substitution of the approximations $I_{j+1/2}^m$ in the FD scheme (7.12) by the Taylor expansion series (7.22) leads to

$$
0 = \frac{\tilde{I}_{j+1/2}^{m+1} - \mathcal{H}(\tilde{I}^m)}{\Delta t} = \tilde{I}_t + a\, \tilde{I}_x + L_{j+1/2}^m
$$

or, equivalently,

$$
\tilde{I}_t + a\, \tilde{I}_x = -L_{j+1/2}^m
\tag{7.23}
$$

with local truncation error $L_{j+1/2}^m = L_{\Delta x}(m\, \Delta t, (j+1/2)\, \Delta x) = \mathcal{O}((\Delta x)^p)$ for $p \in \mathbb{N}_0$. Here, we recall the assumption that the mesh ratio $\lambda = \frac{\Delta x}{\Delta t}$ remains constant, if we refine Δx or Δt. Therefore, the local truncation error depends alone on Δx rather than on both Δx and Δt.

We observe, that we do not exactly solve the transport equation (TPE), but the equation (7.23), which is called *equivalence differential equation* (EDE) or *modified differential equation*. Moreover, from (7.23) we conclude that the FD scheme approximates the differential equation (TPE) at the point $(m\,\Delta t, (j+1/2)\,\Delta x)$, if the truncation error $L_{j+1/2}^m$ tends to zero for $\Delta x \to 0$. In summary, we define:

Definition 7.8.
Let (7.12) *be a FD scheme with truncation error*

$$L_{j+1/2}^m = \frac{1}{\Delta t}\big(\tilde{I}_{j+1/2}^{m+1} - \mathcal{H}(\tilde{I}_{\Delta x}^m)\big) = \mathcal{O}((\Delta x)^p). \tag{7.24}$$

Then the FD scheme is consistent, *if and only if* $p \geq 1$. *Moreover,* p *is called the* consistency order*.*

Let us exemplify the consistency at the Upwind (7.15) and Lax-Wendroff scheme (7.18). Using the relation (7.17) we calculate

$$\tilde{I}_t(t,x) + a\,\tilde{I}_x(t,x) = |a|\,\frac{\Delta x}{2}\left(1 - |a\,\lambda|\right)\tilde{I}_{xx} \tag{7.25}$$

as EDE for the Upwind scheme, where we assumed that $\tilde{I} \in \mathcal{C}^2((0,T)\times\mathbb{R})$ is the exact solution to the transport equation (TPE). For the Lax-Wendroff scheme we assume $\tilde{I} \in \mathcal{C}^3((0,T)\times\mathbb{R})$ and compute

$$\tilde{I}_t(t,x) + a\,\tilde{I}_x(t,x) = a\,\frac{(\Delta x)^2}{6}\left(1 - (a\,\lambda)^2\right)\tilde{I}_{xxx} \tag{7.26}$$

as EDE. Consequently, we conclude that the Upwind scheme is first order accurate, whereas the Lax-Wendroff scheme is second order accurate.

Stability

Lastly, we discuss the stability of a FD scheme. This means, that errors which are unavoidable due to discretisation should not grow to infinity, i.e., there exists a constant $C > 0$ with

$$\|I_{\Delta x}^m\| = \|\mathcal{H}(I_{\Delta x}^{m-1})\| = \ldots = \|\mathcal{H}^m(I_{\Delta x}^0)\| \leq \|\mathcal{H}^m\|\,\|I_{\Delta x}^0\| \leq C\,\|I_{\Delta x}^0\| \quad \text{for } m = 0,\ldots,M.$$

Sufficient for the stability of a FD scheme is, that

$$\|\mathcal{H}\| \leq 1 + D\,\Delta t.$$

In fact, in this case we obtain

$$\|\mathcal{H}^m\| \leq (1 + D\,\Delta t)^m \leq e^{m\,D\,\Delta t} \leq e^{D\,T} \leq C.$$

Now the question is: What is a suitable norm for analysing the stability and, consequently, also the convergence of a FD scheme due to Lax's Equivalence theorem? An ideally norm is usually the L^∞-norm, but convergence in the L^∞-norm is unrealistic for discontinuous solutions. For conservation laws, like the transport equation (TPE), the L^1-norm is a natural norm. As an illustration, we derive for the forward Upwind scheme (7.13) that it is *conditionally L^1-stable* for $0 \leq a\,\lambda \leq 1$:

$$
\begin{aligned}
\left\| I_{j+1/2}^{m+1} \right\|_{L^1} &= \Delta x \sum_{j \in \mathbb{Z}} \left| I_{j+1/2}^{m+1} \right| = \Delta x \sum_{j \in \mathbb{Z}} \left| I_{j+1/2}^{m} - a\,\lambda \left(I_{j+1/2}^{m} - I_{j-1/2}^{m} \right) \right| \\
&\leq \Delta x \sum_{j \in \mathbb{Z}} \left| (1 - a\,\lambda)\, I_{j+1/2}^{m} \right| + \left| a\,\lambda\, I_{j-1/2}^{m} \right| \\
&= \Delta x \left((1 - a\,\lambda) \sum_{j \in \mathbb{Z}} \left| I_{j+1/2}^{m} \right| + a\,\lambda \sum_{j \in \mathbb{Z}} \left| I_{j-1/2}^{m} \right| \right) \\
&= \Delta x \sum_{j \in \mathbb{Z}} \left| I_{j+1/2}^{m} \right| = \left\| I_{j+1/2}^{m} \right\|_{L^1}.
\end{aligned}
$$

Analogously, we can show that the backward Upwind scheme (7.14) is conditionally L^1-stable for $-1 \leq a\,\lambda \leq 0$. The stability condition for a FD scheme (7.12) is often called CFL-condition (for Courant-Friedrich-Lewy). However, for FD schemes, where also negative coefficients $b_{j+1/2}, j \in \mathbb{Z}$ appear in the definition (7.12) of the finite difference operator $\mathcal{H}$, like in the Lax-Wendroff scheme (7.18), it is more difficult to show the L^1-stability. Therefore, the L^2-norm is more frequently used. Because, in this case Parseval's identity is used to show stability in the frequency domain. This technique for proving stability is called *von Neumann analysis*. By using a von Neumann analysis, we can show that both the Upwind and Lax-Wendroff scheme are conditionally L^2-stable for $|a\,\lambda| \leq 1$, for more details we refer to [32].

Convergence

Finally, we deduce the convergence of the Upwind (7.15) and Lax-Wendroff (7.18) scheme from Lax's Equivalence theorem.

Theorem 7.9 (Lax's Equivalence theorem).
Consistency and stability are necessary and sufficient for the convergence of a linear FD scheme. Moreover, the convergence order is equal to the consistency order of the FD scheme.

Proof.
We only show by adopting the work of [36], that consistency and stability is sufficient for convergence. For the necessity we refer to [41].

We define the local approximation error function by

$$
E_{\Delta x}(t, x) = I_{\Delta x}(t, x) - \tilde{I}(t, x),
$$

where we recall that $I_{\Delta x}$ defined in (7.11) denotes the discrete and $\tilde{I}$ the exact solution. Furthermore, we set $E^m(x) = E(m\,\Delta t, x)$.

Next by using the linearity of the FD scheme and the formulation of the local truncation error (7.24) we can express the local approximation error by

$$E_{\Delta x}^{m+1}(x) = \big(\mathcal{H}(E_{\Delta x}^m)\big)(x) - \Delta t\, L_{\Delta x}(m\,\Delta t, x).$$

Applying this relation recursively, we obtain

$$E_{\Delta x}^m(x) = \big(\mathcal{H}^m(E_{\Delta x}^0)\big)(x) - \Delta t \sum_{l=1}^{m} \big(\mathcal{H}^{m-l}\, L_{\Delta x}(l\,\Delta t, \cdot)\big)(x).$$

Now, for global convergence of the FD scheme we have to show that $\|E_{\Delta x}^m\| \to 0$ for all $m = 0, ..., M$, if Δx tends to zero. By exploiting the stability,

$$\|\mathcal{H}^{M-l}\| \le C_S \quad \text{for all } l = 0, ..., M,$$

and consistency,

$$\|L_{\Delta x}(m\,\Delta t, \cdot)\| \le C_L\,(\Delta x)^p \quad \text{for all } m = 0, ..., M$$

of the FD scheme we estimate

$$\|E_{\Delta x}^m\| \le \|\mathcal{H}^m\|\,\|E_{\Delta x}^0\| + \Delta t \sum_{l=1}^{m} \|\mathcal{H}^{m-l}\|\,\|L_{\Delta x}(l\,\Delta t, \cdot)\|$$

$$\le C_S\big(\|E_{\Delta x}^0\| + \Delta t \sum_{l=1}^{m} \|L_{\Delta x}(l\,\Delta t, \cdot)\|\big)$$

$$\le C_S\big(\|E_{\Delta x}^0\| + T\,C_L\,(\Delta x)^p\big)$$

for $m\,\Delta t \le T$. Hence, letting $\Delta x \to 0$ we deduce the statement, if there is no error in the initial data. $\qquad\square$

Flux Limiters

However, the convergence order is not significant for the quality of the numerical solution. In fact, in Figure 7.4 we observe that in the Upwind scheme (7.15) discontinuities of the exact solution are smoothened out, whereas in the Lax-Wendroff scheme (7.18) oscillations occur around discontinuities. Therefore, we use flux limiters to limit these oscillations.

The damping and oscillatory behaviour of the Upwind and Lax-Wendroff scheme, respectively, can be explained by analysing their corresponding EDE's. Indeed, for the Upwind scheme (7.15) we have calculated in (7.25) a convection diffusion equation with numerical viscosity term

$$|a|\,\frac{\Delta x}{2}\,\big(1 - |a\,\lambda|\big)\,I_{xx}.$$

Consequently, for positive viscosity terms oscillations and strong gradients are damped, whereas for negative viscosity terms disturbances are amplified exponentially. Altogether, we again observe, that the scheme is stable if and only if $|a\,\lambda| \leq 1$.

On the other hand, for the Lax-Wendroff scheme (7.18) we have computed in (7.26) a dispersive equation with dispersion error

$$a\,\frac{(\Delta x)^2}{6}\left(1 - (a\,\lambda)^2\right) I_{xxx},$$

which leads to oscillations in the solution.

However, for an accurate scheme there should be neither a damping nor an oscillatory behaviour. In a moment, we derive a sufficient condition for a non oscillating behaviour of a discrete solution to the transport equation (TPE). For this purpose, we recall that the exact solution $\tilde{I}$ to (TPE) is given by

$$\tilde{I}(t,x) = I_0(x - at).$$

Consequently, it holds

$$\min I_0(x) \leq \tilde{I}(t,x) \leq \max I_0(x) \quad \text{for all } (t,x) \in [0,T] \times \mathbb{R}. \tag{7.27}$$

Moreover, by considering the case, where I_0 is a constant function, we conclude, that the coefficients $b_{j+1/2}, j \in \mathbb{Z}$ of a consistent FD scheme have to satisfy the *consistency condition*

$$\sum_{j\in\mathbb{Z}} b_{j+1/2} = 1. \tag{7.28}$$

Finally, to prevent the oscillatory behaviour of a solution, we require that the scheme is monotone, i.e.,

$$I_{j+1/2}^m \geq J_{j+1/2}^m \quad \Rightarrow \quad \mathcal{H}_{j+1/2}(I) = I_{j+1/2}^{m+1} \geq J_{j+1/2}^{m+1} = \mathcal{H}_{j+1/2}(J) \tag{7.29}$$

for all $j \in \mathbb{Z}$ and $m = 0, ..., M - 1$. As a consequence, in this case we obtain

$$\begin{aligned}
I_{\min}^m = \sum_{j\in\mathbb{Z}} b_{j+1/2} I_{\min}^m &\leq \sum_{j\in\mathbb{Z}} b_{j+1/2} I_{j+1/2}^m = I_{j+1/2}^{m+1} \\
&\leq \sum_{j\in\mathbb{Z}} b_{j+1/2} I_{\max}^m = I_{\max}^m,
\end{aligned} \tag{7.30}$$

where

$$I_{\min}^m = \min(I_{\Delta x}^m) \quad \text{and} \quad I_{\max}^m = \max(I_{\Delta x}^m).$$

Subsequently, by an iteratively application of the estimate (7.30), we obtain the discrete formulation of (7.27), i.e.

$$\min(I_{\Delta x}^0) \leq I_{j+1/2}^m \leq \max(I_{\Delta x}^0)$$

for all $j \in \mathbb{Z}$ and $m = 0, ..., M$.

Moreover, there is a simple condition to check, if a FD scheme is monotone.

Lemma 7.10.
Let

$$I_{j+1/2}^{m+1} = \sum_{k \in \mathbb{Z}} b_{k+j+1/2} \, I_{k+j+1/2}^m. \tag{7.31}$$

be a FD scheme, which satisfies the consistency condition (7.28). Then the scheme is monotone, if

$$b_{j+1/2} \geq 0 \quad \text{for all } j \in \mathbb{Z} \tag{7.32}$$

Proof.
It holds

$$I_{j+1/2}^m \leq J_{j+1/2}^m \quad \Rightarrow \quad b_{j+1/2} I_{j+1/2}^m \leq b_{j+1/2} J_{j+1/2}^m.$$

Thus, we immediately deduce the statement. $\qquad \square$

Remark 7.11.
Note, that the formulation (7.31) is equivalent to

$$I_{j+1/2}^{m+1} = I_{j+1/2}^m + \sum_{k \in \mathbb{Z}} b_{k+j+1/2} \left(I_{k+j+1/2}^m - I_{j+1/2}^m \right),$$

if the consistency condition (7.28) is satisfied.

For the Upwind scheme (7.15) we easily compute

$$b_{j-1/2} = \frac{1}{2} \big(a\,\lambda + |a\,\lambda| \big), \quad b_{j+1/2} = 1 - |a\,\lambda| \quad \text{and} \quad b_{j+3/2} = \frac{1}{2} \big(-a\,\lambda + |a\,\lambda| \big).$$

Hence, the Upwind scheme (7.15) is monotone, if the CFL condition $|a\,\lambda| \leq 1$ is satisfied. In contrast, the Lax-Wendroff scheme (7.18) is non-monotone, since either

$$b_{j-1/2} = \frac{\lambda\,a}{2}(\lambda\,a - 1) \quad \text{or} \quad b_{j+3/2} = \frac{\lambda\,a}{2}(\lambda\,a + 1)$$

is negative.

More general, Godunov states that all linear monotone schemes are of first order [32]. Therefore, we present now the concept of flux limiter to obtain a second order monotone

scheme. Here, the main idea is to combine the benefits of the Upwind (7.15) and the Lax-Wendroff scheme (7.18). More precisely, we would like to use the second order accurate Lax-Wendroff scheme in domains, where the solution is smooth. Whereas, in domains, where the solution is discontinuous, we would like to use the monotone Upwind scheme. Unfortunately, we do not know a priori, where the solution is smooth or not. Therefore, we introduce gradient ratios to measure the local smoothness of the solution. The *gradient ratios* at each cell boundary are defined by

$$R_j = \frac{I_{j-1/2} - I_{j-3/2}}{I_{j+1/2} - I_{j-1/2}}, \quad \text{for } a > 0$$

and

$$R_j = \frac{I_{j+3/2} - I_{j+1/2}}{I_{j+1/2} - I_{j-1/2}}, \quad \text{for } a < 0.$$

We remark, that the gradient ratios are depending on the flow direction due to symmetry reasons in the solution. Finally, by using the measure of the gradient ratios we can locally characterise the behaviour of the solution:

$$R_j \approx 1 \qquad \Rightarrow \text{smooth solution}$$
$$R_j = \varepsilon > 0 \qquad \Rightarrow \text{discontinuity}$$
$$R_j = \infty \qquad \Rightarrow \text{discontinuity}$$
$$R_j < 0 \qquad \Rightarrow \text{local extremum}.$$

Finally, we define a numerical flux function by

$$F_j = F_j^{Up} + \Phi(R_j)\big(F_j^{LW} - F_j^{Up}\big), \tag{7.33}$$

where Φ is a *flux limiter* function, which has to be suitably chosen. Ideally, we have $\Phi \approx 1$ in domains, where the solution is smooth and $\Phi \approx 0$ in domains, where the solution is discontinuous. However, in [32] it is discussed, that the flux limiter Φ should satisfy:

$$0 \leq \Phi(r) \leq \min(2r, 2) \quad \text{and} \quad \Phi(r) = 0, \quad \text{for } r \leq 0.$$

This inequality is satisfied for instance by the *Superbee limiter* defined by

$$\Phi(r) := \max(0, \min(2r, 1), \min(r, 2)). \tag{7.34}$$

For a list of further flux limiter functions, we refer to [32].

Finally, we show that the scheme defined by the numerical flux function (7.33) is indeed monotone. We consider the case, where $a > 0$. Then the numerical flux function is given by

$$\begin{aligned} F_j &= a\, I_{j-1/2}^m + \Phi(R_j) \left(\frac{a}{2} \big(I_{j+1/2}^m - I_{j-1/2}^m \big) - \frac{a^2\,\lambda}{2} \big(I_{j+1/2}^m - I_{j-1/2}^m \big) \right) \\ &= a\, I_{j-1/2}^m + \frac{a}{2} \big(1 - a\,\lambda \big)\, \Phi(R_j) \big(I_{j+1/2}^m - I_{j-1/2}^m \big). \end{aligned} \tag{7.35}$$

(a) Exact solution

(b) Solution with Upwind scheme

(c) Solution with LW scheme

(d) Solution with flux limiter scheme
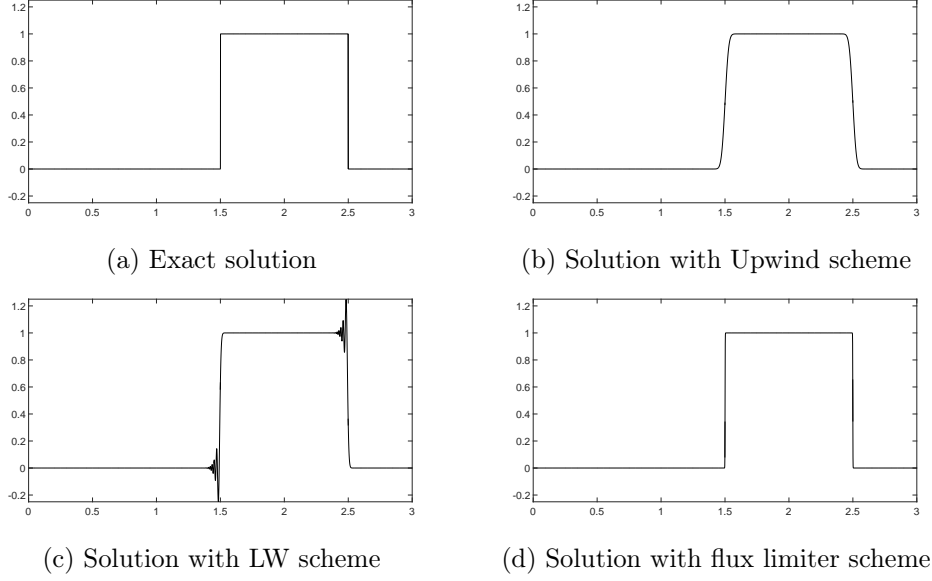
Figure 7.4.: Solution behaviour of FD schemes for the constant transport equation (TPE): Here, problem (TPE) is solved for initial condition $I_0(x) = \chi_{[0.5,1.5]}$ and constant vector field $a = 1$. We use as mesh size $\Delta x = 0.0001$ and as step size $\Delta t = 0.00005$. The exact solution at time $t = 1$ is plotted in (a). The discrete solutions at time $t = 1$ for the different FD schemes are plotted in (b) - (d).

Inserting (7.35) in the conservative formulation (7.19) of a FD scheme leads to

$$
\begin{aligned}
I_{j+1/2}^{m+1} &= I_{j+1/2}^m - a\,\lambda\big(I_{j+1/2}^m - I_{j-1/2}^m\big) \\
&\quad - \frac{a\,\lambda}{2}(1 - a\,\lambda)\Big(\Phi(R_{j+1})\big(I_{j+3/2}^m - I_{j+1/2}^m\big) - \Phi(R_j)\big(I_{j+1/2}^m - I_{j-1/2}^m\big)\Big) \\
&= I_{j+1/2}^m - a\,\lambda\big(I_{j+1/2}^m - I_{j-1/2}^m\big) \\
&\quad - \frac{a\,\lambda}{2}(1 - a\,\lambda)\Big(\frac{\Phi(R_{j+1})}{R_{j+1}} - \Phi(R_j)\Big)\big(I_{j+1/2}^m - I_{j-1/2}^m\big) \\
&= I_{j+1/2}^m - a\,\lambda\Big(1 + \frac{1 - a\,\lambda}{2}\Big(\frac{\Phi(R_{j+1})}{R_{j+1}} - \Phi(R_j)\Big)\Big)\big(I_{j+1/2}^m - I_{j-1/2}^m\big) \\
&= I_{j+1/2}^m + b_{j-1/2}\big(I_{j-1/2}^m - I_{j+1/2}^m\big).
\end{aligned}
$$

Regarding to the monotonicity condition (7.32), we finally conclude that the scheme is monotone, since

$$
b_{j-1/2} = a\,\lambda\Big(1 + \frac{1 - a\,\lambda}{2}\Big(\frac{\Phi(R_{j+1})}{R_{j+1}} - \Phi(R_j)\Big)\Big) \geq 0,
$$

if the CFL condition $|a\,\lambda| \leq 1$ is satisfied.

Considering Figure 7.4 we observe, that the flux limiter scheme defined by the numerical flux (7.33) approximates the exact solution of the transport equation (TPE) very good. In particular, there are no oscillations in the solution and discontinuities are only smoothened out very slightly.

However, note that this scheme is not linear anymore, since the coefficients $b_{j+1/2}$ for $j \in \mathbb{Z}$ are dependent on $I_{\Delta x}^m$.

7.4.2. Conservative Transport Equation

Now we want to generalize the Upwind (7.15) and Lax-Wendroff (7.18) scheme, such that we are also able to solve numerically the optical flow constraint

$$I_t(t,x) + \omega(t,x) \cdot \nabla I(t,x) = 0 \quad \text{with } I(0,x) = I_0(x), \tag{OFC}$$

as well as the conservative transport equation

$$p_t(t,x) + Div\big(\omega(t,x)\,p(t,x)\big) = 0 \quad \text{with } p(0,x) = p_0(x), \tag{cTPE}$$

where $x \in \mathbb{R}$. We start with the numerical treatment of the conservative transport equation (cTPE). Because in this case, we use the numerical fluxes of the Upwind (7.20) and Lax-Wendroff schemes (7.21) to generalize these schemes straightforward. In fact, we only substitute in the numerical flux functions the constant vector field a by the function value of the variable vector field ω evaluated at the current cell boundary. This substitution leads to the following conservative FD scheme:

$$p_{j+1/2}^{m+1} = p_{j+1/2}^m - \lambda\left(F_{j+1}^m(p_{\Delta x}^m) - F_j^m(p_{\Delta x}^m)\right) \tag{7.36}$$

with Upwind flux

$$\begin{aligned} F_j^m(p_{\Delta x}^m) &= \begin{cases} \omega_j^m\, p_{j-1/2}^m &, \text{ for } \omega_j^m \geq 0 \\ \omega_j^m\, p_{j+1/2}^m &, \text{ for } \omega_j^m < 0 \end{cases} \\ &= \frac{1}{2}\,\omega_j^m\left(p_{j+1/2}^m + p_{j-1/2}^m\right) - \frac{1}{2}\left|\omega_j^m\right|\left(p_{j+1/2}^m - p_{j-1/2}^m\right) \end{aligned} \tag{7.37}$$

or Lax-Wendroff flux

$$F_j^m(p_{\Delta x}^m) = \frac{1}{2}\,\omega_j^m\left(p_{j+1/2}^m + p_{j-1/2}^m\right) - \frac{1}{2}\left(\omega_j^m\right)^2 \lambda\left(p_{j+1/2}^m - p_{j-1/2}^m\right), \tag{7.38}$$

respectively.

Consistency

In fact, the conservative Upwind scheme is a first order approximation of the conservative transport equation (cTPE), as the following theorem shows:

Theorem 7.12.
Let $\omega \in \mathcal{C}^1((0,T) \times \mathbb{R})$ and $\tilde{p} \in \mathcal{C}^2((0,T) \times \mathbb{R})$ the exact solution to the conservative transport equation (cTPE). *Then the conservative Upwind scheme defined by* (7.36) *with numerical flux* (7.37) *admits a consisteny order 1.*

Proof.
Letting $(t,x) = (m\,\Delta t, (j+1/2)\,\Delta x)$, we calculate the following Taylor expansion series:

$$\tilde{p}_{j+1/2}^{m+1} = \tilde{p}(t,x) + \tilde{p}_t(t,x)\,\Delta t + \tilde{p}_{tt}(t,x)\,\frac{(\Delta t)^2}{2} + \mathcal{O}((\Delta t)^3),$$

$$\tilde{p}_{j+3/2}^{m} = \tilde{p}(t,x) + \tilde{p}_x(t,x)\,\Delta x + \tilde{p}_{xx}(t,x)\,\frac{(\Delta x)^2}{2} + \mathcal{O}((\Delta x)^3),$$

$$\tilde{p}_{j-1/2}^{m} = \tilde{p}(t,x) - \tilde{p}_x(t,x)\,\Delta x + \tilde{p}_{xx}(t,x)\,\frac{(\Delta x)^2}{2} + \mathcal{O}((\Delta x)^3),$$

$$\omega_{j+1}^{m} = \omega(t,x) + \omega_x(t,x)\,\frac{\Delta x}{2} + \omega_{xx}(t,x)\,\frac{(\Delta x)^2}{8} + \mathcal{O}((\Delta x)^3) \qquad \text{and}$$

$$\omega_{j-1}^{m} = \omega(t,x) - \omega_x(t,x)\,\frac{\Delta x}{2} + \omega_{xx}(t,x)\,\frac{(\Delta x)^2}{8} + \mathcal{O}((\Delta x)^3).$$

Next, we insert these Taylor expansion into the conservative Upwind scheme. However, since the definition of the conservative Upwind flux (7.37) depends on the sign of the vector field ω at the cell boundaries, we use a case analysis and obtain as truncation errors:

(i) For $\omega_j^m \geq 0$ and $\omega_{j+1}^m \geq 0$ we obtain

$$L_{j+1/2}^{m} = \frac{1}{2}(\omega\,\tilde{p}_{xx} + \omega_x\,\tilde{p}_x)\Delta x - \frac{1}{2}\tilde{p}_{tt}\,\Delta t + \mathcal{O}((\Delta x)^2) + \mathcal{O}((\Delta t)^2).$$

(ii) For $\omega_j^m \geq 0$ and $\omega_{j+1}^m < 0$ we obtain

$$L_{j+1/2}^{m} = -\omega\,\tilde{p}_x - \frac{1}{2}\tilde{p}_{tt}\,\Delta t + \mathcal{O}((\Delta x)^2) + \mathcal{O}((\Delta t)^2).$$

Since there exists a root denoted by ξ in the time interval $[j\,\Delta t, (j+1)\,\Delta t]$, we can use a Taylor expansion

$$\omega(x,t) = \omega(\xi,t) + \mathcal{O}(\Delta x) = \mathcal{O}(\Delta x)$$

and obtain

$$L_{j+1/2}^{m} = -\frac{1}{2}\tilde{p}_{tt}\,\Delta t + \mathcal{O}(\Delta x) + \mathcal{O}((\Delta t)^2).$$

(iii) For $\omega_j^m < 0$ and $\omega_{j+1}^m \geq 0$ we obtain

$$L_{j+1/2}^m = \omega \, \tilde{p}_x - \tilde{p}_{tt} \, \frac{\Delta t}{2} + \mathcal{O}((\Delta x)^2) + \mathcal{O}((\Delta t)^2).$$

Since there exists a root denoted by ξ in the time interval $[j \, \Delta t, (j+1) \, \Delta t]$, we can use again a Taylor expansion

$$\omega(x, t) = \omega(\xi, t) + \mathcal{O}(\Delta x) = \mathcal{O}(\Delta x)$$

and obtain

$$L_{j+1/2}^m = -\frac{1}{2} \tilde{p}_{tt} \, \Delta t + \mathcal{O}(\Delta x) + \mathcal{O}((\Delta t)^2).$$

(iv) For $\omega_j^m < 0$ and $\omega_{j+1}^m < 0$ we obtain

$$L_{j+1/2}^m = -\frac{1}{2}(\omega \, \tilde{p}_{xx} + \omega_x \, \tilde{p}_x)\Delta x - \frac{1}{2} \tilde{p}_{tt} \, \Delta t + \mathcal{O}((\Delta x)^2) + \mathcal{O}((\Delta t)^2).$$

Altogether, by recalling $\lambda = \frac{\Delta t}{\Delta x} = const$ we obtain

$$L_{j+1/2}^m = \mathcal{O}(\Delta x).$$

$\square$

Next, we analyse the consistency order of the conservative Lax-Wendroff scheme defined by the numerical flux function (7.38). Here, we use the same Taylor expansion series as in the proof above and obtain as EDE

$$\tilde{p}_t + \text{div}(\omega \, \tilde{p}) = \frac{\Delta t}{2} \left(2 \, \omega \, \omega_x \, \tilde{p}_x + \omega^2 \, \tilde{p}_{xx} - \tilde{p}_{tt} \right),$$

where we assumed that $\omega \in \mathcal{C}^1((0, T) \times \mathbb{R})$ and $\tilde{p} \in \mathcal{C}^2((0, T) \times \mathbb{R})$. Analogously to the constant case (7.17), we substitute the time derivatives by spatial derivatives via

$$\begin{aligned}
\tilde{p}_{tt} &= \left(-\omega \, \tilde{p}_x - \omega_x \, \tilde{p} \right)_t = -\omega_t \, \tilde{p}_x - \omega \, \tilde{p}_{xt} - \omega_{xt} \, \tilde{p} - \omega_x \, \tilde{p}_t \\
&= -\omega_t \, \tilde{p}_x - \omega \left(-\omega \, \tilde{p}_x - \omega_x \, \tilde{p} \right)_x - \omega_{xt} \, \tilde{p} - \omega_x \left(-\omega \, \tilde{p}_x - \omega_x \, \tilde{p} \right) \\
&= -\omega_t \, \tilde{p}_x + \omega \, \omega_x \, \tilde{p}_x + \omega^2 \, \tilde{p}_{xx} + \omega \, \omega_{xx} \, \tilde{p} + \omega \, \omega_x \, \tilde{p}_x - \omega_{xt} \, \tilde{p} + \omega \, \omega_x \, \tilde{p}_x + \omega_x^2 \tilde{p} \\
&= \left(\omega \, \omega_{xx} - \omega_{xt} + \omega_x^2 \right) \tilde{p} + \left(-\omega_t + 3\omega \, \omega_x \right) \tilde{p}_x + \omega^2 \, \tilde{p}_{xx}.
\end{aligned}$$

and obtain

$$\tilde{p}_t + \text{div}(\omega \, \tilde{p}) = \frac{\Delta t}{2} \left(\omega_{xt} - \omega_x^2 - \omega \, \omega_{xx} \right) \tilde{p} + \frac{\Delta t}{2} \left(\omega_t - \omega \, \omega_x \right) \tilde{p}_x.$$

We conclude, that the conservative Lax-Wendroff scheme is only first accurate, too. However, by adopting the thoughts of LeVeque [35], we can rewrite the EDE as

$$\tilde{p}_t(t,x) + \text{div}\left(\omega\left(t - \frac{1}{2}\Delta t,\ x + \frac{1}{2}\,\omega(t,x)\,\Delta t\right)\tilde{p}(t,x)\right) = 0,$$

where we have ignored higher order terms. We observe, that we still solve a conservative transport equation, but with a velocity field which is shifted by less than a grid cell. Hence, under the assumption that the correct conservative transport equation (cTPE) admits a smooth solution, we expect that we obtain with the conservative Lax-Wendroff scheme a discrete solution which looks similar to the exact solution, but slightly offset. In particular, in contrast to the Upwind scheme the solution is not smoothened out (or at least not at $\mathcal{O}(\Delta x)$ level).

Stability

Next, we analyse the stability of the Upwind scheme.

Theorem 7.13 (Stability).
The conservative Upwind scheme defined by the numerical flux function (7.37) is L^1-stable, if the following two conditions are satisfied for all $j \in \mathbb{Z}$ and $m = 0, ..., M - 1$:

$$(i) \qquad\qquad |\lambda\,\omega_j^m| \leq 1, \qquad\qquad\qquad\qquad\qquad (7.39a)$$

$$(ii) \qquad |\lambda(\omega_{j+1}^m - \omega_j^m)| \leq 1, \quad \text{for } \omega_{j+1}^m < 0 \text{ and } \omega_j^m > 0. \qquad (7.39b)$$

Proof.
It holds

$$\left\|p_{\Delta x}^{m+1}\right\| = \Delta x \sum_{j \in \mathbb{Z}} \left|p_{j+1/2}^{m+1}\right|$$

$$= h\left(\sum_{\substack{\omega_{j+1}^m \geq 0 \\ \omega_j^m \geq 0}} \left|p_{j+1/2}^{m+1}\right| + \sum_{\substack{\omega_{j+1}^m < 0 \\ \omega_j^m < 0}} \left|p_{j+1/2}^{m+1}\right| + \sum_{\substack{\omega_{j+1}^m \geq 0 \\ \omega_j^m < 0}} \left|p_{j+1/2}^{m+1}\right| + \sum_{\substack{\omega_{j+1}^m < 0 \\ \omega_j^m \geq 0}} \left|p_{j+1/2}^{m+1}\right|\right)$$

For the first sum we estimate

$$\sum_{\substack{\omega_{j+1}^m \geq 0 \\ \omega_j^m \geq 0}} \left|p_{j+1/2}^{m+1}\right| = \sum_{\substack{\omega_{j+1}^m \geq 0 \\ \omega_j^m \geq 0}} \left|p_{j+1/2}^m - \lambda\left(\omega_{j+1}^m\,p_{j+1/2}^m - \omega_j^m\,p_{j-1/2}^m\right)\right|$$

$$\leq \sum_{\substack{\omega_{j+1}^m \geq 0 \\ \omega_j^m \geq 0}} \left|\left(1 - \lambda\,\omega_{j+1}^m\right)p_{j+1/2}^m\right| + \left|\lambda\,\omega_j^m\,p_{j-1/2}^m\right|$$

$$= \sum_{\substack{\omega_{j+1}^m \geq 0 \\ \omega_j^m \geq 0}} \left(1 - \lambda\,\omega_{j+1}^m\right)\left|p_{j+1/2}^m\right| + \lambda\,\omega_j^m\left|p_{j-1/2}^m\right|.$$

For the second sum we estimate

$$\sum_{\substack{\omega^m_{j+1}<0 \\ \omega^m_j<0}} \left|p^{m+1}_{j+1/2}\right| = \sum_{\substack{\omega^m_{j+1}<0 \\ \omega^m_j<0}} \left|p^m_{j+1/2} - \lambda\left(\omega^m_{j+1}\, p^m_{j+3/2} - \omega^m_j\, p^m_{j+1/2}\right)\right|$$

$$\leq \sum_{\substack{\omega^m_{j+1}<0 \\ \omega^m_j<0}} \left|\left(1 + \lambda\,\omega^m_j\right) p^m_{j+1/2}\right| + \left|\lambda\,\omega^m_{j+1}\, p^m_{j+3/2}\right|$$

$$= \sum_{\substack{\omega^m_{j+1}<0 \\ \omega^m_j<0}} \left(1 + \lambda\,\omega^m_j\right)\left|p^m_{j+1/2}\right| - \lambda\,\omega^m_{j+1}\left|p^m_{j+3/2}\right|.$$

For the third sum we estimate

$$\sum_{\substack{\omega^m_{j+1}\geq 0 \\ \omega^m_j<0}} \left|p^{m+1}_{j+1/2}\right| = \sum_{\substack{\omega^m_{j+1}\geq 0 \\ \omega^m_j<0}} \left|p^m_{j+1/2} - \lambda\left(\omega^m_{j+1}\, p^m_{j+1/2} - \omega^m_j\, p^m_{j+1/2}\right)\right|$$

$$= \sum_{\substack{\omega^m_{j+1}\geq 0 \\ \omega^m_j<0}} \left(1 - \lambda\,\omega^m_{j+1} + \lambda\,\omega^m_j\right)\left|p^m_{j+1/2}\right|$$

For the fourth sum we estimate

$$\sum_{\substack{\omega^m_{j+1}<0 \\ \omega^m_j\geq 0}} \left|p^{m+1}_{j+1/2}\right| = \sum_{\substack{\omega^m_{j+1}<0 \\ \omega^m_j\geq 0}} \left|p^m_{j+1/2} - \lambda\left(\omega^m_{j+1}\, p^m_{j+3/2} - \omega^m_j\, p^m_{j-1/2}\right)\right|$$

$$\leq \sum_{\substack{\omega^m_{j+1}<0 \\ \omega^m_j\geq 0}} \left|p^m_{j+1/2}\right| + \left|\lambda\,\omega^m_{j+1}\, p^m_{j+3/2}\right| + \left|\lambda\,\omega^m_j\, p^m_{j-1/2}\right|$$

$$= \sum_{\substack{\omega^m_{j+1}<0 \\ \omega^m_j\geq 0}} \left|p^m_{j+1/2}\right| - \sum_{\substack{\omega^m_{j+1}<0 \\ \omega^m_j\geq 0}} \lambda\,\omega^m_{j+1}\left|p^m_{j+3/2}\right| + \sum_{\substack{\omega^m_{j+1}<0 \\ \omega^m_j\geq 0}} \lambda\,\omega^m_j\left|p^m_{j-1/2}\right|.$$

Altogether, we get

$$\left\|p^{m+1}_{\Delta x}\right\| = \Delta x \sum_{j\in\mathbb{Z}} \left|p^{m+1}_{j+1/2}\right|$$

$$\leq \|p^m_{\Delta x}\| + \lambda\,\Delta x\left(-\sum_{\omega^m_{j+1}\geq 0} \omega^m_{j+1}\left|p^m_{j+1/2}\right| + \sum_{\omega^m_j<0} \omega^m_j\left|p^m_{j+1/2}\right|\right.$$

$$\left. + \sum_{\omega^m_j\geq 0} \omega^m_j\left|p^m_{j-1/2}\right| - \sum_{\omega^m_{j+1}<0} \omega^m_{j+1}\left|p^m_{j+3/2}\right|\right)$$

$$= \|p_{\Delta x}^m\| + \lambda \Delta x \left(- \sum_{\omega_j^m \geq 0} \omega_j^m \left| p_{j-1/2}^m \right| + \sum_{\omega_j^m < 0} \omega_j^m \left| p_{j+1/2}^m \right| \right.$$

$$\left. + \sum_{\omega_j^m \geq 0} \omega_j^m \left| p_{j-1/2}^m \right| - \sum_{\omega_j^m < 0} \omega_j^m \left| p_{j+1/2}^m \right| \right)$$

$$= \|p_{\Delta x}^m\|.$$

Thus, we conclude the stability with

$$\|\mathcal{H}\| \leq 1.$$

$\square$

Finally, due to Lax's Equivalence theorem we follow from consistency and stability the convergence of the conservative Upwind scheme.

Unfortunately, we are not able to do a stability analysis for the conservative Lax-Wendroff scheme defined by the numerical flux function (7.38).

Monotonicity

Before analysing the monotonicity of the schemes, we remark that we have to redefine the consistency condition (7.28). Because in contrast to the solution of the transport equation (TPE) with constant velocity field, the solution of the conservative transport equation (cTPE) is not necessarily constant along a characteristic. In fact, in Section 3.2.2 we have shown that the exact solution to the conservative transport equation (cTPE) is given by

$$p(t,x) = I_0(y(0)) \exp\left(- \int_0^t \omega_x\big(y(s), s\big) \right),$$

where $y \colon [0, t] \to \mathbb{R}^d$ denotes the solution of the differential equation

$$\dot{y}(\tau) = a\big(\tau, y(\tau)\big) \quad \text{with} \quad y(t) = x.$$

By considering the conservative Upwind (7.37) and Lax-Wendroff scheme (7.38) we observe that in this case the consistency condition is given by

$$\sum_{k \in \mathbb{Z}} b_{k+j+1/2}^m = 1 - \omega_{j+1/2}^m \lambda + \omega_{j-1/2}^m \lambda. \tag{7.40}$$

For a further motivation of this consistency condition, consider the case, where I_0 and ω_x are constant. Then it holds

$$\lambda \left(\omega_{j+1/2}^m - \omega_{j-1/2}^m \right) = \Delta t \, \omega_x$$

for all $j \in \mathbb{Z}$ and $m = 0, ..., M - 1$. As a consequence, we obtain for the discrete solution

$$p_j^M = \left(1 - \Delta t\, \omega_x\right) p_j^{M-1} = \left(1 - \Delta t\, \omega_x\right)^M p_j^0 = \left(1 - \frac{T}{M}\, \omega_x\right)^M p_j^0.$$

Letting $\Delta x \to 0$, leads to

$$p_j^M = \exp\left(- T\, \omega_x\right) p_j^0 = \exp\left(- \int_0^T \omega_x \, \mathrm{d}t\right) p_j^0.$$

Thus, the consistency condition (7.40) is reasonable for the conservative transport equation (cTPE). Nevertheless, also in this case the monotonicity condition

$$b_{j+1/2}^m \geq 0 \quad \text{for all } j \in \mathbb{Z} \text{ and } m = 0, ..., M - 1$$

is sufficient for the same L^∞-boundedness of the discrete solution as for the exact solution.

Theorem 7.14.
The conservative Upwind scheme defined by the numerical flux function (7.37) is monotone, if it satisfies the stability conditions (7.39).

Proof.
We do a case analysis:

(i) for $\omega_j^m \geq 0$ and $\omega_{j+1}^m \geq 0$ we have:

$$b_{j-1/2}^m = \omega_j^m \, \lambda \geq 0 \qquad \text{and}$$
$$b_{j+1/2}^m = 1 - \omega_{j+1}^m \, \lambda \geq 0.$$

(ii) for $\omega_j^m < 0$ and $\omega_{j+1}^m < 0$ we have:

$$b_{j+1/2}^m = 1 + \omega_j^m \, \lambda \geq 0 \qquad \text{and}$$
$$b_{j+3/2}^m = - \omega_{j+1}^m \, \lambda \geq 0.$$

(iii) for $\omega_j^m < 0$ and $\omega_{j+1}^m \geq 0$ we have:

$$b_{j+1/2}^m = \left(1 - \omega_{j+1}^m \, \lambda + \omega_j^m \, \lambda\right) \geq 0.$$

(iv) for $\omega_j^m \geq 0$ and $\omega_{j+1}^m < 0$ we have:

$$b_{j-1/2}^m = \omega_j^m \, \lambda \geq 0,$$
$$b_{j+1/2}^m = 1 \geq 0 \qquad \text{and}$$
$$b_{j+3/2}^m = - \omega_{j+1}^m \, \lambda \geq 0.$$

In summary, we have shown that the conservative Upwind scheme is monotone. $\qquad\square$

On the other hand, the Lax-Wendroff scheme defined by the numerical flux function (7.38) is not monotone, as in the constant case. The non-monotonicity of the Lax-Wendroff scheme is also illustrated in Figure 7.5. Here, we observe for the conservative Upwind and Lax-Wendroff scheme the same damping and oscillating behaviour as in the constant case.

Flux limiters

In this case we also want to combine both schemes by using flux limiters to obtain more accurate approximations. However, to detect jumps in the vector field, we redefine the gradient ratios by

$$R_j^m = \frac{\omega_{j-1}^{m,+}\left(p_{j-1/2}^m - p_{j-3/2}^m\right)}{\omega_j^{m,+}\left(p_{j+1/2}^m - p_{j-1/2}^m\right)}, \quad \text{for } \omega_j^m \geq 0 \tag{7.41a}$$

or

$$R_j^m = \frac{\omega_{j+1}^{m,-}\left(p_{j+3/2}^m - p_{j+1/2}^m\right)}{\omega_j^{m,-}\left(p_{j+1/2}^m - p_{j-1/2}^m\right)}, \quad \text{for } \omega_j^m \leq 0, \tag{7.41b}$$

respectively, where

$$\omega_j^{m,+} = \max(\omega_j^m, 0), \quad \text{and} \quad \omega_j^{m,-} = \min(\omega_j^m, 0).$$

Finally, we use the Superbee flux limiter function (7.34) to combine both schemes, i.e.,

$$F_j(p_{\Delta x}^m) = F_j^{Up}(p_{\Delta x}^m) + \Phi(\theta_j)\, F_j^{HOT}(p_{\Delta x}^m), \tag{7.42}$$

where

$$\begin{aligned} F_j^{HOT}(p_{\Delta x}^m) &= F_j^{LW}(p_{\Delta x}^m) - F_j^{Up}(p_{\Delta x}^m) \\ &= \frac{1}{2}|\omega_j^m|\left(1 - |\omega_j^m|\lambda\right)\left(p_{j+1/2}^m - p_{j-1/2}^m\right). \end{aligned} \tag{7.43}$$

Theorem 7.15.
The scheme defined by (7.19) with numerical flux (7.42) is monotone, if the stability conditions (7.39) of the conservative Upwind scheme are satisfied.

Proof.
We do a case analysis:

(i) for $\omega_j^m \geq 0$ and $\omega_{j+1}^m \geq 0$ we have:

$$p_{j+1/2}^{m+1} = p_{j+1/2}^m - \omega_{j+1}^m \lambda\, p_{j+1/2} + \omega_j^m \lambda\, p_{j-1/2}$$

$$- \frac{1}{2}\,\Phi\!\left(R_{j+1}^m\right) \omega_{j+1}^m \lambda \left(1 - \omega_{j+1}^m \lambda\right) \left(p_{j+3/2}^m - p_{j+1/2}^m\right)$$

$$+ \frac{1}{2}\,\Phi\!\left(R_j^m\right) \omega_j^m \lambda \left(1 - \omega_j^m \lambda\right) \left(p_{j+1/2}^m - p_{j-1/2}^m\right)$$

$$= p_{j+1/2}^m - \omega_{j+1}^m \lambda\, p_{j+1/2} + \omega_j^m \lambda\, p_{j-1/2}$$

$$- \frac{1}{2}\,\frac{\Phi\!\left(R_{j+1}^m\right)}{R_{j+1}^m}\, \omega_j^m \lambda \left(1 - \omega_{j+1}^m \lambda\right) \left(p_{j+1/2}^m - p_{j-1/2}^m\right)$$

$$+ \frac{1}{2}\,\Phi\!\left(R_j^m\right) \omega_j^m \lambda \left(1 - \omega_j^m \lambda\right) \left(p_{j+1/2}^m - p_{j-1/2}^m\right)$$

$$= b_{j-1/2}^m\, p_{j-1/2}^m + b_{j+1/2}^m\, p_{j+1/2}^m$$

with

$$b_{j-1/2}^m = \omega_j^m \lambda \left[1 - \frac{1}{2}\left(\Phi\!\left(R_j^m\right)\left(1 - \omega_j^m\right) - \frac{\Phi\!\left(R_{j+1}^m\right)}{R_{j+1}^m}\left(1 - \omega_{j+1}^m \lambda\right)\right)\right]$$

$$\geq \omega_j^m \lambda \left(1 - \frac{1}{2}\, 2\right) \geq 0$$

and

$$b_{j+1/2}^m = 1 - \omega_{j+1}^m \lambda$$

$$- \frac{1}{2}\,\omega_j^m \lambda \left(\frac{\Phi\!\left(R_{j+1}^m\right)}{R_{j+1}^m}\left(1 - \omega_{j+1}^m \lambda\right) - \Phi\!\left(R_j^m\right)\left(1 - \omega_j^m\right)\right)$$

$$\geq 1 - \omega_{j+1}^m \lambda - \frac{1}{2}\,\omega_j^m \lambda\left(2\left(1 - \omega_{j+1}^m \lambda\right) - 0\right)$$

$$\geq 1 + \left(\lambda\,\omega_j^m\right)\left(\lambda\,\omega_{j+1}^m\right) - \lambda\left(\omega_{j+1}^m + \omega_j^m\right) \geq 0.$$

(ii) for $\omega_j^m < 0$ and $\omega_{j+1}^m < 0$ we have:

$$p_{j+1/2}^{m+1} = p_{j+1/2}^m - \omega_{j+1}^m \lambda\, p_{j+3/2} + \omega_j^m \lambda\, p_{j+1/2}$$

$$+ \frac{1}{2}\,\Phi\!\left(R_{j+1}^m\right) \omega_{j+1}^m \lambda \left(1 + \omega_{j+1}^m \lambda\right) \left(p_{j+3/2}^m - p_{j+1/2}^m\right)$$

$$- \frac{1}{2}\,\Phi\!\left(R_j^m\right) \omega_j^m \lambda \left(1 + \omega_j^m \lambda\right) \left(p_{j+1/2}^m - p_{j-1/2}^m\right)$$

$$= p_{j+1/2}^m - \omega_{j+1}^m \lambda\, p_{j+3/2} + \omega_j^m \lambda\, p_{j+1/2}$$

$$+ \frac{1}{2}\,\Phi\!\left(R_{j+1}^m\right) \omega_{j+1}^m \lambda \left(1 + \omega_{j+1}^m \lambda\right) \left(p_{j+3/2}^m - p_{j+1/2}^m\right)$$

$$- \frac{1}{2}\,\frac{\Phi\!\left(R_j^m\right)}{R_j^m}\, \omega_{j+1}^m \lambda \left(1 + \omega_j^m \lambda\right) \left(p_{j+3/2}^m - p_{j+1/2}^m\right)$$

$$= b_{j+1/2}^m\, p_{j+1/2}^m + b_{j+3/2}^m\, p_{j+3/2}^m$$

with

$$b^m_{j+1/2} = 1 + \omega^m_j \lambda$$
$$+ \frac{1}{2} \omega^m_{j+1} \lambda \left(\frac{\Phi(R^m_j)}{R^m_j} \left(1 + \omega^m_j \lambda\right) - \Phi(R^m_{j+1}) \left(1 + \omega^m_{j+1} \lambda\right) \right)$$
$$\geq 1 + \omega^m_j \lambda + \frac{1}{2} \omega^m_{j+1} \lambda \left(2 \left(1 + \omega^m_j \lambda\right) - 0 \right)$$
$$\geq 1 + \left(\lambda \omega^m_j\right) \left(\lambda \omega^m_{j+1}\right) + \lambda \left(\omega^m_{j+1} + \omega^m_j\right) \geq 0.$$

and

$$b^m_{j+3/2} = -\omega^m_{j+1} \lambda \left[1 - \frac{1}{2} \left(\frac{\Phi(R^m_j)}{R^m_j} \left(1 + \omega^m_j \lambda\right) - \Phi(R^m_{j+1}) \left(1 + \omega^m_{j+1}\right) \right) \right]$$
$$\geq -\omega^m_{j+1} \lambda \left(1 - \frac{1}{2} 2\right) \geq 0$$

(iii) For $\omega^m_j \geq 0$ and $\omega^m_{j+1} < 0$ we have:

$$p^{m+1}_{j+1/2} = p^m_{j+1/2} - \omega^m_{j+1} \lambda p_{j+3/2} + \omega^m_j \lambda p_{j-1/2}$$
$$+ \frac{1}{2} \Phi(R^m_{j+1}) \omega^m_{j+1} \lambda \left(1 + \omega^m_{j+1} \lambda\right) \left(p^m_{j+3/2} - p^m_{j+1/2}\right)$$
$$+ \frac{1}{2} \Phi(R^m_j) \omega^m_j \lambda \left(1 - \omega^m_j \lambda\right) \left(p^m_{j+1/2} - p^m_{j-1/2}\right)$$
$$= b^m_{j-1/2} p^m_{j-1/2} + b^m_{j+1/2} p^m_{j+1/2} + b^m_{j+3/2} p^m_{j+3/2}$$

with

$$b^m_{j-1/2} = \omega^m_j \lambda \left(1 - \frac{1}{2} \Phi(R^m_j) \omega^m_j \lambda \left(1 - \omega^m_j \lambda\right) \right)$$
$$\geq \omega^m_j \lambda \left(1 - \frac{1}{2} 2\right) \geq 0,$$
$$b^m_{j+1/2} = 1 - \frac{1}{2} \left(\Phi(R^m_{j+1}) \omega^m_{j+1} \lambda \left(1 + \omega^m_{j+1} \lambda\right) \right.$$
$$\left. - \Phi(R^m_j) \omega^m_j \lambda \left(1 - \omega^m_j \lambda\right) \right)$$
$$\geq 1 - \frac{1}{2} 2 \geq 0$$

and

$$b^m_{j+3/2} = -\omega^m_{j+1} \lambda \left(1 - \frac{1}{2} \Phi(R^m_{j+1}) \omega^m_{j+1} \lambda \left(1 + \omega^m_{j+1} \lambda\right) \right)$$
$$\geq -\omega^m_{j+1} \lambda \left(1 - \frac{1}{2} 2\right) \geq 0.$$

(iv) For $\omega_j^m < 0$ and $\omega_{j+1}^m \geq 0$ we have $\Phi(R_j) = \Phi(R_{j+1}) = 0$. As a consequence, we obtain the monotone, conservative Upwind scheme.

Altogether, we have shown that the scheme defined by (7.19) with numerical flux (7.42) is monotone. □

(a) exact solution   (b) solution with Upwind scheme

(c) solution with LW scheme   (d) solution with flux limiter scheme
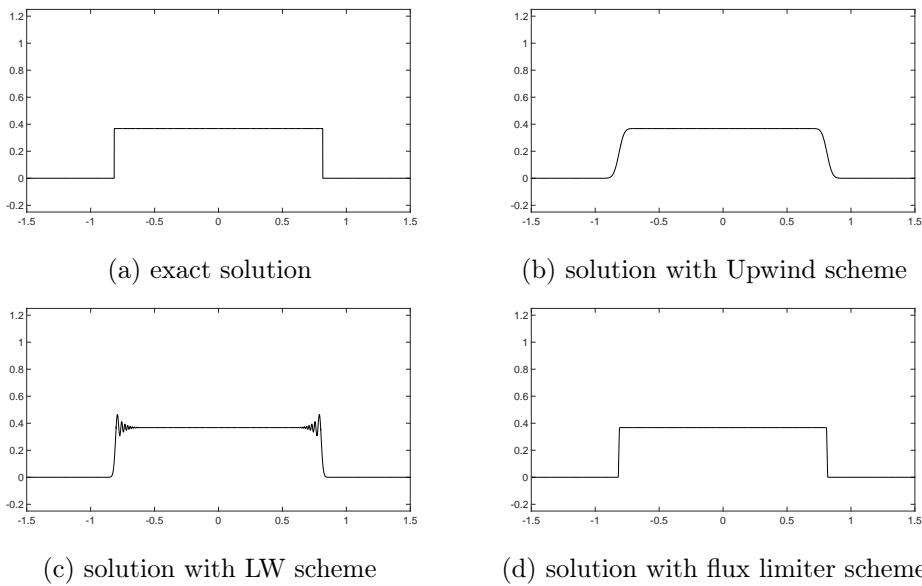
Figure 7.5.: Solution behaviour of FD schemes for the conservative transport equation (cTPE): Here, problem (cTPE) is solved for initial condition $I_0(x) = \chi_{[-0.3,0.3]}$ and vector field $\omega(t,x) = x$. We use as mesh size $\Delta x = 0.0001$ and as step size $\Delta t = 0.00005$. The exact solution at time $t = 1$ is plotted in (a). The discrete solutions at time $t = 1$ for the different FD schemes are plotted in (b) - (d).

Finally, in Figure 7.5 we observe that we obtain very accurate approximations to the exact solution of the conservative transport equation (cTPE), if we use the flux limiter scheme defined by the flux function (7.42).

7.4.3. Non-Conservative Transport Equation

Next, we want to generalize the Upwind (7.15) and Lax-Wendroff scheme (7.18), such that we are able to numerically solve the non-conservative transport equation (OFC).

Non-Conservative Upwind Scheme

For the generalization of the Upwind scheme we first rewrite the scheme for the constant case (7.20) as

$$I_{j+1/2}^{m+1} = I_{j+1/2}^m - \lambda \left(a^+ \, G_j(I_{\Delta x}^m) + a^- \, G_{j+1}(I_{\Delta x}^m) \right),$$

where

$$a^+ = \max(a, 0), \quad a^- = \min(a, 0)$$

and

$$G_j(I_{\Delta x}^m) = I_{j+1/2}^m - I_{j-1/2}^m.$$

Then we generalize the scheme by substituting a by the function value of the vector field ω evaluated at the current cell boundary. This generalization leads to the following non-conservative Upwind scheme:

$$I_{j+1/2}^{m+1} = I_{j+1/2}^m - \lambda \left(\omega_j^{m,+} \, G_j(I_{\Delta x}^m) + \omega_{j+1}^{m,-} \, G_{j+1}(I_{\Delta x}^m) \right), \tag{7.44}$$

where

$$\omega_j^{m,+} = \max(\omega_j^m, 0), \quad \omega_{j+1}^{m,-} = \min(\omega_{j+1}^m, 0)$$

and

$$G_j(I_{\Delta x}^m) = I_{j+1/2}^m - I_{j-1/2}^m.$$

In fact, this scheme approximates the non-conservative transport equation (cTPE).

Theorem 7.16.
Let $\omega \in \mathcal{C}^1((0, T) \times \mathbb{R})$ and $\tilde{I} \in \mathcal{C}^2((0, T) \times \mathbb{R})$ the exact solution of the non-conservative transport equation (OFC). *Then the non-convervative Upwind scheme defined by* (7.44) *admits a consistency order 1.*

Proof.
Analogously to the consistency analysis of the conservative Upwind scheme (Theorem 7.12) we find the truncation errors for the different cases:

(i) For $\omega_j^m \geq 0$ and $\omega_{j+1}^m \geq 0$ we obtain

$$L_{j+1/2}^m = \frac{1}{2}(\omega \, \tilde{I}_{xx} + \omega_x \, \tilde{I}_x)\Delta x - \frac{1}{2}\tilde{I}_{tt} \, \Delta t + \mathcal{O}((\Delta x)^2) + \mathcal{O}((\Delta t)^2).$$

(ii) For $\omega_j^m \geq 0$ and $\omega_{j+1}^m < 0$ we obtain

$$L_{j+1/2}^m = -\frac{1}{2}\tilde{I}_{tt} \, \Delta t + \mathcal{O}(\Delta x) + \mathcal{O}((\Delta t)^2).$$

(iii) For $\omega_j^m < 0$ and $\omega_{j+1}^m \geq 0$ we obtain

$$L_{j+1/2}^m = -\frac{1}{2}\tilde{I}_{tt}\,\Delta t + \mathcal{O}(\Delta x) + \mathcal{O}((\Delta t)^2).$$

(iv) For $\omega_j^m < 0$ and $\omega_{j+1}^m < 0$ we obtain

$$L_{j+1/2}^m = -\frac{1}{2}(\omega\,\tilde{I}_{xx} + \omega_x\,\tilde{I}_x)\Delta x - \frac{1}{2}\tilde{I}_{tt}\,\Delta t + \mathcal{O}((\Delta x)^2) + \mathcal{O}((\Delta t)^2).$$

Altogether, by recalling $\lambda = \frac{\Delta t}{\Delta x} = const$ we obtain

$$L_{j+1/2}^m = \mathcal{O}(\Delta x).$$

$\square$

Non-Conservative Lax-Wendroff Scheme

Comparing the truncation errors of the conservative and the non-conservative Upwind scheme (cf. Theorem 7.12 and Theorem 7.16) we observe that both schemes have the same first order error terms. This fact motivates us to add in the non-conservative case the same error corrections terms to the Upwind scheme as in the conservative case. Consequently, we define the non-conservative Lax-Wendroff scheme as follows

$$I_{j+1/2}^{m+1} = I_{j+1/2}^m - \lambda\left(\omega_j^{m,+}\,G_j(I_{\Delta x}^m) + \omega_{j+1}^{m,-}\,G_{j+1}(I_{\Delta x}^m)\right)$$
$$- \lambda\left(F_{j+1}^{HOT}(I_{\Delta x}^m) - F_j^{HOT}(I_{\Delta x}^m)\right),$$

where F_j^{HOT} is defined in (7.43). Moreover, by using

$$\tilde{I}_{tt} = \left(-\omega\,\tilde{I}_x\right)_t = -\omega_t\,\tilde{I}_x - \omega\,\tilde{I}_{xt}$$
$$= -\omega_t\,\tilde{I}_x - \omega\left(-\omega\,\tilde{I}_x\right)_x = -\omega_t\,\tilde{I}_x + \omega\,\omega_x\,\tilde{I}_x + \omega^2\,\tilde{I}_{xx}$$

we obtain as EDE

$$\tilde{I}_t + \omega\,\tilde{I}_x = \frac{\Delta t}{2}\left(\omega_t + \omega\,\omega_x\right)\tilde{I}_x,$$

where we assumed that $\omega \in \mathcal{C}^1((0,T)\times\mathbb{R})$ and $\tilde{I} \in \mathcal{C}^2((0,T)\times\mathbb{R})$ is the exact solution to the non-conservative transport equation (OFC). This EDE can be rewritten (ignoring higher order terms) as

$$\tilde{I}_t(t,x) + \omega\left(t - \frac{1}{2}\Delta t,\ x - \frac{1}{2}\omega(t,x)\,\Delta t\right)\tilde{I}_x(t,x) = 0.$$

Hence, by using the same argumentation as for the conservative Lax-Wendroff scheme (see page 98), we expect that the solution of the non-conservative Lax-Wendroff scheme is less smoothened out than the solution of the non-conservative Upwind scheme.

Stability

Next, we analyse the stability of the Upwind scheme.

Theorem 7.17 (Stability).
Let $\omega \in \mathcal{C}^1((0,T) \times \mathbb{R})$. Then the non-conservative Upwind scheme (7.44) is L^1-stable, if the following condition is satisfied:

$$|\lambda\,\omega_j^m| \leq 1, \quad \text{for all } j \in \mathbb{Z} \text{ and } m = 0, ..., M-1. \tag{7.45}$$

Proof.
Analogously to the stability analysis of the conservative Upwind scheme, we obtain by using the stability condition (7.45)

$$\left\| I_{\Delta x}^{m+1} \right\| = \Delta x \sum_{j \in \mathbb{Z}} \left| I_{j+1/2}^{m+1} \right|$$

$$= h \left(\sum_{\substack{\omega_{j+1}^m \geq 0 \\ \omega_j^m \geq 0}} \left| I_{j+1/2}^{m+1} \right| + \sum_{\substack{\omega_{j+1}^m < 0 \\ \omega_j^m < 0}} \left| I_{j+1/2}^{m+1} \right| + \sum_{\substack{\omega_{j+1}^m \geq 0 \\ \omega_j^m < 0}} \left| I_{j+1/2}^{m+1} \right| + \sum_{\substack{\omega_{j+1}^m < 0 \\ \omega_j^m \geq 0}} \left| I_{j+1/2}^{m+1} \right| \right)$$

$$= \left\| I_{\Delta x}^m \right\| + \lambda\,\Delta x \left(- \sum_{\omega_j^m \geq 0} \left| \omega_j^m \right| \left| I_{j+1/2}^m \right| + \sum_{\omega_j^m \geq 0} \left| \omega_j^m \right| \left| I_{j-1/2}^m \right| \right.$$

$$\left. - \sum_{\omega_{j+1}^m < 0} \left| \omega_{j+1}^m \right| \left| I_{j+1/2}^m \right| + \sum_{\omega_{j+1}^m < 0} \left| \omega_{j+1}^m \right| \left| I_{j+3/2}^m \right| \right).$$

With the help of the Taylor estimation

$$\left| \omega_j \right| \leq \left| \omega_{j+1} \right| + C\,\Delta x, \quad \text{with } C := \max_{(\xi,\tau)} \left| \omega_x(\xi,\tau) \right|,$$

we obtain

$$\left\| I_{\Delta x}^{m+1} \right\| \leq \left\| I_{\Delta x}^m \right\| + \lambda\,\Delta x \left(- \sum_{\omega_j^m \geq 0} \left| \omega_j^m \right| \left| I_{j+1/2}^m \right| + \sum_{\omega_j^m \geq 0} \left| \omega_{j-1}^m \right| \left| I_{j-1/2}^m \right| \right.$$

$$- \sum_{\omega_{j+1}^m < 0} \left| \omega_{j+1}^m \right| \left| I_{j+1/2}^m \right| + \sum_{\omega_{j+1}^m < 0} \left| \omega_{j+2}^m \right| \left| I_{j+3/2}^m \right|$$

$$\left. + \sum_{\omega_j^m \geq 0} C\,\Delta x \left| I_{j-1/2}^m \right| + \sum_{\omega_{j+1}^m < 0} C\,\Delta x \left| I_{j+3/2}^m \right| \right)$$

$$= \left\| I_{\Delta x}^m \right\| + \lambda \, \Delta x \left(\sum_{\substack{\omega_{j+1}^m \geq 0 \\ \omega_j^m < 0}} \left| \omega_j^m \right| \left| I_{j+1/2}^m \right| - \sum_{\substack{\omega_{j+1}^m < 0 \\ \omega_j^m \geq 0}} \left| \omega_j^m \right| \left| I_{j+1/2}^m \right| \right.$$

$$+ \sum_{\substack{\omega_{j+1}^m \geq 0 \\ \omega_j^m < 0}} \left| \omega_{j+1}^m \right| \left| I_{j+1/2}^m \right| - \sum_{\substack{\omega_{j+1}^m < 0 \\ \omega_j^m \geq 0}} \left| \omega_{j+1}^m \right| \left| I_{j+1/2}^m \right|$$

$$\left. + \sum_{\omega_j^m \geq 0} C \, \Delta x \left| I_{j-1/2}^m \right| + \sum_{\omega_{j+1}^m < 0} C \, \Delta x \left| I_{j+3/2}^m \right| \right) = (*),$$

where we have exploited in the last step, that there are two telescoping sums.

For each of the sums in the second and third last line we note, that ω admits a root in the interval $[(j - 1/2)\Delta x, (j + 1/2)\Delta x]$, which we denote by ξ. Hence, by using the Taylor estimate

$$\left| \omega_{j\pm 1/2} \right| \leq \left| \omega(\xi) \right| + C \, \frac{\Delta x}{2} \leq C \, \Delta x, \quad \text{with } C := \max_{(\xi, \tau)} \left| \omega_x(\xi, \tau) \right|$$

we obtain

$$(*) \leq \left\| I_{\Delta x}^m \right\| + C \, \lambda \, (\Delta x)^2 \left(\sum_{\omega_j^m \geq 0} \left| I_{j-1/2}^m \right| + \sum_{\omega_{j+1}^m < 0} \left| I_{j+3/2}^m \right| + \sum_{\substack{\omega_{j+1}^m \geq 0 \\ \omega_j^m < 0}} \left| I_{j+1/2}^m \right| \right.$$

$$\left. + \sum_{\substack{\omega_{j+1}^m < 0 \\ \omega_j^m \geq 0}} \left| I_{j+1/2}^m \right| + \sum_{\substack{\omega_{j+1}^m \geq 0 \\ \omega_j^m < 0}} \left| I_{j+1/2}^m \right| + \sum_{\substack{\omega_{j+1}^m < 0 \\ \omega_j^m \geq 0}} \left| I_{j+1/2}^m \right| \right)$$

$$\leq \left\| I_{\Delta x}^m \right\| + 6 \, C \, \Delta x \, \lambda \left\| I_{\Delta x}^m \right\|$$

$$= \left(1 + \tilde{C} \, \Delta t \right) \left\| I_{\Delta x}^m \right\|,$$

where $\tilde{C} = C \, \lambda^2$. Consequently, we conclude the stability with

$$\left\| \mathcal{H} \right\| \leq 1 + \tilde{C} \, \Delta t.$$

$\square$

Finally, we follow from consistency and stability the convergence of the conservative Upwind scheme due to Lax's Equivalence theorem.

Flux limiter

In Figure 7.6 the solution behaviour of the non-conservative Upwind and Lax-Wendroff scheme is illustrated. As in the constant case, we observe that in the non-conservative Upwind scheme discontinuities of the exact solution are smoothened out, whereas in the non-conservative Lax-Wendroff scheme oscillations occur around the discontinuities. Therefore, also in this case, we want to combine both schemes by using flux limiters to obtain more accurate approximations.

For the non-conservative transport equation (OFC) the exact solution $\tilde{I}$ is given by

$$\tilde{I}(t, x) = I_0(y(0)),$$

where $y \colon [0, t] \to \mathbb{R}^d$ denotes the solution of the differential equation

$$\dot{y}(\tau) = a\big(\tau, y(\tau)\big) \quad \text{with} \quad y(t) = x.$$

Hence, analogous to the transport equation with constant vector field (TPE), the scheme is monotone if

$$\sum_{j \in \mathbb{Z}} b^m_{j+1/2} = 1 \quad \text{and} \quad b^m_{j+1/2} \geq 0 \quad \text{for all } j \in \mathbb{Z}.$$

For the combination of the non-conservative Upwind and Lax-Wendroff scheme we use the same gradient ratios given by (7.41) as in the conservative case. Finally, we define the following monotone scheme

$$
\begin{aligned}
I^{m+1}_{j+1/2} = I^m_{j+1/2} &- \lambda \left(\omega^{m,+}_j \, G_j(I^m_{\Delta x}) + \omega^{m,-}_{j+1} \, G_{j+1}(I^m_{\Delta x}) \right) \\
&- \lambda \left(\Phi(R_{j+1}) F^{HOT}_{j+1}(I^m_{\Delta x}) - \Phi(R_j) F^{HOT}_j(I^m_{\Delta x}) \right),
\end{aligned}
\tag{7.46}
$$

where F^{HOT}_j is defined in (7.43) and Φ denotes the Superbee flux function (7.34).

In fact, we can show that this scheme is monotone.

Theorem 7.18.
Let $\omega \in \mathcal{C}^1((0, T) \times \mathbb{R})$. Then the scheme defined by (7.46) is monotone, if the stability condition (7.45) of the non-conservative Upwind scheme is satisfied

Proof.
We do a case analysis:

(i) For $\omega_j^m \geq 0$ and $\omega_{j+1}^m \geq 0$ we have:

$$
\begin{aligned}
I_{j+1/2}^{m+1} = {}& I_{j+1/2}^m - \omega_j^m \lambda \left(I_{j+1/2} - I_{j-1/2}\right) \\
& - \frac{1}{2}\, \Phi\!\left(R_{j+1}^m\right) \omega_{j+1}^m \lambda \left(1 - \omega_{j+1}^m \lambda\right) \left(I_{j+3/2}^m - I_{j+1/2}^m\right) \\
& + \frac{1}{2}\, \Phi\!\left(R_j^m\right) \omega_j^m \lambda \left(1 - \omega_j^m \lambda\right) \left(I_{j+1/2}^m - I_{j-1/2}^m\right) \\
= {}& I_{j+1/2}^m + \omega_j^m \lambda \left(I_{j-1/2} - I_{j+1/2}\right) \\
& + \frac{1}{2}\, \frac{\Phi\!\left(R_{j+1}^m\right)}{R_{j+1}^m}\, \omega_j^m \lambda \left(1 - \omega_{j+1}^m \lambda\right) \left(I_{j-1/2}^m - I_{j+1/2}^m\right) \\
& - \frac{1}{2}\, \Phi\!\left(R_j^m\right) \omega_j^m \lambda \left(1 - \omega_j^m \lambda\right) \left(I_{j-1/2}^m - I_{j+1/2}^m\right) \\
= {}& I_{j+1/2}^m + b_{j-1/2}^m \left(I_{j-1/2}^m - I_{j+1/2}^m\right)
\end{aligned}
$$

with

$$
b_{j-1/2}^m = \omega_j^m \lambda \left[1 - \frac{1}{2}\left(\Phi\!\left(R_j^m\right)\left(1 - \omega_j^m \lambda\right) - \frac{\Phi\!\left(R_{j+1}^m\right)}{R_{j+1}^m}\left(1 - \omega_{j+1}^m \lambda\right)\right)\right]
$$

$$
\geq \omega_j^m \lambda \left(1 - \frac{1}{2}\,2\right) \geq 0.
$$

(ii) For $\omega_j^m < 0$ and $\omega_{j+1}^m < 0$ we have:

$$
\begin{aligned}
I_{j+1/2}^{m+1} = {}& I_{j+1/2}^m - \omega_{j+1}^m \lambda \left(I_{j+3/2} - I_{j+1/2}\right) \\
& + \frac{1}{2}\, \Phi\!\left(R_{j+1}^m\right) \omega_{j+1}^m \lambda \left(1 + \omega_{j+1}^m \lambda\right) \left(I_{j+3/2}^m - I_{j+1/2}^m\right) \\
& - \frac{1}{2}\, \Phi\!\left(R_j^m\right) \omega_j^m \lambda \left(1 + \omega_j^m \lambda\right) \left(I_{j+1/2}^m - I_{j-1/2}^m\right) \\
= {}& I_{j+1/2}^m - \omega_{j+1}^m \lambda \left(I_{j+3/2} - I_{j+1/2}\right) \\
& + \frac{1}{2}\, \Phi\!\left(R_{j+1}^m\right) \omega_{j+1}^m \lambda \left(1 + \omega_{j+1}^m \lambda\right) \left(I_{j+3/2}^m - I_{j+1/2}^m\right) \\
& - \frac{1}{2}\, \frac{\Phi\!\left(R_j^m\right)}{R_j^m}\, \omega_{j+1}^m \lambda \left(1 + \omega_j^m \lambda\right) \left(I_{j+3/2}^m - I_{j+1/2}^m\right) \\
= {}& I_{j+1/2}^m + b_{j+3/2}^m \left(I_{j+3/2}^m - I_{j+1/2}^m\right)
\end{aligned}
$$

with

$$
b_{j+3/2}^m = -\omega_{j+1}^m \lambda \left[1 - \frac{1}{2}\left(\Phi\!\left(R_{j+1}^m\right)\left(1 + \omega_{j+1}^m \lambda\right) - \frac{\Phi\!\left(R_j^m\right)}{R_j^m}\left(1 + \omega_j^m \lambda\right)\right)\right]
$$

$$
\geq -\omega_{j+1}^m \lambda \left(1 - \frac{1}{2}\,2\right) \geq 0.
$$

(iii) For $\omega_j^m \geq 0$ and $\omega_{j+1}^m < 0$ we have:

$$
\begin{aligned}
I_{j+1/2}^{m+1} = {} & I_{j+1/2}^m - \omega_j^m \lambda \left(I_{j+1/2} - I_{j-1/2} \right) - \omega_{j+1}^m \lambda \left(I_{j+3/2} - I_{j+1/2} \right) \\
& + \frac{1}{2} \Phi\left(R_{j+1}^m\right) \omega_{j+1}^m \lambda \left(1 + \omega_{j+1}^m \lambda\right) \left(I_{j+3/2}^m - I_{j+1/2}^m \right) \\
& + \frac{1}{2} \Phi\left(R_j^m\right) \omega_j^m \lambda \left(1 - \omega_j^m \lambda\right) \left(I_{j+1/2}^m - I_{j-1/2}^m \right) \\
= {} & I_{j+1/2}^m + b_{j-1/2}^m \left(I_{j-1/2}^m - I_{j+1/2}^m \right) + b_{j+3/2}^m \left(I_{j+3/2}^m - I_{j+1/2}^m \right)
\end{aligned}
$$

with

$$
\begin{aligned}
b_{j-1/2}^m &= \omega_j^m \lambda \left(1 - \frac{1}{2} \Phi\left(R_j^m\right) \left(1 - \omega_j^m \lambda\right) \right) \\
&\geq \omega_j^m \lambda \left(1 - \frac{1}{2} 2 \right) \geq 0
\end{aligned}
$$

and

$$
\begin{aligned}
b_{j+1/2}^m &= -\omega_{j+1}^m \lambda \left(1 - \frac{1}{2} \Phi\left(R_{j+1}^m\right) \left(1 + \omega_{j+1}^m \lambda\right) \right) \\
&\geq -\omega_{j+1}^m \lambda \left(1 - \frac{1}{2} 2 \right) \geq 0.
\end{aligned}
$$

(iv) For $\omega_j^m < 0$ and $\omega_{j+1}^m \geq 0$ we have $\Phi(R_j) = \Phi(R_{j+1}) = 0$ and, consequently, $I_{j+1/2}^{m+1} = I_{j+1/2}^m$.

In Summary, we have shown that the scheme defined by (7.46) is monotone □

Corollary 7.19.
The non-conservative Upwind scheme (7.15) is monotone, if the stability condition (7.45) is satisfied.

Proof.
By setting $\Phi_R = 0$ in the proof of theorem 7.18. □

Finally, in Figure 7.6 we observe that we obtain very accurate approximations to the exact solution of the non-conservative transport equation (OFC), if we use the flux limiter scheme defined in (7.46).

7.4.4. Directional Splitting Approach

This section presents a splitting approach for solving a transport equation in the multi-dimensional case [36]. We exemplify it with the two dimensional case, i.e., we consider the non-conservative transport equation

$$
\begin{aligned}
0 &= I_t(t, x, y) + \omega(t, x, y) \cdot \nabla I(t, x, y) \\
&= I_t(t, x, y) + u(t, x, y) I_x(t, x, y) + v(t, x, y) I_y(t, x, y)
\end{aligned}
\tag{7.47a}
$$

(a) exact solution

(b) solution with Upwind scheme

(c) solution with LW scheme

(d) solution with flux limiter scheme
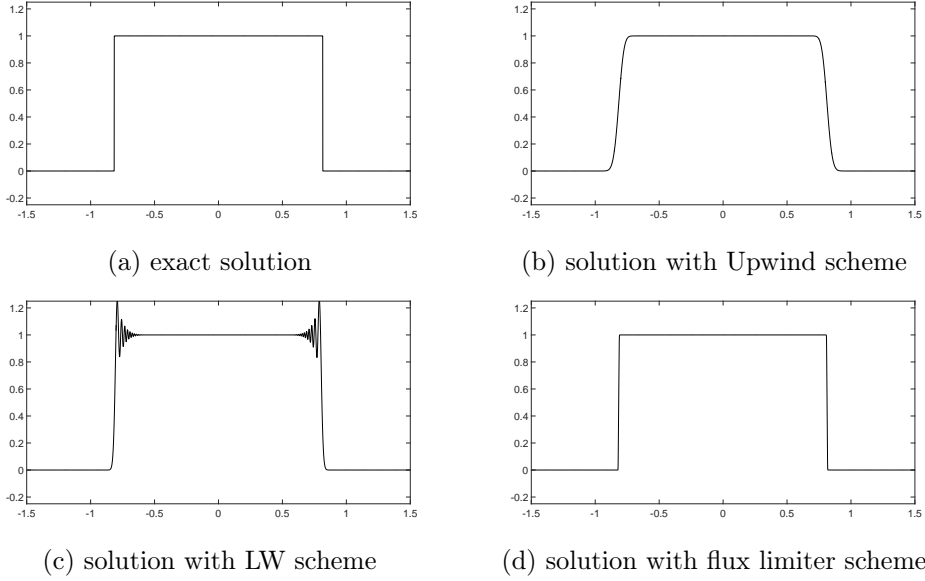
Figure 7.6.: Solution behaviour of FD schemes for the non-conservative transport equation (OFC): Here, problem (OFC) is solved for initial condition $I_0(x) = \chi_{[-0.3,0.3]}$ and vector field $\omega(t,x) = x$. We use as mesh size $\Delta x = 0.0001$ and as step size $\Delta t = 0.00005$. The exact solution at time $t = 1$ is plotted in (a). The discrete solutions at time $t = 1$ for the different FD schemes are plotted in (b) - (d).

with initial condition

$$I(0, x, y) = I_0(x, y), \tag{7.47b}$$

where $x, y \in \mathbb{R}$ and $t \in \mathbb{R}_+$.

We can solve this problem by splitting the problem into two 1-dimensional problems: Firstly, we solve

$$I_t^*(t, x, y) + u(t, x, y) \, I_x^*(t, x, y) = 0 \quad \text{with} \quad I_0^*(0, x, y) = I_0(x, y) \tag{7.48}$$

and secondly, we solve

$$I_t^{**}(t, x, y) + v(t, x, y) \, I_x^{**}(t, x, y) = 0 \quad \text{with} \quad I_0^{**}(0, x, y) = I^*(t, x, y). \tag{7.49}$$

Indeed, the following theorem shows, that $I^{**}(t, x, y)$ is a solution to problem (7.47).

Theorem 7.20 (cf. [36])**.**
Let $I_0 \in \mathcal{C}^1(\mathbb{R}^2)$ and $\omega \in \mathcal{C}(\mathbb{R}_+ \times \mathbb{R}^2; \mathbb{R}^2)$. Assume that the vector field ω is additionally Lipschitz continuous in the space variable. If $I(t, x, y)$ denotes the unique solution to problem (7.47) and $I^{**}(t, x, y)$ denotes the unique solution to problem (7.49), then $I^{**}(t, x, y) = I(t, x, y)$.

Proof.

From the Lipschitz continuity of $\omega = (u, v)^T$ follows that the problem

$$\begin{pmatrix} \dot{x}(s) \\ \dot{y}(s) \end{pmatrix} = \begin{pmatrix} u(s, x, y) \\ v(s, x, y) \end{pmatrix}, \quad \text{with} \quad \begin{pmatrix} \dot{x}(t) \\ \dot{y}(t) \end{pmatrix} = \begin{pmatrix} x \\ y \end{pmatrix} \tag{7.50}$$

is uniquely solvable. We denote the flow of this differential equation (7.50) by

$$\Phi_t^{-s}(x, y) = \begin{pmatrix} \Phi_{t,x}^{-s}(x, y) \\ \Phi_{t,y}^{-s}(x, y) \end{pmatrix}.$$

Next, from Section 3.2.1 we deduce that

$$I^*(t, x, y) = I_0(\Phi_{t,x}^{-t}(x, y), y)$$

is the exact solution of problem (7.48). Subsequently, we compute

$$\begin{aligned}
I^{**}(t, x, y) &= I^{**}(0, x, \Phi_{t,y}^{-t}(x, y)) \\
&= I^*(t, x, \Phi_{t,y}^{-t}(x, y)) \\
&= I_0(\Phi_{t,x}^{-t}(x, y), \Phi_{t,y}^{-t}(x, y)) \\
&= I(t, x, y).
\end{aligned}$$

$\square$

Finally, we can transfer the splitting approach straightforward to the discrete case. For this purpose, we introduce the 1-dimensional finite difference operators

$$\mathcal{H}_{i+1/2, j+1/2}^x(I_{\Delta x}^m) := \sum_{k \in \mathbb{Z}} b_{k+i+1/2} \, I_{k+i+1/2, j+1/2}^m$$

and

$$\mathcal{H}_{i+1/2, j+1/2}^y(I_{\Delta x}^m) := \sum_{k \in \mathbb{Z}} b_{k+j+1/2} \, I_{i+1/2, k+j+1/2}^m$$

in x- and y-direction, respectively.

Subsequently, we numerically solve the non-conservative transport equation (7.47) by solving firstly

$$I_{\Delta x}^* = \mathcal{H}^x(I_{\Delta x}^m) \tag{7.51a}$$

and secondly

$$I_{\Delta x}^{m+1} = \mathcal{H}^y(I_{\Delta x}^*). \tag{7.51b}$$

For a constant vector field $\omega(t, x) = a \in \mathbb{R}^d$ we can show that the splitting approach (7.51) is $p - th$ order accurate, if the finite difference operators $\mathcal{H}^x$ and $\mathcal{H}^y$ admit a consistency order p [36].

Analogously, we can develop a splitting approach for the conservative transport equation (cTPE).

7.5. Finite Difference Schemes for the Elliptic PDEs

In this section we present FD schemes for solving the elliptic PDE problems (7.3) and (7.4) appearing in the computation of the gradient $\nabla J(\omega)$ (cf. Theorem 7.1). Here, we only discuss in detail the discretisation of the elliptic PDEs corresponding to the velocity component u. For the velocity component v we only state the discretisation at the end.

As we have already mentioned in Section 7.3, we approximate each velocity component of $\omega = (u, v)^T$ at the grid points

$$u_{i,j+1/2}^m = u\big(m\,\Delta t, i\,\Delta x, (j+1/2)\,\Delta x\big) \qquad \text{for} \qquad \begin{aligned} i &= 1, ..., N_x - 1, \\ j &= 0, ..., N_y - 1, \\ m &= 0, ..., M, \end{aligned}$$

and

$$v_{i+1/2,j}^m = v\big(m\,\Delta t, (i+1/2)\,\Delta x, j\,\Delta x\big) \qquad \text{for} \qquad \begin{aligned} i &= 0, ..., N_x - 1, \\ j &= 1, ..., N_y - 1, \\ m &= 0, ..., M. \end{aligned}$$

Moreover, we recall that I and p are discretised solutions of the optical flow constraint (OFC) and the adjoint equation (adjEq). Thus, these are only given at the grid points

$$I_{i+1/2,j+1/2}^m = I\big(m\,\Delta t, (i+1/2)\,\Delta x, (j+1/2)\,\Delta x\big) \qquad \text{with} \qquad \begin{aligned} i &= 0, ..., N_x - 1, \\ j &= 0, ..., N_y - 1, \\ m &= 0, ..., M, \end{aligned}$$

and

$$p_{i+1/2,j+1/2}^m = p\big(m\,\Delta t, (i+1/2)\,\Delta x, (j+1/2)\,\Delta x\big) \qquad \text{with} \qquad \begin{aligned} i &= 0, ..., N_x - 1, \\ j &= 0, ..., N_y - 1, \\ m &= 0, ..., M. \end{aligned}$$

For the following discussion, we define at each time level $m = 0, ..., M$ the vectors

$$
\begin{aligned}
u_{\Delta x}^m = \big(& u_{1,1/2}^m, ..., u_{1,N_y-1/2}^m, u_{2,1/2}^m, ..., u_{2,N_y-1/2}^m, ..., \\
& u_{N_x-1,1/2}^m, ..., u_{N_x-1,N_y-1/2}^m \big)^T,
\end{aligned}
\tag{7.52}
$$

$$
\begin{aligned}
v_{\Delta x}^m = \big(& v_{1/2,1}^m, ..., v_{1/2,N_y-1}^m, v_{3/2,1}^m, ..., v_{3/2,N_y-1}^m, ..., \\
& v_{N_x-1/2,1}^m, ..., v_{N_x-1/2,N_y-1}^m \big)^T,
\end{aligned}
\tag{7.53}
$$

$$
\begin{aligned}
I_{\Delta x}^m = \big(& I_{1/2,1/2}^m, ..., I_{1/2,N_y-1/2}^m, I_{3/2,1/2}^m, ..., I_{3/2,N_y-1/2}^m, ..., \\
& I_{N_x-1/2,1/2}^m, ..., I_{N_x-1/2,N_y-1/2}^m \big)^T
\end{aligned}
\tag{7.54}
$$

and

$$
\begin{aligned}
p_{\Delta x}^m = \big(& p_{1/2,1/2}^m, ..., p_{1/2,N_y-1/2}^m, p_{3/2,1/2}^m, ..., p_{3/2,N_y-1/2}^m, ..., \\
& p_{N_x-1/2,1/2}^m, ..., p_{N_x-1/2,N_y-1/2}^m \big)^T.
\end{aligned}
\tag{7.55}
$$

Additionally we set

$$
u_{\Delta x} = \begin{pmatrix} u_{\Delta x}^0 \\ \vdots \\ u_{\Delta x}^M \end{pmatrix}, \quad
v_{\Delta x} = \begin{pmatrix} v_{\Delta x}^0 \\ \vdots \\ v_{\Delta x}^M \end{pmatrix}, \quad
I_{\Delta x} = \begin{pmatrix} I_{\Delta x}^0 \\ \vdots \\ I_{\Delta x}^M \end{pmatrix} \quad \text{and} \quad
p_{\Delta x} = \begin{pmatrix} p_{\Delta x}^0 \\ \vdots \\ p_{\Delta x}^M \end{pmatrix}
\tag{7.56}
$$

7.5.1. Poisson Equation

We start with the approximation of the Poisson equation (7.3). For reducing the computational costs, we use the substitution $\tilde{\omega} = \nabla J(\omega) - \alpha\,\omega$. This leads to the Poisson problems

$$
\begin{aligned}
-\Delta \tilde{u} &= p\, I_{x_1} & &\text{in } \Omega, & &\text{(7.57a)} \\
u &= 0 & &\text{on } \partial\Omega & &\text{(7.57b)}
\end{aligned}
$$

and

$$
\begin{aligned}
-\Delta \tilde{v} &= p\, I_{x_2} & &\text{in } \Omega, & &\text{(7.58a)} \\
v &= 0 & &\text{on } \partial\Omega & &\text{(7.58b)}
\end{aligned}
$$

for each velocity component of $\omega = (u, v)^T$.

Laplace Operator

For the discretisation of the Laplace operator $-\Delta \tilde{u}$ at the inner mesh points of $\tilde{u}$ (cf. Figure 7.7) we use central finite differences to obtain
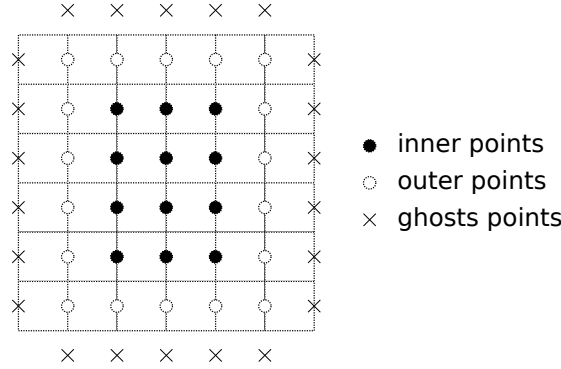
Figure 7.7.: Inner, outer and ghost points for the grid of $\tilde{u}$

$$
\begin{aligned}
&- \Delta \tilde{u}\big(m\,\Delta t, i\,\Delta x, (j+1/2)\,\Delta x\big) \\
&\approx \frac{4\,\tilde{u}^m_{i,j+1/2} - \tilde{u}^m_{i-1,j+1/2} - \tilde{u}^m_{i+1,j+1/2} - \tilde{u}^m_{i,j-1/2} - \tilde{u}^m_{i,j+3/2}}{(\Delta x)^2}
\end{aligned} \tag{7.59}
$$

for $i = 2, ..., N_x - 2, j = 1, ..., N_y - 2$ and $m = 0, ..., M$.

This approximation (7.59) we also like to use at the outer mesh points of $\tilde{u}$ (cf. Figure 7.7), i.e., for $i = 1, ..., N_x - 1, j = 0, ..., N_y - 1$ and $m = 0, ..., M$. But in this case the approximations

$$
\tilde{u}^m_{0,j+1/2}, \quad \tilde{u}^m_{N_x,j+1/2}, \quad \tilde{u}^m_{i,-1/2} \quad \text{and} \quad \tilde{u}^m_{i,N_y+1/2} \tag{7.60}
$$

appear in equation (7.59) at points which do not belong to the mesh grid of $\tilde{u}$ (cf. Figure 7.7). These points in (7.60) are called *ghost points*. However, by exploiting the Dirichlet boundary condition (7.57b) we can eliminate these ghost points. Indeed, in the x-direction we immediately obtain

$$
\tilde{u}^m_{0,j+1/2} = \tilde{u}^m_{N_x,j+1/2} = 0.
$$

In the y-direction we use a quadratic extrapolation, as in the MAC scheme [45] for solving the Stokes problem numerically, see Section 7.6. This means, we compute for the ghost points $\tilde{u}^m_{i,-1/2}$ with $i = 1, ..., N_x - 1$ and $m = 0, ..., M$ an interpolant of $\tilde{u}^m_{i,0}, \tilde{u}^m_{i,1/2}$ and $\tilde{u}^m_{i,3/2}$ and evaluate this interpolant at $u^m_{i,-1/2}$ to obtain the approximation

$$
\begin{aligned}
\tilde{u}^m_{i,-1/2} &\approx \frac{1}{3}\,\tilde{u}^m_{i,3/2} - 2\,\tilde{u}^m_{i,1/2} + \frac{8}{3}\,\tilde{u}^m_{i,0} \\
&= \frac{1}{3}\,\tilde{u}^m_{i,3/2} - 2\,\tilde{u}^m_{i,1/2}.
\end{aligned} \tag{7.61}
$$

Analogously, we obtain for the ghost points $\tilde{u}^m_{i,N_y+1/2}$ the approximation

$$
\begin{aligned}
\tilde{u}^m_{i,N_y+1/2} &\approx \frac{1}{3}\,\tilde{u}^m_{i,N_y-3/2} - 2\,\tilde{u}^m_{i,N_y-1/2} + \frac{8}{3}\,\tilde{u}^m_{i,N_y} \\
&= \frac{1}{3}\,\tilde{u}^m_{i,N_y-3/2} - 2\,\tilde{u}^m_{i,N_y-1/2}
\end{aligned}
\tag{7.62}
$$

for $i = 1, ..., N_x - 1$ and $m = 0, ..., M$.

Inserting (7.61) and (7.62) into the Laplace approximation (7.59) leads to

$$
-\Delta\tilde{u}\big(m\,\Delta t, i\,\Delta x, 1/2\,\Delta x\big) \approx \frac{6\,\tilde{u}^m_{i,1/2} - \tilde{u}^m_{i-1,1/2} - \tilde{u}^m_{i+1,1/2} - \frac{4}{3}\,\tilde{u}^m_{i,3/2}}{(\Delta x)^2}
$$

and

$$
\begin{aligned}
&- \Delta\tilde{u}\big(m\,\Delta t, i\,\Delta x, N_y - 1/2\,\Delta x\big) \\
&\approx \frac{6\,\tilde{u}^m_{i,N_y-1/2} - \tilde{u}^m_{i-1,N_y-1/2} - \tilde{u}^m_{i+1,N_y-1/2} - \frac{4}{3}\,\tilde{u}^m_{i,N_y-3/2}}{(\Delta x)^2},
\end{aligned}
$$

respectively.

Using notation (7.52), we can formulate the discretisation of the Laplace operator $-\Delta\tilde{u}$ at all grid points of $\tilde{u}$ for each time level $m = 0, ..., M$ as a matrix-vector multiplication,

$$
\Big[- \Delta\tilde{u}\big(m\,\Delta t, i\,\Delta x, (j + 1/2)\,\Delta x\big)\Big]_{\substack{i=1,...,N_x-1 \\ j=0,...,N_y-1}} \approx L_u \cdot \tilde{u}^m_{\Delta x}.
$$

Here, the matrix L_u is given by

$$
L_u = \frac{1}{(\Delta x)^2}
\begin{pmatrix}
A_u & -I_u & & & \\
-I_u & A_u & -I_u & & \\
 & \ddots & \ddots & \ddots & \\
 & & -I_u & A_u & -I_u \\
 & & & -I_u & A_u
\end{pmatrix}
\in \mathbb{R}^{(N_x-1)\,N_y \times (N_x-1)\,N_y}
$$

where

$$
A_u =
\begin{pmatrix}
6 & -\frac{4}{3} & & & & & \\
-1 & 4 & -1 & & & & \\
 & -1 & 4 & -1 & & & \\
 & & \ddots & \ddots & \ddots & & \\
 & & & -1 & 4 & -1 & \\
 & & & & -1 & 4 & -1 \\
 & & & & & -\frac{4}{3} & 6
\end{pmatrix}
\in \mathbb{R}^{N_y \times N_y}
$$

and $I_u \in \mathbb{R}^{N_y \times N_y}$ denotes the identity matrix.

Analogously, we find for the Laplace operator $-\Delta \tilde{v}$ in (7.58a) the approximation

$$\left[- \Delta \tilde{v}\big(m \,\Delta t, (i + 1/2)\, \Delta x, j\, \Delta x \big) \right]_{\substack{i=0,\dots,N_x-1 \\ j=1,\dots,N_y-1}} \approx L_v \cdot \tilde{v}^m_{\Delta x}.$$

for $m = 0, \dots, M$, where

$$L_v = \frac{1}{(\Delta x)^2} \begin{pmatrix} A_v & -\frac{4}{3} I_v & & & & & \\ -I_v & B_v & -I_v & & & & \\ & -I_v & B_v & -I_v & & & \\ & & \ddots & \ddots & \ddots & & \\ & & & -I_v & B_v & -I_v & \\ & & & & -I_v & B_v & -I_v \\ & & & & & -\frac{4}{3} I_v & A_v \end{pmatrix} \in \mathbb{R}^{N_x\,(N_y-1) \times N_x\,(N_y-1)}$$

with

$$A_v = \begin{pmatrix} 6 & -1 & & & \\ -1 & 6 & -1 & & \\ & \ddots & \ddots & \ddots & \\ & & -1 & 6 & -1 \\ & & & -1 & 6 \end{pmatrix} \in \mathbb{R}^{(N_y-1)\times(N_y-1)},$$

$$B_v = \begin{pmatrix} 4 & -1 & & & \\ -1 & 4 & -1 & & \\ & \ddots & \ddots & \ddots & \\ & & -1 & 4 & -1 \\ & & & -1 & 4 \end{pmatrix} \in \mathbb{R}^{(N_y-1)\times(N_y-1)}$$

and identity matrix $I_v \in \mathbb{R}^{(N_y-1)\times(N_y-1)}$.

Differentation operator

After discretising the Laplace operators $-\Delta \tilde{u}$ and $-\Delta \tilde{v}$ we have to discretise the right hand sides of the Poisson equations (7.57a) and (7.58a). For the approximation of the spatial derivative I_x in (7.57a) we use central finite differences to obtain

$$I_x\big(m\,\Delta t, i\,\Delta x, (j+1/2)\,\Delta x \big) \approx \frac{I^m_{i+1/2,j+1/2} - I^m_{i-1/2,j+1/2}}{\Delta x}$$

for $i = 1, \dots, N_x - 1, j = 0, \dots, N_y - 1$ and $m = 0, \dots, M$. Using the notation (7.54), we can formulate the discretisation of the spatial derivative I_x at all grid points of $\tilde{u}$ for

each time level $m = 0, ..., M$ as a matrix-vector multiplication,

$$\Big[I_x \big(m\, \Delta t, i\, \Delta x, (j + 1/2)\, \Delta x \big) \Big]_{\substack{i=1,...,N_x-1 \\ j=0,...,N_y-1}} \approx D_x \cdot I_{\Delta x}^m.$$

Here, the matrix D_x is given by

$$D_x = \frac{1}{\Delta x} \begin{pmatrix} -d_x & d_x & & \\ & -d_x & d_x & \\ & & \ddots & \ddots \\ & & & -d_x & d_x \end{pmatrix} \in \mathbb{R}^{(N_x-1)\, N_y \times N_x\, N_y},$$

where $d_x \in \mathbb{R}^{N_y \times N_y}$ denotes the identity matrix.

Analogously, we compute for the spatial derivative I_y in (7.58a) the approximation

$$\Big[I_y \big(m\, \Delta t, (i + 1/2)\, \Delta x, j\, \Delta x \big) \Big]_{\substack{i=0,...,N_x-1 \\ j=1,...,N_y-1}} \approx D_y \cdot I_{\Delta x}^m,$$

where

$$D_y = \frac{1}{\Delta x} \begin{pmatrix} d_y & & & \\ & d_y & & \\ & & \ddots & \\ & & & d_y \end{pmatrix} \in \mathbb{R}^{N_x\, (N_y-1) \times N_x\, N_y},$$

with

$$d_y = \begin{pmatrix} -1 & 1 & & \\ & -1 & 1 & \\ & & \ddots & \ddots \\ & & & -1 & 1 \end{pmatrix} \in \mathbb{R}^{(N_y-1) \times N_y}.$$

Interpolation operator

Lastly, we have to evaluate the adjoint variable p at the grid points of $\tilde{u}$ and $\tilde{v}$, respectively. However, $\tilde{p}$ is a discretised function, too, and is defined on a different grid as $\tilde{u}$ and $\tilde{v}$. Therefore, in equation (7.57a) we have to interpolate p at the grid points of $\tilde{u}$. Hence, by using a linear interpolation in x-direction we obtain

$$p(m\, \Delta t, i\, \Delta x, (j + 1/2)\, \Delta x) \approx \frac{p_{i+1/2,j+1/2}^m + p_{i-1/2,j+1/2}^m}{2}$$

for $i = 1, ..., N_x - 1, j = 0, ..., N_y - 1$ and $m = 0, ..., M$. Again, we can formulate the interpolation of p at all grid points of $\tilde{u}$ for each time level $m = 0, ..., M$ as a matrix-vector multiplication,

$$\Big[p \big(m\, \Delta t, i\, \Delta x, (j + 1/2)\, \Delta x \big) \Big]_{\substack{i=1,...,N_x-1 \\ j=0,...,N_y-1}} \approx P_x \cdot p_{\Delta x}^m.$$

Here, P_x is given by

$$P_x = \frac{1}{2} \begin{pmatrix} p_x & p_x & & & \\ & p_x & p_x & & \\ & & \ddots & \ddots & \\ & & & p_x & p_x \end{pmatrix} \in \mathbb{R}^{(N_x-1)\,N_y \times N_x\,N_y},$$

where $p_x \in \mathbb{R}^{N_y \times N_y}$ is the identity matrix.

Analogously, for the Poisson equation (7.58a) we obtain as interpolation of p in y-direction

$$\left[p\big(m\,\Delta t, (i+1/2)\,\Delta x, j\,\Delta x\big) \right]_{\substack{i=0,\dots,N_x-1 \\ j=1,\dots,N_y-1}} \approx P_y \cdot p_{\Delta x}^m,$$

where

$$P_y = \frac{1}{2} \begin{pmatrix} p_y & & & \\ & p_y & & \\ & & \ddots & \\ & & & p_y \end{pmatrix} \in \mathbb{R}^{N_x\,(N_y-1) \times N_x\,N_y},$$

with

$$p_y = \begin{pmatrix} 1 & 1 & & & \\ & 1 & 1 & & \\ & & \ddots & \ddots & \\ & & & 1 & 1 \end{pmatrix} \in \mathbb{R}^{(N_y-1) \times N_y}.$$

Consistency

Altogether, we obtain as approximation of the Poisson problems (7.57) and (7.58) the linear systems

$$L_u \cdot \tilde{u}_{\Delta x}^m = \big(P_x \cdot p_{\Delta x}^m\big) \odot \big(D_x \cdot I_{\Delta x}^m\big) \quad \text{and} \tag{7.63a}$$

$$L_v \cdot \tilde{v}_{\Delta x}^m = \big(P_y \cdot p_{\Delta x}^m\big) \odot \big(D_y \cdot I_{\Delta x}^m\big), \tag{7.63b}$$

where $\odot$ denotes the component wise vector-multiplication. Hence, we obtain the discrete solutions $\tilde{u}$ and $\tilde{v}$ by solving the linear systems in (7.63). These linear systems can be solved with a complexity of $\mathcal{O}((N_x-1)\,N_y)$ or $\mathcal{O}(N_x\,(N_y-1))$, respectively, by using a multigrid method [12, 27]. However, numerical tests shows that a Gauss elimination is comparable in the computational effort, if we compute the LU factorization beforehand, since the systems are relatively small in this case.

Remark 7.21.
For numerical calculations it is reasonable to multiply the first and the last N_x equations in (7.63a) by a factor of $\frac{3}{4}$, because then the system matrix L_u becomes symmetric. Analogously, we have to rearrange some equations in the linear system (7.63b).

Now the question is: Do the discrete solution $\tilde{u}$ and $\tilde{v}$ converge to the exact solution of the Poisson problems (7.57) and (7.58). As for the transport equation, the convergence can be deduced from the consistency and stability of the scheme. By using Taylor expansion series, we easily compute the consistency order for the different discretisation operators.

Theorem 7.22 (Consistency).

(i) Let $\tilde{u}, \tilde{v} \in \mathcal{C}^4(\Omega)$. Then the approximations $L_u \cdot \tilde{u}$ and $L_v \cdot \tilde{v}$ of the Laplace operators $-\Delta\tilde{u}$ and $-\Delta\tilde{v}$ are second order accurate at the inner grid points and first order accurate at the outer grid points of $\tilde{u}$ and $\tilde{v}$, respectively.

(ii) Let $I \in \mathcal{C}^3(\Omega)$. Then the approximations $D_x \cdot I$ and $D_y \cdot I$ of the spatial derivatives I_x and I_y are second order accurate.

(iii) Let $p \in \mathcal{C}^2(\Omega)$. Then the interpolations $P_x \cdot p$ and $P_y \cdot \tilde{p}$ of p are second order accurate.

Proof.

(i) For the approximation order of the operator L_u we compute at each time level $m = 0, ..., M$

$$\varepsilon^u_{i,j+1/2} = \Big[\Delta\tilde{u}\big(m\,\Delta t, i\,\Delta x, (j+1/2)\,\Delta x\big)\Big]_{\substack{i=1,...,N_x-1 \\ j=0,...,N_y-1}}$$
$$- L_u \cdot \Big[\tilde{u}\big(m\,\Delta t, i\,\Delta x, (j+1/2)\,\Delta x\big)\Big]_{\substack{i=1,...,N_x-1 \\ j=0,...,N_y-1}}.$$

with

$$\varepsilon^u_{i,j+1/2} = \begin{cases} \big(u_{xxxx} + u_{yyyy}\big)\big(m\,\Delta t, i\,\Delta x, (j+1/2)\,\Delta x\big)\frac{(\Delta x)^2}{12} + \mathcal{O}((\Delta x)^3), \\ \qquad \text{for } i = 1, ..., N_x - 1 \text{ and } j = 1, ..., N_y - 2, \\ u_{xxx}\big(m\,\Delta t, i\,\Delta x, (j+1/2)\,\Delta x\big)\frac{\Delta x}{6} + \mathcal{O}((\Delta x)^2), \\ \qquad \text{for } i = 1, ..., N_x - 1 \text{ and } j = \{0, N_y - 1\} \end{cases}.$$

Analogously, we can show the consistency order of the operator L_v.

(ii) For the approximation order of the differentiation operator D_x we compute at each time level $m = 0, ..., M$

$$\Big[I_x\big(m\,\Delta t, i\,\Delta x, (j+1/2)\,\Delta x\big)\Big]_{\substack{i=1,...,N_x-1 \\ j=0,...,N_y-1}}$$
$$- D_x \cdot \Big[I\big(m\,\Delta t, i\,\Delta x, (j+1/2)\,\Delta x\big)\Big]_{\substack{i=1,...,N_x-1 \\ j=0,...,N_y-1}}$$
$$= \Big[I_{xxx}\big(m\,\Delta t, i\,\Delta x, (j+1/2)\,\Delta x\big)\Big]_{\substack{i=1,...,N_x-1 \\ j=0,...,N_y-1}}\frac{(\Delta x)^2}{12} + \mathcal{O}((\Delta x)^3).$$

Analogously, we can show the consistency order of the differentiation operator D_y.

(iii) For the approximation order of the interpolation operator P_x we compute at each time level $m = 0, ..., M$

$$\left[p\big(m\,\Delta t, i\,\Delta x, (j+1/2)\,\Delta x\big)\right]_{\substack{i=1,...,N_x-1 \\ j=0,...,N_y-1}}$$

$$- P_x \cdot \left[p\big(m\,\Delta t, i\,\Delta x, (j+1/2)\,\Delta x\big)\right]_{\substack{i=1,...,N_x-1 \\ j=0,...,N_y-1}}$$

$$= \left[p_{xx}\big(m\,\Delta t, i\,\Delta x, (j+1/2)\,\Delta x\big)\right]_{\substack{i=1,...,N_x-1 \\ j=0,...,N_y-1}} \frac{(\Delta x)^2}{8} + \mathcal{O}((\Delta x)^3).$$

Analogously, we can show the consistency order of the interpolation operator P_y.

$\square$

Stability

For proving the stability of the FD scheme, we use the theory of L_0 and M-matrices.

Definition 7.23.

   (i) *A matrix A is called L_0-matrix, if $a_{ij} \leq 0$ for $i \neq j$.*

   (ii) *A matrix A is called M-matrix, if A is a regular L_0-matrix and any entry of A^{-1} is non negative.*

In particular, helpful for the stability analysis is the following theorem.

Theorem 7.24.
A L_0-matrix is a M-matrix, if and only if a vector $e > 0$ exists with $A\,e > 0$. Additionally, in this case, we have the estimate

$$\|A^{-1}\|_\infty \leq \frac{\|e\|_\infty}{\min\limits_k (Ae)_k}.$$

Proof.
A proof can be found in [27]. $\square$

With the help of this theorem we can show the stability of the FD schemes defined in (7.63). Here, we adapt the thoughts of [27].

Theorem 7.25.
The matrices L_u and L_v are M-matrices, with

$$\|L_u^{-1}\|_\infty \leq 1/4 \quad and \quad \|L_v^{-1}\|_\infty \leq 1/4.$$

Proof.

We start with the matrix L_u. In this case, we consider the function $e^*(x,y) = x\,(1-x)$. Applying the Laplace operator to this function gives

$$\Delta e^* = e^*_{xx} = 2 > 0.$$

Next, we define a vector e by evaluating the function $e^*(x,y)$ at the grid point of $\tilde{u}$. For this vector it holds that

$$e > 0 \quad \text{and} \quad L_u\,e = 2 > 0. \tag{7.64}$$

Here, we have exploited the consistency order of the operator L_u. More precisely, we used that the approximation of the function e^*_{xx} is exact for a quadratic function e^* with zero boundary values and that e^* is constant in the y-direction.

As a consequence of (7.64), we deduce from Theorem 7.24 that L_u is a M-matrix. Moreover, we have

$$\|L_u^{-1}\|_\infty \le \frac{1}{2}\,\|e\|_\infty = \frac{1}{4}.$$

Analogously, we show that L_v is a M-matrix with $\|L_v^{-1}\|_\infty \le \frac{1}{4}$ by using the function $e^*(x,y) = y\,(1-y)$. $\qquad\square$

Convergence

Finally, we obtain the convergence of the FD schemes defined in (7.63).

Theorem 7.26 (Convergence, cf. [27]).
Let $p \in \mathcal{C}^2(\Omega), I \in \mathcal{C}^3(\Omega)$ and $\tilde{u}, \tilde{v} \in \mathcal{C}^4(\Omega)$ be the exact solutions of the Poisson problems (7.57) and (7.58). Then the discrete solutions $\tilde{u}^m_{\Delta x}$ defined in (7.63) converges towards $\tilde{u}$ and the discrete solutions $\tilde{v}^m_{\Delta x}$ defined in (7.63) converges towards $\tilde{v}$ in the $\|\cdot\|_\infty$-norm. The convergence is of second order at the inner grid points and of first order at the outer grid points of $\tilde{u}$ and $\tilde{v}$, respectively.

Proof.

We first consider the Poisson problem (7.57). Let $\tilde{u}$ denote the exact solution of (7.57), $f = p\,I_x$ the continuous and $f^m_{\Delta x} = \left(P_x \cdot p^m_{\Delta x}\right) \odot \left(D_x \cdot I^m_{\Delta x}\right)$ the discretised representation of the right hand side in (7.57a). Moreover, we define the error by

$$e^m_{\Delta x} = \tilde{u}^m_{\Delta x} - \left[\tilde{u}\big(m\,\Delta t, i\,\Delta x, (j + 1/2)\,\Delta x\big)\right]_{\substack{i=1,\dots,N_x-1 \\ j=0,\dots,N_y-1}}$$

for each time level $m = 0, \dots, M$. For convergence, we have to show $\|e^m_{\Delta x}\|_\infty \to 0$ for $\Delta x \to 0$.

At each time level $m = 0, ..., M$ we calculate

$$L_u \cdot e_{\Delta x}^m = L_u \cdot \tilde{u}_{\Delta x}^m - L_u \cdot \left[\tilde{u}\big(m\,\Delta t, i\,\Delta x, (j+1/2)\,\Delta x\big)\right]_{\substack{i=1,...,N_x-1 \\ j=0,...,N_y-1}}$$

$$= f_{\Delta x}^m - \left[\Delta\tilde{u}\big(m\,\Delta t, i\,\Delta x, (j+1/2)\,\Delta x\big)\right]_{\substack{i=1,...,N_x-1 \\ j=0,...,N_y-1}}$$

$$+ \left[\Delta\tilde{u}\big(m\,\Delta t, i\,\Delta x, (j+1/2)\,\Delta x\big)\right]_{\substack{i=1,...,N_x-1 \\ j=0,...,N_y-1}}$$

$$- L_u \cdot \left[\tilde{u}\big(m\,\Delta t, i\,\Delta x, (j+1/2)\,\Delta x\big)\right]_{\substack{i=1,...,N_x-1 \\ j=0,...,N_y-1}}.$$

Consequently , we obtain

$$\|e_{\Delta x}^m\|_\infty \le \|L_u^{-1}\|_\infty \left(\left\|f_{\Delta x}^m - \left[f\big(m\,\Delta t, i\,\Delta x, (j+1/2)\,\Delta x\big)\right]_{\substack{i=1,...,N_x-1 \\ j=0,...,N_y-1}}\right\|_\infty\right.$$

$$+ \left\|\left[\Delta\tilde{u}\big(m\,\Delta t, i\,\Delta x, (j+1/2)\,\Delta x\big)\right]_{\substack{i=1,...,N_x-1 \\ j=0,...,N_y-1}}\right.$$

$$\left.\left. - L_u \cdot \left[\tilde{u}\big(m\,\Delta t, i\,\Delta x, (j+1/2)\,\Delta x\big)\right]_{\substack{i=1,...,N_x-1 \\ j=0,...,N_y-1}}\right\|_\infty\right).$$

Finally, by using the stability and consistency of the scheme, we deduce the statement.

Analogously, we can show the convergence for the Poisson problem (7.58). □

7.5.2. Time-Dependent Elliptic PDE

Next, we discuss the approximation of the time-dependent elliptic PDE (7.4), which appears in the calculation of the gradient $\nabla J(\omega)$, if we use an H^1-regularization in space and time (compare Theorem 7.1). For reducing the computational costs we use in this case the substitution

$$\tilde{\omega} = \nabla J(\omega) - \beta\,\omega.$$

This substitution leads to the following two time-dependent elliptic PDEs

$$
\begin{aligned}
-\tilde{u}_{tt} - \Delta\tilde{u} &= (\beta - \alpha)\,\Delta u + p\,I_{x_1} && \text{in } \Omega_T = (0,T) \times \Omega && \text{(7.65a)} \\
u &= 0 && \text{on } \Gamma_x = (0,T) \times \partial\Omega, && \text{(7.65b)} \\
u_t &= 0 && \text{on } \Gamma_t = \{0,T\} \times \Omega && \text{(7.65c)}
\end{aligned}
$$

and

$$
\begin{aligned}
-\tilde{v}_{tt} - \Delta\tilde{v} &= (\beta - \alpha)\,\Delta v + p\,I_{x_2} && \text{in } \Omega_T = (0,T) \times \Omega && \text{(7.66a)} \\
v &= 0 && \text{on } \Gamma_x = (0,T) \times \partial\Omega, && \text{(7.66b)} \\
v_t &= 0 && \text{on } \Gamma_t = \{0,T\} \times \Omega && \text{(7.66c)}
\end{aligned}
$$

for each velocity component of $\omega = (u,v)^T$.

Elliptic PDE Operator

We start with the approximation of the elliptic PDE operator $-\tilde{u}_{tt} - \Delta\tilde{u}$. For the approximation of the Laplace operator $-\Delta\tilde{u}$ we use the same discretisation as in Section 7.5.1. This discretisation also includes the approximation of the Dirichlet boundary condition (7.65b) in space. The second order time derivative $-u_{tt}$ is discretised by central finite differences, too, i.e.,

$$-\tilde{u}_{tt}\big(m\,\Delta t, i\,\Delta x, (j+1/2)\,\Delta x\big) \approx \frac{2\,\tilde{u}_{i,j+1/2}^m - \tilde{u}_{i,j+1/2}^{m+1} - \tilde{u}_{i,j+1/2}^{m-1}}{(\Delta t)^2}$$

for $i = 1, ..., N_x - 1, j = 0, ..., N_y - 1$ and $m = 1, ..., M - 1$.

Altogether, as in Section (7.5.1), we can formulate the approximation of the elliptic PDE operator at each time level $m = 1, ..., M - 1$ as a summation of matrix-vector multiplications

$$\left[\big(-\tilde{u}_{tt} - \Delta\tilde{u}\big)\big(m\,\Delta t, i\,\Delta x, (j+1/2)\,\Delta x\big)\right]_{\substack{i=1,...,N_x-1 \\ j=0,...,N_y-1}}$$
$$\approx \frac{2\,I_{Tu} \cdot \tilde{u}^m - I_{Tu} \cdot \tilde{u}^{m+1} - I_{Tu} \cdot \tilde{u}^{m-1}}{(\Delta t)^2} + L_u \cdot \tilde{u}^m, \tag{7.67}$$

where $I_{Tu} \in \mathbb{R}^{(N_x-1)\,N_y \times (N_x-1)\,N_y}$ denotes the identity matrix.

Next, we have to discretise the Neumann boundary condition (7.65c). Clearly, it is intuitively to approximate the time derivative at initial and final time by the following approximations

$$\tilde{u}_t\big(0, i\,\Delta x, (j+1/2)\,\Delta x\big) \approx \frac{\tilde{u}_{i,j+1/2}^1 - \tilde{u}_{i,j+1/2}^0}{\Delta t}$$

and

$$\tilde{u}_t\big(T, i\,\Delta x, (j+1/2)\,\Delta x\big) \approx \frac{\tilde{u}_{i,j+1/2}^M - \tilde{u}_{i,j+1/2}^{M-1}}{\Delta t}.$$

for $i = 1, ..., N_x - 1$ and $j = 0, ..., N_y - 1$.

But, in this case numerical tests shows that the resulting stiffness matrix is ill-conditioned.

Hence, for stability reasons we introduce the ghost points $\tilde{u}_{i,j+1/2}^{-1}$ and $\tilde{u}_{i,j+1/2}^{M+1}$ and approximate the Neumann boundary condition (7.65c) at initial and final time by

$$0 = \tilde{u}_t\big(0, i\,\Delta x, (j+1/2)\,\Delta x\big) \approx \frac{\tilde{u}_{i,j+1/2}^1 - \tilde{u}_{i,j+1/2}^{-1}}{2\,\Delta t} \tag{7.68}$$

and

$$0 = \tilde{u}_t\big(T, i\,\Delta x, (j+1/2)\,\Delta x\big) \approx \frac{\tilde{u}_{i,j+1/2}^{M+1} - \tilde{u}_{i,j+1/2}^{M-1}}{2\,\Delta t}. \tag{7.69}$$

for $i = 1, ..., N_x - 1$ and $j = 0, ..., N_y - 1$.

From (7.68) and (7.69) we conclude

$$\tilde{u}_{i,j+1/2}^{-1} \approx \tilde{u}_{i,j+1/2}^{1} \quad \text{and} \quad \tilde{u}_{i,j+1/2}^{M+1} \approx \tilde{u}_{i,j+1/2}^{M-1}. \tag{7.70}$$

Inserting (7.70) in (7.67) leads to

$$\begin{aligned}
&\Big[\big(-\tilde{u}_{tt} - \Delta\tilde{u}\big)\big(0, i\,\Delta x, (j+1/2)\,\Delta x\big)\Big]_{\substack{i=1,...,N_x-1 \\ j=0,...,N_y-1}} \\
&\approx \frac{2\,I_{Tu}\cdot\tilde{u}^0 - 2\,I_{Tu}\cdot\tilde{u}^1}{(\Delta t)^2} + L_u\cdot\tilde{u}^0,
\end{aligned} \tag{7.71}$$

and

$$\begin{aligned}
&\Big[\big(-\tilde{u}_{tt} - \Delta\tilde{u}\big)\big(T, i\,\Delta x, (j+1/2)\,\Delta x\big)\Big]_{\substack{i=1,...,N_x-1 \\ j=0,...,N_y-1}} \\
&\approx \frac{2\,I_{Tu}\cdot\tilde{u}^M - 2\,I_{Tu}\cdot\tilde{u}^{M-1}}{(\Delta t)^2} + L_u\cdot\tilde{u}^M.
\end{aligned} \tag{7.72}$$

Altogether, we can express (7.67), (7.71) and (7.72) as matrix-vector multiplication

$$\Big[\big(-\tilde{u}_{tt} - \Delta\tilde{u}\big)\big(m\,\Delta t, i\,\Delta x, (j+1/2)\,\Delta x\big)\Big]_{\substack{i=1,...,N_x-1 \\ j=0,...,N_y-1 \\ m=0,...,M}} \approx \big(L_{Tu} + T_u\big)\cdot\tilde{u}_{\Delta x},$$

with matrices $L_{Tu}, T_u \in \mathbb{R}^{(M+1)\,(N_x-1)\,N_y \times (M+1)\,(N_x-1)\,N_y}$ defined by

$$L_{Tu} = \begin{pmatrix} L_u & & & \\ & L_u & & \\ & & \ddots & \\ & & & L_u \end{pmatrix}$$

and

$$T_u = \frac{1}{(\Delta t)^2} \begin{pmatrix} 2I_{Tu} & -2I_{Tu} & & & & & \\ -I_{Tu} & 2I_{Tu} & -I_{Tu} & & & & \\ & -I_{Tu} & 2I_{Tu} & -I_{Tu} & & & \\ & & \ddots & \ddots & \ddots & & \\ & & & -I_{Tu} & 2I_{Tu} & -I_{Tu} \\ & & & & -2I_{Tu} & 2I_{Tu} \end{pmatrix}.$$

Analogously, we can express the approximation of the elliptic operator $-\tilde{v}_{tt} - \Delta\tilde{v}$ in equation (7.66a) as matrix-vector multiplication

$$\left[(-\tilde{v}_{tt} - \Delta\tilde{v})\big(m\,\Delta t, i\,\Delta x, (j+1/2)\,\Delta x\big)\right]_{\substack{i=0,\dots,N_x-1 \\ j=1,\dots,N_y-1 \\ m=0,\dots,M}} \approx \left(L_{Tv} + T_v\right) \cdot \tilde{v}_{\Delta x},$$

with matrices $L_{Tv}, T_v \in \mathbb{R}^{(M+1)\,N_x\,(N_y-1)\times(M+1)\,N_x\,(N_y-1)}$ defined by

$$L_{Tv} = \begin{pmatrix} L_v & & & \\ & L_v & & \\ & & \ddots & \\ & & & L_v \end{pmatrix}$$

and

$$T_v = \frac{1}{(\Delta t)^2} \begin{pmatrix} 2I_{Tv} & -2I_{Tv} & & & & \\ -I_{Tv} & 2I_{Tv} & -I_{Tv} & & & \\ & -I_{Tv} & 2I_{Tv} & -I_{Tv} & & \\ & & \ddots & \ddots & \ddots & \\ & & & -I_{Tv} & 2I_{Tv} & -I_{Tv} \\ & & & & -2I_{Tv} & 2I_{Tv} \end{pmatrix}$$

Right Hand Side

Regarding to the previous discussion in this and the last subsection, we approximate the right hand side by

$$\left[(p\,I_x)\big(m\,\Delta t, (i+1/2)\,\Delta x, j\,\Delta xt\big)\right]_{\substack{i=1,\dots,N_x-1 \\ j=0,\dots,N_y-1 \\ m=0,\dots,M}} \approx \left(P_{Tx} \cdot p_{\Delta x}\right) \odot \left(I_{Tx} \cdot I_{\Delta x}\right)$$

and

$$\left[(p\,I_y)\big(m\,\Delta t, (i+1/2)\,\Delta x, j\,\Delta x\big)\right]_{\substack{i=0,\dots,N_x-1 \\ j=1,\dots,N_y-1 \\ m=0,\dots,M}} \approx \left(P_{Ty} \cdot p_{\Delta x}\right) \odot \left(I_{Ty} \cdot I_{\Delta x}\right).$$

Here the matrices are given by

$$
P_{Tx} = \begin{pmatrix} P_x & & & \\ & P_x & & \\ & & \ddots & \\ & & & P_x \end{pmatrix} \qquad \in \mathbb{R}^{(M+1)\,(N_x-1)\,N_y \times (M+1)\,N_x\,N_y},
$$

$$
I_{Tx} = \begin{pmatrix} I_x & & & \\ & I_x & & \\ & & \ddots & \\ & & & I_x \end{pmatrix} \qquad \in \mathbb{R}^{(M+1)\,(N_x-1)\,N_y \times (M+1)\,N_x\,N_y},
$$

$$
P_{Ty} = \begin{pmatrix} P_y & & & \\ & P_y & & \\ & & \ddots & \\ & & & P_y \end{pmatrix} \qquad \in \mathbb{R}^{(M+1)\,N_x\,(N_y-1) \times (M+1)\,N_x\,N_y},
$$

and

$$
I_{Ty} = \begin{pmatrix} I_y & & & \\ & I_y & & \\ & & \ddots & \\ & & & I_y \end{pmatrix} \qquad \in \mathbb{R}^{(M+1)\,N_x\,(N_y-1) \times (M+1)\,N_x\,N_y}.
$$

In summary, we obtain as approximations of the time-dependent elliptic PDEs the linear systems

$$
\left(L_{Tu} + T_u \right) \cdot \tilde{u}_{\Delta x} = (\beta - \alpha)\, L_{Tu} \cdot u_{\Delta x} + \left(P_{Tx} \cdot p_{\Delta x} \right) \odot \left(I_{Tx} \cdot I_{\Delta x} \right) \tag{7.73a}
$$

and

$$
\left(L_{Tv} + T_v \right) \cdot \tilde{v}_{\Delta x} = (\beta - \alpha)\, L_{Tv} \cdot v_{\Delta x} + \left(P_{Ty} \cdot p_{\Delta x} \right) \odot \left(I_{Ty} \cdot I_{\Delta x} \right). \tag{7.73b}
$$

We solve these large linear systems by using the multigrid method [12, 27]. In particular, we apply the algebraic multigrid method PyAMG [6].

Remark 7.27.
For numerical calculations it is reasonable to multiply the equations (7.73a) *and* (7.73b) *for the first and last time step by a factor of* $\frac{1}{2}$, *because then the system matrices* $\left(L_{Tu} + T_u \right)$ *and* $\left(L_{Tv} + T_v \right)$ *become symmetric.*

Convergence

Analogously to the discretisation of the Poisson equation, we can show that the discretisation of the time-dependent elliptic PDE is at least first order accurate and stable.

Theorem 7.28 (Convergence).
Let $p \in \dashv\nabla\}\infty^2((0,T)\times\Omega), I \in \dashv\nabla\}\infty^3((0,T)\times\Omega)$ and $\tilde{u}, \tilde{v} \in \dashv\nabla\}\infty^4((0,T)\times\Omega)$ be the exact solutions of the time-dependent elliptic PDE problems (7.65) and (7.66). Then the discrete solutions $\tilde{u}_{\Delta x}$ defined in (7.73a) converges towards $\tilde{u}$ and the discrete solutions $\tilde{v}_{\Delta x}$ defined in (7.73b) converges towards $\tilde{v}$ in the $\|\cdot\|_\infty$-norm. The convergence is of second order at the inner grid points and of first order at the outer grid points of $\tilde{u}$ and $\tilde{v}$, respectively.

Sketch of the proof.

1. We show the consistency of the schemes (7.73a) and (7.73b).

2. We show the stability of the schemes. For this purpose, we use the function $e^*(t,x,y) = x\,(1-x)$ or, respectively, $e^*(t,x,y) = y\,(1-y)$ to show, that the matrices $(T_u + L_{Tu})$ and $(T_v + L_{Tv})$ are M-matrices, with

$$\|(T_u + L_{Tu})^{-1}\|_\infty \leq 1/4 \quad \text{and} \quad \|(T_v + L_{Tv})^{-1}\|_\infty \leq 1/4.$$

3. Finally, from stability and consistency we deduce the statement analogous to Theorem 7.26

$\square$

7.6. MAC Scheme for the Stokes Equation

In Section 7.2 we have discussed, that we have to solve the Stokes problem (7.8) at each time $t = m\,\Delta t$, if we seek for a divergence free optical flow. For the sake of simplification we set

$$\tilde{\omega} = \begin{pmatrix} \tilde{u} \\ \tilde{v} \end{pmatrix} := \begin{pmatrix} \mathcal{P}(\nabla_u J(\omega)) \\ \mathcal{P}(\nabla_v J(\omega)) \end{pmatrix} \quad \text{and} \quad f = \begin{pmatrix} g \\ h \end{pmatrix} := \begin{pmatrix} \nabla_u J(\omega) \\ \nabla_v J(\omega) \end{pmatrix}.$$

This way, we obtain the Stokes problem

$$
\begin{aligned}
-\Delta\tilde{\omega} + \nabla\lambda &= -\Delta f & &\text{in } \Omega, \\
-\operatorname{div}(\tilde{\omega}) &= 0 & &\text{in } \Omega, \\
\tilde{\omega} &= 0 & &\text{on } \partial\Omega.
\end{aligned}
$$

Next, we discretise the functions $\tilde{u}, \tilde{v}, g, h$ and λ at the following grid points

$$\tilde{u}^m_{i,j+1/2} = \tilde{u}\big(i\,\Delta x, (j+1/2)\,\Delta x, m\,\Delta t\big) \qquad \text{with} \qquad \begin{aligned} & i = 1, ..., N_x - 1 \\ & j = 0, ..., N_y - 1 \\ & m = 0, ..., M \end{aligned}$$

$$\tilde{v}^m_{i+1/2,j} = \tilde{v}\big((i+1/2)\,\Delta x, j\,\Delta x, m\,\Delta t\big) \qquad \text{with} \qquad \begin{aligned} & i = 0, ..., N_x - 1 \\ & j = 1, ..., N_y - 1 \\ & m = 0, ..., M \end{aligned}$$

$$g^m_{i,j+1/2} = g\big(i\,\Delta x, (j+1/2)\,\Delta x, m\,\Delta t\big) \qquad \text{with} \qquad \begin{aligned} & i = 1, ..., N_x - 1 \\ & j = 0, ..., N_y - 1 \\ & m = 0, ..., M \end{aligned}$$

$$h^m_{i+1/2,j} = h\big((i+1/2)\,\Delta x, j\,\Delta x, m\,\Delta t\big) \qquad \text{with} \qquad \begin{aligned} & i = 0, ..., N_x - 1 \\ & j = 1, ..., N_y - 1 \\ & m = 0, ..., M \end{aligned}$$

and

$$\lambda^m_{i+1/2,j+1/2} = \lambda\big((i+1/2)\,\Delta x, (j+1/2)\,\Delta x, m\,\Delta t\big) \qquad \text{with} \qquad \begin{aligned} & i = 0, ..., N_x - 1 \\ & j = 0, ..., N_y - 1 \\ & m = 0, ..., M. \end{aligned}$$

Moreover, we define the vectors $\tilde{u}^m_{\Delta x}, \tilde{v}^m_{\Delta x}, g^m_{\Delta x}, h^m_{\Delta x}$ and $\lambda^m_{\Delta x}$ by combining the function values for each time step $m = 0, ..., M$ in a vector, for instance we have

$$\tilde{u}^m_{\Delta x} := \big(\tilde{u}^m_{1,1/2}, ..., \tilde{u}^m_{1,N_y-1/2}, \tilde{u}^m_{2,1/2}, ..., \tilde{u}^m_{2,N_y-1/2}, ...,$$
$$\tilde{u}^m_{N_x-1,1/2}, ..., \tilde{u}^m_{N_x-1,N_y-1/2}\big)^T,$$

Finally, regarding to the discussion in the previous section, we can discretise the Stokes problem by

$$\begin{pmatrix} L_u & 0 & D_x \\ 0 & L_v & D_y \\ D_x^T & D_y^T & 0 \end{pmatrix} \cdot \begin{pmatrix} \tilde{u}^m_{\Delta x} \\ \tilde{v}^m_{\Delta x} \\ \lambda^m_{\Delta x} \end{pmatrix} = \begin{pmatrix} g^m_{\Delta x} \\ h^m_{\Delta x} \\ 0 \end{pmatrix}. \tag{7.74}$$

This discretisation of the Stokes problem is known as MAC-scheme [28, 45]. In [45] a multigrid method is developed for solving the discrete saddle point problem (7.74) efficiently.

Analogous to the discretisation of the transport equation in Section 7.4 and the elliptic PDEs in Section 7.5, the convergence of the MAC-scheme follows from the consistency and stability of the scheme, the consistency of the matrices L_u, L_v, D_x and D_y we have already shown in Section 7.5. A stability proof can be found in the references of [45]. Hence, the discrete solution of problem (7.74) converges to the exact solution of the Stokes problem, if Δx tends to zero.

8. Numerical Examples

In Chapter 6, we have shown that problem (NP) is a stable approximation of the ill-posed sequence interpolation problem (SIP). Moreover, in Chapter 7, we have developed an algorithm to solve problem (NP) numerically in the case of an H^1-regularization in space (and time). In collaboration with Thrän [43], this algorithm was efficiently implemented in the coding language Julia.

In this chapter we validate the algorithm at sequences of synthetic and real image frames. In particular, at the sequences of synthetic image frames we critically study the behaviour of the algorithm. Furthermore, we numerically solve problem (NP) both with and without the restriction that the optical flow is divergence-free. In this way, we want to validate numerically that we obtain more accurate reconstruction results, if we do not restrict the optical flow to be divergence-free. Here, we emphasize that this is an essential improvement of our theoretical work (see Chapter 5 and 6), in comparison to [15], where the assumption of a divergence-free optical flow is needed to show existence of a solution to problem (NP).

In the following, the test cases are described: Firstly, we generate a reference (or complete) sequence of image frames $S_j, j = 0, ..., K$ with $K = k\,N$ for given $k, N \in \mathbb{N}$. Here, each image frame is of size $N_x \times N_y$ pixel. Secondly, from the sequence of image frames S_j we take every k-th image frame as input sequence $I_n, n = 0, ..., N$, which we aim to interpolate in the sequence interpolation problem (SIP). The relation between both sequences is graphically illustrated in Figure 8.1.
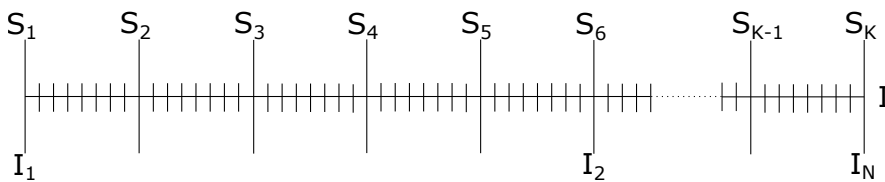
Figure 8.1.: Sampling points of the sequences of reference image frames S_j and input frames I_n; time discretisation points of the reconstructed intensity function I.

To measure the approximation quality of the reconstruction results, we compare the reference sequence of image frames S_j with the reconstructed intensity function I obtained by solving problem (NP). For this aim, we use in the FD schemes as time step

size $\Delta t = \frac{1}{M}$ with $M = LK$ and $L \in \mathbb{N}$, such that Δt and $\Delta x = \frac{1}{\max(N_x, N_y)}$ satisfy the CFL-condition. In doing so, we can evaluate the reconstructed intensity function I at time discretisation points corresponding to the sampling time points of the reference sequence of images S_j, see Figure 8.1. As a consequence, we can measure the quality of the reconstruction I in the L^2-norm with respect to the reference image frames $S_\# := (S_0, ..., S_K)$ by

$$\varepsilon_{L^2}(I, S_\#) := \sum_{j=0}^{K} \| I(j\, L\, \Delta t, \cdot) - S_j \|_{L^2(\Omega)}^2. \tag{8.1}$$

Moreover, we introduce the *peak signal to noise ratio* given by

$$\mathrm{PSNR}(I, S_\#) := 10 \log_{10} \left(\frac{1}{\mathrm{MSE}(I, S_\#)} \right)$$

with

$$\mathrm{MSE}(I, S_\#) := \frac{1}{N_x\, N_y} \sum_{i=0}^{N_x-1} \sum_{l=0}^{N_y-1} (I_j^{i,l} - S_j^{i,l})^2,$$

where

$$I_j^{i,l} := I\big(j\, L\, \Delta t, (i+1/2)\, \Delta x, (l+1/2)\, \Delta x\big)$$

and

$$S_j^{i,l} := S_j\big((i+1/2)\, \Delta x, (l+1/2)\, \Delta x\big).$$

The peak signal to noise ratio is usually used to measure the quality of reconstruction in image processing. Here, large peak to noise ratios correspond to accurate approximations. However, note that we can only measure the peak signal to noise ratio for each image frame separately.

Furthermore, analogously to (8.1), we define the L^2-approximation error of the input samples I_n by

$$\varepsilon_{L^2}(I, I_\#) := \sum_{n=0}^{N} \| I(n\, k\, L\, \Delta t, \cdot) - I_n \|_{L^2(\Omega)}^2$$

with $I_\# := (I_0, ..., I_N)$.

In the gradient method for solving problem (NP) numerically we use for almost any test simulation the parameters $\mathrm{Tol} = 1.0e{-}8, \sigma = 1.0e{-}4$ and $\gamma = 0.9$. The only exception is the Hamburg taxi sequence, in this case we use $\gamma = 0.6$.

134

In the following we examine our regularized image sequence interpolation method for various regularization parameters. For the best parameter setting, which we find empirically, the reconstruction sequences are pictured at the end of this chapter. Moreover in Appendix A.2, we list the L^2-reconstruction error $\varepsilon_{L^2}(I, S_\#)$, the L^2-approximation error of the input samples $\varepsilon_{L^2}(I, I_\#)$, as well as the value of the regularization terms $R^x(\omega)$ and $R^t(\omega)$ for several parameter settings.

Finally, we want to mention that some of the following numerical results are already presented in [43], for the case where the functions I and p and the velocity components u and v are discretised on a collocated grid, whereas we use a staggered grid (cf. discussion at the end of Section 7.3). However, by comparing the numerical results for both kinds of discretisation, we conclude that it is not essential for the reconstruction quality, if we use a staggered or a collocated grid. Hence, it is only necessary to discretise the functions I and p and the velocity components u and v on different grids, if we seek for a reconstruction I corresponding to a divergence free optical flow ω.

8.1. Reconstruction of Translational, Rotational and Deformational Motions

In this section we demonstrate at sequences of synthetic image frames that the algorithm is able to reconstruct translational, rotational and deformational motions of objects. Here, we first introduce a different test sequence for each kind of motion and, subsequently, we discuss the numerical results of all the three test cases.

| Shifted square | Rotated slotted disc | Deformed slotted disc |
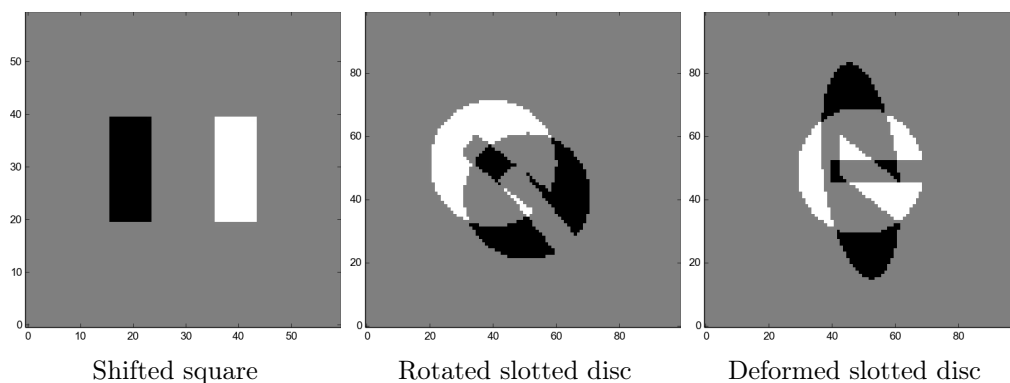
Figure 8.2.: Displacements of the first and second input sample of three different sequences.

As example for the translation we consider a sequence of a shifted square. Here, the $K + 1 = 9$ reference image frames S_j are of size 60×60 pixel. Between two sequential image frames the square is shifted to the left by a distance of one pixel. As input samples I_n we take the first and the last image frame. The displacement of these two input samples is visualized in Figure 8.2. Furthermore, for the reconstruction we use $M = 32$ time steps in the FD schemes.

As example for the rotation we consider a sequence of a rotated slotted disc. Here, the $K + 1 = 13$ reference image frames S_j are of size 100×100 pixel. Between two sequential image frames the slotted disc is rotated around the lower left edge by the radian $0.003\,\pi$. As input samples I_n we take the first and the last image frame. The displacement of these two input samples is visualized in Figure 8.2. Furthermore, for the reconstruction we use $M = 72$ time steps in the FD schemes.

As example for the deformation we consider a sequence of a deformed slotted disc. Here, the $K + 1 = 13$ reference image frames S_j are of size 100×100 pixel. Between two sequential image frames the slotted disc is deformed by the deformation matrix

$$A = \begin{pmatrix} 1.04 & 0.04 \\ 0 & 0.96 \end{pmatrix}.$$

As input samples I_n we take the first and the last image frame. The displacement of these two input samples is visualized in Figure 8.2. Furthermore, for the reconstruction we use $M = 72$ time steps in the FD schemes.

For all these three examples the reconstruction results are visualized in Figure 8.6 - 8.8. We observe, that we obtain for translational, rotational and deformational motions very accurate reconstructions. The structure of the objects are well preserved. Only the edges of the objects are slightly smoothened out.

From Table A.1, A.3 and A.5 we conclude that we obtain better reconstruction results, if we additionally regularize in time. However this improvement is so minimal that it does not satisfy the essentially higher computational costs. The computational costs are much higher in the case of additional time regularization, since the linear systems (7.73) are larger than the linear systems (7.63) for the computation of the gradient $\nabla J(\omega)$. Note, that the linear systems (7.63) arising without time regularization can be solved simultaneously for each time step.

8.2. Reconstruction of Motions Using Divergence Free Optical Flows

Next, we reconstruct the same sequences as in the previous section, but in this case, we seek a reconstruction I corresponding to a divergence-free optical flow ω. The reconstruction results of the translational, rotational and deformational motions are illustrated in Figure 8.9 - 8.11.

We observe that we not only obtain worse reconstruction results for the deformational movement, but also for the translational and rotational movement, if we seek for a divergence-free optical flow. In fact, in the example of the shifted square we observe, that the square is strongly deformed at the intermediate frames. In the two examples of the slotted disc we observe that edges are less sharp than in the case where we do not restrict the optical flow to be divergence-free.

The fact, that we obtain worse reconstructions, if we seek for a divergence free optical flow, can be explained by considering the corresponding optical flows. In Figure 8.12 - 8.14, these are visualized at time $t = 0.5$, where time point t is representative for the complete time interval. In these figures, we detect undesired rotations in the optical flows. These are caused by the requirement, that the optical flow should vanish on the boundary. Hence, due to the Dirichlet boundary condition we cannot obtain for instance a constant translational vector field, which is a divergence-free optical flow for the sequence of a shifted square.

However, in the deformational example the numerical reconstruction results look better as we have expected. Therefore, in the following, we consider a sequence of a zoomed and translated square. Here, the $K + 1 = 17$ reference image frames S_j are of size 60×60 pixel. Between two sequential image frames the square is shifted and zoomed in by one pixel. As input samples I_n we take every eighth image frame. Furthermore, for the reconstruction we use $M = 64$ time steps in the FD schemes. Note that this example can model for instance the respiratory act of a lung (cf. applications of the sequence interpolation problem in Section 1.1).

From Figure 8.15 we conclude that we obtain reasonable reconstruction results, if we do not restrict the optical flow to be divergence-free. However, we cannot reconstruct the zoomed motion, if we use divergence-free optical flows. This is caused by the fact that for representing a zoomed motion, there has to be a source in the optical flow. But in a divergence-free vector field can neither exist a source nor a sink.

8.3. Reconstruction of the Hamburg Taxi Sequence

This section demonstrates that our algorithm is also able to reconstruct sequences of real image frames. As benchmark we consider the Hamburg taxi sequence, consisting of 41 image frames of size 256×190 pixel. For the following numerical simulations we use as reference sequence the first $K + 1 = 21$ image frames S_j, which are displayed in Figure 8.16. From this sequence, we take every fifth image frame as input sequence. Furthermore, for the reconstruction of the Hamburg taxi sequence we use $M = 60$ time steps.

The reconstruction results of the Hamburg taxi sequence are pictured in Figure 8.17 and 8.18. We observe that the approximation of the motions of the white car and the pedestrian are very accurate. But the reconstruction of the motions of the two black

cars driving into the picture are very imprecise.

| Exact frame | Reconstructed image frame $\alpha = 0.01$ | Reconstructed image frame $\alpha = 0.0001$ |

Figure 8.3.: Reconstruction of the 21-th image frame of the Hamburg taxi sequence using an H^1-regularization in space.

The question is, why the algorithm is not able to capture accurately the motion of the two black cars. To answer this question, we first consider Figure 8.3, which displays the last image frame of the reconstructed sequence for two different regularization parameters. From this figure we conclude, that the algorithm is not able to detect a motion of the two black cars for a large regularization parameter α. This behaviour is caused by the requirement that the optical flow should vanish at the boundary of the image, as high velocities in the optical flow close to the boundary imply large gradients of the optical flow at the boundary. But these gradients are penalized stronger by the H^1-regularization term for a larger regularization parameter α. Therefore, the algorithm is only able to detect motions close to the boundary for small regularization parameters α. However, since we do not have any inflow boundary conditions even for small regularization parameters α, the algorithm is not able to preserve the structure of the two black cars. A further problem could be that the two black cars do not provide a large contrast in relation to the background.

Considering the peak to noise ratios in Figure 8.17 and 8.18 we observe that the reconstructions are the best at the sample time points of the input samples I_n.

Moreover, watching the complete reconstructed sequence I on a computer, we observe that we obtain essentially better reconstruction results, if we additionally regularize in time, as without regularization in time, we can observe jumps in time at the sampling time points of the input samples I_n for $n = 1, ..., 4$.

However, solving problem (NP) with an H^1-regularization in space and time is very expensive. This high computational effort is caused by solving the large linear systems in (7.73). The dimension of these linear systems depends on the number of discretisation points in space and time. Hence, to reduce the computational costs, we first

solve a small reconstruction problem (NP) for two sequential image frames I_n and I_{n+1}, with $n = 0, ..., N - 1$, to obtain a good estimate of the optical flow between these two sequential images frames, which we denote by $\omega_{n,n+1}$. Subsequently, we set $\omega^0 = (\omega_{0,1}, \omega_{1,2}, ..., \omega_{n-1,n+1})$ as initial vector field to solve problem (NP) for all input samples $I_n, n = 0, ..., N$. Since ω^0 is a very accurate approximation to an optimal solution we need less iteration steps in the gradient method (Algorithm 7.4) to converge into this. Consequently, the computational costs are reduced, since we have to solve the large linear systems (7.73) less often, for all $M + 1$ time levels.

Finally, we also try to reconstruct the Hamburg taxi sequence using divergence-free optical flows, see Figure 8.19. In this case the reconstruction results are less accurate, since for instance the rear window of the white car and the centre strip of the street are deformed.

8.4. Reconstruction of a Non-Uniform Motion in Time

Up to now one can get the impression that an additional regularization in time leads always to better reconstruction results. To refute this impression we consider a sequence of a square shifted non-uniformly in time. This sequence consists of $K + 1 = 17$ reference image frames S_j of size 60×60 pixel. In the first nine images the square is shifted to the left and in the last nine images it is shifted to the bottom. The speed of the square is again one pixel between two sequential image frames. As input samples I_n we consider every eighth image frame. Furthermore, for the reconstruction we use $M = 64$ time steps in the FD schemes.

Considering the reconstruction results in Figure 8.20, we observe that the numerical results with and without additional regularization in time look similar. However, considering the complete reconstructed sequence I as video on a computer, we observe that the square is moving on a curve with a small radius if we additionally regularize in time. This behaviour can also be observed in the related optical flows, see Figure 8.21 and 8.22. Here, we detect a discontinuous optical flow in time for the H^1-regularization in space only, but a continuous optical flow in time for the H^1-regularization in space and time.

8.5. Reconstruction of Image Sequences with Discontinuous Optical Flows

After presenting many positive reconstruction results, we also want to demonstrate that the algorithm is not able to reconstruct any movement accurately. In Section 6.2.3, we have already discussed that we can only reconstruct continuous optical flows with an H^1-regularization. Therefore, we consider in the following a sequence of two squares touching each other but moving in different directions. This sequence consists of $K + 1 = 33$ reference image frames S_j of size 60×60. As input samples I_n we consider

every eighth image frame. Furthermore, for the reconstruction we use $M = 128$ time steps in the FD schemes.

In Figure 8.23 we observe, as expected, that we do not obtain accurate approximations of the intermediate image frames. Hence, in this case a BV or $W^{1,1+\tau}$-regularization, allowing also discontinuous optical flows, is more suitable to solve the sequence interpolation problem (SIP), as discussed in Section 6.2.3.

However, for solving problem (NP) with BV or $W^{1,1+\tau}$-regularization numerically there are two challenges. Firstly, for the gradient method we have to discuss how to compute a descent direction in the Non-Hilbert space setting, as already mentioned in Remark 7.5. Secondly, in the consistency analysis of the Upwind and Lax-Wendroff schemes for the numerical solution of the optical flow constraint (OFC) and the adjoint equation (adjEq), we have required that the vector field ω is continuously differentiable. In fact, numerical tests show that the FD schemes developed in Section 7.4.2 and 7.4.3 are not able to locally resolve the transport problem exactly or at least approximately in surroundings where the vector field ω admits a discontinuity.

| initial value | exact solution | discrete solution |
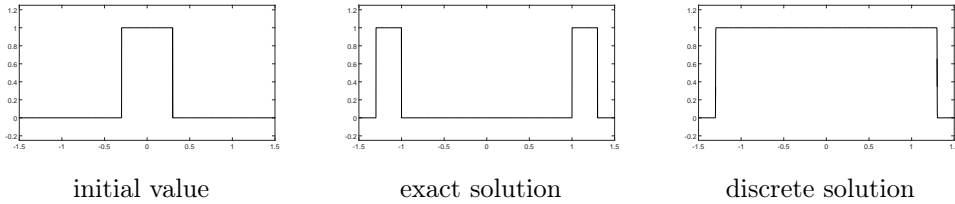
Figure 8.4.: Solution behaviour of FD schemes for the non-conservative transport equation (OFC) with discontinuous vector field ω: Here, problem (OFC) is solved for an initial condition $I_0(x) = \chi_{[-0.3,0.3]}$ and a vector field $\omega(t, x) = \chi_{x \in [0, \infty)} - \chi_{x \in (-\infty, 0)}$. We use as mesh size $\Delta x = 0.0001$ and as step size $t = 0.00005$. The discrete solution at time $t = 1$ is obtained by using the flux limiter FD scheme (7.46).

In Figure 8.4, we have numerically solved the 1-dimensional optical flow constraint (OFC) for a given discontinuous vector field

$$\omega(t, x) = \begin{cases} 1 & \text{for } x \geq 0, \\ -1 & \text{for } x < 0, \end{cases}$$

but the numerical solution corresponds to the vector field

$$\omega_\varepsilon(t, x) = \begin{cases} 1 & \text{for } x \geq \varepsilon, \\ \frac{x}{\varepsilon} & \text{for } -\varepsilon < x < \varepsilon, \\ -1 & \text{for } x \leq \varepsilon, \end{cases}$$

with $\varepsilon > 0$ sufficiently small, which is a continuous approximation of ω.

8.6. Reconstruction of Image Sequences with Small Sampling Rates

In Remark 7.5, we have mentioned that the gradient method (Algorithm 7.4) converges only to a local minimum, which is not necessarily a global minimum. As a consequence, our numerical method has problems to reconstruct a sequence, if the sampling rate of the input samples are too small.

Displacement of 20 pixel   Displacement of 24 pixel
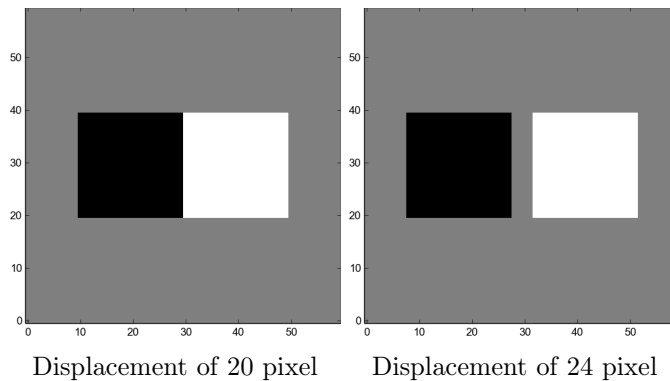
Figure 8.5.: Displacements of the first and second input sample of sequences of a shifted square with small sampling rates.

We demonstrate this fact at the sequence of a shifted square. Here, the image frames are of size 60×60 pixel and the pixel itself of size 20×20 pixel. In the first case, the square is shifted to the left from the first to the second input sample with constant speed by a distance of 20 pixel and in the second test case by a distance of 24 pixel. The displacement of both test cases are pictured in Figure 8.5. In particular, we note that in the first test case the supports of the squares in the first and the second image frame are touching each other, whereas in the second case, there is no interaction between the supports. Furthermore, we use in each of these test cases two different initial vector fields in the gradient method (Algorithm 7.4) to reconstruct numerically the sequences. In fact, we use both a zero vector field as initial vector field, $\omega^0(t, x) = 0$, and a constant vector field $\omega^0(t, x) = (-1, 0)^T$, which is a good estimation of the exact optical flow.

The reconstruction results are illustrated in Figure 8.24 and 8.25. We observe in the case where we use a zero initial vector field, that we are only able to reconstruct the sequence, if the supports of the two squares in the first and second image frame are overlapping or at least touching each other. On the other hand, in the case where we use an initial vector field close to the exact optical flow in the gradient method, we are able to reconstruct the sequence in both cases. However, the reconstruction in the first case is much better.

In summary, to be able to reconstruct a sequence, we have to guarantee either that the supports of corresponding objects in two sequential image frames are overlapping or at least touching each other, or that we use in the gradient method (Algorithm 7.4) a close estimate to the exact optical flow as initial vector field. Otherwise, the algorithm has too less information to reconstruct the sequence accurately. In particular, the reconstruction results are the better the more a priori information we put into the solution process.

8.7. Reconstruction of Perturbed Image Sequences

In the last section we show numerically that problem (NP) with an H^1-regularization in space is a stable approximation of the sequence interpolation problem (SIP). In particular, we verify empirically the parameter choice rule stated in Corollary 6.13.

As test example we consider the sequences of a shifted square and a rotated slotted disc introduced in Section 8.1. Moreover, in this case, we add to the input samples I_n a normally distributed noise with variance ε and mathematical expectation 0.

However, due to the requirement that the optical flow vanishes on the spatial boundary, a constant vector field may not be used as minimal norm solution for the sequence of a shifted square (with unperturbed image samples). Also, for the sequence of a rotated slotted disc we do not know a priori a minimal norm solution. Therefore, we can only verify the stability empirically.

As analysed in Corollary 6.13, for a given noise level $\varepsilon > 0$, we have to choose the regularization parameter α, such that

$$\alpha(\varepsilon) \to 0, \quad \text{and} \quad \frac{\varepsilon^2}{\alpha(\varepsilon)} \to 0 \quad \text{for} \quad \varepsilon \to 0. \tag{8.2}$$

In the following, we test $\alpha(\varepsilon) = \varepsilon, \alpha(\varepsilon) = \varepsilon^2$ and $\alpha(\varepsilon) = 0.01$ as parameter choices. We note that $\alpha = 0.01$ is the regularization parameter for which we obtain the best reconstruction results for the unperturbed sequence of a shifted square (cf. Section 8.1). Moreover, we note that only the parameter choice rule $\alpha(\varepsilon) = \varepsilon$ satisfies the requirement (8.2) for all noise levels $\varepsilon > 0$.

The reconstruction of the optical flow, for various noise levels $\varepsilon > 0$ and regularization parameters α, is illustrated for the sequences of a shifted square in Figure 8.26 and for the sequence of a rotated slotted disc in Figure 8.27. Considering the reconstruction results of both test examples for $\varepsilon = 0.02$ and $\varepsilon = 0.03$ with $\alpha = 0.01$, we conclude that the reconstruction of the optical flow tends to be unstable, if $\alpha(\varepsilon) < \varepsilon$. Moreover, for small noise levels, i.e., for instance $\varepsilon = 0.01$, the reconstruction results of the optical flow are also unstable for $\alpha(\varepsilon) = \varepsilon^2$. Furthermore, in the case of $\alpha(\varepsilon) = \varepsilon$ for the regularization parameter, we obtain for all noise levels $\varepsilon > 0$ a stable reconstruction of the optical flow.

In summary, we have empirically verified Corollary 6.13, which states how to choose the

regularization parameter α depending on the noise level ε. At this point, we also remark that for unperturbed image sequences the best reconstruction parameter α is nonzero, since numerical discretisation errors have similar effects on the solution process as noise in the measurements.

Finally, in Figure 8.28 we also picture the corresponding reconstructed sequences for a noise level $\varepsilon = 0.03$ with regularization parameter $\alpha = 0.03$. Here, we observe that the method is also able to reconstruct the intensity function I of perturbed image sequences, but it is not able to regularize the noise in the images. Indeed, the noise is only slightly denoised, but this is caused by the damping behaviour of the FD scheme, or to be more precise by the Upwind scheme, for solving the optical flow constraint (OFC) numerically. Therefore, it is reasonable to denoise the input samples a priori, for instance by using variational or filter methods [14], before we reconstruct the image sequences.
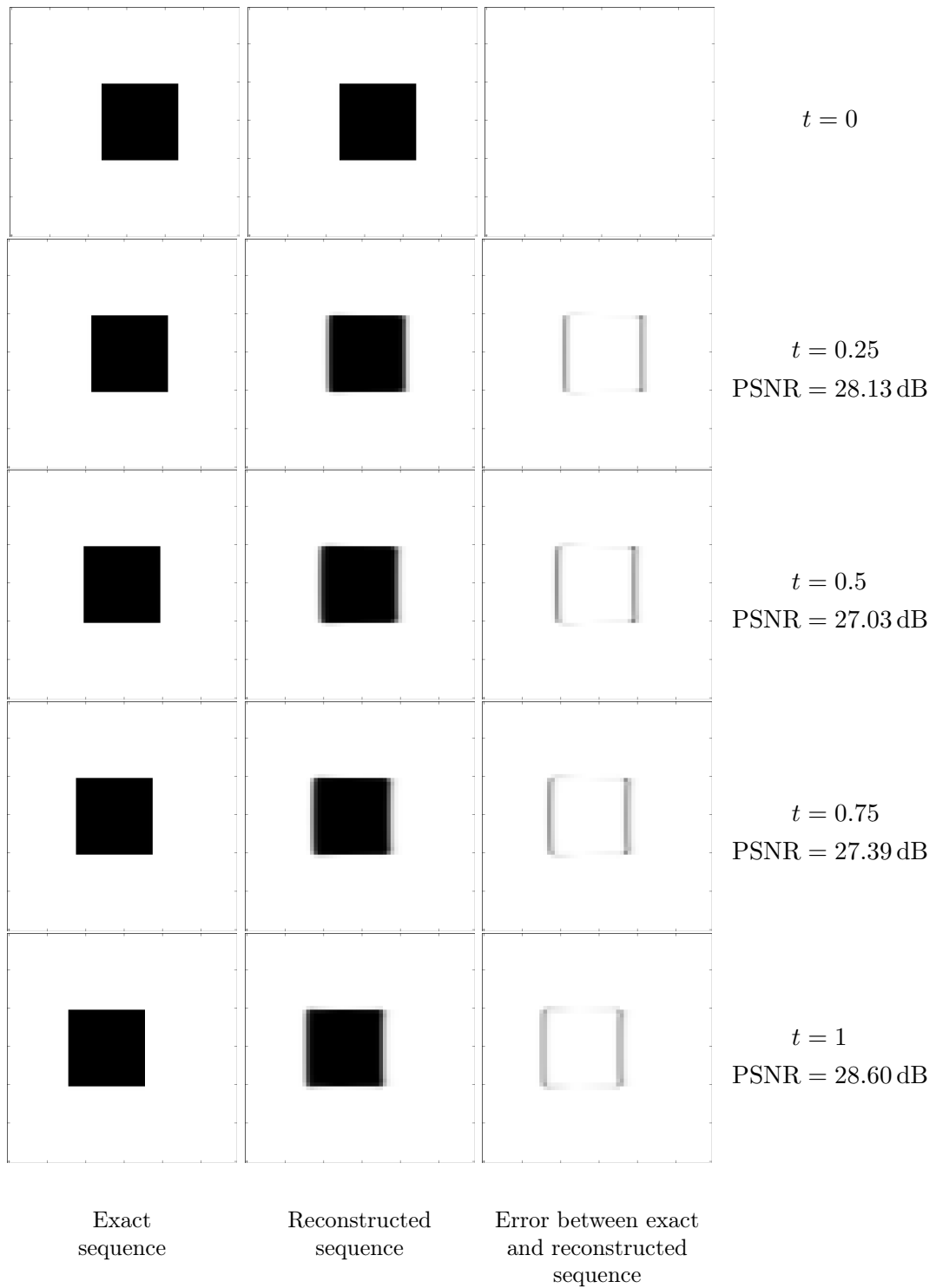
Figure 8.6.: Reconstructed sequence of a shifted square by using an H^1-regularization in space and time with regularization parameters $\alpha = 0.00001$ and $\beta = 0.01$.

Exact sequence	Reconstructed sequence	Error between exact and reconstructed sequence	
			$t = 0$
			$t = 0.25$ PSNR $= 24.17\,\mathrm{dB}$
			$t = 0.5$ PSNR $= 24.03\,\mathrm{dB}$
			$t = 0.75$ PSNR $= 24.29\,\mathrm{dB}$
			$t = 1$ PSNR $= 25.75\,\mathrm{dB}$
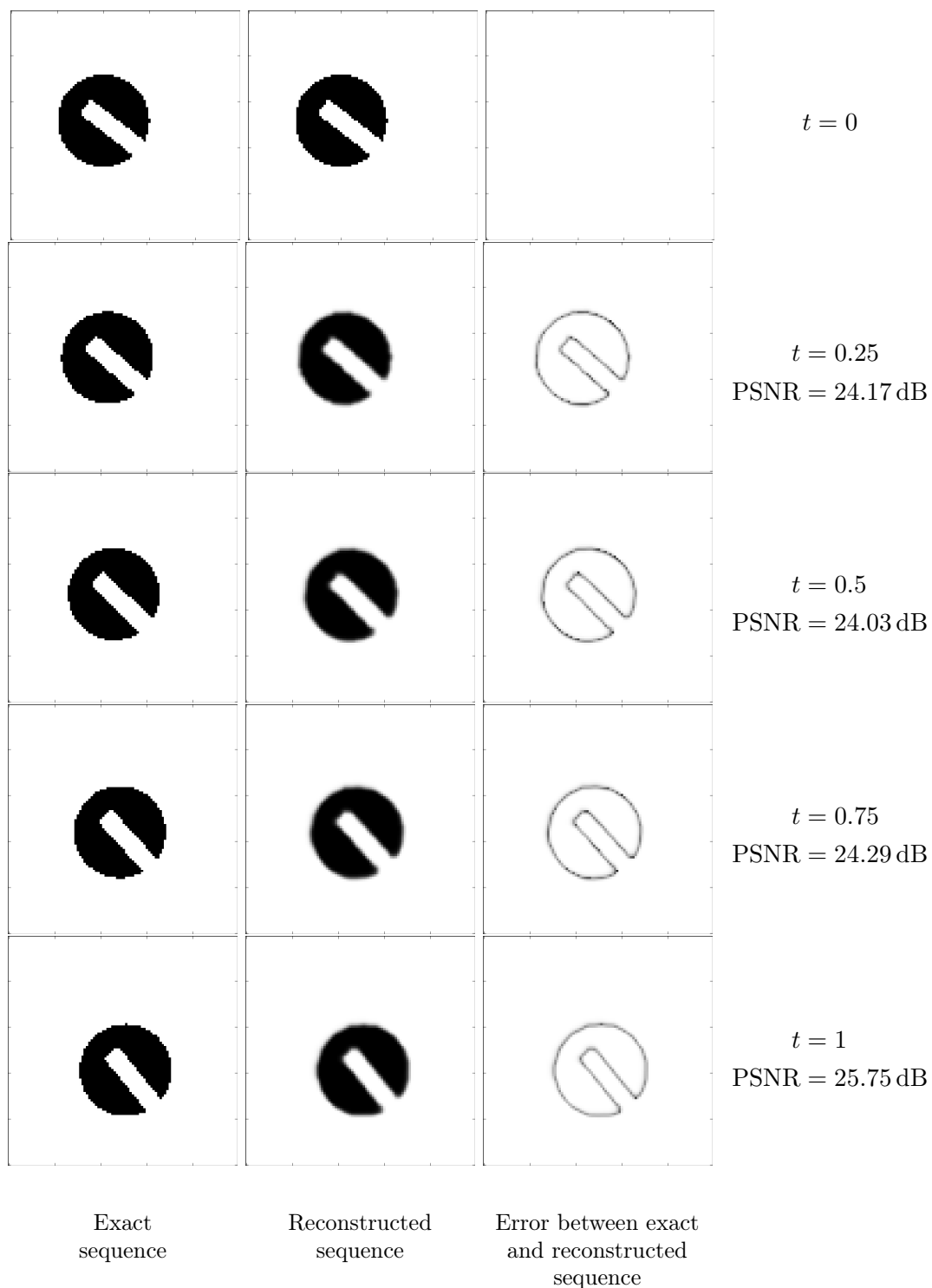
Figure 8.7.: Reconstructed sequence of a rotated slotted disc by using an H^1-regularization in space and time with regularization parameters $\alpha = 0.00001$ and $\beta = 0.01$.

Exact sequence	Reconstructed sequence	Error between exact and reconstructed sequence	
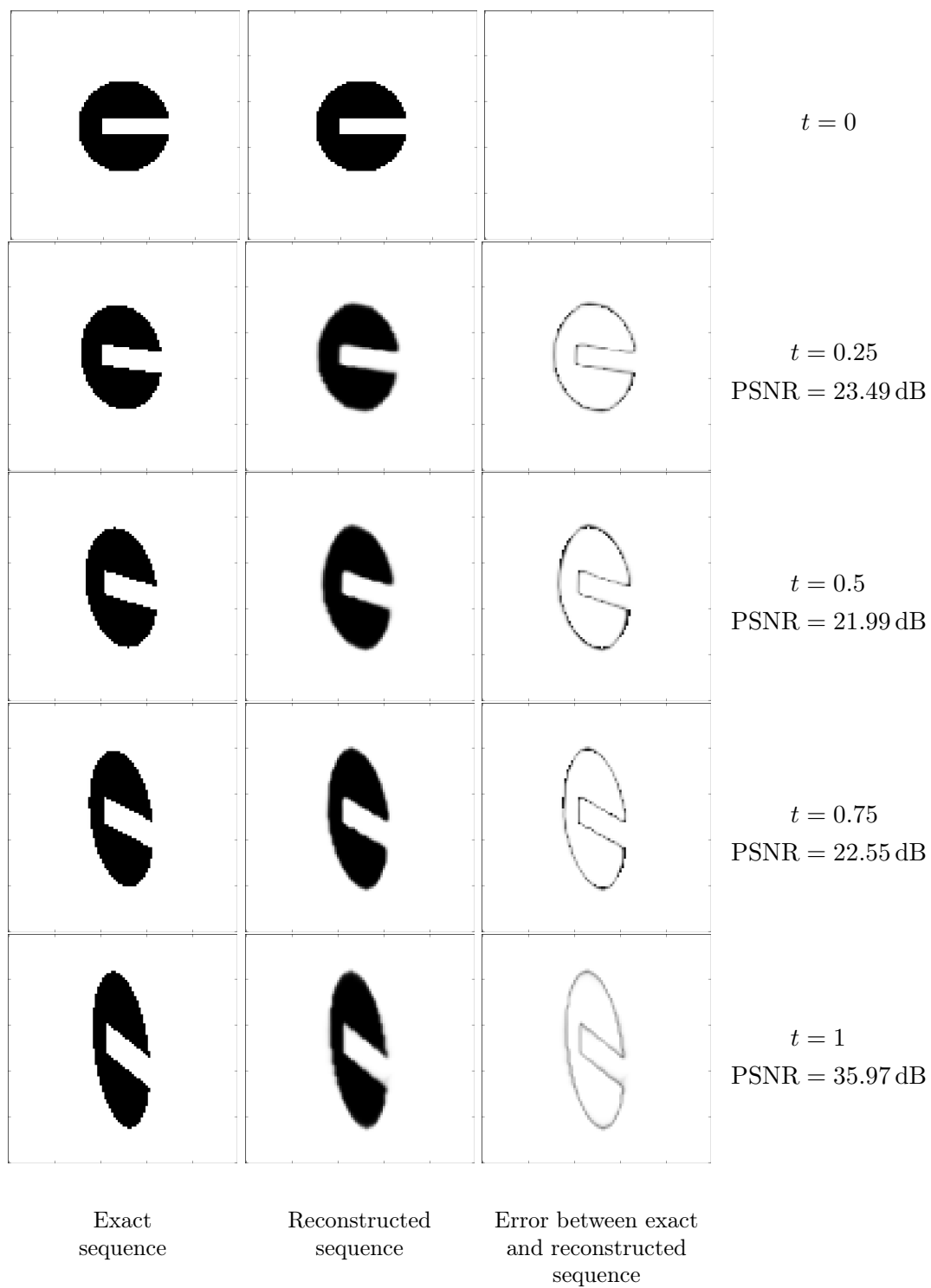
Figure 8.8.: Reconstructed sequence of a deformed slotted disc by using an H^1-regularization in space and time with regularization parameters $\alpha = 0.000001$ and $\beta = 0.0001$.

			$t = 0$
			$t = 0.25$ $\text{PSNR} = 27.54\,\text{dB}$ $\text{PSNR} = 22.87\,\text{dB}$
			$t = 0.5$ $\text{PSNR} = 26.44\,\text{dB}$ $\text{PSNR} = 21.55\,\text{dB}$
			$t = 0.75$ $\text{PSNR} = 26.82\,\text{dB}$ $\text{PSNR} = 22.80\,\text{dB}$
			$t = 1$ $\text{PSNR} = 28.35\,\text{dB}$ $\text{PSNR} = 26.27\,\text{dB}$
Exact sequence	Non-divergence-free $\alpha = 0.01$	Divergence-free $\alpha = 0.001$	
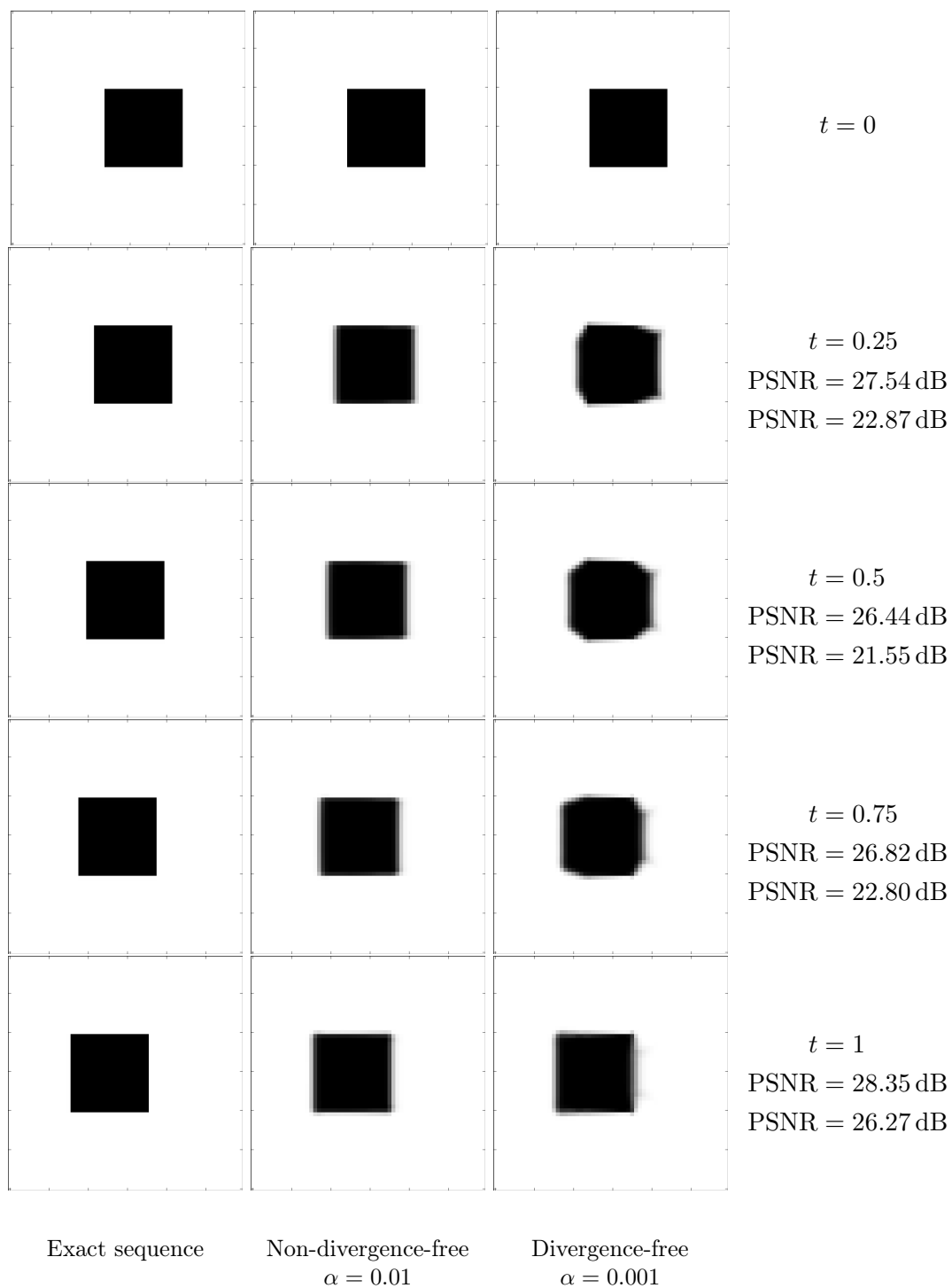
Figure 8.9.: Reconstructed sequences of a shifted square corresponding to a divergence-free and a non-divergence-free optical flow with H^1-regularization in space.

			$t = 0$
			$t = 0.25$ PSNR $= 23.67\,\mathrm{dB}$ PSNR $= 21.39\,\mathrm{dB}$
			$t = 0.5$ PSNR $= 23.52\,\mathrm{dB}$ PSNR $= 20.68\,\mathrm{dB}$
			$t = 0.75$ PSNR $= 23.71\,\mathrm{dB}$ PSNR $= 21.02\,\mathrm{dB}$
			$t = 1$ PSNR $= 26.72\,\mathrm{dB}$ PSNR $= 25.09\,\mathrm{dB}$
Exact sequence	Non-divergence-free $\alpha = 0.01$	Divergence-free $\alpha = 0.001$	
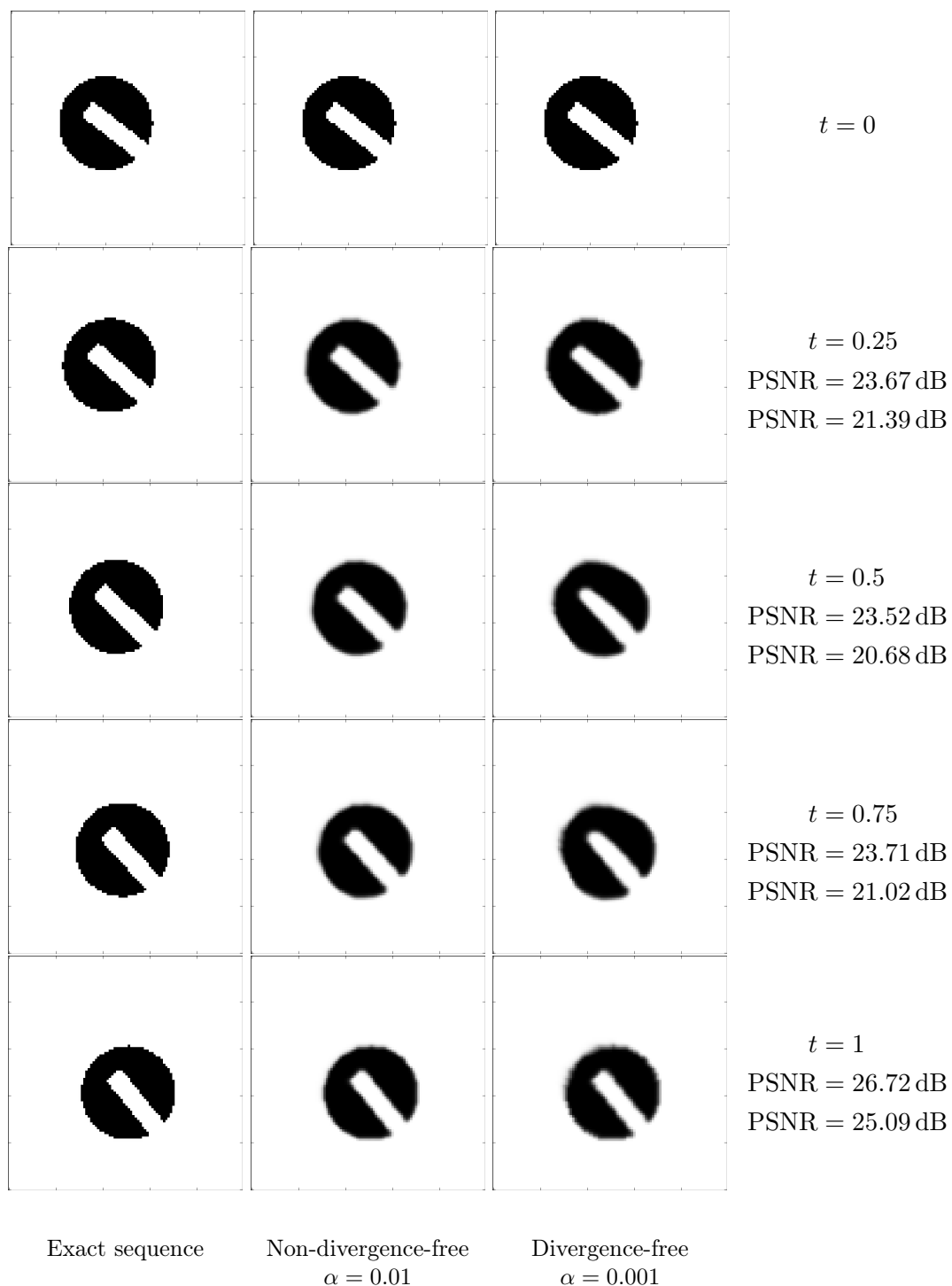
Figure 8.10.: Reconstructed sequences of a rotated slotted disc corresponding to a divergence-free and a non-divergence-free optical flow with H^1-regularization in space.

			$t = 0$
			$t = 0.25$ PSNR = 23.79 dB PSNR = 22.86 dB
			$t = 0.5$ PSNR = 23.19 dB PSNR = 22.47 dB
			$t = 0.75$ PSNR = 23.25 dB PSNR = 22.99 dB
			$t = 1$ PSNR = 23.30 dB PSNR = 25.23 dB

Exact sequence	Non-divergence-free $\alpha = 0.1$	Divergence-free $\alpha = 0.01$
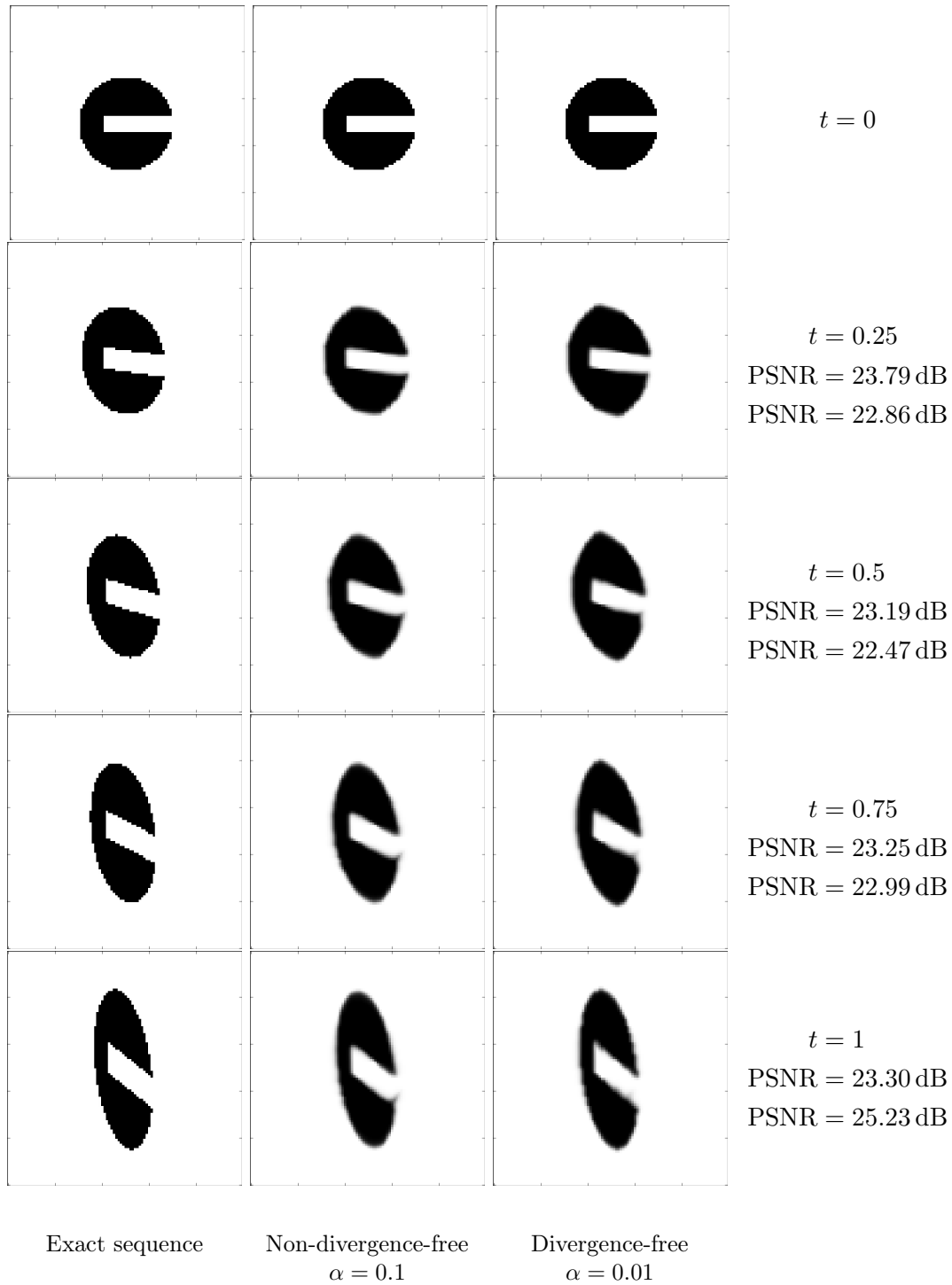
Figure 8.11.: Reconstructed sequences of a deformed slotted disc corresponding to a divergence-free and a non-divergence-free optical flow with H^1-regularization in space.

Non-divergence-free
$\alpha = 0.01$

Divergence-free
$\alpha = 0.001$
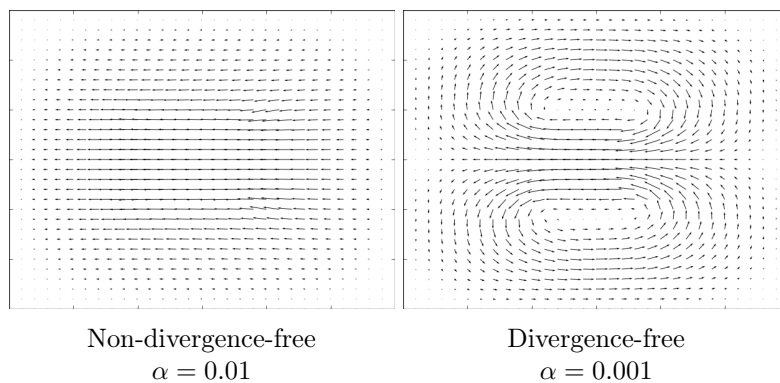
Figure 8.12.: Divergence-free and non-divergence-free optical flow of a shifted square at time $t = 0.5$ with an H^1-regularization in space.

Non-divergence-free
$\alpha = 0.01$

Divergence-free
$\alpha = 0.001$
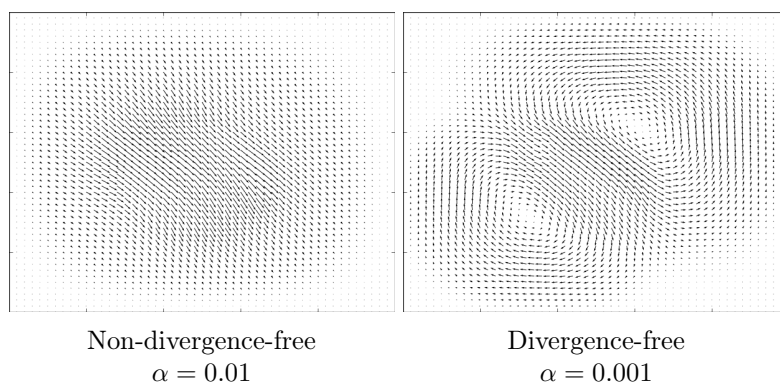
Figure 8.13.: Divergence-free and non-divergence-free optical flow of a rotated slotted disc at time $t = 0.5$ with an H^1-regularization in space.

Non-divergence-free
$\alpha = 0.1$

Divergence-free
$\alpha = 0.01$
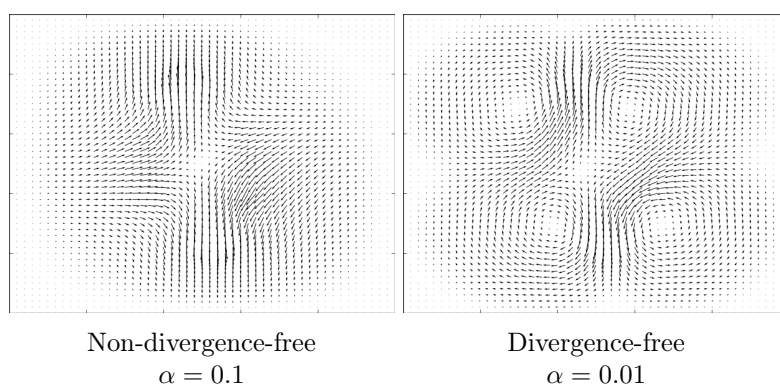
Figure 8.14.: Divergence-free and non-divergence-free optical flow of a deformed slotted disc at time $t = 0.5$ with H^1-regularization in space.

| Exact Sequence | Non-divergence-free
$\alpha = 0.0001$ | Divergence-free
$\alpha = 0.01$ | Divergence-free
$\alpha = 0.0001$ |
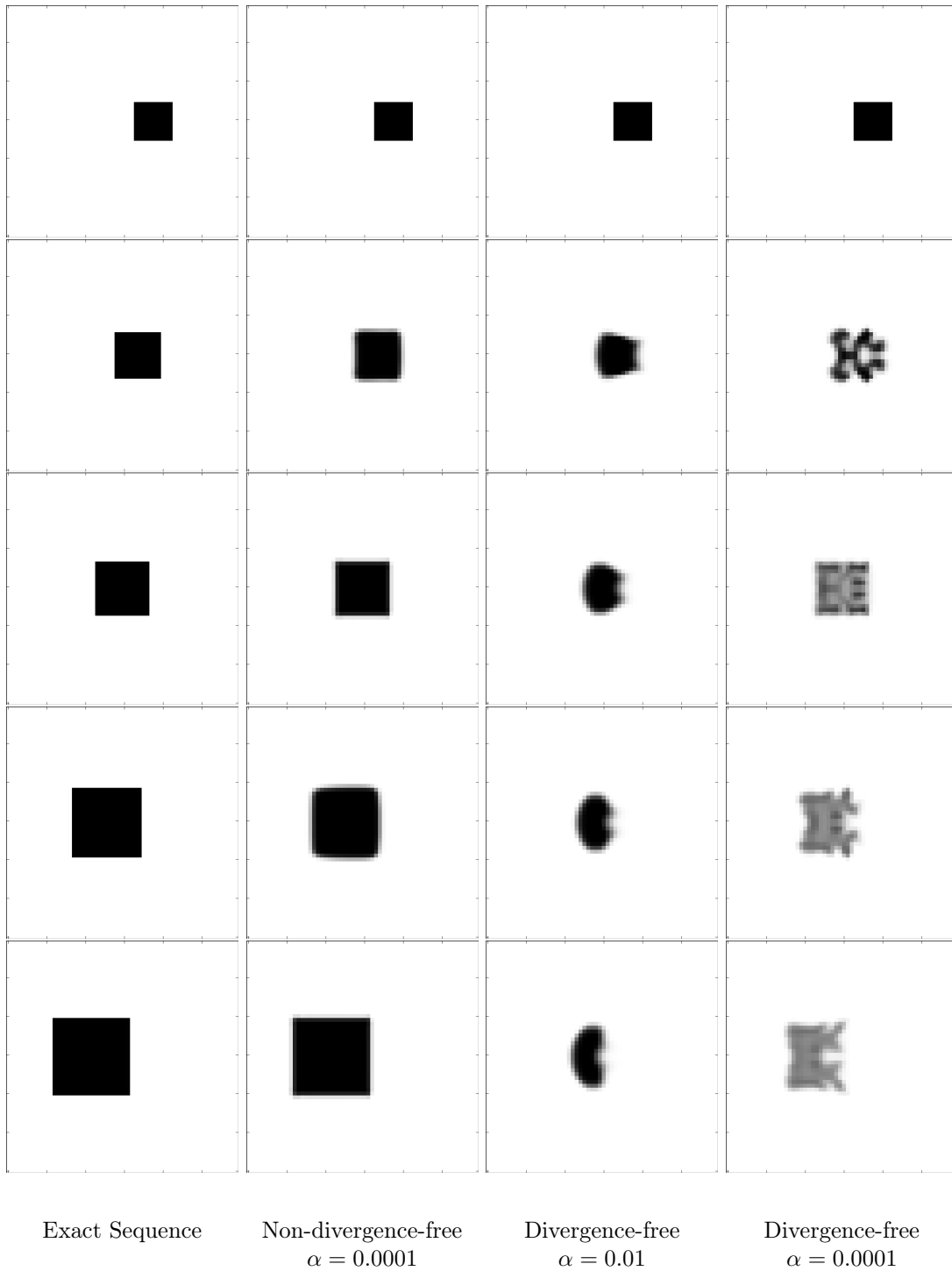
Figure 8.15.: Reconstructed sequences of a zoomed and translated square corresponding to a divergence-free and a non-divergence-free optical flow with H^1-regularization in space.

Frame 1   Frame 2   Frame 3   Frame 4

Frame 5   Frame 6   Frame 7   Frame 8

Frame 9   Frame 10   Frame 11   Frame 12

Frame 13   Frame 14   Frame 15   Frame 16

Frame 17   Frame 18   Frame 19   Frame 20

Frame 21
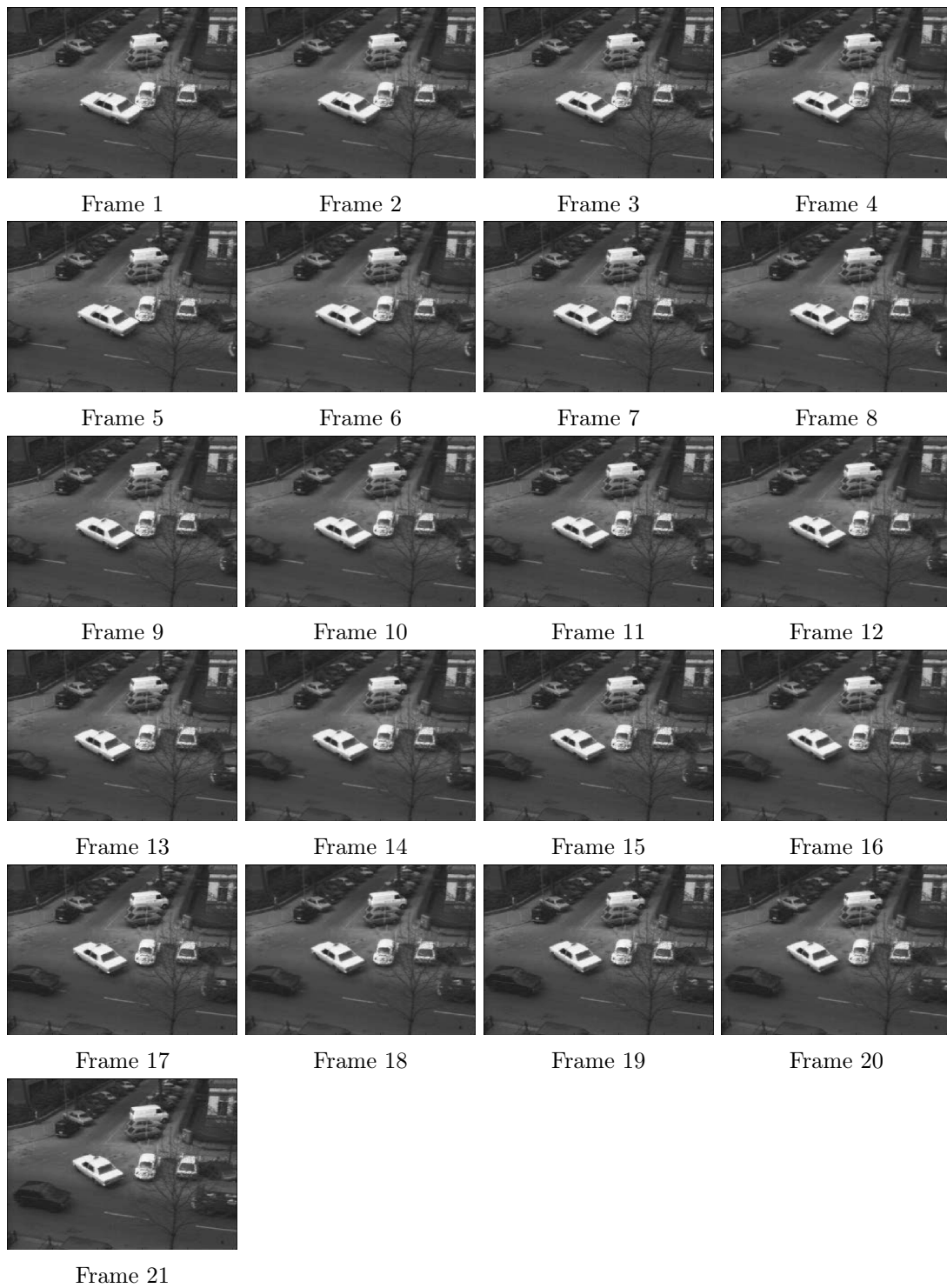
Figure 8.16.: Hamburg taxi sequence: Illustration of the first 21 frames of the Hamburg Taxi sequence line by line.

Exact	PSNR: 34.75 dB	PSNR: 33.18 dB	PSNR: 33.60 dB
PSNR: 34.48 dB	PSNR: 36.77 dB	PSNR: 34.18 dB	PSNR: 34.02 dB
PSNR: 33.77 dB	PSNR: 34.62 dB	PSNR: 35.98 dB	PSNR: 34.39 dB
PSNR: 33.70 dB	PSNR: 34.08 dB	PSNR: 34.01 dB	PSNR: 36.10 dB
PSNR: 34.51 dB	PSNR: 34.28 dB	PSNR: 33.40 dB	PSNR: 33.98 dB

PSNR: 35.55 dB
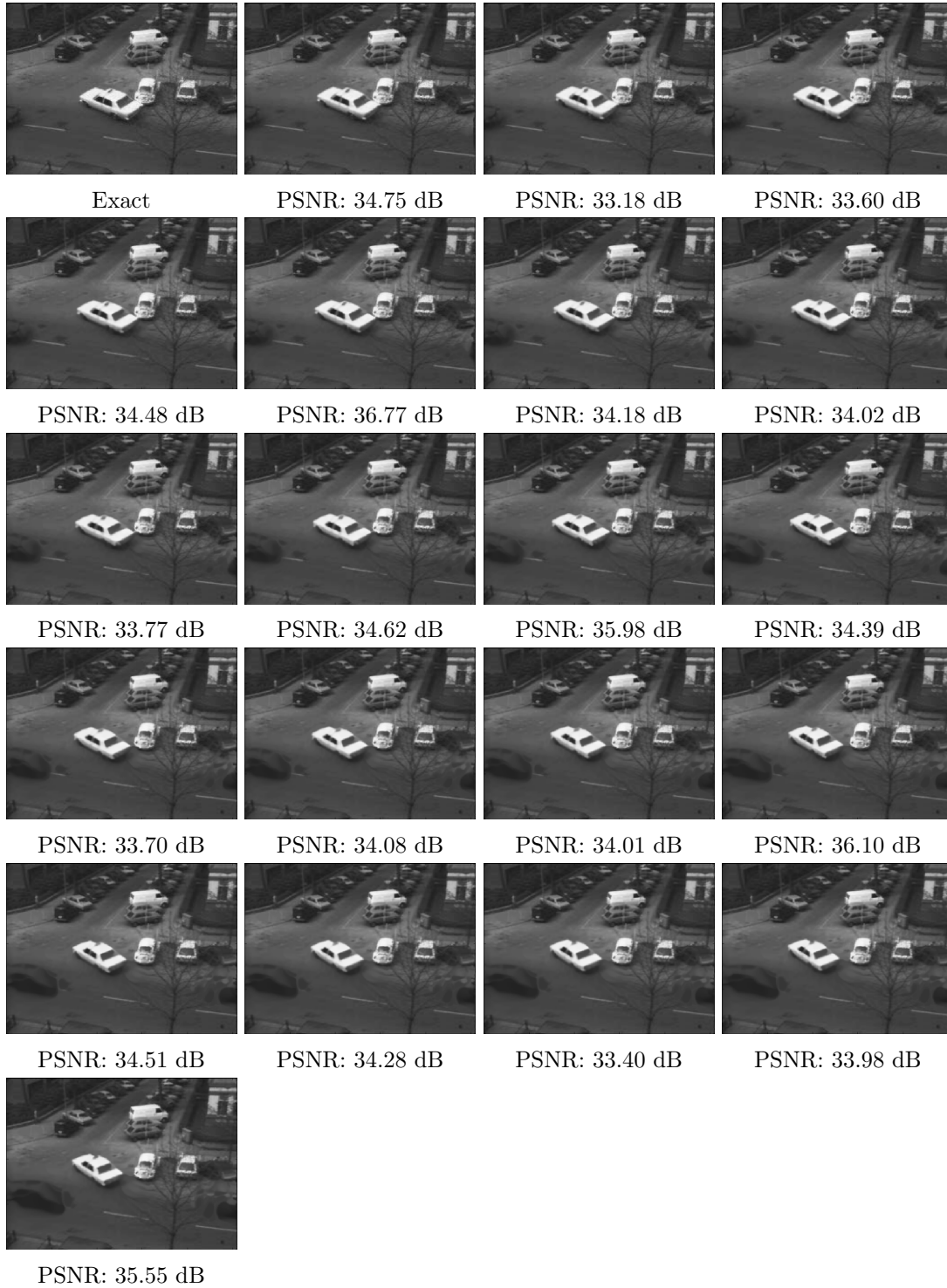
Figure 8.17.: Reconstructed Hamburg taxi sequence by using an H^1-regularization in space and time with regularization parameters $\alpha = \beta = 0.0001$. The reconstructed image frames are displayed line by line.

Exact PSNR: 33.68 dB PSNR: 32.55 dB PSNR: 32.98 dB

PSNR: 34.16 dB PSNR: 35.82 dB PSNR: 33.34 dB PSNR: 32.51 dB

PSNR: 32.40 dB PSNR: 33.21 dB PSNR: 34.33 dB PSNR: 33.34 dB

PSNR: 32.82 dB PSNR: 32.34 dB PSNR: 32.43 dB PSNR: 33.96 dB

PSNR: 32.93 dB PSNR: 32.06 dB PSNR: 31.08 dB PSNR: 31.81 dB

PSNR: 32.76 dB
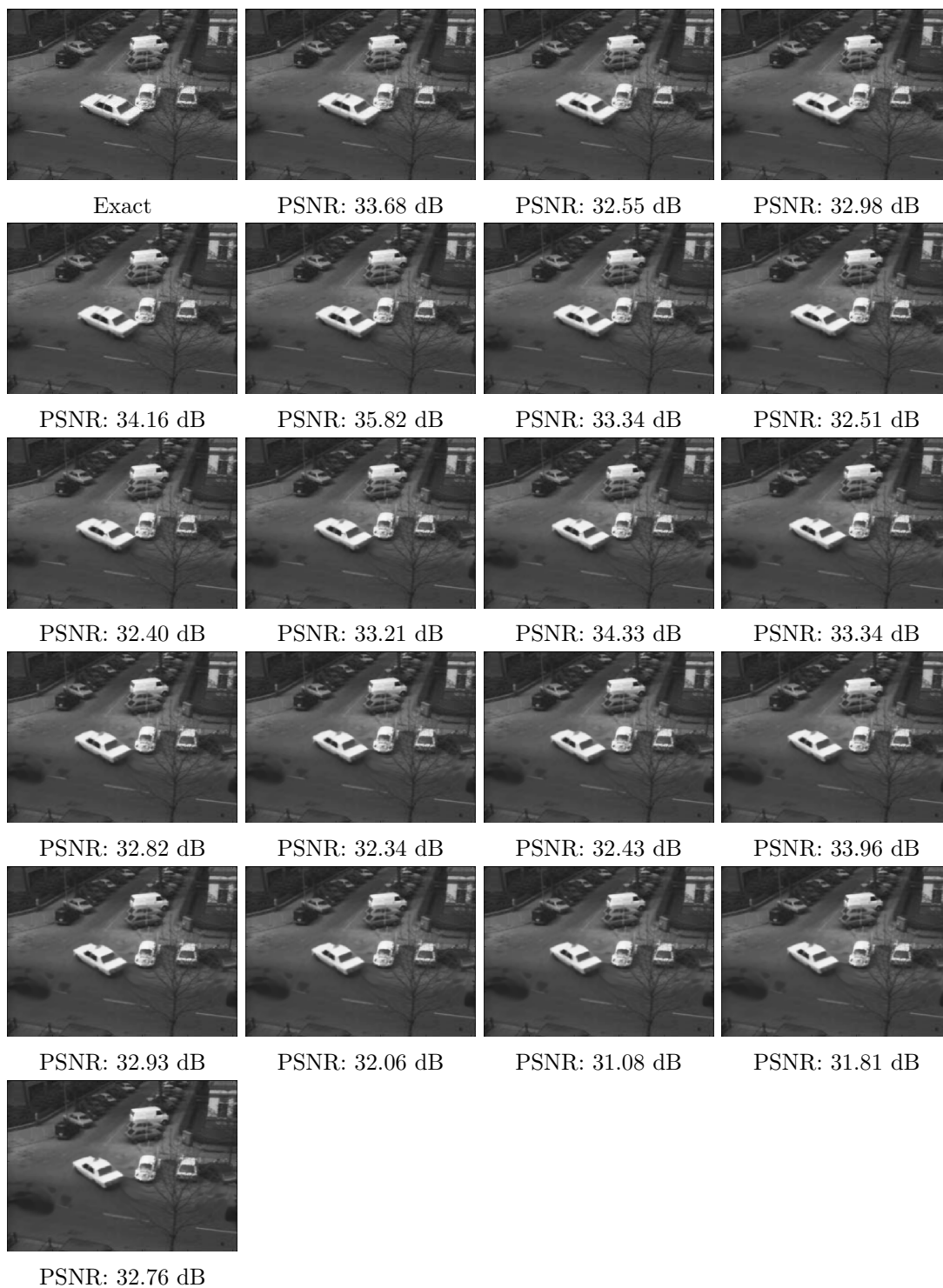
Figure 8.18.: Reconstructed Hamburg taxi sequence by using an H^1-regularization in space with regularization parameter $\alpha = 0.001$. The reconstructed image frames are displayed line by line.

Exact	PSNR: 34.05 dB	PSNR: 31.13 dB	PSNR: 30.94 dB
PSNR: 32.27 dB	PSNR: 34.21 dB	PSNR: 31.37 dB	PSNR: 29.54 dB
PSNR: 29.39 dB	PSNR: 30.78 dB	PSNR: 31.95 dB	PSNR: 30.26 dB
PSNR: 29.02 dB	PSNR: 29.37 dB	PSNR: 29.73 dB	PSNR: 30.71 dB
PSNR: 29.53 dB	PSNR: 28.64 dB	PSNR: 28.26 dB	PSNR: 28.92 dB

PSNR: 29.26 dB
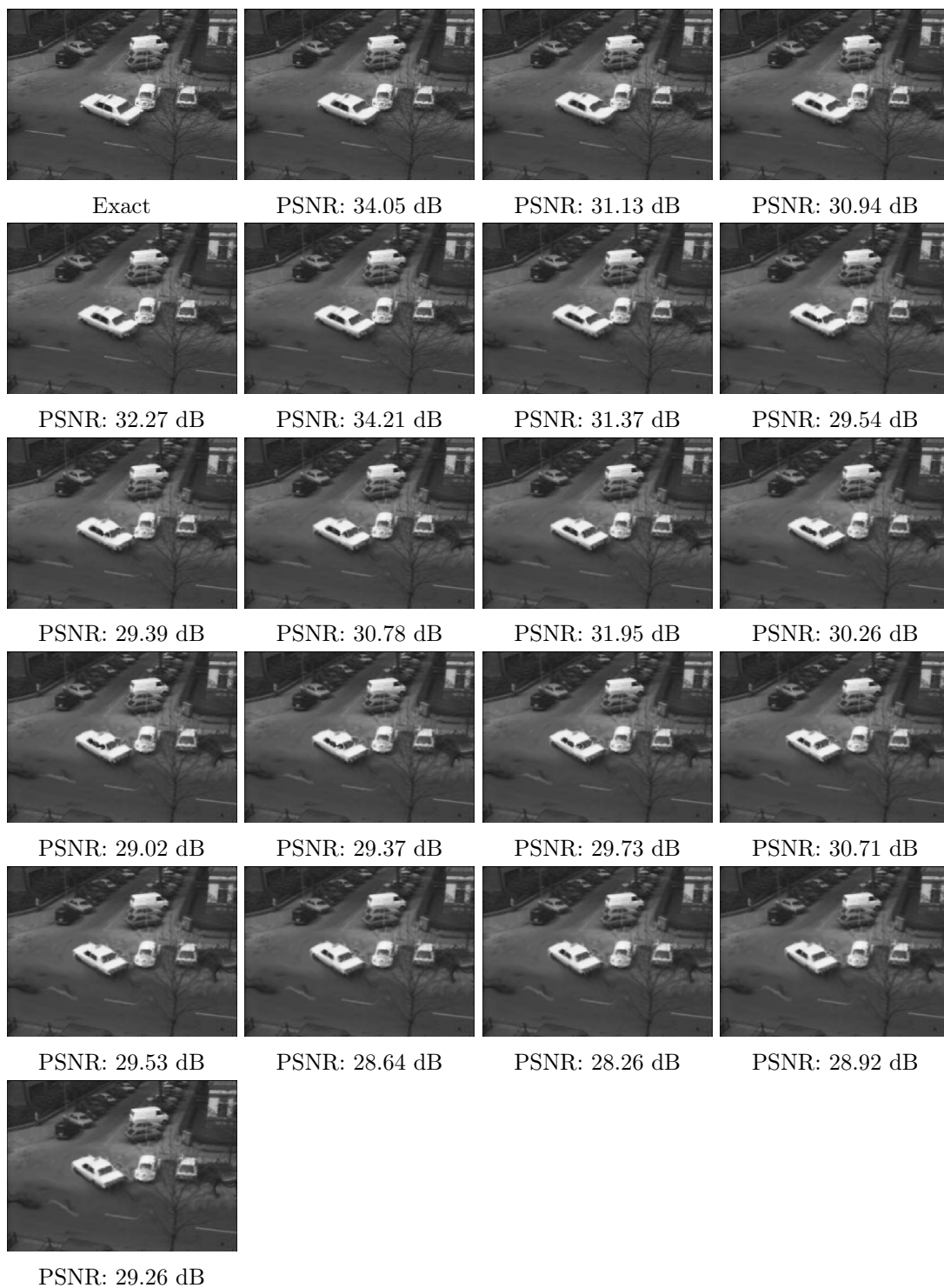
Figure 8.19.: Reconstructed Hamburg taxi sequence corresponding to a divergence-free optical flow by using an H^1-regularization in space with regularization parameter $\alpha = 0.0001$. The reconstructed image frames are displayed line by line.
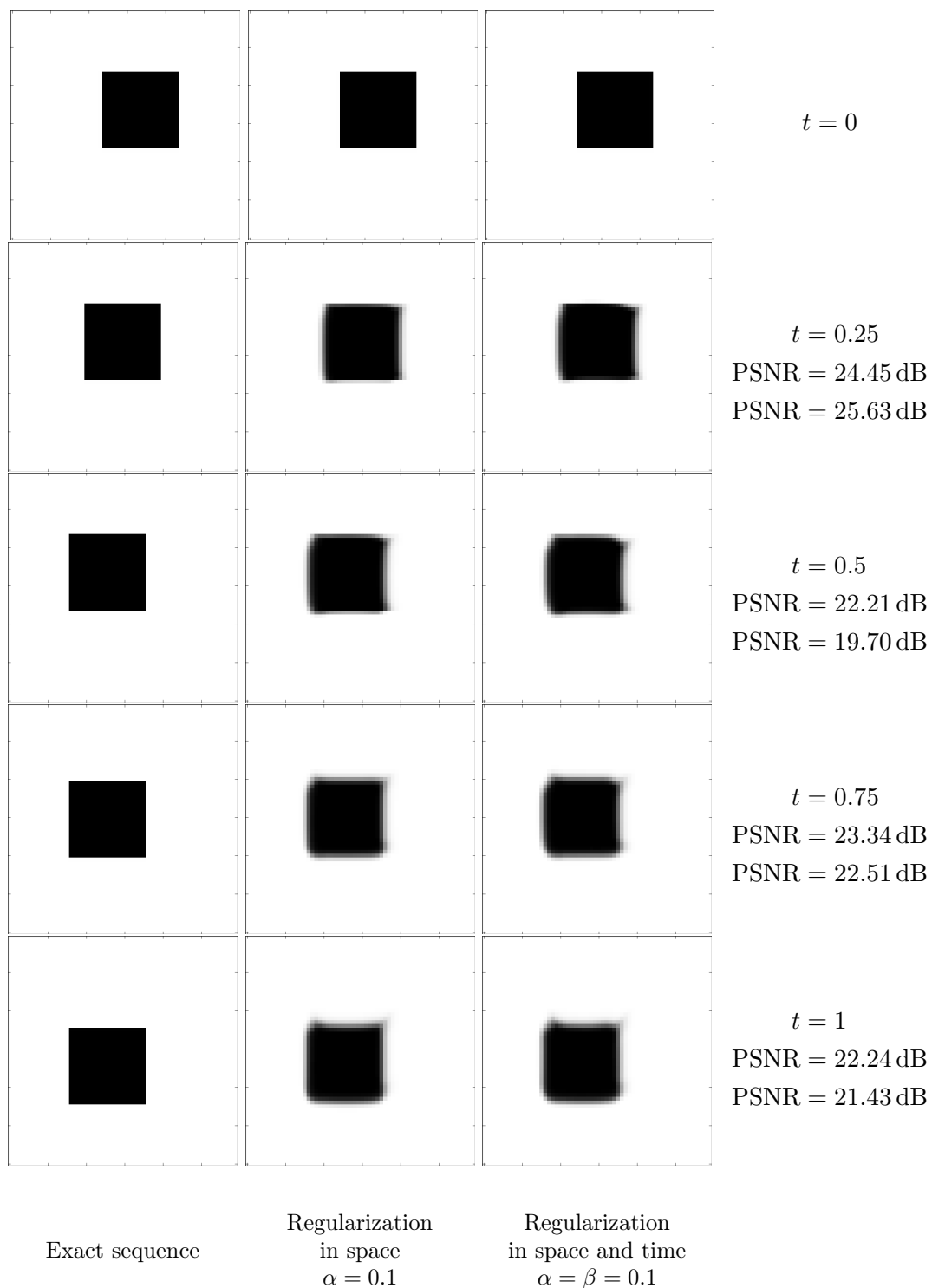
Figure 8.20.: Reconstructed sequence of a square shifted non-uniformly in time with H^1-regularization in space (and time).

$$t = 0.40625 \qquad t = 0.5 \qquad t = 0.515625 \qquad t = 609375$$
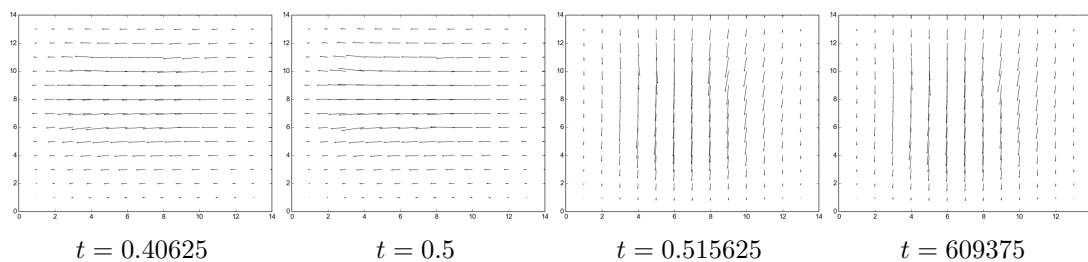
Figure 8.21.: Reconstructed optical flow of a square shifted non-uniformly in time by using an H^1-regularization in space with regularization parameter $\alpha = 0.1$.

$$t = 0.21875 \qquad t = 0.3125 \qquad t = 0.40625 \qquad t = 0.5$$

$$t = 0.515625 \qquad t = 609375 \qquad t = 0.703125 \qquad t = 0.796875$$
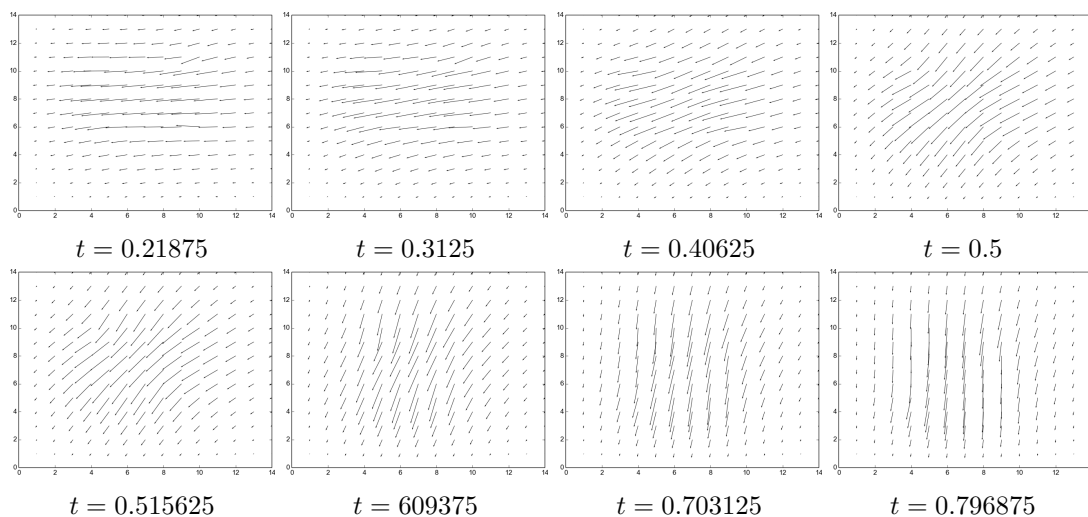
Figure 8.22.: Reconstructed optical flow of a square shifted non-uniformly in time by using an H^1-regularization in space and time with regularization parameters $\alpha = \beta = 0.1$.
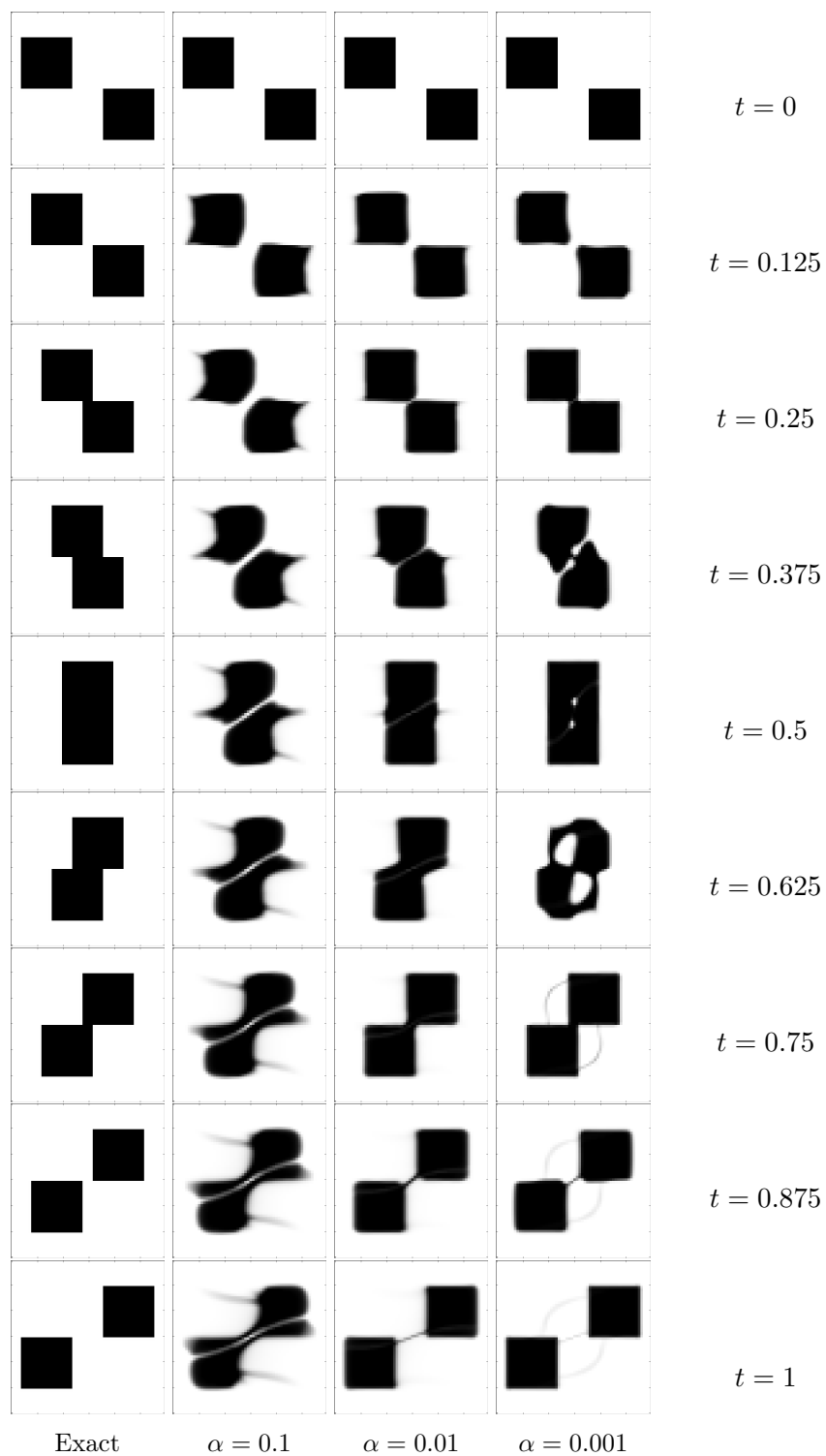
Figure 8.23.: Reconstructed sequence of two squares touching each other but moving in different directions with H^1-regularization in space.

		$t = 0$
		$t = 0.25$ PSNR $= 22.30\,\mathrm{dB}$ PSNR $= 25.36\,\mathrm{dB}$
		$t = 0.5$ PSNR $= 21.55\,\mathrm{dB}$ PSNR $= 24.30\,\mathrm{dB}$
		$t = 0.75$ PSNR $= 23.14\,\mathrm{dB}$ PSNR $= 24.99\,\mathrm{dB}$
		$t = 1$ PSNR $= 26.03\,\mathrm{dB}$ PSNR $= 26.43\,\mathrm{dB}$
Exact sequence	Reconstructed seq. $s = 0.0$	Reconstructed seq. $s = -1.0$
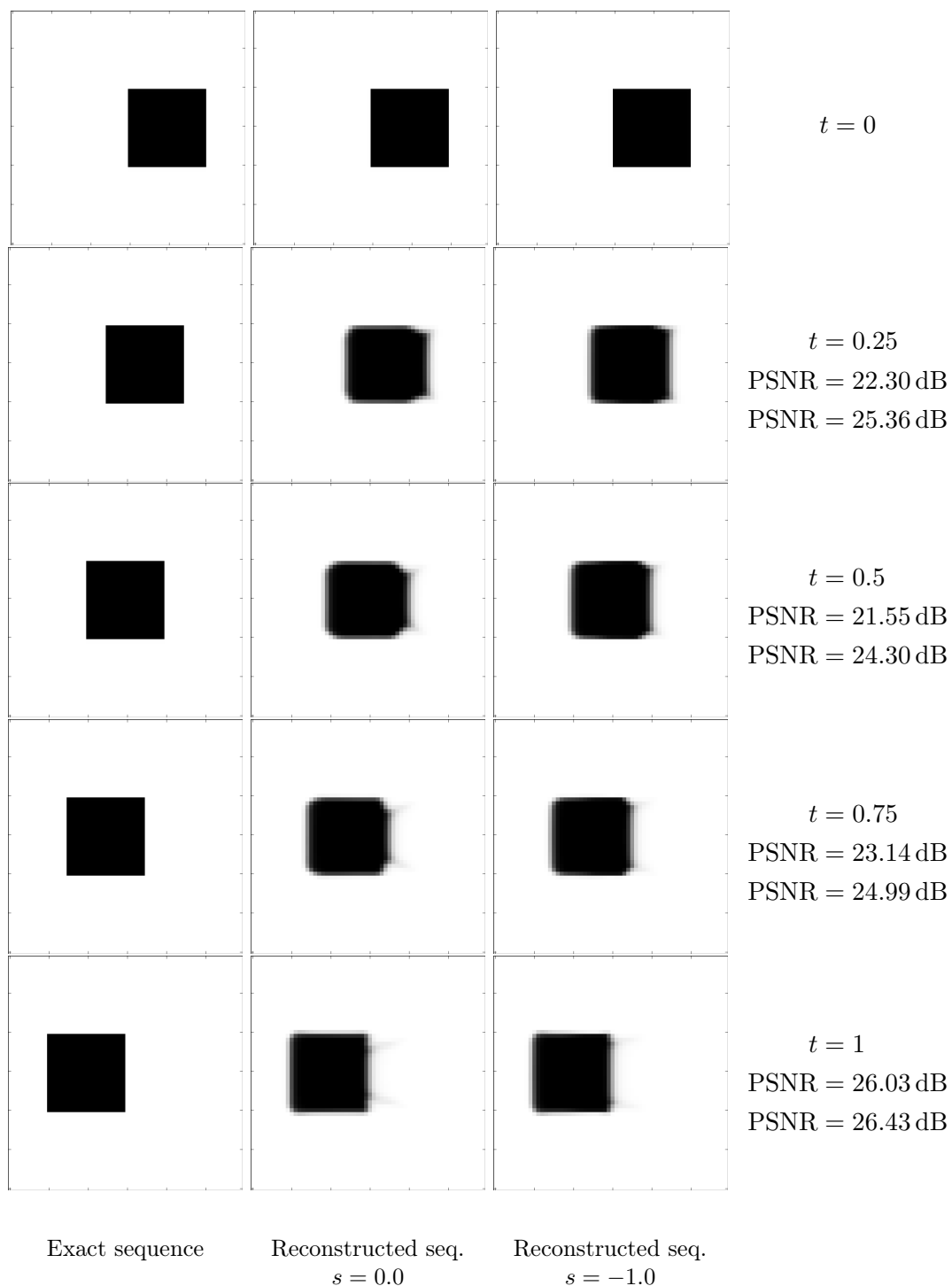
Figure 8.24.: Reconstructed sequence of a shifted square with a displacement of 20 pixel between the first and second input frame. For the reconstruction we use an H^1-regularization in space and time with regularization parameters $\alpha = 0.001$ and $\beta = 0.01$. As initial vector field in the gradient method (cf. Algorithm 7.4) we use $\omega^0 = (s, 0)^T$.

Exact sequence   Reconstructed seq.   Reconstructed seq.
$s = 0.0$ $s = 1.0$
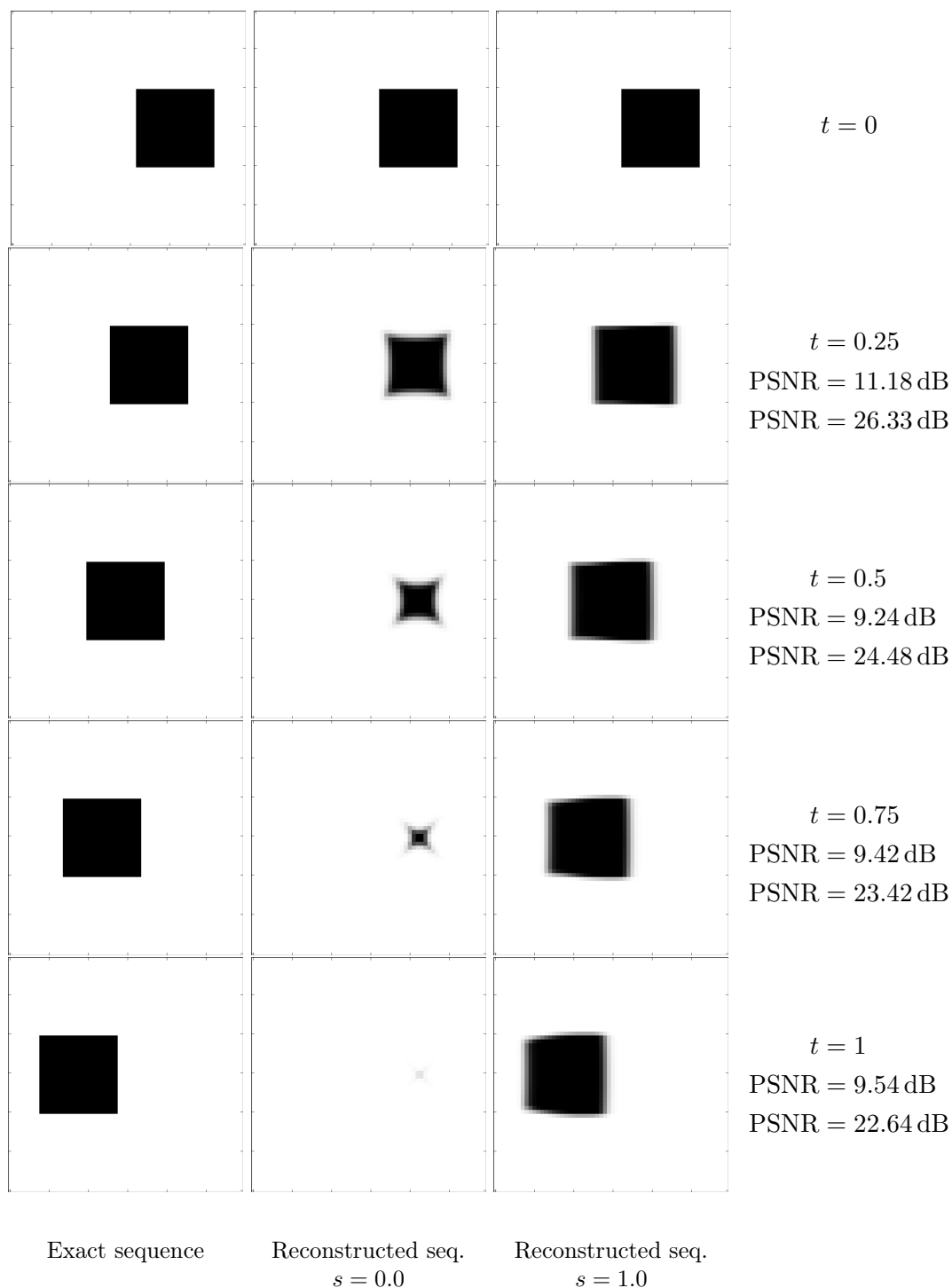
Figure 8.25.: Reconstructed sequence of a shifted square with a displacement of 24 pixel between the first and second input frame. For the reconstruction we use an H^1-regularization in space and time with regularization parameters $\alpha = 0.001$ and $\beta = 0.01$. As initial vector field in the gradient method (cf. Algorithm 7.4) we use $\omega^0 = (s,0)^T$.

$\varepsilon = 0.01$

$\alpha = 0.01$ $\qquad \alpha = 0.0001 \qquad \alpha = 0.1$

$\varepsilon = 0.05$

$\alpha = 0.01$ $\qquad \alpha = 0.0025 \qquad \alpha = 0.05$

$\varepsilon = 0.1$

$\alpha = 0.01$ $\qquad \alpha = 0.01 \qquad \alpha = 0.1$

$\varepsilon = 0.2$

$\alpha = 0.01$ $\qquad \alpha = 0.04 \qquad \alpha = 0.2$

$\varepsilon = 0.3$

$\alpha = 0.01$ $\qquad \alpha = 0.09 \qquad \alpha = 0.3$
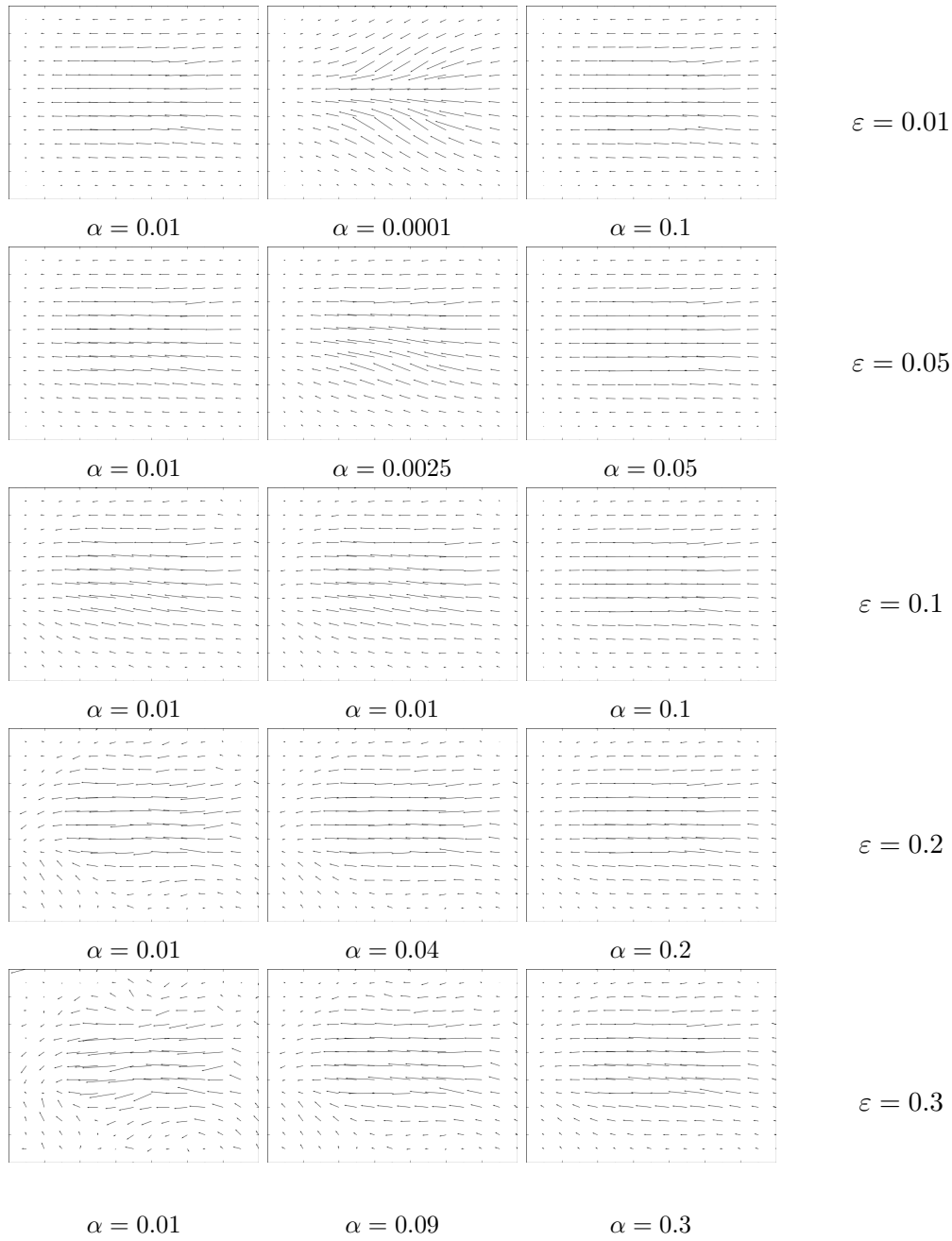
Figure 8.26.: Reconstructed optical flows at time $t = 0$ of a sequence of a shifted square perturbed by various noise levels ε. For the reconstruction we use an H^1-regularization in space with parameter choices $\alpha(\varepsilon) = 0.01$, $\alpha(\varepsilon) = \varepsilon^2$ and $\alpha(\varepsilon) = \varepsilon$.

161
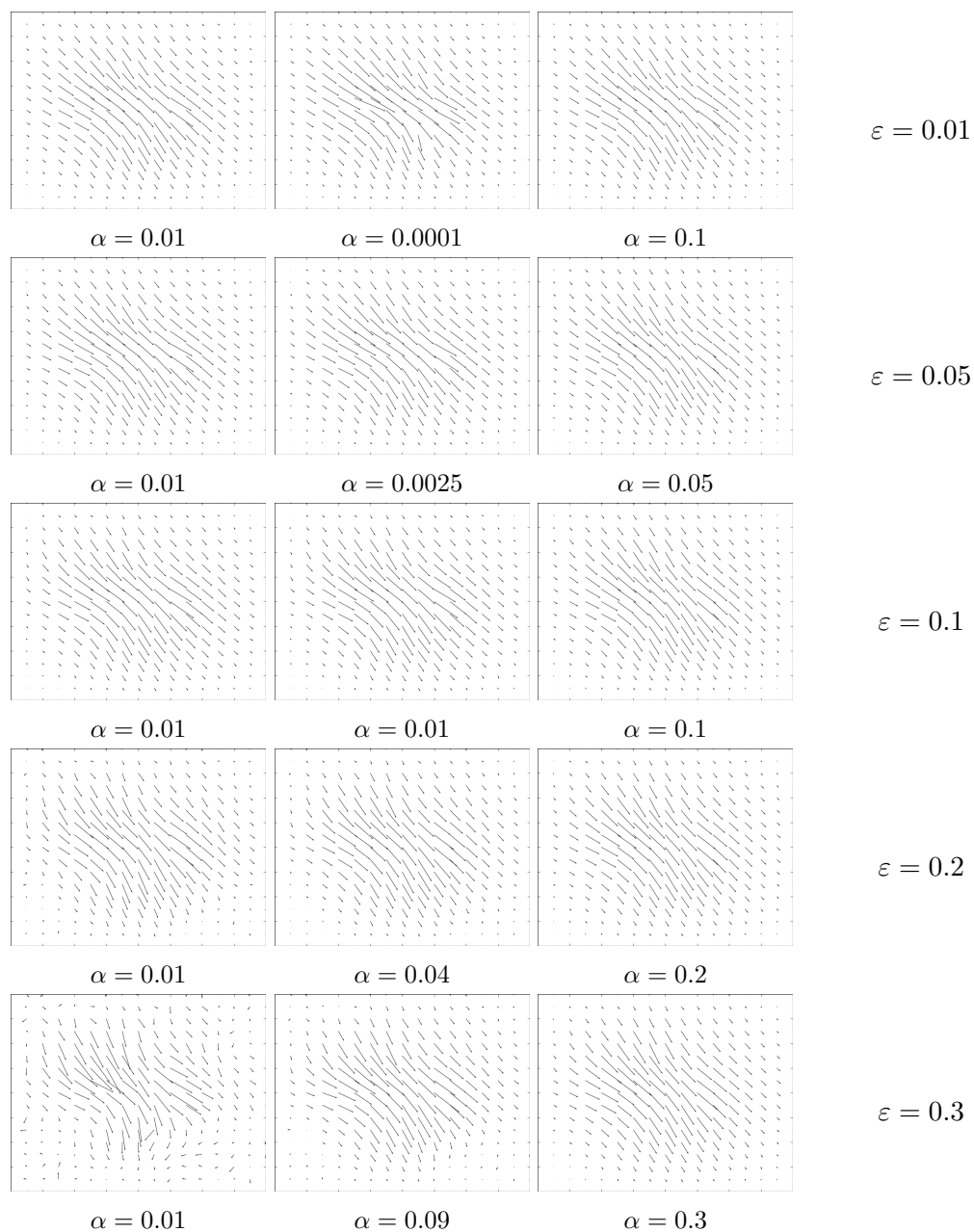
Figure 8.27.: Reconstructed optical flows at time $t = 0$ of a sequence of a rotated slotted disc perturbed by various noise levels ε. For the reconstruction we use an H^1-regularization in space with parameter choices $\alpha(\varepsilon) = 0.01$, $\alpha(\varepsilon) = \varepsilon^2$ and $\alpha(\varepsilon) = \varepsilon$.
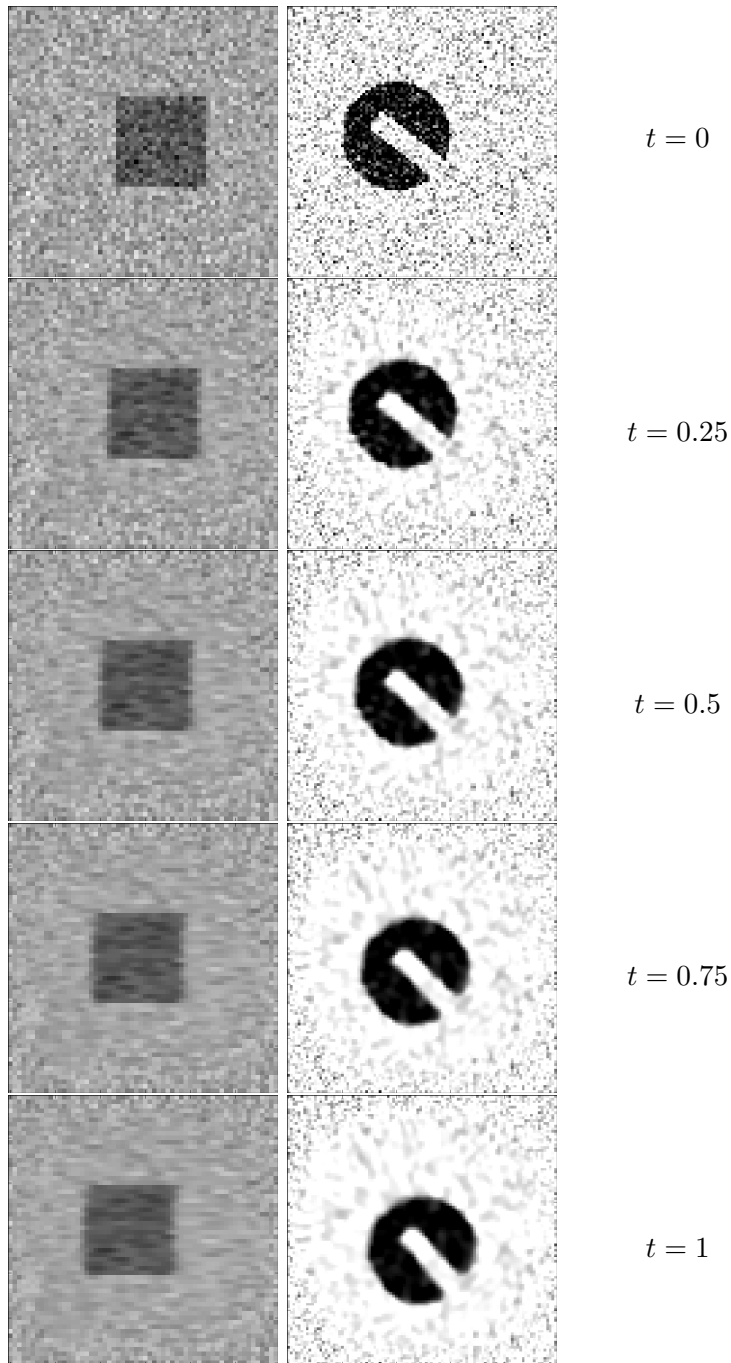
Figure 8.28.: Reconstruction of a perturbed sequence of a shifted square and a rotated disc: The H^1-regularization parameter α is equal to the noise level $\varepsilon = 0.3$

9. Conclusion and Outlook

Adapting the work of [10], we have shown that the solution operator

$$\mathcal{T} : \mathcal{U} \times \mathcal{Z} \to \mathcal{Y},$$
$$(\omega, I_0) \mapsto I$$

of the optical flow constraint (OFC) with $\mathcal{U} := \left(L^p((0,T), W_0^{1,q}(\Omega))\right)^d$, $\mathcal{Z} := L^\infty(\Omega)$ and $\mathcal{Y} := \mathcal{C}([0,T], L^r(\Omega))$, for some $1 < p, q < \infty$ and $1 \le r < \infty$, admits a unique weak solution and is weak-* sequentially closed. For proving these properties, we emphasize in comparison to [10] that we have omit the assumption $\mathrm{div}(\omega) \in L^1((0,T), L^\infty(\Omega))$ by requiring instead that the vector field ω vanishes on the spatial boundary $\partial\Omega$.

With this established theory on weak solutions to the optical flow constraint (OFC), we have shown the local ill-posedness of the sequence interpolation problem (SIP). Therefore, in the following, we have considered the regularized problem (NP). For this regularized problem (NP), we have shown that convexity and $\mathcal{U}$-coercivity of the regularization term is sufficient for the existence of an optimal solution, if the function spaces $\mathcal{U}, \mathcal{Y}$ and $\mathcal{Z}$ are specified as above. In particular, in comparison to [15], we do not need the requirement that the optical flow ω is divergence-free. Assuming additionally the existence of a bilinear form $(\cdot, \cdot)_R$ with $(\cdot, \cdot)_R = R(\omega)$, where $R(\omega)$ denotes the energy of the solution, we have shown that the regularized problem (NP) is a stable approximation of the sequence interpolation problem (SIP).

Furthermore, we have verified the existence and stability condition for an H^1-regularization in space (and time). Since we are not able to reconstruct a discontinuous optical flow with an H^1-regularization, we have also motivated a $W^{1,1+\tau}$-regularization. However, for this $W^{1,1+\tau}$-regularization we can only verify the existence condition, but not the stability condition. Thus, a next step is to analyse the stability of problem (NP) also for a $W^{1,1,+\tau}$-regularization.

For solving problem (NP) with H^1-regularization in space (and time) numerically we have presented the gradient method. Moreover, we have shown that the calculation of the gradient of the cost functional defined in (NP) involves the solution of a conservative, a non-conservative transport equation and an elliptic PDE.

In the literature, the first order Upwind and the second order Lax-Wendroff scheme are well known for the numerical solution of a transport equation with constant vector field. Generalized Upwind and Lax-Wendroff schemes are motivated in [35] to solve the conservative (cTPE) or the non-conservative transport equation (OFC) with variable coefficient vector field, respectively, but these schemes are only motivated for

time-independent and monotone vector fields, i.e., $\omega(x) \geq 0$ or $\omega(x) \leq 0$ for all $x \in \Omega \subset \mathbb{R}^d$. However, we have shown that these generalized schemes are reasonable for time-dependent and non-monotone vector fields, too, by doing a consistency analysis. Additionally, in contrast to [35], we have proven the L^1-stability of the generalized Upwind schemes and, consequently, the convergence of these schemes due to Lax's Equivalence theorem. Nevertheless, we were not able to show the stability of the generalized Lax-Wendroff schemes. Since the Upwind and the Lax-Wendroff schemes admit a damping or an oscillatory behaviour for discontinuous solutions, respectively, we have also generalized the concept of flux limiters to obtain, finally, very accurate approximations of the exact solution.

For solving the Poisson equation (7.3) or the time-dependent elliptic PDE (7.4), respectively, depending on the kind of H^1-regularization, we have presented finite difference schemes on a staggered grid and have additionally analysed the convergence of these schemes.

Moreover, we have used a projected gradient method to numerically solve problem (NP) with H^1-regularization in space for divergence-free optical flows. Here, the orthogonal projection is given by solving a Stokes problem, for which we used the MAC scheme [28, 45].

Finally, we have tested the developed reconstruction method with sequences of synthetic and real image frames. We have seen that we obtain accurate reconstruction results for various kinds of test sequences. In particular, the reconstructed sequences look much more accurate, if we do not restrict the optical flow to be divergence-free. An additional regularization in time usually leads to more accurate reconstruction results, but the computational costs are much higher. Moreover, we have seen that we are also able to reconstruct perturbed image sequences, however, to obtain more accurate reconstructions it is reasonable to denoise the input samples a priori, for instance by using variational or filter methods [14], before we reconstruct the image sequences.

Nevertheless, we have also presented negative reconstruction results. We have demonstrated that a sufficiently large sampling rate is necessary to reconstruct the sequence. Furthermore, we have observed that we obtain imprecise reconstruction results, if we try to reconstruct a sequence corresponding to a discontinuous optical flow. Thus, in this case, it seems to be more appropriate to use a $W^{1,1+\tau}$-regularization instead of a H^1-regularization. However, for solving problem (NP) with $W^{1,1+\tau}$-regularization numerically, there are two challenges: Firstly, for applying a descent method we have to discuss how to compute a descent direction in the Non-Hilbert space setting. Secondly, in the consistency analysis of the finite difference schemes for the two semi-linear transport equation we have assumed that the vector field is continuously differentiable. In particular, we have numerically illustrated that it is necessary to have at least a continuous vector field in order to obtain for convergence.

In future research, it is of interest to show existence and stability of an optimal solution

to problem NP with BV-regularization. However, for this aim one has to generalize the theory on weak solutions to the transport equation presented in Chapter 5. Furthermore, it is appropriate to construct more application-oriented regularization terms. For instance, in the case of the reconstruction of a periodical lung movement, see Section 1.1, it is reasonable to incorporate the periodicity into the construction of a suitable regularization term.

A. Appendices

A.1. Mathematical Tools

Gronwall's Inequality

Theorem A.1 (Gronwall's Inequality)**.**
Let us consider a function $y \in L^\infty((0,T))$, a non-negative function $g \in L^1((0,T))$ and $y_0 \in \mathbb{R}$, such that

$$y(t) \leq y_0 + \int_0^t g(x)y(s)\,\mathrm{d}s, \text{ for almost all } t \in [0,T],$$

we then have

$$y(t) \leq y_0 \exp\left(\int_0^t g(s)\,\mathrm{d}s\right), \text{ for almost all } t \in [0,T].$$

Proof.
A proof can be found in [10]. □

Riesz Representation Theorem

Theorem A.2 (Riesz Representation Theorem)**.**
Let $\mathcal{U}$ be a Hilbert space. Then for each $u^* \in \mathcal{U}^*$ there exists a unique element $u \in \mathcal{U}$ such that

$$\langle u^*, v \rangle_{\mathcal{U}^*\mathcal{U}} = (u,v)_{\mathcal{U}} \quad \text{for all } v \in \mathcal{U}.$$

Proof.
A proof can be found in [22]. □

Mollifier Functions

Definition A.3 (Mollifying Kernel)**.**
A function $\eta_\varepsilon \colon \mathbb{R}^d \to \mathbb{R}$ satisfying

  (i) $\eta_\varepsilon \in \mathcal{C}^\infty(\mathbb{R})$,

  (ii) $\eta_\varepsilon(x) = 0$ if $\|x\| \geq \varepsilon$ and

(iii) $\int\limits_{\mathbb{R}^d} \eta_\varepsilon(x)\,\mathrm{d}x = 1$

is called mollifying kernel.

Example A.4.

An example for a mollifying kernel function is given by

$$\eta_\varepsilon(x) = \frac{1}{\varepsilon^d}\,\eta\left(\frac{x}{\varepsilon}\right) \quad\textit{with}\quad \eta(x) = \begin{cases} C\,\exp\left(\frac{1}{\|x\|-1}\right), & \textit{if } \|x\| < 1, \\ 0 & \textit{if } \|x\| \geq 1 \end{cases},$$

where $C > 0$ is chosen such that $\int\limits_{\mathbb{R}^d} \eta(x)\,\mathrm{d}x = 1$.

Theorem A.5.

Let $f\colon \Omega \to \mathbb{R}$ be locally integrable, where $\Omega \subset \mathbb{R}^d$ denotes an open set. Then the mollification

$$f^\varepsilon := \eta_\varepsilon * f = \int\limits_\Omega \eta_\varepsilon(y-x)\,f(x)\,\mathrm{d}x = \int\limits_{B_\varepsilon(0)} \eta_\varepsilon(x)\,f(y-x)\,\mathrm{d}x$$

satisfies the following properties:

(i) $f^\varepsilon \in \mathcal{C}^\infty(\Omega)$,

(ii) *If $f \in W^{k,p}_{loc}(\Omega)$ for $k \geq 0$ and $1 \leq p < \infty$, then $f^\varepsilon \to f$ in $W^{k,p}_{loc}(\Omega)$,*

(iii) *If $f \in L^\infty(\Omega)$ then*

$$\|f^\varepsilon\|_{L^\infty(\Omega)} \leq \|f\|_{L^\infty(\Omega)}.$$

Proof.

A proof can be found in [10, 22]. $\qquad\square$

A.2. Reconstruction Error Tables

Sequence of a shifted square

α	β	$\varepsilon_{L^2}(I, I_{\#})$	$R^x(w)$	$R^t(w)$	$\varepsilon_{L^2}(I, S_{\#})$
1.0	0	0.0408894	0.0195241	—	0.1687872
0.1	0	0.0016856	0.0904738	—	0.0103012
0.01	0	0.0007934	0.1215116	—	0.0088547
0.001	0	0.0004609	0.2736055	—	0.0251710
0.0001	1.0	0.0426604	0.0238407	0.0000126	0.1738395
0.0001	0.1	0.0034537	0.0808816	0.0003115	0.0162044
0.0001	0.01	0.0007676	0.1101567	0.0005925	0.0076095
0.0001	0.001	0.0002939	0.6842077	0.0083964	0.0299832
0.0001	0.0001	0.0001990	1.0506960	0.0092256	0.0249581
0.0001	0	0.0003227	0.6046728	—	0.0266026
0.00001	1.0	0.0426604	0.0238407	0.0000126	0.1738395
0.00001	0.1	0.0034557	0.0808732	0.0003115	0.0162122
0.00001	0.01	0.0007689	0.1100615	0.0005898	0.0075905
0.00001	0.001	0.0002991	0.6702750	0.0087828	0.0308453
0.00001	0.0001	0.0000546	3.2234587	0.0586445	0.0199274
0.00001	0	0.0001685	2.2470854	—	0.0230358
0.000001	1.0	0.0426604	0.0238407	0.0000126	0.1738395
0.000001	0.1	0.0034559	0.0808724	0.0003115	0.0162130
0.000001	0.01	0.0007690	0.1100533	0.0005898	0.0075909
0.000001	0.001	0.0002998	0.6679422	0.0087916	0.0308981
0.000001	0.0001	0.0000570	3.1604764	0.0581509	0.0199347
0.000001	0	0.0001675	2.3003158	—	0.0230356

Table A.1.: Reconstruction errors of the sequence of a shifted square with H^1-regularization in space (and time).

α	$\varepsilon_{L^2}(I, I_{\#})$	$R^x(w)$	$\varepsilon_{L^2}(I, S_{\#})$
1.0	0.0766965	0.0036079	0.3331124
0.1	0.0210634	0.2674898	0.0972726
0.01	0.0015624	0.5979424	0.0281177
0.001	0.0013551	0.6443516	0.0272281
0.0001	0.0013676	0.6493764	0.0274012
0.00001	0.0013691	0.6498385	0.0274221
0.000001	0.0013693	0.6498738	0.0274245

Table A.2.: Reconstruction errors of the sequence of a shifted square corresponding to divergence-free optical flows with H^1-regularization in space.

Sequence of a Rotated Slotted Disc

α	β	$\varepsilon_{L^2}(I, I_\#)$	$R^x(w)$	$R^t(w)$	$\varepsilon_{L^2}(I, S_\#)$
1.0	0	0.0530422	0.0274057	—	0.3333650
0.1	0	0.0023306	0.1187019	—	0.0347119
0.01	0	0.0010456	0.1715070	—	0.0289935
0.001	0	0.0004327	0.4624819	—	0.0335455
0.0001	1.0	0.0715671	0.0134948	0.0000019	0.4725609
0.0001	0.1	0.0041077	0.1084378	0.0005221	0.0437760
0.0001	0.01	0.0013458	0.1554576	0.0006009	0.0251414
0.0001	0.001	0.0003977	0.5270669	0.0106730	0.0438550
0.0001	0.0001	0.0002103	1.4270353	0.0151329	0.0407300
0.0001	0	0.0001946	1.2625379	—	0.0373066
0.00001	1.0	0.0715677	0.0134942	0.0000019	0.4725650
0.00001	0.1	0.0041098	0.1084289	0.0005221	0.0437896
0.00001	0.01	0.0013470	0.1554290	0.0006013	0.0251411
0.00001	0.001	0.0004081	0.5066461	0.0104281	0.0438572
0.00001	0.0001	0.0001248	2.9633698	0.0509185	0.0388167
0.00001	0	0.0001236	3.0675683	—	0.0386363
0.000001	1.0	0.0715678	0.0134941	0.0000019	0.4725654
0.000001	0.1	0.0041100	0.1084280	0.0005221	0.0437910
0.000001	0.01	0.0013471	0.1554121	0.0006013	0.0251422
0.000001	0.001	0.0004092	0.5047413	0.0104040	0.0438637
0.000001	0.0001	0.0001274	2.8873269	0.0496286	0.0389513
0.000001	0	0.0001214	3.2675397	—	0.0388214

Table A.3.: Reconstruction errors of the sequence of a rotated slotted disc with H^1-regularization in space (and time).

α	$\varepsilon_{L^2}(I, I_\#)$	$R^x(w)$	$\varepsilon_{L^2}(I, S_\#)$
1.0	0.095817	0.0045192	0.6491899
0.1	0.029228	0.3327146	0.1975529
0.01	0.002204	0.8336318	0.0672619
0.001	0.001662	0.9774344	0.0594704
0.0001	0.001663	1.0274754	0.0687344
0.00001	0.001664	1.0345181	0.0703559
0.000001	0.001665	1.0351035	0.0704735

Table A.4.: Reconstruction errors of the sequence of a rotated slotted disc corresponding to divergence-free optical flows with H^1-regularization in space.

Sequence of a Deformed Slotted Disc

α	β	$\varepsilon_{L^2}(I, I_\#)$	$R^x(w)$	$R^t(w)$	$\varepsilon_{L^2}(I, S_\#)$
1.0	0	0.0541446	0.0154944	—	0.3507497
0.1	0	0.0030686	0.1437075	—	0.0347495
0.01	0	0.0007967	0.2241521	—	0.0396388
0.001	0	0.0003966	0.4499184	—	0.0419242
0.0001	1.0	0.0556237	0.0191065	0.0000029	0.3633331
0.0001	0.1	0.0079759	0.1149621	0.0004178	0.0600367
0.0001	0.01	0.0011012	0.1873393	0.0012604	0.0387245
0.0001	0.001	0.0003378	0.5542712	0.0039807	0.0450397
0.0001	0.0001	0.0002410	1.0126889	0.0053151	0.0415047
0.0001	0.00001	0.0002384	1.0391236	0.0052561	0.0425266
0.0001	0.000001	0.0002386	1.0379240	0.0052230	0.0426698
0.0001	0	0.0002572	1.0056332	—	0.0400081
0.00001	1.0	0.0556237	0.0191065	0.0000029	0.3633331
0.00001	0.1	0.0079822	0.1149337	0.0004177	0.0600712
0.00001	0.01	0.0011038	0.1871399	0.0012566	0.0386234
0.00001	0.001	0.0003374	0.5940005	0.0048613	0.0466787
0.00001	0.0001	0.0001206	4.5450961	0.0642661	0.0366305
0.00001	0.00001	0.0000514	10.394610	0.1383527	0.0389100
0.00001	0.000001	0.0000745	8.4994390	0.0910993	0.0423499
0.00001	0	0.0000793	7.2240719	—	0.0374487
0.000001	1.0	0.0556237	0.0191065	0.0000029	0.3633331
0.000001	0.1	0.0079829	0.1149307	0.0004176	0.0600751
0.000001	0.01	0.0011041	0.1871159	0.0012557	0.0386032
0.000001	0.001	0.0003369	0.6037685	0.0050650	0.0470821
0.000001	0.0001	0.0001236	4.4252753	0.0625341	0.0366030
0.000001	0.00001	0.0000550	9.7496855	0.1346559	0.0376110
0.000001	0.000001	0.0000478	11.124098	0.1454806	0.0414245
0.000001	0	0.0000558	8.5173526	—	0.0387115

Table A.5.: Reconstruction errors of the sequence of a deformed slotted disc with H^1-regularization in space (and time).

α	$\varepsilon_{L^2}(I, I_\#)$	$R^x(w)$	$\varepsilon_{L^2}(I, S_\#)$
1.0	0.07348	0.0071287	0.4769818
0.1	0.01366	0.2409445	0.0943595
0.01	0.00166	0.4548931	0.0367352
0.001	0.00149	0.5076143	0.0486661
0.0001	0.00150	0.5266466	0.0561469
0.00001	0.00150	0.5312745	0.0581530
0.000001	0.00150	0.5313846	0.0581957

Table A.6.: Reconstruction errors of the sequence of a deformed slotted disc corresponding to divergence-free optical flows with H^1-regularization in space.

Hamburg Taxi Sequence

α	β	$\varepsilon_{L^2}(I, I_\#)$	$R^x(w)$	$R^t(w)$	$\varepsilon_{L^2}(I, S_\#)$
0.1	0	0.002960	0.0318061	—	0.0125639
0.01	0.1	0.004472	0.0224558	0.0001521	0.0188795
0.01	0.01	0.001643	0.0754064	0.0002613	0.0073241
0.01	0.001	0.001975	0.0975452	0.0005261	0.0088826
0.01	0.0001	0.002011	0.0981767	0.0005387	0.0090426
0.01	0	0.001625	0.0776516	—	0.0073495
0.001	0.1	0.004832	0.0209534	0.0001428	0.0205293
0.001	0.01	0.001848	0.0580432	0.0002260	0.0080981
0.001	0.001	0.000876	0.3391609	0.0018302	0.0045319
0.001	0.0001	0.000966	0.3639413	0.0018683	0.0049124
0.001	0	0.000865	0.4000184	—	0.0057658
0.0001	0.1	0.004525	0.0221229	0.0001609	0.0190382
0.0001	0.01	0.001871	0.0567308	0.0002233	0.0081940
0.0001	0.001	0.000925	0.2730913	0.0018145	0.0046653
0.0001	0.0001	0.000497	1.5191372	0.0117026	0.0037903
0.0001	0	0.000646	1.1200451	—	0.0058440
0.00001	0	0.000596	2.0220189	—	0.0062645

Table A.7.: Reconstruction errors of the Hamburg taxi sequence with H^1-regularization in space (and time).

α	$\varepsilon_{L^2}(I, I_\#)$	$R^x(w)$	$\varepsilon_{L^2}(I, S_\#)$
0.1	0.0066085	0.0506745	0.0276675
0.01	0.0034784	0.1392780	0.0149428
0.001	0.0025952	0.3777087	0.0121350
0.0001	0.0018757	1.6042912	0.0116976
0.00001	0.0015862	4.8558390	0.0125374

Table A.8.: Reconstruction errors of the Hamburg taxi sequence corresponding to divergence-free optical flows with H^1-regularization in space.

Sequence of a Shifted Square with Small Sampling Rates

α	β	$\varepsilon_{L^2}(I, I_\#)$	$R^x(w)$	$R^t(w)$	$\varepsilon_{L^2}(I, S_\#)$
0.1	0	0.0087668	0.5449230	—	0.1560610
0.01	0.1	0.0412068	0.3553432	0.0058322	0.5121763
0.01	0.01	0.0010915	0.7199260	0.0170612	0.0842981
0.01	0.001	0.0017685	1.0393142	0.0102129	0.1616442
0.01	0.0001	0.0018473	1.0578231	0.0102708	0.1680175
0.01	0	0.0010850	0.7265789	—	0.0897608
0.001	0.1	0.0461224	0.3318105	0.0050671	0.5677260
0.001	0.01	0.0015001	0.6669125	0.0162611	0.0696352
0.001	0.001	0.0007254	1.0819721	0.0160256	0.1274802
0.001	0.0001	0.0007614	1.1535154	0.0148010	0.1450653
0.001	0	0.0007140	1.0948725	—	0.1141870
0.0001	0.1	0.0465915	0.3296218	0.0049998	0.5729969
0.0001	0.01	0.0015407	0.6644622	0.0162914	0.0704683
0.0001	0.001	0.0005343	1.3635645	0.0359247	0.1278299
0.0001	0.0001	0.0002658	2.8478479	0.0657637	0.1275120
0.0001	0	0.0003364	2.3795128	—	0.1092872

(a) $s = 0.0$

α	β	$\varepsilon_{L^2}(I, I_\#)$	$R^x(w)$	$R^t(w)$	$\varepsilon_{L^2}(I, S_\#)$
0.1	0	0.0086804	0.5456315	—	0.1525052
0.01	0.1	0.0352665	0.3864818	0.0069553	0.4139140
0.01	0.01	0.0010273	0.7086062	0.0163091	0.0528549
0.01	0.001	0.1111271	429.2333333	0.0	2.5264803
0.01	0.0001	0.1111271	429.2333333	0.0	2.5264805
0.01	0	0.0010220	0.7151667	—	0.0568795
0.001	0.1	0.0395952	0.3727236	0.0059550	0.4526643
0.001	0.01	0.0013747	0.6731850	0.0158545	0.0373767
0.001	0.001	0.1108414	60.7535360	0.1546196	1.9884821
0.001	0.0001	0.1111271	429.2333333	0.0	2.5264797
0.001	0	0.0009663	61.6021579	—	0.8948088
0.0001	0.1	0.1161107	274.8218915	0.0002631	2.3755303
0.0001	0.01	0.0017456	12.8713526	0.0443369	0.0872941
0.0001	0.001	0.0008605	13.5221351	0.4709798	0.7612734
0.0001	0.0001	0.1111271	351.4933660	0.0	2.4763118
0.0001	0	0.1111271	351.4933693	—	2.4763097

(b) $s = -1.0$

Table A.9.: Reconstruction error of the sequence of a shifted square with a displacement of 20 pixel between the first and second input frame. For the reconstruction we use an H^1-regularization in space (and time). As initial vector field in the gradient method (cf. Algorithm 7.4) we use $\omega^0 = (s, 0)^T$.

α	β	$\varepsilon_{L^2}(I,I_\#)$	$R^x(w)$	$R^t(w)$	$\varepsilon_{L^2}(I,S_\#)$
0.1	0	0.1233588	0.2106779	—	2.4315137
0.01	0.1	0.1356338	0.1289962	0.0004600	2.5369626
0.01	0.01	0.1118213	0.4696491	0.0045157	2.2789681
0.01	0.001	0.1124093	0.5899820	0.0010273	2.3033771
0.01	0.0001	0.1124249	0.5963778	0.0010113	2.3038625
0.01	0	0.1118026	0.4705484	—	2.2881158
0.001	0.1	0.1367454	0.1236507	0.0004268	2.5464423
0.001	0.01	0.1125601	0.4128740	0.0051687	2.2899354
0.001	0.001	0.1111796	0.6640022	0.0046871	2.2583180
0.001	0.0001	0.1112166	0.8015708	0.0019366	2.2680534
0.001	0	0.1111781	0.6647838	—	2.2638409
0.0001	0.1	0.1368577	0.1231224	0.0004233	2.5474019
0.0001	0.01	0.1126451	0.4080816	0.0050695	2.2918230
0.0001	0.001	0.1112260	0.6088675	0.0068410	2.2601270
0.0001	0.0001	0.1111391	0.8953971	0.0027032	2.2562945
0.0001	0	0.1111387	0.9002893	—	2.2610964

(a) $s = 0.0$

α	β	$\varepsilon_{L^2}(I,I_\#)$	$R^x(w)$	$R^t(w)$	$\varepsilon_{L^2}(I,S_\#)$
0.1	0	0.0143404	0.7572673	—	0.3189827
0.01	0.1	0.0653838	0.4296010	0.0074990	0.9455068
0.01	0.01	0.0011125	1.0110308	0.0322261	0.0960655
0.01	0.001	0.1111271	430.1388889	0.0	2.9420984
0.01	0.0001	0.1111271	430.1388889	0.0	2.9420987
0.01	0	0.0011145	1.0159514	—	0.0965659
0.001	0.1	0.0107878	68.3399336	0.0032978	0.1223610
0.001	0.01	0.0015608	0.9726897	0.0321679	0.0652380
0.001	0.001	0.0009507	62.3399153	0.4458951	1.1370688
0.001	0.0001	0.1111271	430.1388889	0.0	2.9420970
0.001	0	0.0007153	62.1918545	—	0.8431889
0.0001	0.1	0.0038804	75.6061937	0.0033047	0.0564983
0.0001	0.01	0.0019162	22.7863000	0.0326374	0.1103731
0.0001	0.001	0.0009270	13.7750578	0.5286805	0.7435570
0.0001	0.0001	0.1111276	352.2775196	0.0000193	2.8346096
0.0001	0	0.1111275	352.2784745	—	2.8336539

(b) $s = -1.0$

Table A.10.: Reconstruction error of the sequence of a shifted square with a displacement of 24 pixel between the first and second input frame. For the reconstruction we use an H^1-regularization in space (and time). As initial vector field in the gradient method (cf. Algorithm 7.4) we use $\omega^0 = (s,0)^T$.

Sequence of a Non-Uniform Shifted Square

α	β	$\varepsilon_{L^2}(I, I_\#)$	$R^x(w)$	$R^t(w)$	$\varepsilon_{L^2}(I, S_\#)$
1.0	1.0	0.0168745	0.0202187	0.0000215	0.139581
1.0	0.1	0.0123704	0.0314041	0.0000139	0.126878
1.0	0.01	0.0123704	0.0314041	0.0000139	0.126874
1.0	0.001	0.0123704	0.0314041	0.0000139	0.126873
1.0	0.0001	0.0123704	0.0314041	0.0000139	0.126873
1.0	0	0.0155400	0.0211992	—	0.137396
0.1	1.0	0.0123704	0.0314041	0.0000139	0.126943
0.1	0.1	0.0018991	0.0467318	0.0000684	0.100665
0.1	0.01	0.0023064	0.0567916	0.0000369	0.102811
0.1	0.001	0.0022594	0.0590211	0.0000371	0.102639
0.1	0.0001	0.0022586	0.0592458	0.0000373	0.102641
0.1	0	0.0019204	0.0462407	—	0.101279
0.01	1.0	0.0123704	0.0314041	0.0000139	0.126945
0.01	0.1	0.0025928	0.0450368	0.0000305	0.102833
0.01	0.01	0.0009349	0.0906686	0.0007613	0.100889
0.01	0.001	0.0015556	0.0630102	0.0000523	0.101425
0.01	0.0001	0.0015471	0.0628872	0.0000527	0.101433
0.01	0	0.0014582	0.0610583	—	0.101888

Table A.11.: Reconstruction errors of the sequence of a square shifted non-uniformly in time with H^1-regularization in space (and time).

Sequence of a Zommed In and Translated Square

α	$\varepsilon_{L^2}(I, I_\#)$	$R^x(w)$	$\varepsilon_{L^2}(I, S_\#)$
1.0	0.1502174	0.0229685	0.7879874
0.1	0.0093030	0.3946709	0.0571559
0.01	0.0021992	0.5775282	0.0345540
0.001	0.0010034	1.0760683	0.0376729
0.0001	0.0004997	2.6106347	0.0365505
0.00001	0.0000438	15.1928514	0.3342139
0.000001	0.0000251	18.8350627	0.9556858

Table A.12.: Reconstruction errors of the sequence of a zoomed and translated square with H^1-regularization in space

α	$\varepsilon_{L^2}(I, I_{\#})$	$R^x(w)$	$\varepsilon_{L^2}(I, S_{\#})$
1.0	0.1881278	0.0024436	1.0200542
0.1	0.1082107	0.3187858	0.5613986
0.01	0.0961134	0.6080348	0.4939423
0.001	0.0804334	3.2771032	0.4188005
0.0001	0.0792281	4.9593496	0.4161314
0.00001	0.0789296	6.0930110	0.4188976
0.000001	0.0788969	6.1607504	0.4189676

Table A.13.: Reconstruction errors of the sequence of a zoomed and translated square corresponding to divergence-free optical flows with H^1-regularization in space.

Sequence of 2 Squares

α	β	$\varepsilon_{L^2}(I, I_{\#})$	$R^x(w)$	$R^t(w)$	$\varepsilon_{L^2}(I, S_{\#})$
0.1	0.1	0.1580246	3.5969446	0.2804023	0.9966773
0.1	0.01	0.8029649	1.5095130	0.0397222	5.7206019
0.1	0.001	0.8012935	1.5798865	0.0407218	5.7089464
0.1	0.0001	0.8043194	1.5482181	0.0396037	5.7314469
0.1	0	0.1344879	3.7854122	—	0.8597478
0.01	0.1	0.63373140	1.2983100	0.1294037	4.5162212
0.01	0.01	0.0186932	7.6175590	0.7941471	0.2176909
0.01	0.001	0.2498397	14.0477121	1.5004131	1.8367867
0.01	0.0001	0.2631647	13.7954890	1.4397018	1.9268570
0.01	0	0.0118425	6.8706031	—	0.1776370
0.001	0.1	0.6659123	1.1778707	0.1210922	4.7427469
0.001	0.01	0.0315497	6.5316704	0.8511410	0.3087130
0.001	0.001	0.0122320	21.0542835	3.1831973	0.5685495
0.001	0.0001	0.0151115	28.2647311	3.8723581	0.6456766
0.001	0	0.0051925	23.0014706	—	0.5069380
0.0001	0.1	0.6726119	1.1503725	0.1168902	4.8015562
0.0001	0.01	0.0335007	6.4729011	0.8700972	0.3263297
0.0001	0.001	0.0091589	20.3245727	3.3519227	0.3469311
0.0001	0.0001	0.0060490	44.6464421	6.4345632	0.6252176
0.0001	0	0.0026752	40.3241770	—	0.5584646

Table A.14.: Reconstruction errors of the sequence of two squares touching each other but moving in different directions with H^1-regularization in space (and time).

Bibliography

[1] R. Acar and C. R. Vogel: *Analysis of bounded variation penalty methods for ill-posed problems.* Inverse Problems, 10, 1217-1229, 1994.

[2] H. W. Alt: *Lineare Funktionalanalysis: Eine anwendungsorientierte Einführung.* Springer, Berlin, 2012.

[3] L. Ambrosio, N. Fusco, and D. Pallara: *Functions of Bounded Variation and Free Discontinuity Problems.* Clarendon Press, Oxford, 2000.

[4] G. Aubert, R. Deriche, and P. Kornprobst: *Computing optical flow via variational techniques.* SIAM J. Appl. Math, 60 (1), 156-182, 1999.

[5] G. Aubert and L. Vese: *A variational method in image recovery.* SIAM J. Numer. Anal., 34 (5), 1948-1979, 1997.

[6] W. N. Bell, L. N. Olson, and J. B. Schroder: *PyAMG: Algebraic Multigrid Solvers in Python.* Release 3.0, 2015. url: `http://www.pyamg.org`.

[7] M. Bergounioux: *On Poincare-Wirtinger inequalities in spaces of functions of bounded variation.* <hal-00515451v1>, 2010.

[8] A. Borzi, K. Ito, and K. Kunisch: *An optimal control approach to optical flow computation.* Int. J. Numer. Meth. Fluids, 40, 231-240, 2002.

[9] A. Borzi, K. Ito, and K. Kunisch: *Optimal control formulation for determining optical flow.* SIAM J. Sci. Comput., 24 (3), 818-847, 2002.

[10] F. Boyer and P. Fabrie: *Mathematical Tools for the Study of the Incompressible Navier-Stokes Equations and Related Models.* Springer, New York, 2013.

[11] H. Brezis: *Functional Analysis, Sobolev Spaces and Partial Differential Equations.* Springer, New York, 2011.

[12] W. L. Briggs, V. E. Henson, and S. F. McCormick: *A Multigrid Tutorial.* SIAM, Philadelphia, 2000.

[13] C. Brune: *Berechnung des Optischen Flusses und Kantenerkennung mit Optimierungsmethoden.* Diploma Thesis, Department of Mathematics and Computer Science, University of Münster, 2007.

[14] T. F. Chan and J. Shen: *Image Processing and Analysis: Variational, PDE, Wavelet, and Stochastic Methods.* SIAM, Philadelphia, 2005.

[15] K. Chen: *Optimal Control based Image Sequence Interpolation.* Phd Thesis, Department of Mathematics and Computer Science, University of Bremen, 2011.

[16] I. Cohen: *Nonlinear Variational method for optical flow computation.* Proceedings of the 8th SCIA, 523-530, 1993.

[17] G. Crippa: *The flow associated to weakly differentiable vector fields.* Phd Thesis, Department of Mathematics, University of Zurich, 2008.

[18] R. Deriche, P. Kornprobst, and G. Aubert: *Optical-flow estimation while preserving its discontinuities: A variational approach.* Proc. Second Asian Conference on Computer Vision, 290-295, 1995.

[19] R. J. DiPerna and P. L. Lions: *Ordinary differential equations, transport theory and Sobolev spaces.* Invent. math, 98, 511-547, 1989.

[20] I. Ekeland and R. Temam: *Convex Analysis and Variational Problems.* North-Holland, Amsterdam, 1976.

[21] H. W. Engl, M. Hanke-Bourgeois, and A. Neubauer: *Regularization of Inverse Problems.* Kluwer, Dordrecht, 2000.

[22] L. C. Evans: *Partial Differential Equations.* American Math. Soc., Providence, 2010.

[23] Federal Statistical Office in Germany: *Krebs war 2013 die zweithäufigste Todesursache.* News release, 34, 02.02.2015, url: `https://www.destatis.de/DE/PresseService/Presse/Pressemitteilungen/2015/02/PD15_034_232.html`.

[24] C. Geiger and C. Kanzow: *Numerische Verfahren zur Lösung unrestringierter Optimierungsaufgaben.* Springer, Berlin, 1999.

[25] V. Girault and P. A. Raviart: *Finite Element Approximation of the Navier-Stokes Equations.* Springer, Berlin, 1979.

[26] E. Giusti: *Minimal Surfaces and Functions of Bounded Variation.* Birkhäuser, Boston, 1984.

[27] C. Großmann and H.-G. Roos: *Numerik partieller Differentialgleichungen.* Teubner, Stuttgart, 1992.

[28] F. H. Harlow and J. E.Welch: *Numerical calculation of time-dependent viscous incompressible flow of fluid with free surface.* The Physics of Fluids, 8 (12), 2182-2189, 1965.

[29] H. Heuser: *Gewöhnliche Differentialgleichungen : Einführung in Lehre und Gebrauch.* Vieweg + Teubner, Wiesbaden, 2009.

[30] W. Hinterberger and O. Scherzer: *Models for image interpolation based on the optical flow.* Computing, 66, 231-247, 2001.

[31] M. Hinze, R. Pinnau, M. Ulbrich and S. Ulbrich: *Optimization with PDE Constraints.* Springer, Dordrecht, 2009.

[32] C. Hirsch: *Numerical Computation of Internal and External Flows. Volume 1: Fundamentals of Computational Fluid Dynamics.* Butterworth-Heinemann, Amsterdam, 2007.

[33] B. K. P. Horn and B. G. Schunk: *Determining optical flow.* Artificial Intelligence, 17, 185-203, 1981.

[34] C. T. Kelley: *Iterative Methods for Optimization.* SIAM, Philadelphia, 1999.

[35] R. J. LeVeque: *Finite-Volume Methods for Hyperbolic Problems.* Cambridge Univ. Press, Cambridge, 2004.

[36] R. J. LeVeque: *Numerical Methods for Conservation Laws.* Birkhäuser, Basel, 1992.

[37] H. Logemann and E.P. Ryan: *Ordinary Differential Equations : Analysis, Qualitative Theory and Control.* Springer, London, 2014.

[38] A. K. Louis: *Inverse und schlecht gestellte Probleme.* Teubner, Stuttgart, 1989.

[39] V. A. Morozov: *Methods for Solving Incorrectly Posed Problems.* Springer, New York, 1984.

[40] L. Perko: *Differential Equations and Dynamical Systems.* Springer, New York, 1991.

[41] R. D. Richtmyer and K. W. Morton: *Difference Methods for Initial-Value Problems.* Interscience Publ., New York, 1967.

[42] A. Rieder: *Keine Probleme mit Inversen Problemen: Eine Einführung in ihre stabile Lösung.* Vieweg, Wiesbaden, 2003.

[43] J. Thrän: *Implementation eines Optimierungsverfahrens zur Rekonstruktion lückenhafter Bildsequenzen.* Diploma Thesis, Department of Mathematics, University of Hamburg, 2016.

[44] F. Tröltzsch: *Optimale Steuerung partieller Differentialgleichungen : Theorie, Verfahren und Anwendungen.* Vieweg + Teubner, Wiesbaden, 2009.

[45] M. Wang and L. Chen: *Multigrid methods for the Stokes equations using distributive Gauss-Seidel relaxations based on the least squares commutator.* J. Sci. Comput., 56 (2), 409-431, 2013.

[46] J. Weickert and C. Schnörr: *Variational optic flow computation with a spatiotemporal smoothness constraint.* Journal of Mathematical Imaging and Vision, 14, 245-255, 2001.

[47] Welt der Physik/Wissenschaft aktuell: *Wie funktioniert eine optische Computermaus?.* 15.12.2008, url: `http://www.weltderphysik.de/thema/hinter-den-dingen/elektronische-geraete/optische-computermaus/`

[48] Wikipedia - The Free Encyclopedia: *Barberpole illusion.* url: `https://en.wikipedia.org/wiki/Barberpole_illusion`.

[49] E. Zeidler: *Nonlinear Functional Analysis and its Applications II/A: Linear Monotone Operators.* Springer, New York, 1990.

Abstract

In this thesis, we study a sequence interpolation problem: Given a sequence of image frames at discrete points in time, find a continuous function in time, which interpolates these image frames. We solve this problem by using optical flows. Since the reconstruction problem is unstable, we regularize it. This regularization leads to a non-linear minimization problem subject to the optical flow constraint, which is characterized by a semi-linear transport equation.

To analyse existence and stability of a solution to the regularized reconstruction problem, we first discuss weak solutions of transport equations. Here, we adapt the work of [10] to show – without any restriction on the divergence of the vector field – that the non-linear solution operator of the transport equation is weak-* sequentially closed and admits a unique weak solution.

Finally, with the help of this theory we state sufficient conditions on the regularization term and the involved function spaces, which guarantee existence and stability of an optimal solution to the regularized reconstruction problem. Here, we do not need to restrict the optical flow to be divergence-free, in contrast to [15]. We verify the existence condition for an H^1-regularization in space (and time), as well as for a $W^{1,1+\tau}$-regularization in space. Moreover, we verify the stability condition for both H^1-regularizations.

For solving the reconstruction problem with H^1-regularization numerically we apply the gradient method. However, the computation of the gradient involves the solution of a conservative, a non-conservative transport equation and an elliptic partial differential equation. Therefore, we present numerical efficient finite difference schemes for solving these differential equations. In particular, in the numerically analysis of the finite difference schemes for the two semi-linear transport equations we obtain new results.

Finally, we test the robustness of the developed reconstruction method with sequences of synthetic and real image frames. In particular, we compare our reconstruction results with reconstructions correspondig to divergence-free optical flows.

Zusammenfassung

In dieser Arbeit untersuchen wir folgendes Rekonstruktionsproblem: Zu einer gegebenen Sequenz von Bildern zu diskreten Zeitpunkten suchen wir eine stetige Funktion in der Zeit, welche diese Bilder interpoliert. Wir lösen dieses Problem mit Hilfe von optischen Flüssen. Da das Rekonstruktionsproblem instabil ist, regularisieren wir dieses. Diese Regularisierung führt zu einem nichtlinearen Minimierungsproblem unter der Nebenbedingung einer optischen Fluss Restriktion, welche durch eine semilineare Transportgleichung charakterisiert wird.

Um die Existenz und Stabilität einer Lösung für das regularisierte Rekonstruktionsproblem zu analysieren, diskutieren wir zunächst schwache Lösungen von Transportgleichungen. Hierbei modifizieren wir die Resultate in [10], um auch ohne Restriktionen an die Divergenz des Vektorfeldes zu zeigen, dass der nichtlineare Lösungsoperator der Transportgleichung schwach-* folgenabgeschlossen ist und eine eindeutige Lösung besitzt.

Mit Hilfe dieser Theorie geben wir schließlich hinreichende Bedingungen an den Regularisierungterm und die involvierten Funktionenräume an, welche die Existenz und Stabilität einer optimalen Lösung zum regularisierten Rekonstruktionsproblem gewährleisten. Hierbei benötigen wir, im Gegensatz zu [15], nicht die Restriktion, dass der optische Fluss divergenzfrei ist. Wir verifizieren die Existenz-Bedingung sowohl für die H^1-Regularisierung im Ort (und in der Zeit) als auch für die $W^{1,1+\tau}$-Regularisierung im Ort. Außerdem, verfizieren wir die Stabilitäts-Bedingung für beide H^1-Regularisierungen.

Um das Rekonstruktionsproblem mit H^1-Regularisierung numerisch zu lösen, verwenden wir das Gradientenverfahren. Die Berechnung des Gradienten erfordert allerdings das Lösen einer konservativen, einer nicht konservativen Transportgleichung und einer elliptischen partiellen Differentialgleichung. Daher präsentieren wir numerisch effiziente finite Differenzen-Verfahren, um diese Differentialgleichungen zu lösen. Insbesondere erhalten wir in der numerischen Analyse der finiten Differenzenverfahren für die zwei semilinearen Transportgleichungen neue Resultate.

Schließlich testen wir die Robustheit des entwickelten Rekonstruktionsverfahrens an künstlichen und realen Bildsequenzen. Insbesondere vergleichen wir unsere Rekonstruktionsergebnisse mit Rekonstruktionen, welche zu divergenzfreien optischen Flüssen korrespondieren.

Eidesstattliche Erklärung

Hiermit erkläre ich an Eides statt, dass ich die vorliegende Dissertationsschrift selbst verfasst und keine anderen als die angegebenen Quellen und Hilfsmittel benutzt habe.

Hamburg, 21. Dezember 2016   _____

                                                    Unterschrift